DYNA

Journal of the Facultad de Minas, Universidad Nacional de Colombia - Medellin Campus
DYNA 93 (240), January - March, 2026 - ISSN 0012-7353

Facultad de Minas
Sede Medellín

UNIVERSIDAD NACIONAL DE COLOMBIA

DYNA

http://dyna.medellin.unal.edu.co/

DYNA is an international journal published by the Facultad de Minas, Universidad Nacional de Colombia, Medellín Campus since 1933. DYNA publishes peer-reviewed scientific articles covering all aspects of engineering. Our objective is the dissemination of original, useful and relevant research presenting new knowledge about theoretical or practical aspects of methodologies and methods used in engineering or leading to improvements in professional practices. All conclusions presented in the articles must be based on the current state-of-the-art and supported by a rigorous analysis and a balanced appraisal. The journal publishes scientific and technological research articles, review articles and case studies.

DYNA publishes articles in the following areas:

Organizational Engineering
Civil Engineering
Materials and Mines Engineering
Geosciences and the Environment
Systems and Informatics
Chemistry and Petroleum
Mechatronics
Bio-engineering
Other areas related to engineering

Publication Information

DYNA (ISSN 0012-73533, Printed; 2346-2183, online).
Is published by the Facultad de Minas, Universidad Nacional de Colombia, with a quarterly periodicity (January - March, April - June, July - September and October - December).
Circulation License Resolution 000584 de 1976 from the Ministry of the Government.

Contact information:
Web page: https://revistas.unal.edu.co/index.php/dyna
E-mail: dyna@unal.edu.co
Mail address:
Revista DYNA
Facultad de Minas
Universidad Nacional de Colombia - Medellín Campus
Carrera 80 No. 65-223 Bloque M9 - Of.:107
Telephone: (574) (604) 4255343
Medellín - Colombia

Notice
All statements, methods, instructions and ideas are only responsibility of the authors and not necessarily represent the view of the Universidad Nacional de Colombia. The publisher does not accept responsibility for any injury and/or damage for the use of the content of this journal.
The concepts and opinions expressed in the articles are the exclusive responsibility of the authors.

Institutional Exchange Request
DYNA may be requested as an institutional exchange through the e-mail: canjebib_med@unal.edu.co or to the postal address:

Biblioteca Central “Efe Gómez”
Universidad Nacional de Colombia, Sede Medellín
Calle 59A No 63-20
Teléfono: (574) (604) 430 97 86
Medellín - Colombia

Indexing and Databases

DYNA is admitted in:

The National System of Indexation and Homologation of Specialized Journals CT+I-PUBLINDEX, Category C

Science Citation Index Expanded
SCImago Journal & Country Rank - SJR
SCOPUS
SciELO Scientific Electronic Library Online
Chemical Abstract - CAS
Scientific Electronic Library on Line - SciELO
GEOREF
PERIÓDICA Data Base
Latindex
Actualidad Iberoaméricana
Redalyc - Scientific Information System
Directory of Open Acces Journals - DOAJ
PASCAL
CAPES
UN Digital Library - SINAB
EBSCO Host Research Databases

Publisher’s Office
Néstor Ricardo Rojas Reyes, Director
Mónica del Pilar Rada Tobón, Editorial Coordinator
Catalina Cardona Álvarez, Editorial Assistant
Jean Franco Salas Guerrero, Editorial Assistant

Todograficas Ltda., Diagramming

Reduced Postal Fee
Tarifa Postal Reducida # 2014-287 4-72.
La Red Postal de Colombia, expires Dec. 31st, 2026

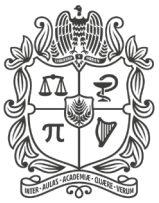

UNIVERSIDAD
NACIONAL
DE COLOMBIA

DYNA

DYNA
http://dyna.medellin.unal.edu.co/

Universidad Nacional de Colombia

DYNA
http://dyna.medellin.unal.edu.co/

Universidad Nacional de Colombia

Journal DYNA, 93 (240), January - March, 2026. Medellín. ISSN 0012-7353 Printed, ISSN 2346-2183 Online

CONTENTS

Our Cover

Photograph showing the transparency of the water, which at first sight reveals the aquatic vegetation of the natural reservoir. Taken on March 8, 2025.

In the article: Landsat 8-based estimation of total suspended solids (1.3-43 mg/L) using NDWI, MNDWI and AWEI indices at Tecocomulco Ramsar Wetland, Mexico

Authors
Ismael Ortega-García, René Cruz-Guerrero & German Cuaya-Simbro

DYNA
http://dyna.medellin.unal.edu.co/

Universidad Nacional de Colombia

Revista DYNA, 93 (240), enero - marzo, 2026. Medellín. ISSN 0012-7353 Impreso, ISSN 2346-2183 En línea

CONTENIDO

Nuestra Carátula

Fotografía que muestra la transparencia del agua, que a primera vista revela la vegetación acuática del reservorio natural. Tomada el 8 de marzo de 2025.

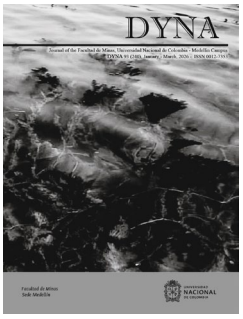

En el artículo: Estimación basada en Landsat 8 de sólidos suspendidos totales (1.3-43 mg/L) usando los índices NDWI, MNDWI y AWEI en el Humedal Ramsar de Tecocomulco, México

Autores
Ismael Ortega-García, René Cruz-Guerrero & German Cuaya-Simbro

DYNA
http://dyna.medellin.unal.edu.co/

UNIVERSIDAD NACIONAL DE COLOMBIA

Influence of dissolved organic carbon on the limnochemical characteristics of a tropical endorheic wetland during a hydrological period: El Eneal Wetland, Colombia

Wilfer David Guzmán-López, Lina Claudia Giraldo, Fabio Vélez-Macías, & Néstor Aguirre

Escuela ambiental, Facultad de Ingeniería, Universidad de Antioquia, Medellín, Colombia. wilfer.guzman@udea.edu.co, lina.giraldo@udea.edu.co, fabio.velez@udea.edu.co, nestor.aguirre@udea.edu.co

Received: April 21st, 2025. Received in revised form: November 7th, 2025. Accepted: November 12th, 2025.

Abstract
The progressive darkening of inland waters globally has been attributed to increasing dissolved organic carbon (DOC) concentrations, yet this phenomenon remains understudied in tropical systems. This research investigated DOC's influence on the limnochemical characteristics of a tropical endorheic wetland through two sampling campaigns during different hydrological periods. DOC was measured alongside key limnological variables, with relationships analyzed through descriptive statistics and principal component analysis. Results demonstrated significant positive correlations between DOC and electrical conductivity ($r=0.78$, $p<0.001$) and turbidity ($r=0.74$, $p<0.001$), while inverse correlations emerged with bicarbonates ($r=-0.80$, $p<0.001$), ORP ($r=-0.61$, $p<0.001$), and chlorophyll-a ($r=-0.75$, $p<0.001$). However, these associations likely reflect synchronous responses to increasing water levels rather than direct DOC effects. Our findings suggest DOC potentially regulates phytoplankton biomass and optical properties in this tropical wetland system.

Keywords: DOC; tropical; wetland; limnochemistry; DOM; endorheic

Influencia del carbono orgánico disuelto en las características limnoquímicas de un humedal endorreico tropical durante un período hidrológico: Humedal El Eneal, Colombia

Resumen
El oscurecimiento progresivo de aguas continentales se ha atribuido al incremento de carbono orgánico disuelto (COD), fenómeno poco estudiado en sistemas tropicales. Esta investigación evaluó la influencia del COD en las características limnoquímicas de un humedal endorreico tropical mediante dos campañas de muestreo en diferentes periodos hidrológicos. Se midió el COD junto con parámetros limnológicos, analizando relaciones mediante estadística descriptiva y análisis de componentes principales. Los resultados mostraron correlaciones positivas significativas entre COD y conductividad eléctrica ($r=0,78$, $p<0,001$) y turbidez ($r=0,74$, $p<0,001$), y correlaciones inversas con bicarbonatos ($r=-0,80$, $p<0,001$), ORP ($r=-0,61$, $p<0,001$) y clorofila-a ($r=-0,75$, $p<0,001$). Estas asociaciones probablemente reflejan respuestas sincrónicas al aumento del nivel hídrico más que efectos directos del COD. Los hallazgos sugieren que el COD regula potencialmente la biomasa fitoplanctónica y las propiedades ópticas del sistema.

Palabras clave: DOC; humedal tropical; limnoquímica; DOM; endorreico

1. Introduction

In recent decades, a growing body of research has documented a progressive darkening of continental water bodies worldwide, a phenomenon known as "brownification" [1-3] This change in coloration of aquatic ecosystems not only represents a visible alteration but also carries profound ecological and biogeochemical implications that affect the structure and functioning of these systems [4,5].

Research has established that this darkening is primarily

How to cite: Guzmán-López, W.D., Giraldo, L.C., Vélez-Macías, F. and Aguirre, N., Influence of dissolved organic carbon on the limnochemical characteristics of a tropical endorheic wetland during a hydrological period: El Eneal Wetland, Colombia DYNA, (93)240, pp. 9-18, January - March, 2026.

linked to increasing concentrations of dissolved organic carbon (DOC) in water bodies [6]. DOC, composed of humic and fulvic substances derived from the decomposition of terrestrial plant material, has exhibited increasing trends in temperate and boreal regions, attributed to factors such as changes in land use, reduction of acid deposition, and notably, global climate change [7,8].

In contrast to the extensive research conducted at middle and high latitudes, there is a notable paucity of studies documenting analogous processes in tropical aquatic ecosystems, particularly in endorheic systems [9]. In Brazil, for instance, studies in urban wetlands have demonstrated that DOC significantly contributes to light attenuation, impacting primary productivity [10,11]. However, the existing literature has focused on lentic systems connected to hydrographic networks, thereby leaving a gap in the understanding of tropical endorheic wetlands. These wetlands are particularly vulnerable to the effects of DOC due to their hydrological isolation and dependence on rainfall inputs [9,12].

Tropical endorheic wetlands are recognized as ecosystems particularly vulnerable to the impacts of climate change and anthropogenic disturbances, distinguished by their hydrological isolation and dependence on precipitation-derived inputs [9,12]. These wetlands act as biodiversity reservoirs, providing vital ecosystem services such as water regulation, carbon sequestration, and flood mitigation [13]. However, the comprehension of their limnological processes, particularly those associated with carbon cycling, remains substantially underdeveloped [9].

The role of DOC in these ecosystems is of particular interest, as it has been shown to play a central role through complex regulatory mechanisms. These mechanisms include the absorption of photosynthetically active radiation (PAR), which reduces light penetration available for primary productivity, and the formation of complexes with essential nutrients, which limits their bioavailability for phytoplankton [14,15]. This dynamic alters the optical properties of water, increasing solar radiation absorption in the blue and ultraviolet spectral regions, with direct repercussions for photic zone depth and primary production [16-18].

In this context, this research addresses two key questions: (1) How does DOC influence the limnochemical characteristics of El Eneal wetland? and (2) What role do seasonal fluctuations in limnimetric level play in these interactions? To answer these questions, in situ measurements of physical and chemical variables were combined with descriptive and multivariate analysis. The results will provide insight into the ecology of these unique systems and offer valuable information for their management and conservation over time.

2. Materials and methods

2.1 Study area

The El Eneal wetland is located in the municipality of San Onofre, Sucre Department, Colombia, between the coordinates W75° W76° and N9° N10° (Fig. 1). This water body, which is part of the Sanguare Civil Society Nature Reserve (598 ha), is the result of the isolation of an ancient coastal lagoon, a process that began approximately fifty years ago. This transformation has led to the emergence of a limnetic aquatic environment, which in turn has favored the colonization of freshwater species and the subsequent disappearance of marine species [19,20].

The wetland, which covers an area of 36 hectares and has a perimeter of 4.6 km, is situated between 0 and 3 meters above sea level. The topography of the area is characterized by Pleistocene soils from the Magdalena formation and alluvial sediments [19,20]. Seismic studies have identified diapiric submarine structures that have been colonized by reefs in the area [21].

The climate of the region is characterized by an annual precipitation of 1000 mm, a mean temperature of 27°C, and a bimodal rainfall regime, with dry periods from December to April and from July to September, and rainy periods from April to May and from October to November [22,23]. The region is also subject to the influence of trade winds, which contribute an average wind speed of 3.3 meters per second.

2.2 Sampling stations and periods

Two sampling campaigns were conducted in February and December of 2024. These periods correspond to the high water (February) and low water (December) seasons of the system. Within these campaigns, 10 sampling points were selected using the Random Point tool of ArcGIS Pro software to ensure independence between samples and avoid bias in the collected data. It is noteworthy that the same sites were sampled during both campaigns (Fig. 1).

2.3 Field measurements

Samples were collected at a depth of 10 centimeters at all ten sampling sites. At each site, a comprehensive assessment of the physical and chemical variables was conducted. In situ measurements were performed using WTW 2FD47D and Hach HQ40D multiparametric equipment, both of which had been previously calibrated. Additionally, a HACH 2100Q turbidimeter was utilized for turbidity measurement and a 20-centimeter Secchi disk was employed to estimate water

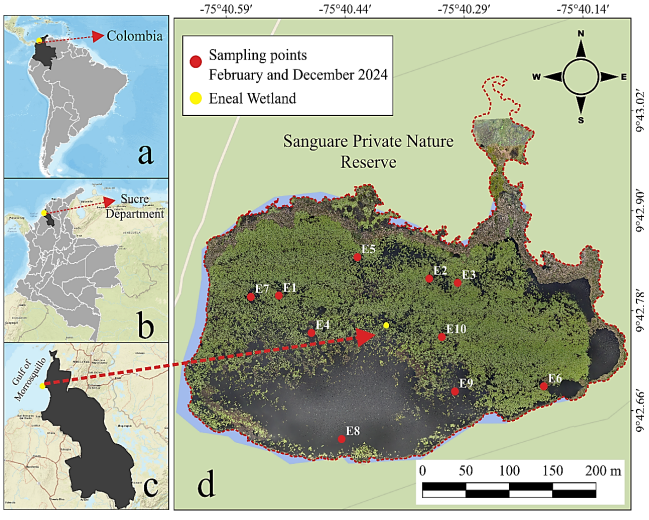

Figure 1. Study Area
Source: Own elaboration

Figure 2. *in situ* measurement of variables.
Source: Own elaboration

transparency. Samples intended for laboratory analysis were stored in sterilized bottles and preserved in thermal coolers at temperatures between 0 and 4°C until processing at the University of Antioquia laboratories (Fig 2).

Amber glass bottles with a capacity of 150 milliliters were utilized for the storage of DOC and TOC samples. For bicarbonates (HCO_3^-), carbonates (CO_3^{2-}), and sulfates (SO_4^{2-}), 250-ml HDPE bottles were utilized. The containers used for nutrients (NO_3^-, NO_2^-, NH_4^+ and PO_4^{3-}) were also 250 ml HDPE bottles. Finally, samples of chlorophyll-a were collected in 1000 ml amber plastic bottles.

Table 1 details the analyzed variables, differentiating those measured in situ from those determined in the laboratory, along with the equipment used and the methodologies applied.

Table 1.
Variables analyzed in this study.

Variable	Unit	Equipment	Methodology
Environmental Variables			
Ambient temperature	°C	Thermometer / meteorological station	IDEAM data
Precipitation	mm/month	Meteorological station	IDEAM data
Physical Variables			
Water temperature	°C	Multiparameter HQ40d	*In situ*
Turbidity	NTU	Turbidimeter Hach 2100Q	*In situ*
Transparency	m	Secchi disk	*In situ*
Water level	m	Limnimeter	*In situ*
Chemical Variables			
pH	pH units	Multiparameter WTW	*In situ*
Conductivity	µS/cm	Multiparameter WTW	*In situ*
Dissolved oxygen	mgO_2/L	Multiparameter WTW	*In situ*
Redox potential	mV	Multiparameter HQ40d	*In situ*
Chlorophyll-a	µg/L	Spectrophotometry	Laboratory
Ammonium (NH_4^+)	$mgNH_4^+/L$	Photometer	*In situ*
Nitrite (NO_2^-)	$mgNO_2/L$	Photometer	*In situ*
Nitrate (NO_3^-)	$mgNO_3/L$	Photometer	*In situ*
Phosphate (PO_4^{3-})	$mgPO_4^{3-}/L$	Photometer	*In situ*
Sulfate (SO_4^{2-})	$mgSO_4/L$	Ion chromatography (SM 4110-B)	Laboratory
Bicarbonate (HCO_3^-)	$mgCaCO_3/L$	Titrimetric (SM 2320-B)	Laboratory
Carbonate (CO_3^{2-})	$mgCaCO_3/L$	Titrimetric (SM 2320-B)	Laboratory
Dissolved organic carbon (DOC)	mgDOC/L	SM 5310 B, Ed. 23, 2017	Laboratory
Total organic carbon (TOC)	mgTOC/L	ASTM D7573-18 ae1	Laboratory

Source: Own elaboration

2.4 Laboratory analysis

The determination of DOC and TOC was conducted at the Pollution Diagnostic Laboratory (GDECON) of the University of Antioquia in accordance with standardized protocols outlined in the Standard Methods for the Examination of Water and Wastewater [24]. The determination of bicarbonates (HCO_3^-), carbonates (CO_3^{2-}), and sulfates (SO_4^{2-}) was conducted at the Environmental Studies Laboratory (LEA) of the aforementioned university. These determinations were made using titrimetric techniques and ion chromatography. Finally, the concentration of chlorophyll-a was analyzed at the Sanitary Hydrobiology Laboratory of the University of Antioquia, following the spectrophotometric methodology proposed by Aguirre 2013 [25].

The determination of nutrients (NO_3^-, NO_2^-, NH_4^+ and PO_4^{3-}) was carried out at the Sanitary Hydrobiology Laboratory of the University of Antioquia. For this, samples were initially filtered through 0.45 µm Whatman GF/F glass fiber filters and analyzed using the Visocolor colorimetric kit, with readings performed on a PF-12 portable photometer.

2.5 Statistical analysis

Statistical analysis was conducted using R 4.4.3 software [26]. Initially, variables with observations below the quantification limit or, alternatively, those with more than 20% observations below the quantification limit, were excluded from the analysis. Subsequently, a descriptive analysis was performed on the remaining variables, calculating measures of central tendency (mean, median) and dispersion (standard deviation, interquartile range). Additionally, box plots were constructed to visualize and compare the variation of these variables during the evaluated periods.

For the multivariate analysis, a correlation matrix was initially constructed using Spearman's coefficient, given that many variables did not meet the normality assumption. This approach facilitated the identification of significant associations between DOC and limnological variables. Subsequently, variables with correlation coefficients greater than 0.6 or less than -0.6, and with a coefficient of variation exceeding 20%, were selected. Finally, with the variables that met both criteria, a principal component analysis (PCA) was performed with the objective of reducing the dimensionality of the data and analyzing their underlying structure.

3 Results

3.1 Water level

The water level of the wetland, measured monthly between February and December 2024, was linked to the bimodal rainfall regime of the region. The minimum level was recorded in April (1.40 m), while the maximum level was reached in December (3.10 m). Additionally, it was observed that the wetland's response to the increase in water level was delayed with respect to the maximum peak of precipitation recorded in October, as evidenced in Figure 3a.

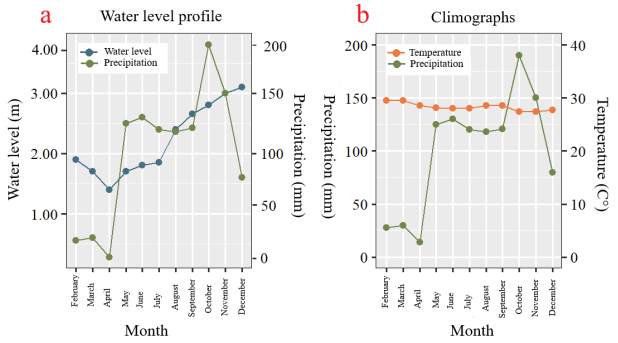

Figure 3. Water level profile and climograph for the year 2024.
Source: Own elaboration

On the other hand, the climograph showed characteristic ambient temperature behavior for the region, where temperatures remained relatively high and constant throughout the year. Values fluctuated within a narrow range between approximately 28°C and 32°C, without presenting significant seasonal variations. It was observed that the warmest months corresponded to the January-February period, with a slight decrease during the intermediate months and a subtle increase towards September-October (Fig. 3b).

Table 2.
Summary statistics of the analyzed variables.

Variable	DOC	COT	HCO_3^-	pH	E.C	ORP	Turb	DO	PO_4^{3-}	Temp	Chl-a
February (n=8)											
Mean	12.77	14.43	101.48	7.22	850.75	195.36	6.91	3.85	0.26	31.54	0.54
Median	12.78	14.46	101.42	7.17	852	201.15	6.69	4.03	0.2	32	0.6
SD	0.29	0.52	0.67	0.15	4.40	52.22	0.69	1.55	0.11	1.37	0.29
Max.	13.31	15.39	102.42	7.42	855	266.8	7.79	5.52	0.5	32.9	1.04
Min.	12.3	13.6	100.7	7.02	843	128.3	6.18	1.56	0.2	29.3	0.15
December (n=10)											
Mean	11.81	12.72	116.29	6.87	443.1	481.65	3.98	3.02	0.54	32.59	1.48
Median	11.81	12.86	116.42	6.91	438	546.5	3.81	3.1	0.5	32.6	1.22
SD	0.26	0.37	1.46	0.13	10.76	222.47	0.6	1.45	0.16	0.86	0.46
Max.	12.19	13.09	118.39	7.02	468	748	4.79	4.87	0.8	34.5	2.38
Min.	11.45	12.15	113.84	6.53	437	160.6	3.27	1.07	0.3	31.4	1.19

Abbreviation: SD = Standard Deviation; E.C = Electrical Conductivity (µS/cm); Turb. = Turbidity;DO = Dissolved Oxygen; Temp. = Temperature; Chl-a = Chlorophyll-a;PO3−4 = Phosphates.
Source: Own elaboration

3.2 Physical and chemical variables

Table 2 presents a summary of the descriptive statistics for variables that did not show values below the quantification limit during the months of February and December 2024. It is worth noting that, for February, only eight observations were analyzed, as two of the DOC data points were identified as outliers. The decision was made to eliminate all observations from this sampling point. The reason for these atypical values is that, when navigating through the wetland, sediment solids were resuspended, which affected the sample taken. In contrast, during the December sampling, environmental conditions were calmer and no sediment resuspension occurred, resulting in no outliers for that month.

DOC showed a decreasing trend between sampling periods. In February, a mean of 12.77 mg/L was recorded (range: 12.30-13.31 mg/L, SD=0.29), while in December it decreased to 11.81 mg/L (range: 11.45-12.19 mg/L, SD=0.26). TOC followed a similar pattern, reducing from 14.43 mg/L in February (SD=0.52) to 12.72 mg/L in December (SD=0.37), with less variability in the latter period (Fig. 4a and 4b).

Throughout the evaluated period, average concentrations were 12.24 mg/L for DOC and 13.48 mg/L for TOC, with low standard deviations (DOC: 0.56; TOC: 0.97). For DOC, 25% of the data were below 11.80 mg/L and 75% below 12.73 mg/L, while for TOC these percentiles were 12.80 mg/L and 14.36 mg/L, respectively (Fig. 4a and 4b).

On the other hand, bicarbonates (HCO_3^-) showed behavior opposite to that of organic and total carbon species, registering an increase in December. The lowest concentrations were observed in February, with a mean of 101.48 mg $CaCO_3$/L and an SD of 0.67, while in December they increased to reach a mean of 116.29 mg $CaCO_3$/L and a standard deviation of 1.46 (Fig. 4c). The mean bicarbonate concentration in the system was 109.71 mg $CaCO_3$/L with an overall SD of 7.66.

Regarding carbonates (CO_3^{2-}), these remained at very low levels during both sampling periods, recording values below the detection limit (< 1.00 mg $CaCO_3$/L).

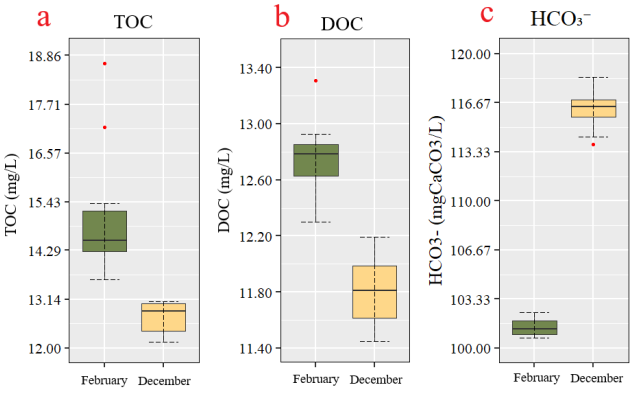

Figure 4. Carbon species.
Source: Own elaboration

Electrical conductivity and oxidation-reduction potential (ORP) showed contrasting changes between both sampling periods. In February, the average electrical conductivity was 850.75 µS/cm, with an SD of 4.40. Meanwhile, in December, conductivity was reduced by almost half, recording a mean of 443.10 µS/cm, accompanied by an increase in data dispersion (SD = 10.76). On the other hand, ORP showed inverse behavior: in February, values were significantly lower, with a mean of 195.36 mV and relatively low variability (SD = 52.22). In December, ORP increased considerably, reaching an average of 481.65 mV, with a range oscillating between 160.60 mV and 748.00 mV, reflecting greater redox variability in December (SD = 222.47) (Fig 5a and 5b).

Water temperature and dissolved oxygen levels presented slight variations between both sampling periods. In February, water temperature ranged between 29.30°C and 32.90°C with a mean of 31.54°C and an SD of 1.37. This compared with December, when the mean rose to 32.59°C and the SD decreased to 0.86. Dissolved oxygen, meanwhile, exhibited opposite behavior: in February, the average value was 3.85 mg/L, with an SD of 1.55, while in December it decreased to 3.02 mg/L, with a slight reduction in variability (SD = 1.45). Overall, the system has average water temperatures of 32.12°C and dissolved oxygen levels of 3.39 mg/L. (Fig. 5c and 5d)

The turbidity of the system showed a decrease between February and December, consistent with transparency levels and total suspended solids (TSS), the latter measured only in December. In February, average turbidity was 6.91 NTU, with a standard deviation of 0.694. During December, these values decreased, reaching a mean of 3.98 NTU (SD = 0.60). In this same period, water transparency varied between 0.60 m and 0.75 m, while TSS remained between <5 mg/L and 15 mg/L. (Fig. 5e)

The pH showed a slight trend toward more alkaline values in February and more acidic in December, remaining near neutrality in both periods. In February, values ranged between 7.02 pH units and 7.42 pH units, with a mean of 7.22 pH units and a standard deviation of 0.15. In December, however, values were more acidic, with an average of 6.87 and an SD of 0.13 (Fig. 5f).

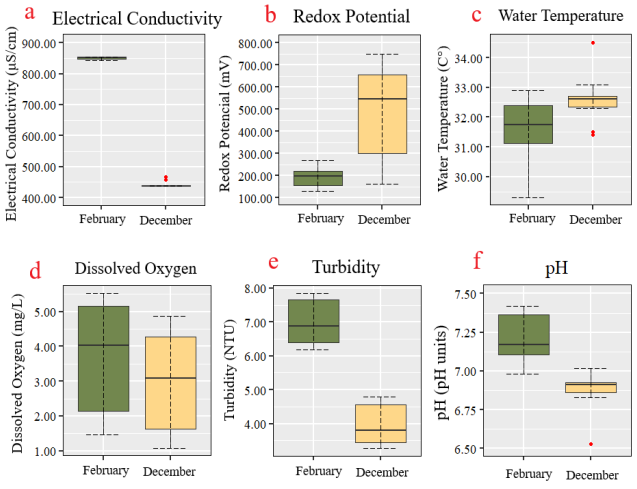

Figure 5. Physical and chemical variables.
Source: Own elaboration

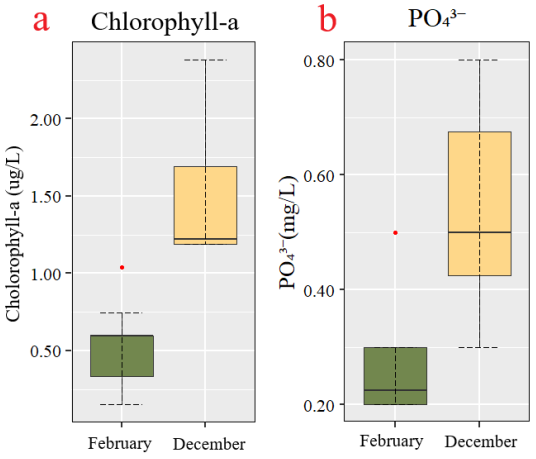

Figure 6. Chlorophyll and phosphates.
Source: Own elaboration

The concentration of chlorophyll-a, an indicator of primary biomass, increased from February to December. In February, 25% of the data was below 0.33 µg/L and 75% below 0.59 µg/L, with a mean of 0.54 µg/L. By December, the average rose to 1.48 µg/L (SD = 0.46) (Fig. 6a).

Phosphorus (PO_4^{3-}) oscillated between 0.20 and 0.80 mg/L, with an average of 0.40 mg/L. In February, the mean was 0.26 mg/L (SD = 0.11), with relatively homogeneous variation among sampling stations. In December, the concentration nearly doubled (0.54 mg/L, SD = 0.16), with maximum values at E4 and E5 (0.7-0.8 mg/L respectively) and minimums at E1, E2, E7, and E9 (0.2 mg/L) (Fig. 6b).

Regarding nitrogenous species, these exhibited different patterns of seasonal variation. For example, in February, nitrate (NO_3^-) concentrations ranged between 1.1 and 1.9 mg/L with a mean of 1.36 mg/L and SD of 0.21. Meanwhile, in December, all measurements remained below the detection limit (<1.0 mg/L). On the other hand, nitrites (NO_2^-) presented a mean of 0.012 mg/L and SD = 0.004 in February, and records for December were below the detection limit (<0.02 mg/L).

Ammonium (NH_4^+), for its part, showed a decrease between both periods. In February, average values were 0.79 mg/L (SD = 0.16), with some stations recording concentrations below the detection limit (< 0.40 mg/L). In December, all stations recorded levels below 0.5 mg/L.

3.3 Correlation matrix

After completing the descriptive analysis, a correlation analysis was conducted with all variables, except those that presented values below the quantification limit (QL) or, failing that, more than 30% of the data had records below the QL. Of these selected variables, more than 30% did not follow a normal distribution, so the Spearman coefficient was chosen to evaluate the degree of association between these variables.

Fig. 7 shows the results obtained from evaluating the degree of relationship between the different variables and

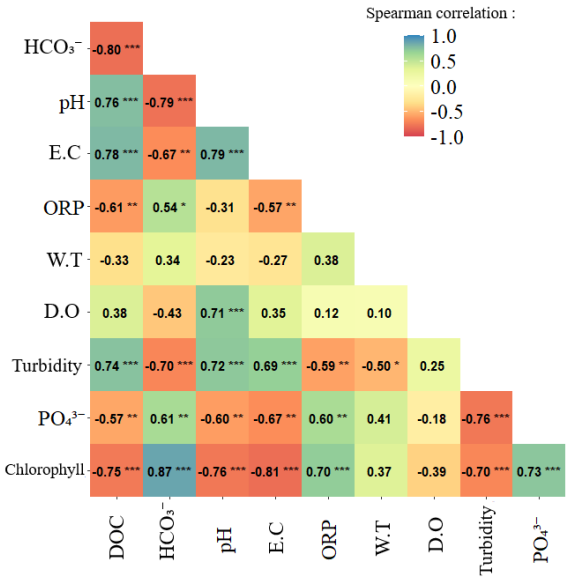

Note: The significance of the correlation is indicated by an asterisk (*) next to each coefficient: ∗ $p < 0.05$; ∗∗ $p < 0.01$; ∗∗∗ $p < 0.001$.
Figure 7. Spearman correlation matrix.
Source: Own elaboration

their statistical significance. First, a strong negative association is observed between DOC and bicarbonate concentrations (HCO_3^-), with a correlation coefficient of -0.80 ($p < 0.001$), indicating that as bicarbonate levels increase, dissolved organic carbon concentrations tend to decrease.

pH showed a positive and significant correlation with DOC ($r = 0.76$, $p < 0.001$), suggesting that higher pH values are associated with higher DOC concentrations. Similarly, electrical conductivity showed a strong positive correlation with DOC ($r = 0.78$, $p < 0.001$), suggesting that waters with higher dissolved solute content present higher levels of dissolved organic carbon.

Turbidity also showed a strong positive correlation with DOC ($r = 0.74$, $p < 0.001$), implying that higher levels of suspended particles in the water are closely related to an increase in dissolved organic carbon concentrations.

On the other hand, oxidation-reduction potential (ORP) presented a moderate negative correlation with DOC ($r = -0.61$, $p < 0.01$), implying that more reducing conditions, characterized by low ORP values, are associated with an increase in dissolved organic carbon concentrations. Likewise, phosphates (PO_4^{3-}) showed a moderate negative correlation with DOC ($r = -0.57$, $p < 0.05$). This result suggests that an increase in phosphate concentrations is associated with a reduction in dissolved organic carbon levels. Finally, chlorophyll-a presented a strong negative correlation with DOC ($r = -0.57$, $p < 0.05$), indicating that higher chlorophyll concentrations, linked to photosynthetic activity and algal biomass, are related to lower dissolved organic carbon concentrations.

Regarding water temperature ($r = -0.33$) and dissolved oxygen ($r = 0.38$), these did not show significant correlations with DOC, indicating that a clear relationship cannot be established between both variables and DOC in this analysis.

Table 3.
Spearman correlation coefficients and coefficients of variation (CV) associated with COD.

Variable	Spearman	CV (%)
HCO_3^-	-0.8	7.08
pH	0.76	3.19
E.C.	0.78	32.3
ORP	-0.61	63.9
Water Temp	-0.33	3.64
DO	0.38	45.7
Turbidity	0.74	30.4
PO_4^{3-}	-0.57	47.1
Chlorophyll-*a*	-0.75	60.1

Source: Own elaboration

3.4 Principal component analysis

Table 3 presents the Spearman coefficient and coefficient of variation for each of the evaluated variables. These results show which variables meet the established criteria. In particular, the variables that satisfy these criteria are electrical conductivity (EC), oxidation-reduction potential (ORP), turbidity, and chlorophyll-a.

The PCA was performed with the selected variables. This identified a dimensional structure in the variation of the limnochemical variables of El Eneal wetland. The eigenvalues and cumulative variance showed that the first two principal components explained 88.55% of the total variability of the data. The first principal component (PC1) captured 77.59% of the variability, while the second component (PC2) added an additional 10.96%.

PC1 was primarily defined by electrical conductivity (EC), which showed a contribution of 23.34%, followed by turbidity, with a contribution of 21.49%, and chlorophyll, with 20.45%. DOC also contributed slightly to this component, with 17.21%, while ORP showed a similar contribution, with 17.52%. This component captures most of the variability in the data and represents a combination of all variables, with greater weight on EC, turbidity, and chlorophyll-a.

On the other hand, PC2 was marked by a high contribution from ORP, which explained 40.98% of the variance in this component, followed by DOC, with a contribution of 31.42%. Chlorophyll-a also contributed, albeit to a lesser extent, with 15.86%. This component highlights the relationship between ORP and DOC, suggesting a significant association between these two variables.

Additionally, $\cos^2$ values (quality of representation of variables in the components) indicate that electrical conductivity (EC) and turbidity are well represented in PC1, with values of 0.95 and 0.91, respectively. DOC also showed moderate representation in PC1, with a $\cos^2$ value of 0.67, and a positive correlation of 0.82 with this component. On the other hand, in PC2, DOC showed a correlation of 0.42, indicating a weaker but still significant relationship with this component. ORP, for its part, showed high representation in PC2, with a $\cos^2$ value of 0.68 and a correlation of 0.47, highlighting its importance in the structure of the second component.

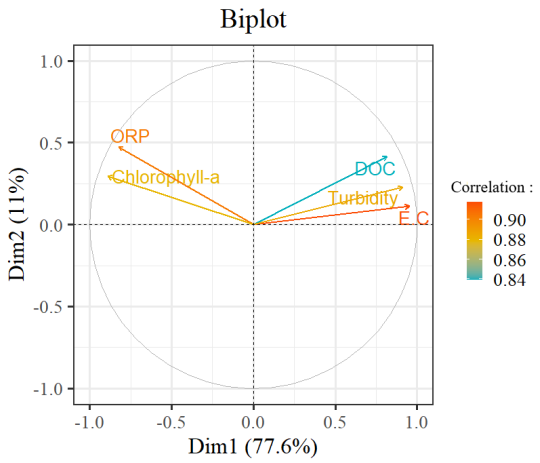

Figure 8. Biplot of Principal Component Analysis.
Source: Own elaboration

The graphical representation of the biplot (Figure 8) allowed visualization of the correlations between the limnochemical variables studied. DOC showed a strong positive correlation with electrical conductivity (EC), evidenced by the proximity and similar orientation of their vectors in the biplot. Additionally, a moderate positive correlation was observed with turbidity, in the angle of their vectors. On the other hand, DOC presented a moderate negative correlation with redox potential (ORP) and chlorophyll, indicated by the opposite position of their vectors in the graph.

Regarding the component equations, the first principal component (PC1) is dominated by positive contributions from electrical conductivity (EC), turbidity, and DOC, with loadings of 0.48, 0.46, and 0.41, respectively. On the other hand, chlorophyll-a and ORP show significant negative contributions, with loadings of -0.47 and -0.38, respectively, indicating an inverse relationship with this component (eq 1).

$$CP_1 = 0.41DOC - 0.48E.C. - 0.41ORP - 0.46Turbidity - 0.40\ Chl\text{-}a \quad (1)$$

The second principal component (PC2) is mainly influenced by ORP, which has a loading of 0.64, highlighting its central role in this component. DOC and turbidity also contribute, albeit to a lesser extent, with loadings of 0.56 and 0.30, respectively. Chlorophyll-*a* and electrical conductivity (EC) have contributions of 0.39 and 0.15, suggesting that this component is more related to redox processes in the system (eq 2).

$$CP_2 = 0.56DOC - 0.15E.C. - 0.64ORP - 0.30Turbidity - 0.3\ Chl\text{-}a \quad (2)$$

4 Discussion

4.1 Water level

The results obtained from the principal component analysis indicate that the dynamics of DOC in El Eneal wetland are primarily influenced by the variables that dominate the first component (PC1), which explains 77.59% of the data variability. Despite DOC having a strong contribution to the variance of PC2, according to Kaiser's criterion, PC1 is the most relevant because it presents an eigenvalue greater than 1, while PC2 has a lower eigenvalue, suggesting that the first component should be the primary focus of analysis [27].

Within PC1, electrical conductivity emerged as the most influential variable, with a contribution of 23.34%. Its decreasing trend as water level increased suggests a dilution process in this endorheic system, a phenomenon previously documented by Ríos et al. (2008; 2009) [19,20], who noted how hydrological increase dilutes dissolved solutes, altering multiple physicochemical parameters.

This dilution process not only affects conductivity but also explains the synchronous behavior of DOC, evidenced by its strong correlation ($r = 0.78$, $p < 0.001$) and significant contribution (17.10%) to the variance of PC1. It is essential to highlight that this correlation does not indicate a direct causal relationship between electrical conductivity and DOC, but rather that both variables are responding independently, yet similarly, to the same factor: the increase in water volume that causes the simultaneous dilution of both parameters [9,12].

The strong positive correlation between turbidity and DOC ($r = 0.74$, $p < 0.001$) reinforces this interpretation, as when DOC is diluted during periods of higher water levels, its concentration decreases and, consequently, so does the water color. This occurs because DOC, particularly in the form of humic and fulvic substances, imparts dark hues to the water. During December, higher water levels notably improved transparency, as demonstrated by the low values of suspended solids (< 5 mg/L - 10 mg/L) and the consequent reduction in both turbidity and transparency.

4.2 DOC Mineralization

In addition to the dilution effect, our results point toward a possible increase in DOC mineralization during periods of higher water levels. This hypothesis is based on the significant inverse correlation between DOC and ORP ($r = -0.61$, $p < 0.001$). The increase in water level in December, along with the greater presence of vegetation, appears to have generated more oxidative conditions that favored the microbial decomposition of DOC and the consequent release of CO_2 [28,29].

This interpretation is reinforced by the inverse correlation between DOC and bicarbonates ($r = -0.80$, $p < 0.001$). Although the latter were not included in the PCA due to their low coefficient of variation (<20%), their increase during periods of higher water levels suggests that the CO_2 released during DOC decomposition is transformed into bicarbonates. This transformation process aligns with previous research on organic matter mineralization in similar aquatic systems [30,31].

However, this hypothesis should be approached with caution, as the formation of bicarbonates could also be influenced by other factors, such as the near-neutral pH (6.7-7.2) that characterizes the El Eneal wetland. These conditions allow the CO_2 released from DOC degradation to rapidly

transform into bicarbonates (HCO_3^-), which would explain the absence of carbonates (CO_3^{2-}) and the predominance of the bicarbonate form in the system [30,31].

4.3 Biological processes

The biological processes in the system appear to be closely conditioned by the concentration of DOC. In the principal component analysis, chlorophyll-a showed a high contribution to the first component (20.45%) and a significant negative correlation with DOC ($r = -0.75$, $p < 0.001$), suggesting that a decrease in DOC concentration associated with dilution processes favors phytoplankton growth. This effect is reinforced by the inverse relationship between chlorophyll-a and turbidity, as the lower presence of suspended particles allows greater light penetration and, consequently, improved photosynthetic activity, as also noted by Ríos et al. [19,20].

Furthermore, Jackson and Hecky (1980) [33] highlighted that DOC can form complexes with essential trace elements such as iron, reducing their bioavailability and limiting phytoplankton metabolism. Similarly, previous studies [3,16] have reported that DOC can bind to key nutrients like phosphorus and nitrogen, decreasing their availability to photosynthetic organisms.

Additionally, various authors [34-36] have indicated that, at high concentrations, DOC acts as an absorbent of photosynthetically active radiation (PAR), significantly reducing light penetration in the water column. This light limitation directly affects photosynthesis and, consequently, phytoplankton development.

Collectively, these mechanisms could explain the low productivity recorded in the system (25–27 mgC/h/m² in February and December respectively) by Macías et al. 2024 [37], a condition that, as documented by Ríos et al. [19,20], has been persistent in the wetland, which is classified as oligoproductive. For example, high DOC concentrations darken the water, reducing light penetration and limiting photosynthetic activity, which in turn constrains phytoplankton growth. Therefore, DOC dynamics emerges as a regulating factor of key ecological processes, although further experimental studies are needed to validate these hypotheses.

4.4 Nutrients

On the other hand, nutrient dynamics did not show significant relationships with DOC, except for phosphorus, which presented a significant inverse relationship ($r = -0.75$, $p < 0.001$). This relationship has been interpreted by various authors as a consequence of DOC's ability to bind to phosphorus compounds, forming stable associations that limit its availability in the aquatic environment. This interaction is particularly relevant in systems where DOC concentrations are high, as this compound acts as a "sink" for nutrients, reducing the bioavailable fraction for biological processes. In this case, the decrease in DOC in December could have facilitated the release of phosphorus into the water column, contributing to the increase in its concentration during this period [3,16].

Although nitrogen species did not show a significant correlation with DOC, this could be influenced by limitations in the detection of these variables. Many of the measurements were below the quantification limit, making it difficult to identify possible relationships. This aspect highlights the need to employ analytical methods with lower quantification limits for a more precise assessment of the interaction between DOC and nitrogen forms. In previous studies where DOC has been the response variable, associations with nitrogen species have been found, suggesting that this relationship could exist but may not have been detected in this case due to methodological restrictions.

4.5 Unrelated variables

No significant relationships were found between DOC and dissolved oxygen ($r = 0.38$) or water temperature ($r = -0.33$), variables that were also not prominent in the PCA. While these results suggest an absence of direct influence, scientific literature indicates that DOC can affect water temperature through infrared radiation absorption. Rüdiger et al. [38], Bonelli et al. [39], and Sahay et al. [40] have documented how chromophoric dissolved organic matter (CDOM) absorbs light, contributing to water warming and modulating thermal transfer. The lack of correlation observed may be attributed to methodological limitations of this preliminary study, including a reduced number of observations (only two periods) and potential measurement inaccuracies due to temperature effects on multiparametric equipment. Implementation of the Winkler method for dissolved oxygen determination could provide more accurate measurements and facilitate a more robust assessment of its relationship with DOC.

5 Conclusions and recommendations

This research determined that DOC influences the limnological characteristics of El Eneal wetland through dilution processes and optical alterations of water. During high water periods, the increase in water level dilutes DOC, electrical conductivity, and turbidity, generating synchronous behavior among these variables. This suggests that their correlations depend primarily on water volume rather than direct interactions. Additionally, an inverse correlation between DOC and bicarbonates was identified, suggesting a mineralization process during the water level increase phase. Similarly, an inverse relationship with phosphorus was observed, indicating possible adsorption mechanisms, likely associated with DOC's capacity to form organic complexes with this nutrient. On the other hand, no significant relationship was found between DOC and nitrogenous compounds. The negative correlation between DOC and chlorophyll-a suggests that DOC reduces light availability for phytoplankton due to absorption and scattering of solar radiation, directly affecting its productivity. This effect is supported by the decrease in primary productivity of this system. As a recommendation, it is proposed to expand the study with a greater number of samplings and include additional variables, such as trace metals, specific optical parameters (e.g., absorbance and

fluorescence of organic matter), and dissolved organic matter fractions (e.g., humic substances), in order to deepen understanding of DOC's role in the dynamics of this ecosystem.

Acknowledgements

The authors of this article thank the GeoLimna research group, the GIGA research group, the Environmental School of the Faculty of Engineering at the University of Antioquia, and the Sanguaré Natural Reserve for their invaluable support in the development of this work and the project "Morphometric and Hydrobiological Evolution of El EnealWetland." El EnealWetland is a strategic wetland for water supply due to the support in this research.

References

[1] Fork, M.L., Karlsson, J., and Sponseller, R.A., Dissolved organic matter regulates nutrient limitation and growth of benthic algae in northern lakes through interacting effects on nutrient and light availability. Limnology and Oceanography Letters, 5(6), pp. 417-424, 2020. DOI: https://doi.org/10.1002/lol2.10166.

[2] Horppila, J., Keskinen, S., Nurmesniemi, M., Nurminen, L., Pippingsköld, E., Rajala, S., Sainio, K., and Estlander, S., Factors behind the threshold-like changes in lake ecosystems along a water colour gradient: the effects of dissolved organic carbon and iron on euphotic depth, mixing depth and phytoplankton biomass. Freshwater Biology, 68(6), pp. 1031-1040, 2023. DOI: https://doi.org/10.1111/fwb.14083.

[3] Pagano, T., Bida, M., and Kenny, J., Trends in levels of allochthonous dissolved organic carbon in natural water: a review of potential mechanisms under a changing climate. Water, 6(10), pp. 2862-2897, 2014. DOI: https://doi.org/10.3390/w6102862.

[4] Stetler, J.T., Knoll, L.B., Driscoll, C.T., and Rose, K.C., Lake browning generates a spatiotemporal mismatch between dissolved organic carbon and limiting nutrients. Limnology and Oceanography Letters, 6(4), pp. 182-191, 2021. DOI: https://doi.org/10.1002/lol2.10194.

[5] Senar, O.E., Creed, I.F., and Trick, C.G., Lake browning may fuel phytoplankton biomass and trigger shifts in phytoplankton communities in temperate lakes. Aquatic Sciences, 83(2), art. 21, 2021. DOI: https://doi.org/10.1007/s00027-021-00780-0.

[6] Rodríguez-Cardona, B.M., Houle, D., Couture, S., Lapierre, J-F., and Del Giorgio, P.A., Long-term trends in carbon and color signal uneven browning and terrestrialization of northern lakes. Communications Earth and Environment, 4(1), art. 338, 2023. DOI: https://doi.org/10.1038/s43247-023-00999-9

[7] Meyer-Jacob, C., Michelutti, N., Paterson, A.M., Cumming, B.F., Keller, W., and Smol, J.P., The browning and re-browning of lakes: divergent lake-water organic carbon trends linked to acid deposition and climate change. Scientific Reports, 9(1), art. 16676, 2019. DOI: https://doi.org/10.1038/s41598-019-52912-0

[8] Yang, L., Zhang, S., Yin, L., and Zhang, B., Global occupation of wetland by artificial impervious surface area expansion and its impact on ecosystem service value for 2001–2018. Ecological Indicators, 142, art. 109307, 2022. DOI: https://doi.org/10.1016/j.ecolind.2022.109307

[9] Sobek, S., Tranvik, L.J., Prairie, Y.T., Kortelainen, P., and Cole, J.J., Patterns and regulation of dissolved organic carbon: an analysis of 7,500 widely distributed lakes. Limnology and Oceanography, 52(3), pp. 1208-1219, 2007. DOI: https://doi.org/10.4319/lo.2007.52.3.1208

[10] Tadeu, C.M.O., Brandão, L.P.M., Bezerra-Neto, J.F., Pujoni, D.G.F., and Barbosa, F.A.R., Photodegradation of autochthonous and allochthonous dissolved organic matter in a natural tropical lake. Limnologica, 87, art. 125846, 2021. DOI: https://doi.org/10.1016/j.limno.2020.125846

[11] Brandão, L.P.M., Brighenti, L.S., Staehr, P.A., Asmala, E., Massicotte, P., Tonetta, D., Barbosa, F.A.R., Pujoni, D., and Bezerra-Neto, J.F., Distinctive effects of allochthonous and autochthonous organic matter on CDOM spectra in a tropical lake. Biogeosciences, 15(9), pp. 2931-2943, 2018. DOI: https://doi.org/10.5194/bg-15-2931-2018

[12] Harvey, J.W., and McCormick, P.V., Groundwater's significance to changing hydrology, water chemistry, and biological communities of a floodplain ecosystem, Everglades, South Florida, USA. Hydrogeology Journal, 17(1), pp. 185-201, 2009. DOI: https://doi.org/10.1007/s10040-008-0379-x

[13] Junk, W.J., World wetlands classification: a new hierarchic hydro-ecological approach. Wetlands Ecology and Management, 32, pp. 975-1001, 2024. DOI: https://doi.org/10.1007/s11273-024-10010-7

[14] Olson, C.R., Solomon, C.T., and Jones, S.E., Shifting limitation of primary production: experimental support for a new model in lake ecosystems. Ecology Letters, 23(12), pp. 1800-1808, 2020. DOI: https://doi.org/10.1111/ele.13606

[15] Solomon, C.T., Jones, S.E., Weidel, B.C., Buffam, I., Fork, M.L., Karlsson, J., Larsen, S., Lennon, J.T., Read, J.S., Sadro, S., and Saros, J.E., Ecosystem consequences of changing inputs of terrestrial dissolved organic matter to lakes: current knowledge and future challenges. Ecosystems, 18(3), pp. 376-389, 2015. DOI: https://doi.org/10.1007/s10021-015-9848-y

[16] Kelly, P.T., Solomon, C.T., Zwart, J.A., and Jones, S.E., A framework for understanding variation in pelagic gross primary production of lake ecosystems. Ecosystems, 21(7), pp. 1364-1376, 2018. DOI: https://doi.org/10.1007/s10021-018-0226-4

[17] Lønborg, C., Carreira, C., Jickells, T., and Álvarez-Salgado, X.A., Impacts of Global Change on Ocean Dissolved Organic Carbon (DOC) Cycling. Frontiers in Marine Science, 7, art. 0466, 2020. DOI: https://doi.org/10.3389/fmars.2020.00466

[18] Kutser, T., Pierson, D.C., Kallio, K.Y., Reinart, A., and Sobek, S., Mapping Lake CDOM by satellite remote sensing. Remote Sensing of Environment, 94(4), pp. 535-540, 2005. DOI: https://doi.org/10.1016/j.rse.2004.11.009

[19] Ríos, E.L., Palacio, J.A., and Aguirre, N.J., Variabilidad fisicoquímica del agua en la ciénaga El Eneal, reserva natural Sanguaré municipio de San Onofre-Sucre, Colombia. Revista Facultad de Ingeniería Universidad de Antioquia, (46), pp. 39-45, 2008.

[20] Ríos, E.L., Palacio, J.A., and Aguirre, N.J., Primary productivity and humic substances in the swamp el eneal, San onofre Sucre-Colombia. Revista Facultad de Ingeniería Universidad de Antioquia, (47), pp. 67-72, 2009.

[21] Patiño, F., and Amaya, F., Estudio ecológico del Golfo de Morrosquillo, Universidad Nacional de Colombia, pp. 11-14, 1993.

[22] Mira, J.D., Urrego, L.E., and Monsalve, K., Determinantes naturales y antrópicos de la distribución, estructura y composición florística de los manglares de la reserva natural Sanguaré, Colombia. Revista de Biología Tropical, 67(4), pp. 810-824, 2019. DOI: http://dx.doi.org/10.15517/rbt.v67i4.30833

[23] Castaño, L., Estudio preliminar de la Ciénaga la Boquilla, Municipio de San Onofre, MSc. Thesis, Facultad de Ciencias Exactas y Naturales, Universidad de Antioquia, 1999.

[24] APHA., Standard methods for the examination of water and wastewater, 23rd ed., Washington D.C: American Public Health Association, 2017.

[25] Aguirre, N., Hidrobiología sanitaria. Ude@, Escuela Ambiental, Facultad de Ingeniería, Universidad de Antioquia, 202, 2013. ISBN 978-958-8790-55-8.

[26] R., Core, Team., R., A language and environment for statistical computing. R., Foundation for statistical computing, Vienna, Austria, [online], 2018. Available at: http://www.R-project.org/.

[27] Ďuriš, V., Bartkova, R., and Tirpáková, A., Principal component analysis and factor analysis for an Atanassov IF data set. Mathematics, 9(17), Art. 2067, 2021. DOI: https://doi.org/10.3390/math9172067

[28] Wetzel, R.G., Limnology: lake and river ecosystems, 1, Academic Press, 2001.

[29] Roldán-Pérez, G., and Ramírez-Restrepo, J.J., Fundamentos de limnología neotropical, 2022.

[30] Tranvik, L.J., Downing, J.A., Cotner, J.B., Loiselle, S.A., Striegl, R.G., Ballatore, T.J., Dillon, P., Finlay, K., Fortino, K., Knoll, L.B., Kortelainen, P.L., Kutser, T., Larsen, S., Laurion, I., Leech, D.M., McCallister, S.L., McKnight, D.M., Melack, J.M., Overholt, E., and Weyhenmeyer, G.A., Lagos y embalses como reguladores del ciclo del

carbono y del clima. Limnología y Oceanografía, [online]. 54(6), pp. 2298–2314, 2009. Available at: https://www.jstor.org/stable/20622833
[31] Reithmaier, G.M.S., Cabral, A., Akhand, A., et al., Química de carbonatos y secuestro de carbono impulsada por el afloramiento de carbono inorgánico de manglares y marismas. Nat Commun, 14, art. 8196, 2023. DOI: https://doi.org/10.1038/s41467-023-44037-w
[32] Dubourg, P., North, R.L., Hunter, K., Vandergucht, D.M., Abirhire, O., Silsbe, G.M., and Hudson, J.J., Light and nutrient co-limitation of phytoplankton communities in a large reservoir: Lake Diefenbaker, Saskatchewan, Canada. Journal of Great Lakes Research, 41(2), pp. 129-143, 2015. DOI: https://doi.org/10.1016/j.jglr.2015.10.001
[33] Jackson, T.A., and Hecky, R.E., Depression of primary productivity by humic matter in lake and reservoir waters of the boreal forest zone. Canadian Journal of Fisheries and Aquatic Sciences, 37(12), pp. 2300-2317, 1980. DOI: https://doi.org/10.1139/f80-277
[34] Finstad, A.G., Helland, I.P., Ugedal, O., Hesthagen, T., and Hessen, D.O., Unimodal response of fish yield to dissolved organic carbon. Ecology Letters, 17(1), pp. 36-43, 2014. DOI: https://doi.org/10.1111/ele.12201
[35] Williamson, C., Overholt, E., Pilla, R., et al., Ecological consequences of long-term browning in lakes. Scientific Reports, 5, art. 18666, 2016. DOI: https://doi.org/10.1038/srep18666
[36] Sherbo, B.A., Tonin, J., Paterson, M.J., Hann, B.J., Kozak, J., and Higgins, S.N., The effects of terrestrial dissolved organic matter on phytoplankton biomass and productivity in boreal lakes. Freshwater Biology, 68(12), pp. 2109-2119, 2023. DOI: https://doi.org/10.1111/fwb.14178
[37] Maciás-Echeverri, L., and Aguirre, N.J., Caracterización del fitoplancton y zooplancton como bioindicadores de calidad del agua en la ciénaga del Eneal, Colombia. BSc. Thesis, Universidad de Antioquia, Medellín, 2024.
[38] Röttgers, R., Novak, M.G., and Belz, M., Measurement of light absorption by chromophoric dissolved organic matter using a type-II liquid capillary waveguide: assessment of an achievable accuracy. Applied Optics, 63, pp. 3811-3824, 2024. DOI: https://doi.org/10.1364/AO.516580
[39] Bonelli, A.G., Vantrepotte, V., Jorge, D.S.F., Demaria, J., Jamet, C., Dessailly, D., and Loisel, H., Colored dissolved organic matter absorption at global scale from ocean color radiometry observation: spatio-temporal variability and contribution to the absorption budget. Remote sensing of environment, 265, art. 112637, 2021. DOI: https://doi.org/10.1016/j.rse.2021.112637
[40] Sahay, A., Ali, S.M., Raman, M., Gupta, A., Motwani, G., Thakker, R., and Shanmugam, P., Empirically derived coloured dissolved organic matter absorption coefficient using in-situ and Sentinel 3/OLCI in coastal waters of India. International Journal of Remote Sensing, 43(4), pp. 1430-1450, 2022. DOI: https://doi.org/10.1080/01431161.2022.2040754

W.D. Guzman-López, received the BSc. Eng. in Environmental Engineering in 2020, from the Universidad de Antioquia, Colombia. Currently, he is a Master's student in Environmental Engineering and a part-time lecturer at the Faculty of Engineering, Universidad de Antioquia. His research focuses on water quality, wetland ecosystems, and dissolved organic carbon (DOC) dynamics.
ORCID: 0009-0007-4494-1231

L.C. Giraldo, received the BSc. and MSc. in Environmental Engineering, and the PhD in Engineering, all of them from the Universidad de Antioquia, Colombia. She is a full-time faculty member at the Faculty of Engineering, Universidad de Antioquia. Her research interests include water treatment, aquatic ecology, and environmental management.
ORCID: 0000-0002-1801-6612

F.V. Macías, received the BSc. and MSc. in Environmental Engineering from the Universidad de Antioquia, Colombia, and the PhD in Geography from Heinrich-Heine-Universität Düsseldorf, Düsseldorf, Germany. He is a retired faculty member of the Faculty of Engineering, Universidad de Antioquia. His research experience includes water quality, environmental modeling, and ecological restoration.
ORCID: 0000-0001-6348-6405

N. Aguirre, received the BSc. and MSc. in Biology from the Universidad de Antioquia, Colombia. PhD in Natural Resources, Universität Giessen, Germany. He is a full-time faculty member at the Faculty of Engineering, Universidad de Antioquia. His research focuses on aquatic ecosystems, water quality, and environmental engineering.
ORCID: 0000-0002-0847-7335

DYNA
http://dyna.medellin.unal.edu.co/

UNIVERSIDAD NACIONAL DE COLOMBIA

Safety risk assessment in a drinking water treatment plant using the NTP 330 method

María Belén Vinces-Obando[a], Luis David Balarezo-Saltos[b*], Carlos Alfredo Salas-Macías[a], Fernando Ramón Isea-León[b], Rodolfo Patricio Panta-Vélez[b] & Dayana Elizabeth Briones-Bermúdez[c]

[a] *Departamento de Ciencias Agronómicas, Facultad de Ingeniería Agroambientales, Universidad Técnica de Manabí, Santa Ana, Ecuador. maria.vinces@utm.edu.ec, carlos.salas@utm.edu.ec*
[b] *Departamento de Acuicultura, Pesca y Recursos Naturales Renovables, Facultad de Acuicultura y Ciencias del Mar, Universidad Técnica de Manabí, Bahía de Caráquez, Ecuador. luis.balarezo@utm.edu.ec, fernando.isea@utm.edu.ec, rodolfo.panta@utm.edu.ec*
[c] *Departamento de Laboratorio Clínico, Facultad de Ciencias de la Salud, Universidad Estatal del Sur de Manabí, Jipijapa, Ecuador. briones-dayana0165@unesum.edu.ec*

Received: June 25th, 2025. Received in revised form: November 14th, 2025. Accepted: November 21st, 2025.

Abstract
In Ecuador, the lack of attention to occupational safety in small and medium-sized enterprises, which constitute 98% of the total, has increased workplace accidents. To assess this situation, a Checklist based on the Guide of the National Institute for Occupational Safety and Health (INSHT) of the Ministry of Labor was applied. The methodology was then adapted to evaluate specific working conditions in SMEs and the NTP 330 method was used, which considers criteria such as efficiency, exposure, probability, and consequences to determine the risk level. Fifty-eight hazards were identified, including falls of people from different levels, falling objects due to collapse, and blows or cuts caused by tools, each with an incidence of 10%. The distribution area presented the highest number of risks (15), and the high-risk level predominated. The application of the method allowed for a comprehensive assessment, highlighting the urgent need for preventive measures.

Keywords: safety risks; risk assessment; drinking water treatment plant.

Evaluación de riesgos de seguridad en una planta de tratamiento de agua potable mediante el método NTP 330

Resumen
En Ecuador, la falta de atención a la seguridad laboral en las pequeñas y medianas empresas, que constituyen el 98 % del total, ha incrementado los accidentes laborales. Para evaluar esta situación, se aplicó una Lista de Verificación basada en la Guía del Instituto Nacional de Seguridad y Salud en el Trabajo (INSHT) del Ministerio de Trabajo. Luego, se adaptó la metodología para evaluar condiciones laborales específicas de PYMES y se utilizó el método NTP 330, que considera criterios como eficiencia, exposición, probabilidad y consecuencias para determinar el nivel de riesgo. Se identificaron 58 peligros, destacando la caída de personas a diferentes niveles, caída de objetos por derrumbe y golpes o cortes con herramientas, cada uno con una incidencia del 10 %. El área de distribución presentó el mayor número de riesgos (15) y predominó el nivel de riesgo alto. La aplicación del método permitió una evaluación integral, destacando la necesidad urgente de medidas preventivas.

Palabras clave: riesgos de seguridad; evaluación de riesgos; planta de tratamiento de agua potable.

1 Introduction

Since the 20th century, occupational safety has gained importance globally, driving the development of techniques and methods aimed at preventing occupational risks. However, many of these methodologies are not applied adequately, since risk level assessments are often inaccurate [1]. This situation has led to approximately 330 million occupational accidents being recorded worldwide towards the end of that century, of which 2.4 million

How to cite: Vinces-Obando, M.B., Balarezo-Saltos, L.D., Salas-Macías, C.A., Isea-León, F.R., Panta-Vélez, R.P. and Briones-Bermúdez, D.E., Safety risk assessment in a drinking water treatment plant using the NTP 330 method DYNA, (93)240, pp. 19-26, January - March, 2026.

resulted in fatalities [2,3]. Until 2016, the highest deaths or disability-adjusted life years per capita were recorded in Oceania, Southeast Asia and central sub-Saharan Africa [4].

Additionally, non-fatal occupational accidents are estimated to generate an economic burden equivalent to 4% of global GDP annually, reflecting their significant impact on the global economy. These figures are especially alarming in low- and middle-income countries, where informal sectors and high-risk industries, such as agriculture and mining, predominate, exacerbating occupational injuries and deaths due to limited implementation of preventive and occupational safety measures [5].

In Latin America and the Caribbean, efforts to establish effective preventive processes have increased. However, many institutions prioritize other aspects over occupational safety, which makes adequate risk management difficult [6]. Unlike developed countries, where preventive guarantees are a priority, greater vulnerability in work environments persists in the region [7].

In Ecuador, the lack of interest in occupational safety issues is evident, even though 98% of organizations are small businesses, where it would be feasible to implement specific risk controls. This lack of action has contributed to the increase in workplace accidents [8,9]. In addition, the absence of solid preventive policies and their lack of implementation have generated a constant exposure of workers to occupational risks, further weakening occupational safety in the country [10,11]. Likewise, occupational safety faces serious challenges, especially in strategic sectors where the risks associated with productive activities are high. Even though 98% of organizations are small businesses, there is a notable lack of interest in the implementation of preventive measures, which could facilitate a more specific control of occupational risks. This situation has led to an increase in unsafe working conditions and a gradual weakening of safety policies [8].

In this context, water treatment plants present a particularly challenging work environment, given that their operations involve complex processes and constant handling of specialized equipment and chemicals. These activities generate significant occupational risks that require rigorous management and adequate preventive measures [9]. However, limited application of safety policies and lack of access to training programs aggravate workers' exposure to accidents.

2 Materials and methods

2.1 Characterization of the plant under study

The water treatment plant under study (located at geographic coordinates x: 563,064.22 m, y: 988,1079.89 m), built at the beginning of the 21st century, was designed to meet the growing demand of a rapidly growing population, ensuring access to clean and safe water. With a production capacity of approximately 90,000 m³ per day, the plant operates continuously through a water treatment process that includes stages such as pretreatment, coagulation and flocculation, sedimentation, filtration, disinfection, and storage before distribution. This infrastructure, equipped with high-quality electromechanical components and supervised by a team of specialized operators and technicians, faces challenges such as variability in raw water quality due to extreme weather events, increased demand, and the impacts of climate change.

In response, treatment processes have been optimized and investments have been made in monitoring technologies to ensure its efficient operation. However, these operations entail significant occupational hazards associated with equipment handling, exposure to chemicals, and working in conditions that require constant attention. Assessing and managing these risks is critical to protecting the physical and mental integrity of the 33 workers involved in the various stages of the process. Therefore, implementing effective preventive measures not only contributes to employee safety but also to meeting quality and sustainability objectives in the supply of drinking water.

2.2 Risk identification

To identify occupational risks in the workplace, an observational study was previously carried out using a "Check-list", in which the risk factors were highlighted based on the considerations of the instrument of the "Guide of the National Institute for Safety and Hygiene at Work in Construction" [12].

Subsequently, the practical methodology for identifying working conditions in small and medium-sized companies of the INSHT [13] was used and adapted. Considering the accident risks (safety) detailed in table 1.

Table 1.
Most common forms of occupational risks (safety).

Cod.	Risk of accident
10	Person falls from a different level.
20	Fall of people at the same level.
30	Falling objects due to collapse or landslides.
40	Falling objects during handling.
50	Falling detached objects.
60	Stepping on objects.
70	Collisions with stationary objects.
80	Collisions with moving objects.
90	Bumps/cuts from objects or tools.
100	Projection of fragments or particles.
110	Entrapment by or between objects.
120	Entrapment due to overturning machines or vehicles.
130	Overexertion.
140	Exposure to extreme ambient temperatures.
150	Thermal contacts.
161	Direct electrical contacts.
162	Indirect electrical contacts.
170	Exposure to harmful or toxic substances.
180	Contact with caustic and/or corrosive substances.
190	Exposure to radiation.
200	Explosions.
211	Fires. Starting factors.
212	Fires. Spread.
213	Fires. Fighting methods.
214	Fires. Evacuation.
220	Accidents caused by living beings.
230	Vehicle collisions or hits.

Source: INSHT, 2000.

2.3 Risk assessment

The risk assessment was carried out based on the NTP 330 method [14,15], a methodology that differs from the others, because the weighting of the levels is not subject to the evaluator's subjectivity, for this purpose, the security risks are evaluated through the interaction of specific criteria or levels [16]. The method consists of determining the deficiency based on the level of exposure, which subsequently yields the corresponding probability, as illustrated in Fig. 1. From this probability, the consequence level can be established, and ultimately, the overall risk level is determined, as detailed below:

1) Deficiency level:
   - Very poor: Significant risk factors have been detected that make it highly possible for failures to occur. The set of preventive measures in place regarding risk is ineffective.
   - Deficient: A significant risk factor has been identified that needs to be corrected. The effectiveness of the set of preventive measures is significantly reduced.
   - Improvable: Minor risk factors have been detected. The effectiveness of the set of existing preventive measures with respect to risk is not significantly reduced.
2) Exposure level:
   - Continuous: If the worker is working for a long time.
   - Frequent: If the worker is there several times during his/her workday, although for short periods of time.
   - Occasional: If the worker is ever on duty during his/her workday and has a short period of time.
   - Sporadic: Irregularly.
3) Probability level:

   Where:
   - Very High: Poor situation with continued exposure or very poor situation with frequent exposure. Risk materialization usually occurs frequently.
   - High: Poor situation with frequent or occasional exposure or very poor situation with occasional or sporadic exposure. The risk may materialize several times in the working life cycle.
   - Average: Poor situation with sporadic exposure or improvable with continuous or frequent exposure. The risk may materialize once a year.
   - Low: Situation could be improved with occasional or sporadic exposure. The risk is not expected to materialize, although it may be conceivable.
4) Level of consequence:

   Based on the result of the probability level, the focus is on determining the level of consequence of the risk using Fig. 2.

NTP method 330		Exposure Level			
		Continue	Frequent	Occasional	Sporadic
Level of Deficiency	Very poor	Very high	Very high	High	High
	Deficient	Very high	High	High	Average
	Improvable	Average	Average	Low	Low

Figure 1. Probability level.
Source: INSHT, 2000.

NTP method 330		Probability			
		Very high	High	Average	Low
Consequence	Mortal	Serious and imminent	Serious and imminent	High	High
	Very serious	Serious and imminent	High	Half	Half
	Serious	High	Half	Half	Low
	Mild	Half	Half	Low	Tolerable.

Figure 2. Level of consequence.
Source: INSHT, 2000.

Where:
- Mortal: One or more dead.
- Very serious: Serious injuries that may be irreparable.
- Serious: Injuries with temporary work incapacity.
- Mild: Minor injuries that do not require hospitalization.

5) Determine the level of risk:

Based on the result obtained in figure 2, the action to be taken based on the level of risk of the worker's activity is considered:
- Serious and imminent: Stop the activity. Correct and check the effectiveness of the correction.
- High: Urgent correction and adoption of control measures.
- Half: Correction and adoption of control measures.
- Low: Improve if possible.
- Tolerable: Satisfactory situation.

2.4 Jobs descriptions

Table 2 outlines the working conditions associated with each job position across the organization, assessing the risk levels of five operational areas as detailed below:

Table 2.
Description of the areas of work under study.

Area	Description
Operator of the collection and mechanical roughing area	As this is the first process where raw water is captured, the operator has the task of frequently cleaning the bulky materials that are carried by the channel flow and that are trapped in the mechanical roughing. Subsequently, all the waste is transported by a conveyor belt to a container.
Rapid mix process operator	Before the chemicals are integrated into the treatment processes, operators are tasked with transporting the substances from a chemical storage warehouse using a forklift to a first mixing point, where they are conveyed via pipelines to the xiphoid tank and the agitator.
Operator of the decanted water filtration stage	The operator has the power to manually clean the decanters and filters every 15 days. These are also operated by control stations.
Distribution area operator	In this position, workers are in charge of controlling the operations and functionality of the pumps for the corresponding distribution of drinking water.
Laboratory area operator	The laboratory manager and his assistant are responsible for frequently measuring the corresponding parameters for controlling water quality processes.

Source: The authors.

3 Results

3.1 Risk identification

Based on the execution of the "Check List" and the practical methodology for identifying working conditions in small and medium-sized companies of the INSHT, table 3 details the total number of risks and safety risk factors that were determined in the work positions evaluated at the drinking water treatment plant.

Table 3.
Risk identification results.

Cod	Risks	Risk factors
10	Person falls from a different level	Lack of protective railings in water catchment areas.
		Use of stairs in poor condition.
		Railings surrounding the xiphoid tank in poor condition.
		Unstable railings around the decanters.
		Use of unstable railings.
		Lack of protection staircase.
20	Fall of people at the same level	Lack of Personal Protective Equipment for cleaning decanters.
		Wet floor.
		Slippery floor.
30	Falling objects due to collapse or landslides	Mechanical roughing in deterioration.
		Forklift with lack of maintenance
		Unstable stacked sacks.
		Lack of selective shelving
		Use of improvised structures for cleaning decanters.
		Use of a ladder with imperfections.
40	Falling objects during handling	Incorrect handling of the forklift.
50	Falling detached objects	Use of inappropriate tools for cleaning decanters.
		Lack of maintenance to railings and stairs.
60	Stepping on objects	Presence of objects in the mechanical grinding circulation routes.
		Presence of unnecessary materials on the decanter circulation paths.
		Presence of objects on the circulation routes of the distribution area.
70	Collisions with stationary objects	Lack of signage in the roughing area.
		Signs in poor condition during the rapid mixing process.
		Lack of signage in the distribution area.
		Slippery floor.
		Small workplace space.
80	Collisions with moving objects	Loss of control of the forklift.
90	Bumps/cuts from objects or tools	Lack of protective elements in mechanical grinding.
		Handling of rakes for bulky materials trapped in the grates.
		Handling obsolete tools.
		Lack of maintenance at the decanter control stations.
		Use of inappropriate materials.
		Poor labeling of some materials and substances.
100	Projection of fragments or particles	Conveyor belt without protective elements.
		Elements of obsolete checkpoints.
		Lack of protection in the pump area.
110		Handling of the conveyor belt.
		Lack of signage during the rapid mixing process.
	Entrapment by or between objects	Improvisation of tools for operator mobility on decanters.
120	Entrapment due to overturning machines or vehicles	Forklift trapped between bags.
130	Overexertion	Manual handling of some bags.
161	Direct electrical contacts	Electrical connection in the distribution area with lack of maintenance.
162	Indirect electrical contacts	Inadequate electrical system for mechanical roughing.
		Electrical system with lack of maintenance at the control stations.
		Electrocution due to the presence of water near the electrical connections of the pumps.
		Handling of electrical equipment.
170	Exposure to harmful or toxic substances	Lack of special masks.
		Frequent use of chemical reagents.
180	Contact with caustic and/or corrosive substances	Use of chemical substances for the analysis of water parameters.
200	Explosions	Alteration of pump operation.
		Use of flammable substances.
211	Fires. Starting factors	Contact of the electrical system with drinking water.
		Incorrect handling of electrical equipment.
		Incorrect handling of flammable substances.
212	Fires. Spread	Presence of drinking water near electrical systems.
214	Fires. Evacuation	Signs in poor condition.
220	Accidents caused by living beings	Bite or sting from an animal that is carried by the current into the catchment area.
230	Vehicle collisions or hits	Lack of pedestrian traffic routes in the area where the forklift operates.

Source: The authors.

Given the results obtained from the identification of risks in the water treatment plant, Fig. 3 shows the risks that had the greatest impact on the tasks performed by the workers. Where: falls of a person from different levels; falling objects due to collapse or landslides and blows/cuts from objects or tools, obtained a 10% higher frequency than the other risks.

3.2 Risk assessment

The assessment of safety risks at the drinking water treatment plant showed that the highest incidence of risks occurred in the distribution area, categorizing the risk levels into "serious and imminent", "high" and "medium", showing a total of 15 risk levels, as shown in Fig. 4.

Fig. 5 shows the general results of the safety risk assessment at the drinking water treatment plant, showing that the most representative level was "high" with 48.28% incidence, leading to the need for "urgent corrections and adoption of control measures". It is important to note that tolerable levels were not obtained in this investigation.

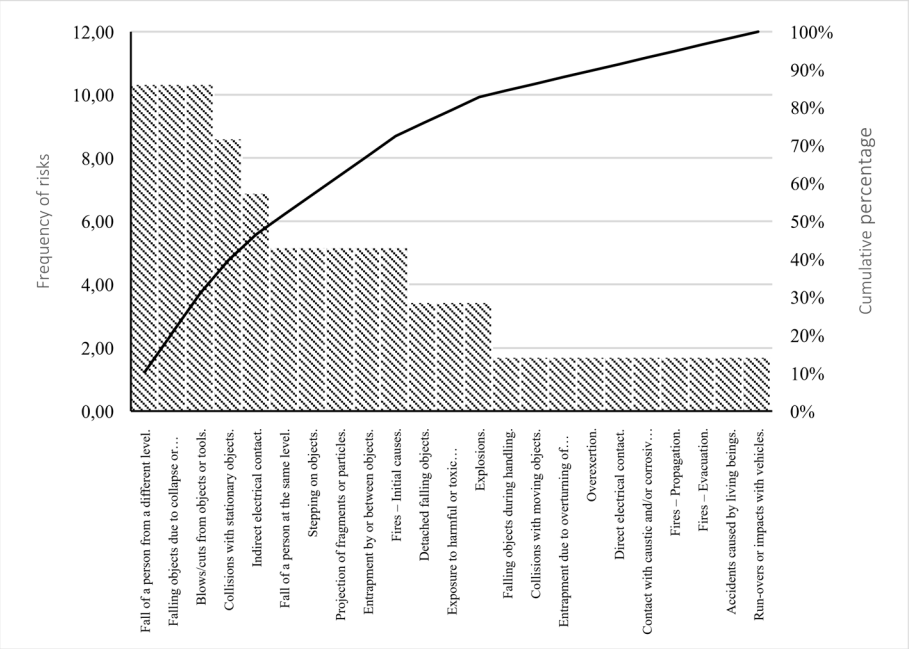

Figure 3. Results of the identification of safety risks at the drinking water treatment plant.
Source: The authors.

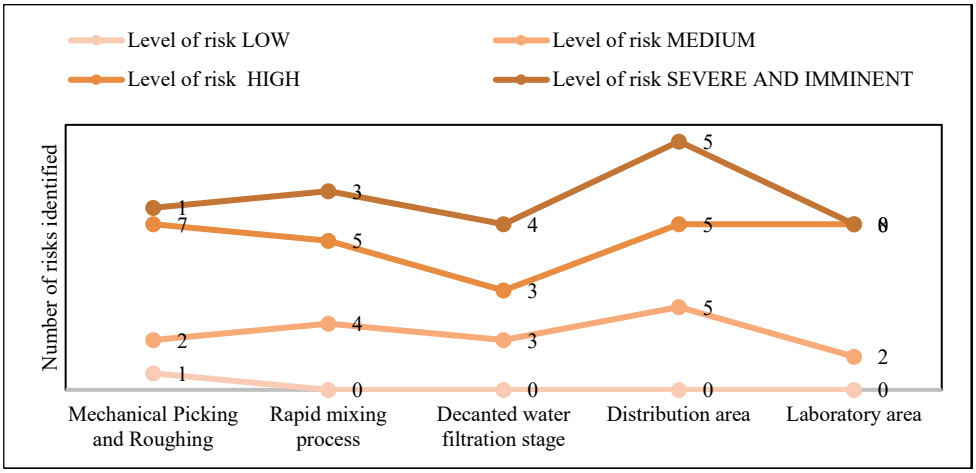

Figure 4. Results of the security risk levels in the evaluated jobs.
Source: The authors.

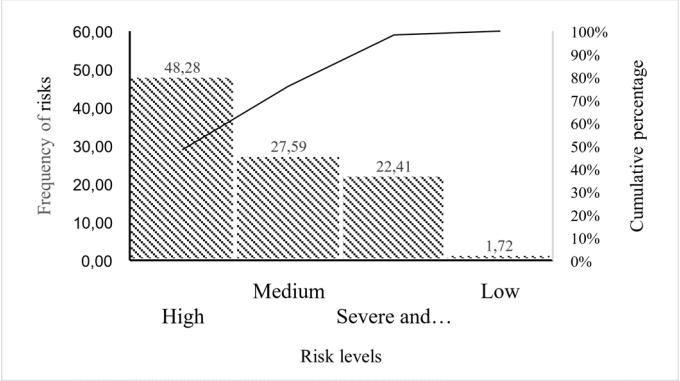

Figure 5. Overall result of safety risk levels at the water treatment plant.
Source: The authors.

4 Discussion

The results of this study identified the most common risks as “person falling from a different level”, “objects falling from a collapse or landslide” and “blows/cuts from objects or tools”. These risks are common in companies of this nature due to the structural and operational form of their processes [17]. In particular, the risk of falling from a different level is intrinsically related to other types of risks, due to the chain of events that this type of accident can trigger [18]. Previous studies have determined that falls from a height represent up to 50% of occupational risks in various companies [19], which corroborates the relevance of these findings in the context of the evaluated water treatment plant.

The distribution area stood out as the zone with the highest incidence of risks. This situation is associated with the dependence on pumps, whose maintenance and operation involve multiple risk factors that affect not only the physical safety of workers, but also their overall health, influencing occupational diseases, fatigue and job dissatisfaction [20]. This combination of physical and psychosocial risks emphasizes the importance of comprehensive safety management in industrial environments.

In terms of assessment, the “high” risk level was the most representative, covering 48.28% of the assessed working conditions. This classification highlights the need to implement “urgent corrections and adoption of control measures”, measures aimed at the3 elimination, reduction or mitigation of the identified risks [14,15,21]. The application of these corrective actions not only positively impacts the quality of working life of workers, but also strengthens the institutional image and competitiveness of companies through effective preventive management models [22].

In general terms, the application of the NTP 330 method revealed that the high incidence of risks associated with falls from different levels and falling objects is closely linked to the operational characteristics of the evaluated plant [23]. Maintenance activities involving pumps, valves, and pipelines require continuous movement across platforms and metal structures which, due to frequent moisture exposure, substantially increase the likelihood of severe accidents [24]. The identification of 58 hazards reflects not only the inherent complexity of the production process but also the inadequacy of the preventive controls currently in place.

These findings are consistent with previous studies conducted in similar facilities, thereby reinforcing the validity of the analysis and underscoring the urgency of implementing comprehensive corrective measures [17,23,24]. Such measures should integrate engineering interventions, improvements in operational infrastructure, and systematic training and preventive management programs designed to reduce both the probability and severity of the identified incidents [25].

5 Conclusions

The findings of this study indicate that the predominant occupational risks identified in the evaluated drinking water treatment plant originate mainly from deficiencies in infrastructure maintenance, inadequate safety signaling, and the use of obsolete equipment. The distribution area emerged as the most critical zone due to the operational demands of the pump systems, which expose workers to physical hazards and contribute to broader impacts on their well-being, including fatigue, stress, and susceptibility to occupational illnesses. The identification of multiple high-risk conditions evidences the limited effectiveness of the preventive measures currently implemented.

The high proportion of risks classified as “high level” underscores the urgent need to implement corrective actions and more robust control mechanisms aimed at eliminating or mitigating hazardous conditions. Intervention strategies should prioritize engineering controls, modernization of equipment, improvement of signage and accessibility, and the strengthening of maintenance and operational protocols. These actions are essential not only to reduce the probability and severity of incidents but also to establish a safer and more efficient operational environment.

The application of the NTP 330 method proved instrumental in identifying critical areas and establishing intervention priorities, providing a structured and systematic assessment of exposure levels, control efficiency, probability of occurrence, and severity. In addition, this comprehensive approach reinforces the importance of adopting an integrated risk-management framework that incorporates engineering solutions, organizational policies, and continuous training. Strengthening occupational safety not only protects workers’ physical and mental integrity but also contributes to the long-term sustainability of plant operations and supports progress toward the Sustainable Development Goals by ensuring a reliable and safe supply of potable water.

References

[1] Céspedes, G., and Martínez, M., An analysis of occupational health and safety in the Cuban business system. Latin American Journal of Social Law; [online]. (22), 2016. Available at: https://www.scielo.org.mx/scielo.php?script=sci_arttext&pid=S1870-46702016000100001

[2] Toro, J., Vega, V., and Romero, A., Occupational accidents and occupational diseases and their application in ordinary justice. Journal of University and Society, [online]. 13(2), pp. 357-362. 2021. Available at: http://scielo.sld.cu/pdf/rus/v13n2/2218-3620-rus-13-02-357.pdf

[3] Takala, J., Global estimates of traditional occupational risks. Scandinavian Journal of Work, Environment and Health, Supplement; [online]. (1), pp. 62–67. 2005. Available at https://www.sjweh.fi/show_abstract.php?abstract_id=940

[4] Driscoll, T., Rushton, L., Hutchings, S.J., Straif, K., Steenland, K., Abate, D., Abbafati, C., Acharya, D., Adebayo, O.M., Afshari, M., Akinyemiju, T., Alahdab, F., Anjomshoa, M., Antonio, C.A.T., Aremu, O., Ataro, Z., Ayala-Quintanilla, B.P., Mattar-Banoub, J.A., Barker-Collo, S.L., y Lim, S., Global and regional burden of disease and injury in 2016 arising from occupational exposures: a systematic analysis for the Global Burden of Disease Study 2016. In Occupational and Environmental Medicine., 77(3). pp. 133-141, 2019. DOI: https://doi.org/10.1136/oemed-2019-106008

[5] Abdalla, S., Apramian, S.S., Cantley, L.F., y Cullen, M.R., Occupation and Risk for Injuries. In Disease Control Priorities, 3ª Edition, Injury Prevention and Environmental Health. 1(1), Art. 120694, 2017. DOI: https://doi.org/10.1596/978-1-4648-0522-6_ch6

[6] Silva, M., Merino, P., Benavidez, F., López, M., and Gómez, A., Occupational health in Ecuador: a comparison with surveys on working conditions in Latin America. Brazilian Journal of Occupational Health. [online]. 45(20), 2020. Available at: https://www.scielo.br/j/rbso/a/tHMyXrBb9cwQQ4rbkbcWbvP/?lang=es

[7] Giuffrida, A., Iunes, R.F., and Savedoff, W.D., Occupational risks in Latin America and the Caribbean: Economic and health dimensions. In Health Policy and Planning. 17(3), pp. 235-246, 2002. DOI: https://doi.org/10.1093/heapol/17.3.235

[8] Alcívar, D., Espinoza, A., Arteaga, M., and Escobar, K., ENEMDU Ecuador: study of the perception of safety and health. Revista Salud UIS. 2020; [online]. 52(3), pp. 215–223. 2018. Available at: http://www.scielo.org.co/pdf/suis/v52n3/2145-8464-suis-52-03-215.pdf

[9] López-López, J.C., and Alcívar-Espín, R.A., Industrial safety and occupational health strategies: the case of a water treatment plant in Ecuador. Journal of Business and Entrepreneurial Studies. 7(3), Art. 341, 2023. DOI: https://doi.org/10.37956/jbes.v7i3.341

[10] Flores, C., Capa, C., and Capa, L., Occupational health and safety management to reduce workplace accidents in companies in Machala-Ecuador. Journal of University and Society. [online]. 10(2), pp. 304-309. 2018. Available at: http://scielo.sld.cu/pdf/rus/v10n2/2218-3620-rus-10-02-310.pdf

[11] Acosta-Pérez, P.B., Espinosa-Pinos, C.A., Acuña-Mayorga, J.M., and Lascano-Arias, G., Occupational Risks: a comparative study of the most common indicators in Uruguay, Cuba and Ecuador. ECTM, IEEE 7th Ecuador Technical Chapters Meeting. pp. 1-4, 2023. DOI: https://doi.org/10.1109/ETCM58927.2023.10309063

[12] Ministry of labor. basic guide to the prevention of occupational risks in construction. [online]. 2022. [cited January 9th, 2023]. Available at: https://www.trabajo.gob.ec/wp-content/uploads/2024/01/Guia-basica-de-prevencion-de-riesgos-laborales-en-la-construccion.pdf

[13] National Institute for Safety and Hygiene at Work (INSHT). Evaluation of working conditions in small and large companies. [online]. 2000. [cited on January 9th, 2023]. Available at: https://www.insst.es/documents/94886/211340/Condiciones_trabajo_PYMES.pdf/0452965e-d0bb-408d-9806-fac257562168?t=1587581004696

[14] National Institute for Safety and Hygiene at Work (INSHT). NTP 330: Simplified system for the assessment of accident risks. [online]. 1993. [cited on January 9th, 2023]. Available at: https://www.insst.es/documents/94886/326827/ntp_330.pdf/e0ba3d17-b43d-4521-905d-863fc7cb800b

[15] Vitrián, F.J., Núñez, J.M., Román, F., Arévalo, T., Occupational risk prevention techniques: safety at work and industrial hygiene. UNIR, editor: 978-84-15626-11-4(Volume II); 2018.

[16] Moyano, J., Jácome, M., García, A., Orozco, J., and Fuertes, V., Evaluation of mechanical risks in engineering workshops and laboratories applying the NTP 330 standard. Perfiles Magazine, [online]. 17(1), pp. 41–62 2017. Available at: http://ceaa.espoch.edu.ec:8080/revista.perfiles/Articulos/Perfiles17Art6.pdf

[17] Del-Pezo, O., Occupational health and safety management model for the drinking water company, "Aguas de la peninsula–AGUAPEN SA". [Thesis prior to obtaining the master's degree in quality, environment and safety management systems]. Guayaquil: Universidad Politécnica Salesiana. 2013.

[18] Wong, L., Wang, Y., Law, T., y Lo, C.T., Association of root causes in fatal fall-from-height construction accidents in Hong Kong. Journal of Construction Engineering and Management, 142(7), pp. 1-12. 2016. Available at: http://dx.doi.org/10.1061/(ASCE)CO.1943-7862.0001098

[19] Zlatar, T., Lago, E.M.G., Soares, W.A., Baptista, J.S., y Barkokébas Junior, B., Falls from height: analysis of 114 cases. 29, Art. 91, 2019. DOI: https://doi.org/10.1590/0103-6513.20180091.

[20] Lovely, L., y Sekar, F., Preventing musculoskeletal disorders due to manual material handling in the production process of clean water. Journal Industrial Servicess, 10(1), pp. 125–132. 2024. DOI: http://dx.doi.org/10.62870/jiss.v10i1.24471

[21] International Labour Organization (ILO). Occupational safety and health inspection, training module for inspectors. [online]. 2017. [cited 10th September 2024]. Available at: https://www.ilo.org/sites/default/files/wcmsp5/groups/public/@americas/@ro-lima/@ilo-buenos_aires/documents/publication/wcms_592318.pdf

[22] Yturralde, J., and Franco, O., Workplace accidents in public and private companies in Ecuador in the period 2014-2015. Dominio de las Ciencias, 6(2), pp. 1022–1043. 2020. DOI: http://dx.doi.org/10.23857/dc.v6i2.1263.

[23] Krasnova, A., and Radygina, E., Occupational safety when working at height. Sbornik Naučnyh Trudov Angarskogo Gosudarstvennogo Tehničeskogo Universiteta, 2024(1), pp. 363–366. 2024. DOI: https://doi.org/10.36629/2686-7788-2024-1-363-366.

[24] Delshah, M., Rahimpour, H.R., and Rahimpour, M.R., Chemicals transporting systems safety: pumps, pipelines, and valves. Elsevier BV pp. 227–242. 2023. DOI: https://doi.org/10.1016/b978-0-323-95163-0.00006-2

[25] Benson, C., Obasi, I.C., Akinwande, D.V., and Ile, C., The impact of interventions on health, safety and environment in the process industry. Heliyon. 10(1), Art. e23604, 2024. DOI: https://doi.org/10.1016/j.heliyon.2023.e23604

M.B. Vinces-Obando, is Professor at the Faculty of Agro-Environmental Engineering at the Technical University of Manabí. She is BSc. Eng in Environmental Engineering, MSc. in Environmental and Energy Management, and is currently a PhD candidate in Environmental Sciences. Her research focuses on waste management, environmental sustainability studies, and environmental protection.
ORCID: 0000-0002-3310-6202

L.D. Balarezo-Saltos, is support professor at the Faculty of Aquaculture and Marine Sciences, Sucre University of Peru. MSc. in Environmental Engineering and a MSc. in Integrated Management Systems for occupational risk prevention, quality, the environment, and corporate social responsibility. He also holds a degree in Occupational Health and Safety and is an internal auditor for the ISO 45001 standard. He is currently a PhD student in Environmental Sciences at the National University of Piura, Peru. His research focuses on environmental technologies, environmental management, and climate finance. He is a member of the Biodiversity and Ecology in Aquatic Systems Research Group.
ORCID: 0000-0003-0259-7632

C.A. Salas Macías, He earned his degree in Agricultural Engineering from the Eloy Alfaro Lay University of Manabí (ULEAM) in 2005. In 2010, MSc. of Science in Tropical Agroforestry from the Tropical Agricultural Research and Higher Education Center (CATIE), and in 2011, a MSc. of Agricultural Administration and Marketing from ULEAM. In 2017, and Dr. of Philosophy in Environmental Engineering and Sciences from the National Agrarian University of La Molina (UNALM), Peru. He subsequently completed a postdoctoral fellowship at the University of Salamanca, Spain. He is currently pursuing complementary MBA studies in Data Science and Analytics, as well as a postdoctoral fellowship in Research Methodology and Scientific Production. He is a Senior Lecturer in the Faculty of Agroenvironmental Engineering at the Technical University of Manabí. His research focuses on the study of dry forests and sustainable production systems. He is a member of the FAGROCLIM research group and the DRYFLOR network.
ORCID: 0000-0002-1641-1571

F.R. Isea-León, is Bsc. Eng. in Agricultural Engineering in, 1995, with a Msc. Scientiarum in Food Science and Technology obtained in 2001 and PhD in Applied Sciences obtained in 2008. I worked at the Universidad Nacional Experimental Sur del Lago (UNESUR), located in Santa Barbara of Zulia, Venezuela, from January 2010 to June 2017. I held the position of Executive Director of the Foundation for the Development of Science and Technology in Zulia State (Territorial Unit Fundacite-Zulia), belonging to the Ministry of Science Technology from July 17, 2014 until May 30, 2017. Then from October 2017 to the present I exercise functions as Senior Lecturer I and researcher of the subjects Biochemistry, Microbiology, Nutrition of Aquatic Organisms and Degree Development II. Currently I also exercise management functions as Vice-Dean of Postgraduate Research and Linking of the Technical University of Manabí. My research areas of interest are the following: Physicochemical and microbiological quality of raw materials and feeds for aquatic organisms. Formulation and elaboration of alternative feeds for fish and shrimp nutrition. Evaluation of attractants in the feeding of aquatic organisms.
ORCID: 0000-0002-3766-5108

R.P. Panta-Vélez, is a BSc. in Aquaculture and a MSc. in Sustainable Bioresource and Environmental Management. He is a professor and researcher with 17 years of experience in Aquaculture at the Technical University of Manabí. He is currently Vice Dean of the Renewable Natural Resources program. He specializes in Fisheries Biology, captive reproduction of organisms, mollusk farming, and water quality in aquaculture. He also serves as a technical advisor in water quality analysis for shrimp and fish farming in the province of Manabí, Ecuador. He is a member of the RIEAE Network, the AQUACIBUS Network, and the Ecuadorian Limnology Network, as well as the Biodiversity and Ecology of Aquatic Systems Research Group "BIOECOSYSTEM" at the Technical University of Manabí. He has participated in several research projects (UTM-Fundacyt, UTM-Provincial Development Agency of the province of Manabí, ADPM-AECI, UTM-Subsecretariat of Aquaculture, SARCE, RIEAE, UTM Research Institute) and is currently the director of the project "Evaluation of Water Quality and Biodiversity in the Chone River Estuary." He has been the advisor for 12 undergraduate theses, the reviewer for 13 undergraduate theses, and the advisor and co-advisor for 8 master's theses, all in the field of Aquaculture and Fisheries. He has published 11 papers in indexed journals and has been a speaker at several national and international conferences.
ORCID: 0000-0003-2969-0765

D.E. Briones-Bermúdez, is a BSc. in Clinical Laboratory Sciences in 2025. Currently pursuing a Master's degree in Quality and Patient Safety Management at the Pontifical Catholic University of Ecuador. Has worked in a private clinical laboratory, where he has gained experience in the collection and processing of biological samples as well as the use of equipment and techniques for clinical analysis. His areas of interest include laboratory procedures for clinical diagnosis, sample processing and analysis, and strengthening professional practice in healthcare settings, as well as risk management and regulatory compliance.
ORCID: 0009-0000-4499-480X

DYNA
http://dyna.medellin.unal.edu.co/

UNIVERSIDAD NACIONAL DE COLOMBIA

Smart audit in real time: automated visual analysis from mobile devices

Francisco Gerardo Huamanchumo-Trujillo [a], Alejandro Roman Campos-Gamarra [a], Rodrigo Alonso Guevara-Saldaña [a] & Alberto Carlos Mendoza-de los Santos [b]

[a] *Escuela de Ingeniería de Sistemas, Universidad Nacional de Trujillo, Trujillo, Perú. t1023300821@unitru.edu.pe, t1513300121@unitru.edu.pe, t1053300621@unitru.edu.pe*
[b] *Departamento de Ingeniería de Sistemas, Universidad Nacional de Trujillo, Trujillo, Perú, amendozad@unitru.edu.pe*

Received: June 8th 2025. Received in revised form: November 4th, 2025. Accepted: November 21st, 2025

Abstract
This study presents Smart Audit in Real Time, a mobile system designed to automate the visual inspection of technological infrastructures using OpenAI GPT-4o Vision. The application captures images, identifies auditable elements, and generates structured reports aligned with international IT auditing standards. A dataset of 50 images from different operational environments was analysed, producing 207 findings grouped into four categories: physical security, ergonomics, environmental conditions, and regulatory compliance. The system achieved an overall accuracy of 83% and an average F1-score of 0.65, with a mean response time of 15.8 seconds per evaluation. A chi-square test applied to the confusion matrix confirmed a statistically significant association between predicted and actual categories, supporting the reliability of the classification. The results show that automated visual auditing from mobile devices can efficiently detect operational risks and produce consistent evaluative outputs without expert intervention. This research contributes to the digital transformation of IT auditing by improving accessibility, precision, and real-time decision-making.

Keywords: digital inspection; visual recognition; contextual verification; operational management; automated review; intelligent processing.

Auditoría inteligente en tiempo real: análisis visual automatizado desde dispositivos móviles

Resumen
Este estudio presenta Smart Audit in Real Time, un sistema móvil diseñado para automatizar la inspección visual de infraestructuras tecnológicas mediante OpenAI GPT-4o Vision. La aplicación captura imágenes, identifica elementos auditables y genera reportes estructurados alineados con normas internacionales de auditoría de TI. Se analizó un conjunto de 50 imágenes procedentes de diversos entornos operativos, obteniéndose 207 hallazgos clasificados en cuatro categorías: seguridad física, ergonomía, condiciones ambientales y cumplimiento normativo. El sistema alcanzó una exactitud global del 83% y un F1-score promedio de 0.65, con un tiempo medio de respuesta de 15.8 segundos por evaluación. Una prueba de chi-cuadrado aplicada a la matriz de confusión confirmó una asociación estadísticamente significativa entre las categorías reales y las predichas, respaldando la confiabilidad del modelo. Los resultados evidencian que la auditoría visual automatizada desde dispositivos móviles puede detectar eficientemente riesgos operativos y generar evaluaciones consistentes sin intervención experta. Esta investigación contribuye a la transformación digital de la auditoría de TI, mejorando la accesibilidad, la precisión y la toma de decisiones en tiempo real.

Palabras clave: inspección digital; reconocimiento visual; verificación contextual; gestión operativa; revisión automatizada; procesamiento inteligente.

1 Introduction

In recent years, IT audits have changed substantially as organizations operate in more distributed settings that demand strict compliance and dependable operational security. In this landscape, mobile tools for assessing technological environments offer a practical alternative to conventional approaches, which tend to rely on static procedures and often miss physical or contextual risks that do not appear in documentation. Ongoing digital transformation together with

How to cite: Huamanchumo-Trujillo, F.G., Campos-Gamarra, A.R., Guevara-Saldaña, R.A. and Mendoza-de los Santos, A.C., Smart audit in real time: automated visual analysis from mobile devices DYNA, (93)240, pp. 27-35, January - March, 2026.

mobile work practices and a growing dependence on interconnected infrastructures has increased the need for quicker, more flexible, and automated audit processes. As a result, the way risks are detected, recorded, and addressed is shifting, especially in facilities where physical conditions directly affect the reliability of information systems.

Audits can no longer focus solely on software checks or network monitoring; they also need visual evidence from the physical environment of cable organization, ventilation, access control, and equipment layout among others. Building on this idea, this work introduces a smart audit approach for real-time assessments using a mobile device. The device camera captures environmental images, and artificial-intelligence models identify auditable elements. The system flags issues such as tangled wiring, missing signage, blocked areas, or poor airflow and produces an automatically structured report that states the problem, the relevant regulation, a suggested corrective action, and the associated risk. Because the process is automated end-to-end, personnel with limited audit experience can still obtain consistent, professional results.

The spread of accessible, portable technologies has changed how auditors interact with systems. Mobile platforms make it possible to document environmental aspects of order, physical security, and ventilation that are frequently overlooked in purely logical reviews [1]. In public-sector settings, AI helps surface vulnerabilities that merit both ethical and technical attention [2]. Beyond recognizing deficiencies, intelligent tools standardize how findings are captured and traced. Automatically generated reports derived from image analysis align observations with international standards, improving documentation structure, traceability, and transparency throughout the audit process [3]. This brings tangible advantages where fast, accurate reporting is essential.

Complementary advances reinforce this direction. The combination of blockchain and cloud accounting with AI strengthens the integrity and traceability of audit evidence [4]. Reviews of AI methods in cybersecurity show that automated analysis can reveal complex or subtle vulnerabilities that are hard to detect with manual procedures [5]. In management and performance audits, intelligent models have shortened analysis cycles and improved effectiveness [6,7]. On the computer-vision side, techniques such as quantized scene detection and mobile augmented reality enable real-time identification of physical risks directly from smartphones [8-13]. Moreover, lightweight AI models have proven practical for mobile deployment, supporting device-based audit tasks without excessive resource demands [14]. Taken together, these developments point to a more holistic view of IT auditing in which visual inspection complements logical analysis to improve accuracy, speed, and the quality of recorded evidence. The intention is not to replace human auditors, but to extend their capabilities through context-aware AI and mobile computing.

Despite these benefits, mobile intelligence audits face limitations. Dependence on network connectivity can restrict operation in constrained environments, and image capture raises privacy and ethical concerns when sensitive content or personnel appear in the frame. Ensuring interpretability, transparency, and responsible use of AI tools is therefore essential for sustainable adoption in professional practice.

2 Design

The proposed software design focuses on developing a functional mobile application built with the Dart programming language and the Flutter framework, ensuring high compatibility with Android devices. The system architecture is divided into three modules: the user interface, the image-processing engine, and the PDF-report generator. This modular structure allows each component to be updated or extended independently, enabling future integrations and improvements.

The main workflow begins when the user captures or selects an image from the device's camera or gallery. The image is then encoded and sent to the analytics service, which processes it in the background and returns a structured audit report containing the detected findings, the applicable regulatory framework, the suggested corrective actions, and the corresponding risk level.

A dedicated REST API manages communication between the mobile client and the analysis service, while an integrated control converts the generated report into a ready-to-archive or shareable PDF file.

From a technical standpoint, specific performance optimizations were implemented for mobile operation. The adoption of deep-learning models for real-time detection on devices with limited computational resources validates the feasibility of this system [15]. In addition, the mobile computer-vision framework is regarded as a technological revolution that enables contextual recognition and intelligent image capture for audit purposes [16]. Finally, super-resolution techniques were applied to enhance image clarity without compromising performance, improving the quality of the visual reports produced directly on the mobile device [17].

3 Materials and Methods

The following technologies were used:

- Mobile device: A mobile device with an Android operating system (version 14) was used to capture the images of the environment to be audited. The device has a high-resolution camera, which allows clear visual evidence to be obtained for automated analysis.
- Make/Model: Galaxy A55 5G
- Operating system: Android version 14
- Dart: It is a modern programming language optimized for the development of user interfaces created by Google. It is an object-oriented language with static typing that allows you to develop efficient and high-performance applications. Dart is the primary language used in Flutter, making it easy to create reactive, cross-platform mobile interfaces from a single codebase.
- Flutter: It is an open-source framework developed by Google for the creation of mobile, web, and desktop applications. It allows you to develop native apps for Android and iOS using a single codebase written in Dart. Flutter provides a rich set of customizable widgets,

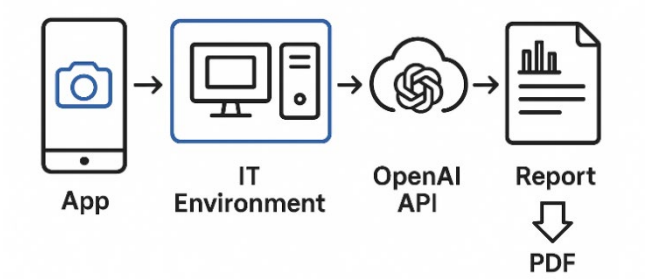

Figure 1. Process of generating a computer audit report.
Source: Authors.

responsive architecture, and built-in tools to facilitate modern interface design and agile development.

- OpenAI GPT-4 Vision: It is an artificial intelligence service capable of interpreting both text and images. This version of the GPT-4 model has multimodal capabilities, allowing it to analyze visual content and generate natural language responses from images. In this project, it is used to perform automatic audits from photographs captured from mobile devices. The image is sent to the model along with a prompt text, and the model returns a detailed analysis in the form of text.
- Internet connection: The system requires an active and stable internet connection to communicate with OpenAI's API. This connection is essential to send images to the AI server, receive the corresponding textual analysis, and subsequently process this information within the mobile app.
- Output format and PDF generation: Once the AI-generated analysis is received, this text is transformed into a PDF document using libraries available in Flutter. This PDF file serves as evidence of the audit performed and can be stored locally, shared digitally, or printed. The generation of PDFs allows the results to be structured and preserved in a widely accepted and portable format.

The system was developed in four phases, each aimed at solving a key component of the system. Each of these phases was developed and integrated in a modular way to ensure the correct functioning of the complete system. Fig. 1 illustrates the process of generating a computer audit report. Phases are briefly described below:

- Phase 1: Interface development.
- Phase 2: Image selection functionality.
- Phase 3: OpenAI API integration
- Phase 4: Generating the PDF file

3.1 Interface development:

Since the main purpose of the software is to capture an image of the environment in real-time to perform an automated computer audit, the development of a mobile application was necessary because of the need to use the device's camera immediately and accessible to the user.

For its implementation, Flutter, a cross-platform development framework created by Google, was chosen. Flutter allows you to build native apps for both Android and iOS from a single codebase, speeding up development and making it easier to maintain your project.

The graphical interface was designed with a minimalist and functional approach, allowing the user to perform the main actions clearly and directly. Next, the code used in the rendering of the interface is presented in Fig. 2. This visual foundation sets the starting point for the next phases of the system, focused on user interaction and intelligent processing of the captured image.

3.2 Image select functionality

This phase focuses on incorporating the functionality that allows the user to provide the image that will serve as an input for the computer audit. Two options are provided, as shown in Fig. 3: Capture a new photo or select an existing image from the device's gallery.

```
Widget build(BuildContext context) {
  return Scaffold(
    appBar: AppBar(title: const Text("Auditoría por Imagen")),
    body: SafeArea(
      child: Padding(
        padding: const EdgeInsets.all(16.0),
        child: Column(
          children: [
            if (_imagen != null)
              Image.file(_imagen!, height: 200, fit: BoxFit.cover),
            const SizedBox(height: 12),
            Row(
              mainAxisAlignment: MainAxisAlignment.spaceAround,
              children: [
                ElevatedButton.icon(
                  onPressed: () => _seleccionarImagen(ImageSource.gallery),
                  icon: const Icon(Icons.image),
                  label: const Text("Galería"),
                ),
                ElevatedButton.icon(
                  onPressed: () => _seleccionarImagen(ImageSource.camera),
                  icon: const Icon(Icons.camera),
                  label: const Text("Cámara"),
                ),
              ],
            ),
            const SizedBox(height: 12),
            ElevatedButton.icon(
              onPressed: _imagen == null || _procesando ? null : _enviarImagen,
              icon: const Icon(Icons.send),
              label: const Text("Hacer auditoría"),
            ),
            const SizedBox(height: 16),
            Expanded(
              child: _procesando
                  ? const Center(child: CircularProgressIndicator())
                  : TextField(
                      controller: _respuestaController,
                      maxLines: null,
                      readOnly: true,
                      expands: true,
                      decoration: const InputDecoration(
                        border: OutlineInputBorder(),
                        hintText: "Aquí aparecerá el resultado de la auditoría...",
                      ),
                    ),
            ),
            const SizedBox(height: 12),
            Padding(
              padding: const EdgeInsets.only(top: 8.0),
              child: ElevatedButton.icon(
                onPressed: _respuesta.isEmpty ? null : _descargarPDF,
                icon: const Icon(Icons.download),
                label: const Text("Descargar PDF"),
              ),
            ),
          ],
        ),
      ),
    ),
  );
}
```

Figure 2. The code snippet corresponding to the construction of the interface
Source: Authors.

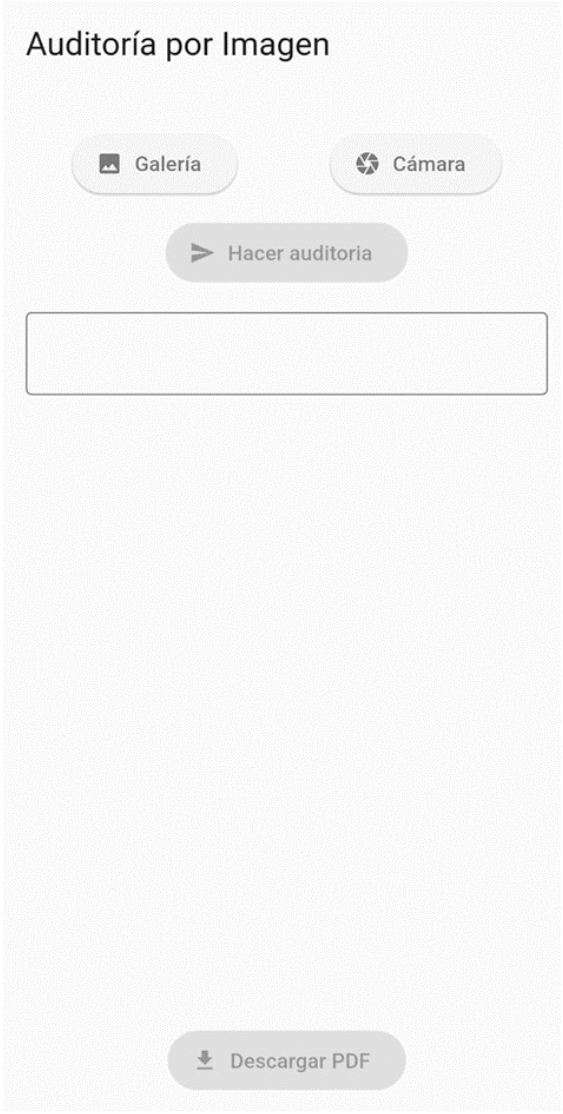

Figure 3. Mobile device interface.
Source: Authors.

3.1.1 Main functionality: Select image

The function responsible for handling image selection is presented in Fig. 4, which includes the corresponding implementation code. This feature allows you to get an image from the specified source (camera or gallery) using the image_picker package. Once selected, the image is saved locally, and the status of the application is updated.

```
Future<void> _seleccionarImagen(ImageSource origen) async {
    final XFile? seleccionada = await _picker.pickImage(source: origen);
    if (seleccionada != null) {
      setState(() {
        _imagen = File(seleccionada.path);
        _respuesta = '';
        _respuestaController.clear();
      });
    }
  }
```

Figure 4. The function in charge of managing the selection of the image
Source: Authors.

```
inAxisAlignment: MainAxisAlignment.spaceAround,
children: [
  ElevatedButton.icon(
    onPressed: () => _seleccionarImagen(ImageSource.gallery),
    icon: const Icon(Icons.image),
    label: const Text("Galería"),
  ),
  ElevatedButton.icon(
    onPressed: () => _seleccionarImagen(ImageSource.camera),
    icon: const Icon(Icons.camera),
    label: const Text("Cámara"),
  ),
],
```

Figure 5. Button code for image selection.
Source: Authors.

Figure 6. User interface for image selection or capture.
Source: Authors.

```
final bytes = await _imagen!.readAsBytes();
final base64 = base64Encode(bytes);
final dataUrl = '$base64';
```

Figure 7. Base64 encoded image in data URL format
Source: Authors.

3.2.1 Selection Interface: Camera or Gallery

The user interface offers two clearly differentiated buttons, one to access the gallery, and one to use the device's camera. The implementation code is shown in Fig. 5, and the interface is shown in Fig. 6, where the user can select an image for processing.

3.3 OpenAI API integration

Once the image has been obtained from the camera or gallery, the next step is to send it to the OpenAI API, where the captured environment will be visually analyzed with GPT-4o and the results will be exported to an audit report.

3.3.1 Converting the image to base format64

Before sending, the image must be base64 encoded in data URL format, which is the format required by the API to process images, the code used is in Fig. 7.

Message preparation and payload, the message that will be sent to the API is constructed. This includes:

- A prompt with detailed instructions on how to audit the image.
- The image in base format64.
- The artificial intelligence model to be used (GPT-4o).

Next, in Fig. 8 the message that will be sent to the API is constructed. This includes:

```dart
final payload = {
  "model": "gpt-4o",
  "messages": [
    {
      "role": "user",
      "content": [
        {
          "type": "text",
          "text": "..."
        },
        {
          "type": "image_url",
          "image_url": {"url": dataUrl}
        }
      ]
    }
  ],
  "max_tokens": 4096
};
```

Figure 8. Code to call the artificial intelligence model to use (gpt-4o).
Source: Authors.

Inside "text" will go the prompt which will be: You are a professional computer auditor. Analyze the submitted image in detail, showing a technology-related facility (e.g., computers, servers, networks, cabling, infrastructure, etc.). Identifies all visible problems, deficiencies or bad practices that may affect the safety, operation, availability or regulatory compliance of technological systems.\n\nConsider aspects such as:\n- Physical security\n- Organization of the environment\n- Cable and energy management\n- Environmental conditions and ventilation\n- Ergonomics and accessibility\n- Signage, cleaning and order\n- Fire protection, theft or accidents\n- Asset management or tagging\n- Physical access controls\n- Operational continuity\n- Any other relevant aspect that can be observed\n\nFor each finding detected:\n1. Clearly describe the observed problem.\n2. It mentions the applicable regulatory framework (ISO/IEC, NIST, COBIT, ITIL, EIA/TIA, etc.). \n3. Propose an action plan or specific corrective measures.\n4. Indicate the risks associated if the problem is not corrected.\n\nAnswer in Spanish and structure the report by separating each finding as if it were part of a professional audit. If no visible problems are detected, it indicates that the installation complies with observable good practices.

To process OpenAI API response, the content is decoded and the analysis generated by the model is extracted. Then, the interface is updated to show the results to the user. The code used for this section is shown in Fig.9.

```dart
final respuesta = await http.post(
  Uri.parse("https://api.openai.com/v1/chat/completions"),
  headers: {
    "Content-Type": "application/json; charset=UTF-8",
    "Authorization": "Bearer api_key"
  },
  body: jsonEncode(payload),
);

final data = json.decode(utf8.decode(respuesta.bodyBytes));
final contenido = data["choices"][0]["message"]["content"];
```

Figure 9. Code to extract the analysis generated by the model
Source: Authors.

This section transforms the picture into a detailed report that identifies various findings related to security, environment organization, technology infrastructure, and regulatory compliance. Each finding includes a description of the observed problem, the applicable regulatory framework, a proposed action plan, and the associated risks in the event of failure to implement the suggested corrective measures. Considering that the "Authorization" will be the api_key generated on the OpenAI website.

3.4 Generation of the pdf file:

Once the structured analysis of the image has been received by the API, the application allows you to generate a file in PDF format containing all the findings; the coding used is shown in Fig. 10. This functionality is essential for documenting, sharing, or backing up analysis results in a readable and portable format.

```dart
Future<void> _descargarPDF() async {
    try {
      if (_respuesta.isEmpty) {
        ScaffoldMessenger.of(context).showSnackBar(
          const SnackBar(content: Text("No hay contenido para exportar.")),
        );
        return;
      }

      final pdf = pw.Document();

      pdf.addPage(
        pw.MultiPage(
          pageFormat: PdfPageFormat.a4,
          build: (pw.Context context) => [
            pw.Text(
              _respuesta,
              style: pw.TextStyle(fontSize: 12),
            ),
          ],
        ),
      );

      final directory = await getApplicationDocumentsDirectory();
      final path = '${directory.path}/auditoria_respuesta.pdf';
      final file = File(path);
      await file.writeAsBytes(await pdf.save());

      ScaffoldMessenger.of(context).showSnackBar(
        SnackBar(content: Text("PDF guardado en: $path")),
      );

      await OpenFile.open(path);
    } catch (e) {
      ScaffoldMessenger.of(context).showSnackBar(
        SnackBar(content: Text("Error al generar PDF: $e")),
      );
    }
  }
```

Figure 10. Code to extract the PDF from everything analyzed by the function
Source: Authors.

The PDF document is built from the previously generated textual content and organizes each finding in a clear structure, facilitating its reading and subsequent analysis. Each section of the report is composed of the following elements:

- Observed problem: Describes the inconvenience detected from the visual analysis of the image, such as security failures, disorder, bad wiring practices, among others.
- Applicable regulatory framework: Indicates which norms, standards or good practices (such as ISO/IEC, NIST, COBIT, ITIL, etc.) are related to the problem identified.
- Action plan: Details of the concrete measures that must be applied to correct the problem observed.
- Associated risks: It sets out the possible consequences that could arise if the suggested action plan is not carried out.

An actual extract of the content that can be generated after analyzing an image is shown in Fig. 11 below. For testing purposes, an image of the development environment used by one of the authors was used.

Figure 11. Image of the environment where the application is developed
Source: Authors.

The audit findings were:

Technology Installation Audit Report
1. Organization of the Environment
- *Observed Problem*: The artboard is disorganized with various elements, including a fan on top of documents or notebooks.
- *Applicable Regulatory Framework*: ITIL, IT Service Management, focus on an orderly work environment.
- *Action Plan*: Organize the workspace, removing unnecessary elements and ensuring that devices such as fans are not on documents that may be important.
- *Associated Risks*: Disorganization can lead to loss of important documents, distractions, and reduced efficiency.

2. Cable and Power Management
- *Observed Problem*: The cables are placed without visible organization, which could lead to clutter or accidents.
- *Applicable Regulatory Framework*: ISO/IEC 14763-2 on the management and design of cabling installations.
- *Action Plan*: Implement cable management systems such as trunking or clips to keep wiring tidy and prevent tripping.
- *Associated Risks*: Possible physical accidents, service interruptions or damage to equipment.

3. Environmental Conditions and Ventilation
- *Observed Problem*: The use of fans indicates that there could be ventilation or temperature control problems.
- *Applicable Regulatory Framework*: ASHRAE, standards for environmental conditions in data centers.
- *Action Plan*: Assess the need for more efficient or suitable HVAC systems for the workspace.
- *Associated Risks*: Overheating of equipment, reduction of hardware life, less comfort for the user.

4. Ergonomics and Accessibility
- *Observed Issue*: The keyboard and mouse layout may not be ergonomic, which may lead to long-term discomfort or injury.
- *Applicable Regulatory Framework*: ISO 9241 ergonomics guidelines.
- *Action Plan*: Evaluate and adjust the position of the input devices according to the best ergonomic practices.
- *Associated Risks*: Injuries may repetitive strain, reduced productivity.

5. Fire Protection
- *Observed Problem*: No smoke detectors or fire extinguishers visible in the image.
- *Applicable Regulatory Framework*: NFPA 75, Fire Protection of Information Processing Equipment.
- *Action Plan*: Ensure the installation of appropriate smoke detectors and fire extinguishers in the vicinity of the technological installation.
- *Associated Risks*: Risk of fire damage to equipment and data, jeopardizing safety and operational continuity.

Conclusions
The installation shows several opportunities for

improvement in terms of organization, safety and ergonomics. We recommend implementing the aforementioned corrective measures to ensure a safe, efficient, and compliant environment.

4 Results

To evaluate the effectiveness of the AI-based IT auditing system, a representative dataset of 50 images was created, reflecting diverse technological environments. Stratified sampling was used to ensure coverage of common audit settings: 17 corporate offices, 10 remote workspaces, 11 software development areas, and 12 computer rooms or educational labs.

Based on the number of auditable findings, images were classified as simple (1–3 elements, 15 images), moderately complex (4–6 elements, 22 images), and complex (over 6 elements, 13 images). This categorization allowed analyzing how visual complexity affected system performance. An analysis of the dataset identified 207 auditable findings distributed across four predefined categories: Physical Security, Ergonomics, Environmental Issues, and Regulatory Compliance (Table 1). The findings averaged 4.14 per image, reflecting the complexity of real technological environments where multiple issues often coexist. The simplest image contained a single finding, corresponding to a well-organized remote workspace, while the most complex image showed nine findings, associated with an educational laboratory exhibiting multiple deficiencies.

Table 1.
Auditable findings categories

Category	Quantity
security	53
ergonomics	57
environmental	48
compliance	49
Total	**207**

Source: Authors.

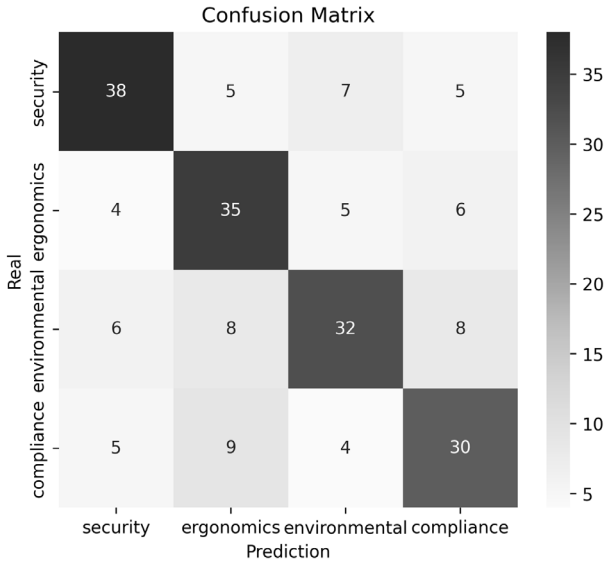

Figure 12. Confusion matrix elaborated using data collected from analysis.
Source: Authors.

Table 2.
Results of Chi-square test applied to the confusion matrix.

Statistic	Value	df	p-value	Critical Value	Decision
χ^2	180.87	9	3.32×10^{-34}	16.91	Reject H_0

Source: Authors.

With the dataset constructed, the IT auditing system was evaluated to assess its accuracy in identifying and classifying the 207 findings. The quantitative results were summarized in a confusion matrix (Figure 12), which highlights both correct detections and characteristic error patterns.

A chi-square (χ^2) test of independence was applied to the confusion matrix to verify whether the distribution of classifications differed significantly among the four categories. The null hypothesis (H_0) assumed no association between predicted and actual findings. As shown in Table 2, the test confirmed a statistically significant relationship between both variables, indicating that the audit system classification performance is consistent and reliable across all categories.

Performance metrics for each category were also calculated and are shown in Table 3. The application exhibited its best performance in identifying issues related to physical security and environmental problems, achieving 72% and 61% accuracy, respectively. These values are consistent with the visual nature of these issues, which tend to present clear, common, and distinguishable patterns suitable for automated analysis. Conversely, findings related to ergonomics and regulatory compliance achieved lower accuracy rates, both at 61%, which may be attributed to the wide variety of existing regulatory frameworks and their respective versions.

Additionally, tests were performed to obtain the application's response time. Using the same set of analyzed images, response time was collected across all stages involved in generating the audit report, as shown in Table 4.

The evaluation of the intelligent IT auditing system revealed consistent performance across multiple categories of auditable findings, with an overall F1 score of 0.65 and an average processing time of 15.8 seconds per image. These

Table 3.
Performance metrics

Category	Precision	Sensitivity	F1 Score	Accuracy
security	0.72	0.69	0.70	0.85
ergonomics	0.61	0.70	0.65	0.82
environmental	0.67	0.59	0.63	0.82
compliance	0.61	0.63	0.62	0.82
Average	0.65	0.65	0.65	0.83

Source: Authors.

Table 4.
Response time per stage

Stage	Average response time (sec)
Image capture	2.3
Image Processing	10.7
Preparation of the PDF report	2.8
Total	**15.8**

Source: Authors

results indicate a satisfactory balance between detection accuracy and operational efficiency, supporting the viability of image-based auditing as a complementary approach to traditional IT audit practices.

The findings align with the broader trend of technology-assisted auditing described in [18], where it was demonstrated that technology-based audit techniques significantly improve efficiency and task completion rates. Similarly, the developed system achieves substantial time reductions by automating visual inspection tasks that would otherwise require manual evaluation. This is consistent with the strategies proposed in [2], that emphasize the use of artificial intelligence, machine learning, and automation to enhance IT auditing through anomaly detection and process optimization. While both studies focus on data-centric or procedural automation, the present system extends these concepts into computer vision, allowing the automated identification of auditable findings directly from images of technological environments. This adaptation exemplifies how AI can evolve from purely data-driven analytics to visually contextual intelligence, expanding its applicability in IT auditing.

In the context of artificial intelligence applications to auditing, [19] conceptualized AI as a transformative enabler for real-time monitoring, anomaly detection, and data-driven decision-making, while [3] empirically demonstrated that AI enhances the accuracy and speed of financial audits by automating fraud detection and anomaly analysis. Building on both perspectives, the proposed system operationalizes these principles within IT auditing, applying AI to the visual domain rather than numerical or textual data. This integration of computer vision enables the recognition of physical, ergonomic, and environmental non-compliance indicators, broadening the scope of AI-based auditing beyond financial or transactional contexts. The system thus provides tangible evidence that AI can effectively support not only abstract data analysis but also the spatial and contextual assessment of technological infrastructures.

Furthermore, [20] argued that Agile methodologies enhance IT audit effectiveness by promoting adaptability, iterative improvement, and stakeholder collaboration. Although the proposed system does not explicitly follow an Agile framework, its modular architecture and rapid-feedback cycle align with Agile principles, enabling continuous refinement of detection models and real-time response to new risk patterns. Integrating this system into Agile audit workflows could therefore strengthen its adaptability and extend its practical use in dynamic organizational environments.

Finally, as noted by [21] and reinforced by [7], the rapid emergence of AI technologies has outpaced the evolution of auditing standards, creating a regulatory gap concerning transparency, interpretability, and ethical responsibility. The present study reflects this dual reality: while AI-driven systems, such as the one developed here, achieve substantial efficiency and precision improvements, they also depend on data representativeness and require human oversight to ensure trustworthiness. These findings underscore the urgent need for updated standards and ethical frameworks that explicitly address the integration of AI in auditing, ensuring the reliability, fairness, and accountability of such systems.

5 Conclusions and recommendations

The developed intelligent auditing application successfully automates the evaluation of technological environments through image recognition. Using a dataset of 50 images containing 207 auditable findings, the system achieved an average F1 score of 0.65 and an overall accuracy of 83%, with a mean processing time of 15.8 seconds per image. A chi-square (χ^2) statistical test applied to the confusion matrix ($\chi^2 = 180.88$, $df = 9$, $p < 0.001$) confirmed a significant association between the predicted and actual findings, indicating that the audit system performance is not due to chance. These results validate the reliability and effectiveness of the proposed solution as a consistent and efficient tool to support IT audit processes. Moreover, as discussed previously, the system's performance aligns with trends reported in the literature, where artificial intelligence and automation significantly enhance audit efficiency and precision. The integration of visual-intelligence techniques extends these advances to IT auditing, demonstrating that image-based analysis can complement traditional approaches and contribute to the digital transformation of auditing practices.

Although the system relies on an internet connection to send images and generate the audit via GPT, this does not represent a significant limitation, as it is designed for IT environments where connectivity is generally available, and running an AI model directly on a mobile device would be too resource intensive. Using GPT involves a low associated cost, and in the future, local models could be considered to reduce dependence on cloud computing services. Regarding privacy, data is limited to the generated report, which is stored only on the user's device, so its security depends on who has access to the phone. Finally, image interpretation is exclusively aimed at identifying issues in the facility and generating a useful report for corrective actions; it is not intended for malicious purposes, highlighting the need for ethical and responsible use of the tool.

References

[1] Jessica-del-Milagro, P.T., Artificial intelligence in government auditing: emerging ethical challenges. Ciencia Latina Revista Científica Multidisciplinar, 8(4), pp. 5984–5998, 2024. DOI: https://doi.org/10.37811/cl_rcm.v8i4.12812

[2] Reyes, A., AI strategies applied to computer auditing. Technology Rain Journal, 2(2), pp. e18, 2023. DOI: https://doi.org/10.55204/trj.v2i2.e18

[3] Valladares-Albarracín, J.J., and Ordóñez-Parra, Y.L., The application of artificial intelligence in accounting auditing. Multidisciplinary Journal of Research Perspectives, [online]. 4(special), pp. 73–85, 2024. Available at: https://rperspectivasinvestigativas.org/index.php/multidiscipinaria/article/view/172

[4] Tapia-Salvatierra, A.J., Impact of artificial intelligence, blockchain and cloud accounting on the transformation of accounting and auditing practices in Mexico: opportunities, challenges and integration strategies. Ciencia Latina Revista Científica Multidisciplinar, 8(4), pp. 12491–12510, 2024. DOI: https://doi.org/10.37811/cl_rcm.v8i4.13450

[5] Torres, A.B., Rendón, F.G., and Gutiérrez, J.F., Revisión de las técnicas de inteligencia artificial aplicadas en seguridad informática. Revista Ontare, 7, pp. 98–115, 2020. DOI: https://doi.org/10.21158/23823399.v7.n0.2019.2612

[6] Galán-Toral, A.X., and Torres-Palacios, M.M., Optimization of management audit processes through the application of artificial intelligence. EMAC case. Cienciamatria, 10(2), pp. 189–209, 2024. DOI: https://doi.org/10.35381/cm.v10i2.1325

[7] Tosca-Magaña, S.A., Vázquez-Vidal, V., and Martinez-Ortiz, M., The digital revolution in accounting: the impact of artificial intelligence on auditing. FACE: Journal of the Faculty of Economic and Business Sciences, 24(2), pp. 71–78. 2024. DOI: https://doi.org/10.24054/face.v24i2.3119

[8] Ignatov, A., Malivenko, G., Timofte, R., Chen, S., Xia, X., Liu, Z., Zhang, Y., Zhu, F., Li, J., Xiao, X., Tian, Y., Wu, X., Kyrkou, C., Chen, Y., Zhang, Z., Peng, Y., Lin, Y., Dutta, S., Das, S.D., and Shah, N.A., Fast and accurate quantized camera scene detection on smartphones, Mobile AI 2021 Challenge: report. 2021 IEEE/CVF Conference on Computer Vision and Pattern Recognition Workshops (CVPRW), pp. 2558–2568. 2021. DOI: https://doi.org/10.1109/cvprw53098.2021.00289

[9] Bustelo, J.L., The intersection between artificial intelligence (AI), complex thinking, and bias audit methodology. Ibero-American Journal of Complexity and Economic Sciences, 2(4), pp. 5–16, 2024. DOI: https://doi.org/10.48168/ricce.v2n4p5

[10] Lucero, L., The role of computer auditing in the era of personal data protection in Ecuador. Technology Rain Journal, 2(2), pp. e17, 2023. DOI: https://doi.org/10.55204/trj.v2i2.e17

[11] Alcocer-Yunda, V.H., Ausay-Carrillo, C.F., Ávila-Pita, S.P., and Sani-Paguay, A.A., Artificial intelligence and digital transformation in auditing to combat fraud and corruption. Revista Científica Multidisciplinaria InvestiGo, 6(15), pp. 316–328. 2025. DOI: https://doi.org/10.56519/39hf4095

[12] Dastagir, R.V., Jami, J.T., Chanda, S., Hafiz, F., Rahman, M., Dey, K., Rahman, M.M., Qureshi, M., and Chowdhury M.M., AI-driven smartphone solution for digitizing rapid diagnostic test kits and enhancing accessibility for the visually impaired. ArXiv (Cornell University). Art. 7, 2024. DOI: https://doi.org/10.48550/arxiv.2411.18007

[13] Li, X., Tian, Y., Zhang, F., Quan, S., and Xu, Y., Object detection in the context of mobile augmented reality. 2020 IEEE International Symposium on Mixed and Augmented Reality (ISMAR), pp. 156–163. 2020. DOI: https://doi.org/10.1109/ismar50242.2020.00037

[14] Li, Y., Dang, X., Tian, H., Sun, T., Wang, Z., Ma, L., Klein, J., and Bissyandé, T.F., An empirical study of AI techniques in mobile applications. Journal of Systems and Software, 219, Art. 112233, 2025. DOI: https://doi.org/10.1016/j.jss.2024.112233

[15] Feng, R., Chen, S., Xie, X., Meng, G., Lin, S.W., and Liu, Y., A performance-sensitive malware detection system using deep learning on mobile devices. IEEE Transactions on Information Forensics and Security, 16, pp. 1563–1578, 2021. DOI: https://doi.org/10.1109/tifs.2020.3025436

[16] Suo, J., Zhang, W., Gong, J., Yuan, X., Brady, D.J., and Dai, Q., Computational imaging and artificial intelligence: the next revolution of mobile vision. Proceedings of the IEEE, 111(12), pp. 1607–1639, 2023. DOI: https://doi.org/10.1109/jproc.2023.3338272

[17] Ignatov, A., Perevozchikov, G., Timofte, R., Zhang, Z., Gao, T., Yang, Y., Zhu, S., Wang, S., Yoon, K., Gankhuyag, G., Moon, H.C., Jeong, T., Kim, Y., Lee, S., Baek, J., Jeong, J., Park, E., Lee, J., Lee, H., and Kim, S., Quantized image super-resolution on mobile NPUs, Mobile AI 2025 Challenge: Report. 2025 IEEE/CVF Conference on Computer Vision and Pattern Recognition Workshops (CVPRW), pp. 1899–1912. 2025. DOI: https://doi.org/10.1109/cvprw67362.2025.00179

[18] Eulerich, M., Masli, A., Pickerd, J., and Wood, D.A., The impact of audit technology on audit task outcomes: evidence for technology-based audit techniques. Contemporary Accounting Research, 40(2), pp. 981–1012. 2023. DOI: https://doi.org/10.1111/1911-3846.12847

[19] Leocádio, D., Malheiro, L., and Reis, J., Artificial intelligence in auditing: a conceptual framework for auditing practices. Administrative Sciences, 14(10), Art. 238, 2024. DOI: https://doi.org/10.3390/admsci14100238

[20] Ilori, O., Nwosu, E., and Naiho, A., Enhancing IT audit effectiveness with agile methodologies: a conceptual exploration. Engineering Science and Technology Journal, 5(6), pp. 1969–1994, 2024. DOI: https://doi.org/10.51594/estj.v5i6.1217

[21] Gauthier, J., and Brender, N., How do the current auditing standards fit the emergent use of blockchain? Managerial Auditing Journal, 36(3), pp. 365–385. 2021. DOI: https://doi.org/10.1108/MAJ-12-2019-2513

F. G. Huamanchumo Trujillo
Systems Engineering Student School of Systems Engineering National University of Trujillo.
ORCID: 0009-0007-1937-4036

A. R. Campos Gamarra
Systems Engineering Student School of Systems Engineering National University of Trujillo
ORCID: 0009-0009-8492-1133

R. A. Guevara Saldaña
Systems Engineering Student School of Systems Engineering National University of Trujillo
ORCID: 0009-0002-6323-3517

A. C. Mendoza de los Santos
PhD in Systems Engineering and Informatics Department of Systems Engineering National University of Trujillo
ORCID: 0000-0002-0469-915X

DYNA
http://dyna.medellin.unal.edu.co/

UNIVERSIDAD NACIONAL DE COLOMBIA

Landsat 8-based estimation of total suspended solids (1.3-43 mg/L) using NDWI, MNDWI and AWEI indices at Tecocomulco Ramsar Wetland, Mexico

Ismael Ortega-García, René Cruz-Guerrero & German Cuaya-Simbro

Instituto Tecnológico del Oriente del Estado de Hidalgo, Tecnológico Nacional de México, Sahagún, Hidalgo, México. 23030537m@itesa.edu.mx, rcruz@itesa.edu.mx, gcuaya@itesa.edu.mx

Received: May 11th, 2025. Received in revised form: November 5th, 2025. Accepted: December 1st, 2025.

Abstract
This study integrates Landsat 8 multispectral imagery and three water segmentation indices (NDWI, MNDWI, AWEI) to estimate Total Suspended Solids (TSS) concentrations in Tecocomulco Lagoon, a Ramsar wetland in Hidalgo, Mexico. Using Google Earth Engine for image acquisition and Python-based processing with Rasterio and NumPy libraries, we applied the TSS algorithm: TSS = (RED/NIR) × F, where F=10 was calibrated against in-situ measurements. Eight spectral bands were processed from cloud-free images (<50% coverage) captured between January-December 2023. Results showed TSS concentrations ranging from 1.3 to 43 mg/L, with strong correlation ($r=0.89$, $p<0.05$) against CONAGUA reference data from three monitoring sites. Statistical validation yielded RMSE=4.2 mg/L, MAE=3.5 mg/L, and $R^2=0.79$. The combined use of three indices improved water body segmentation accuracy compared to single-index approaches. This methodology provides cost-effective monitoring for the 1,769-ha wetland, supporting conservation efforts for 15 duck species and the endangered Ambystoma mexicanum. The approach offers a replicable framework for TSS monitoring in similar high-sedimentation wetlands.

Keywords: remote sensing; Tecocomulco; Ramsar; satellite images.

Estimación basada en Landsat 8 de sólidos suspendidos totales (1.3-43 mg/L) usando los índices NDWI, MNDWI y AWEI en el Humedal Ramsar de Tecocomulco, México

Resumen
Este estudio integra imágenes multiespectrales de Landsat 8 y tres índices de segmentación de agua (NDWI, MNDWI, AWEI) para estimar las concentraciones de Sólidos Suspendidos Totales (SST) en la Laguna de Tecocomulco, un humedal Ramsar en Hidalgo, México. Utilizando Google Earth Engine para la adquisición de imágenes y procesamiento basado en Python con las bibliotecas Rasterio y NumPy, aplicamos el algoritmo de SST: SST = (ROJO/NIR) × F, donde F=10 fue calibrado con mediciones in situ. Se procesaron ocho bandas espectrales a partir de imágenes libres de nubes (<50% de cobertura) capturadas entre enero y diciembre de 2023. Los resultados mostraron concentraciones de SST que oscilaron entre 1.3 y 43 mg/L, con una fuerte correlación ($r=0.89$, $p<0.05$) respecto a los datos de referencia de CONAGUA provenientes de tres sitios de monitoreo. La validación estadística arrojó RMSE=4.2 mg/L, MAE=3.5 mg/L y $R^2=0.79$. El uso combinado de los tres índices mejoró la precisión de la segmentación del cuerpo de agua en comparación con los enfoques de índice único. Esta metodología proporciona un monitoreo eficaz para el humedal de 1,769 ha, apoyando los esfuerzos de conservación de 15 especies de patos y del Ambystoma mexicanum, especie en peligro de extinción. El enfoque ofrece un marco replicable para el monitoreo de SST en humedales similares con alta sedimentación.

Palabras clave: teledetección; Tecocomulco; Ramsar; imágenes satelitales.

How to cite: Ortega-García, I., Cruz-Guerrero, R. and Cuaya-Simbro, G., Landsat 8-Based estimation of total suspended solids (1.3-43 mg/L) using NDWI, MNDWI and AWEI indices at Tecocomulco Ramsar Wetland, Mexico DYNA, (93)240, pp. 36-45, January - March, 2026.

1. Introduction

There is currently a growing concern about water resources, due to the increase in temperature caused by climate change, which together with human activities, directly impact the disappearance of aquatic ecosystems, as in the case of Tecocomulco and other lakes in the basin of the Valley of Mexico [1], which has driven the application of computer vision technologies for the analysis of images captured by satellites, which orbit the earth performing environmental monitoring missions. Traditionally, water quality assessment is performed by in situ sampling that is subsequently analyzed in the laboratory, processes that are costly and limited in terms of spatial and temporal coverage. The Tecocomulco lagoon, recognized as a Ramsar site since 2003, faces problems derived from agricultural practices, indiscriminate logging, urbanization, and untreated waste, which have deteriorated water quality and consequently affected biodiversity and the health of riparian communities [2].

Nowadays, remote sensing is a promising alternative that allows obtaining data on a large spatial scale, through access to collections of satellite images and spatial data sets. Computational processing facilitates the interpretation of large volumes of data, extracting patterns and quantifying physicochemical parameters from the measurement of their reflectance on the Earth's surface, by measuring solar radiation, the images obtained are representations of wavelengths ranging from infrared to ultraviolet [3]. In addition, the use of satellites for earth surface observation has been constantly improved since the first space missions in the 1960s, capturing increasingly accurate images and data through sensors, such as Operational Land Imager (OLI) and Thermal Infrared Sensor (TIRS) of the Landsat missions led by the National Aeronautics Administration of the United States NASA.

Remote sensing as a technological discipline based on sciences such as physics, computing or geography, allows the application of techniques for the study of the earth's surface. Currently, the images obtained by the satellite missions of various space agencies are available for access and download in various digital platforms, such as: Google Earth Engine (GEE), Copernicus, USGS Browser Earth, etc. This article reports the research where the amount of Total Suspended Solids (TSS), considered as an optically active parameter, is calculated [4]. The calculation was made from images taken by the Landsat 8 satellite, which captures the study area every 16 days, allowing to regularly identify variations in water quality, making it possible to perform environmental monitoring of a wetland of great ecological importance such as Tecocomulco.

Previous studies have successfully applied TSS algorithms to various water bodies. Ritchie et al. (1987) [5] established the foundational correlation between red and NIR bands for sediment detection. Gómez & Dalence (2014) [6] validated similar approaches in the Bogotá River, achieving correlations of $r>0.85$. However, applications to high-altitude endorheic wetlands with significant agricultural impact remain limited. This study addresses this gap by adapting established algorithms to the unique conditions of Tecocomulco, an endorheic wetland at 2,514 m.a.s.l. characterized by high sedimentation and turbidity rates due to agricultural erosion [2], with fluctuating water levels influenced by seasonal precipitation patterns [1].

The Tecocomulco lagoon is located in the state of Hidalgo and comprises a regular area of 1,769 ha, with coordinates 19º52'N 098º23'W [7], this body of water arose during the Plio-Cuaternary (~3 million years ago) due to tectonic processes associated with the subduction of the Cocos plate under the North American plate. Volcanic activity in this area included the formation of dacite rock domes, basaltic lava flows and scoria cones, aligned with regional northeast-southeast oriented faults [8]. The volcanic activity created depressions and structures that facilitated the accumulation of water, contributing to the formation of lake bodies such as the Tecocomulco lagoon, whose location can be observed in Fig. 1, according to the visualization platform of the National Water Information System (SINA) of the National Water Commission, a Mexican state agency.

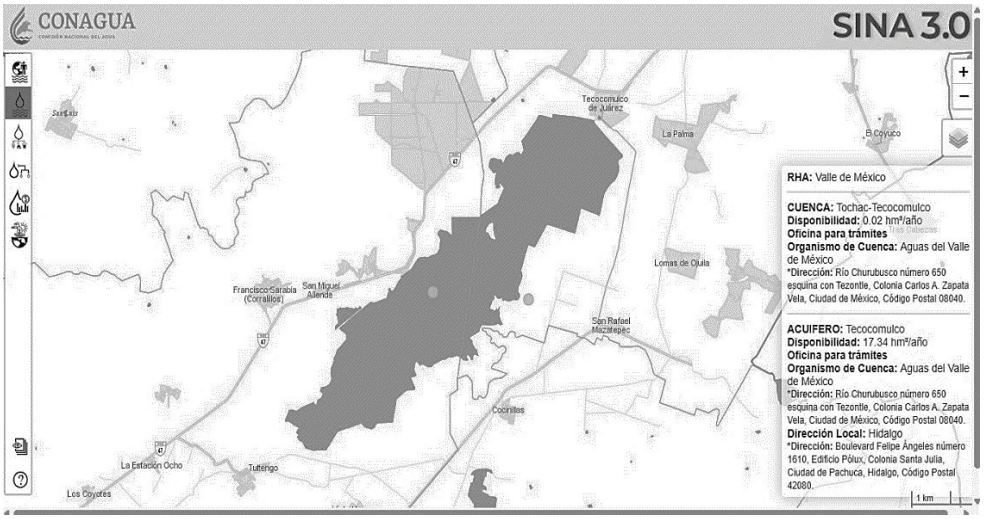

Figure 1. Screenshot of the SINA website where the country's main water bodies are monitored.
Source: Own elaboration. https://sinav30.conagua.gob.mx:8080/SINA/?opcion=acuiferos

Likewise, the Tecocomulco endorheic basin is located at 2514 (m.a.s.l.) and is considered part of the remnants of the ancient freshwater wetland system, which dominated the valley of Mexico basin in the center of the country 500 years ago. The underlying aquifers are recharged through the lake, whose water level is fluctuating due to the impact of meteorological phenomena causing extended periods of rain or drought [1]. The site is notable for the presence of 15 species of ducks, with congregations of ruddy ducks Oxyura jamaicensis of up to 5000 individuals, and coots Gallinula chloropus of up to 3000 [2].

The endangered salamander Ambystoma mexicanum also inhabits this body of water, threatened by invasive species such as the Asian carp (Cyprinus carpo), a non-endemic species that is commercially exploited by local fishermen. Given such a diverse biological environment, there are portions of fauna for waterfowl hunting, which is practiced during the winter and is a relevant economic activity for some people in the communities. Erosion of the basin caused by agricultural activities, logging, and overgrazing have caused a high rate of sedimentation and turbidity in the lake, which is identified in the Ramsar site catalog with the number 1322 [7].

The importance of the Tecocomulco lagoon has been internationally recognized since 2003 with its declaration as a Ramsar site, a category that emerged in 1971 in the convention that Mexico signed as a contracting party, as did 90% of the member states of the United Nations [7]. This importance lies in its ecological value due to its biodiversity and the environmental functions that characterize this lentic wetland. Its importance is key in the central migratory route of the North American region, which is evidenced by the birds such as the white pelican (Pelecanus erythrorhynchos), the Mexican duck (Anas diazi), the white heron (Ardea alba), the gray crane (Grus canadensis) and endangered species such as the common scoter (Emberiza schoeniclus) [9]. It also serves as a refuge during the nesting stages, which are critical for the development of these species.

With a significant reduction in recent decades, the natural reservoir located in the municipalities of Tepeapulco, Apan and Cuautepec in the state of Hidalgo is of great importance for international associations such as Ducks Unlimited de México, A.C. (DUMAC), who offer relevant information on Ramsar sites on their map server, as can be seen in Fig. 2. (DUMAC), who offer relevant information of the Ramsar sites in their cartographic server, as can be seen in Fig. 2, this project allows the visualization of wetlands of great importance for migratory species, where through various layers presents the characteristics of wetland coverage, as a sample of the development of useful computer applications for water management.

Research question: Can the Landsat 8 spectral band algebra (RED/NIR relationship) accurately estimate TSS concentrations in aquatic areas segmented by multiple indices in the Tecocomulco lagoon, as validated by measurements from government institutions?

Objectives:

- Demonstrate the opportunity in the use of satellite imagery for the analysis of physico-chemical parameters of water in the Tecocomulco Lagoon.
- To apply and validate computational algorithms for segmentation and pattern recognition and computational processing in different areas of aquatic coverage shown in satellite images of the Tecocomulco wetland.
- Compare the results obtained for SST parameters with historical measurements reported by official agencies.

Figure 2. Geographic location of the Tecocomulco lagoon as seen on the DUMAC map server, which presents coverage characteristics of wetlands relevant to migratory species.
Source: Own elaboration

2. Methods and materials

2.1 Measurement of reflectance and spectral signature

Reflectance is an optical property of all surfaces and describes the portion of incident radiation that is capable of being reflected by that surface. It is commonly expressed as a percentage and is the physical principle that allows the inference of crustal characteristics in remote sensing. The measurement of reflectance is performed through sensors that are capable of capturing the reflected radiation at different wavelengths of the electromagnetic spectrum, in Fig. 3 can be seen the different wavelengths of which only a small portion is visible to the human eye.

For the capture of satellite images, according to Richards and Jia (2006) [3], a typical process can be considered as one that involves the capture of data through a sensor that captures the radiation from the earth's surface, followed by the correction of solar irradiance before reflection, then corrections that normalize light absorption and scattering to obtain more accurate values, finally reflecting in a reflectance value that can be used for computational analysis of multispectral images in remote sensing studies.

Each material on the earth's surface has a spectral signature, which can be considered as a graphic representation of the reflectance or emissivity as a function of the wavelength emitted by that material, so that vegetation, buildings or water have a unique spectral signature that is due to their physical-chemical properties and allows the identification of different materials on the earth's surface, through computational algorithms that operate directly with images and data captured by satellite sensors, which record the reflectance of lengths in specific ranges of the electromagnetic spectrum.

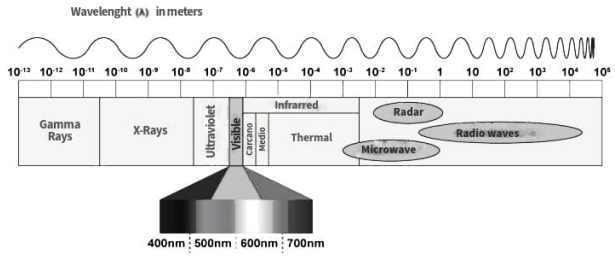

Figure 3. Graphical representation of the electromagnetic spectrum showing the wavelengths at which light is transmitted, indicating the spectrum visible to the human eye.
Source: Own elaboration

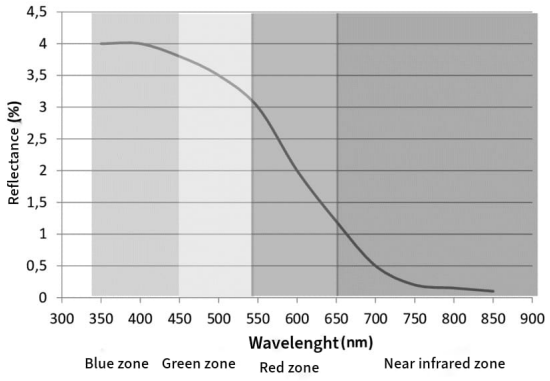

Figure 4. Graphical representation of the spectral signature of water in its pure form.
Source: Own elaboration

In Fig. 4 we can observe the spectral signature of water in its purest form, according to a study by Drozd & Fernandez (2016) [10] where different spectral signatures are analyzed for segments of the Uruguay River. It should be noted that the composition of surface water bodies becomes more complex as there are more variables, such as aquatic vegetation, climatic conditions or irregularities caused by the topographic circumstances of the terrain under study [10].

2.2 Water quality and total suspended solids

According to Richards & Jia (2016) [3], water quality is the set of physical, chemical and biological characteristics that determine its suitability for a specific use, among which human consumption, agriculture, industry, recreation and conservation of the aquatic ecosystem can be considered. These conditions can be affected mainly by the presence of chemical substances such as heavy metals, nutrients (nitrates and phosphates) and the presence of biological agents such as viruses or bacteria, affecting public health, the effectiveness of agriculture and the sustainability of the ecosystem in general.

The physical conditions of the water, such as turbidity, temperature, amount of suspended solids and color, can influence the life of aquatic organisms and the economic activities carried out by the population around the body of water, such as recreational and tourist activities, which have a direct impact on the economy of the communities.

The measurement of Total Suspended Solids (TSS) can be considered relevant in the determination of water quality as it is an indicator of pollution, since suspended particles can include sediments, organic matter, microorganisms and chemical contaminants. Therefore, high TSS levels can signal a deterioration of water quality due to increased human activities such as agricultural runoff or excessive erosion of

Figure 5. Photograph showing the transparency of the water, which at first sight reveals the aquatic vegetation of the natural reservoir. Taken on March 8, 2025.
Source: Own elaboration.

the watershed. The impact of high TSS levels in the water body darkens the aquatic environment, causing a decrease in light penetration, affecting the photosynthesis of algae and aquatic plants, thus altering the food chain and generating direct effects on biodiversity [3] The measurement of this parameter can be an indicator of water quality, because it reveals the dry weight of the particles present in the water column and is represented in units of mg/L [4]. Fig. 5 shows an image captured in the water mirror of the Tecocomulco lagoon, where the level of transparency of the reservoir can be observed in some areas.

2.3 Determination of the study area

The study of a water body requires the georeferential location to delimit the geographic area to be analyzed. This procedure is key in obtaining the results sought, known as ROI. The region of interest is defined by the coordinates of the longitude and latitude vertices of the area from which the satellite images are obtained. In our case, this delimitation was performed using USGS Explorer, as shown in Fig. 6, where the polygon was defined with the coordinates: [-98.442135, 19.833731, -98.335018, 19.906703], indicating the vertices that delimit the area and are subsequently used in the access platform for Landsat 8 collections.

2.4 Calculation of indices for water body segmentation and TSS measurement through band algebra

Once the study area was chosen, it was necessary to segment the aquatic coverage surface, since this is where the TSS calculation will be performed. For this task, there are several computer vision algorithms, such as edge detection and the application of filters. However, those that are best suited to work with georeferenced images, such as satellite collections, are the calculation of indices, which performs direct algebraic operations on the spectral bands, represented as matrices of reflectance of each of the pixels of the image, as shown in Fig. 7.

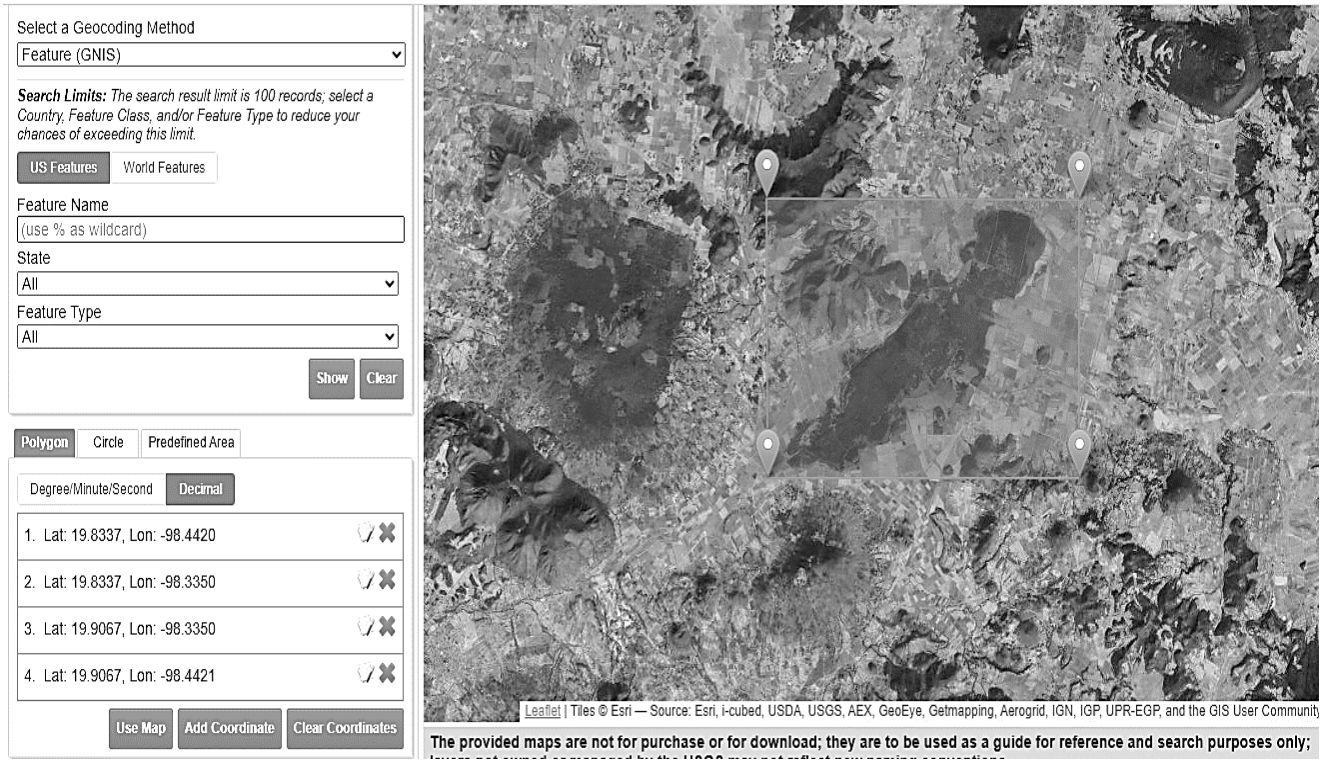

Figure 6. Definition of the region of interest: drawing a polygon in the USGS Earth Explorer platform to delimit the area comprising the Tecocomulco lagoon.
Source: Own elaboration

The use of indices to differentiate surface water from other elements of the landscape, due to their spectral properties, is one of the ways in which a water body can be segmented using the spectral bands of a satellite image. The NDWI index (Normalized Difference Water Index), proposed by McFeeters in 2013, uses the green and near-infrared (NIR) bands of satellite images, taking advantage of the high absorption of water in the wavelength range between 700 and 2500 nm of the NIR band and its moderate reflectance in the green, which allows for the highlighting of water masses. However, this index can overestimate urban areas and suffer interference from vegetation, thus reducing the area represented compared to the actual surface of the reservoir [11].

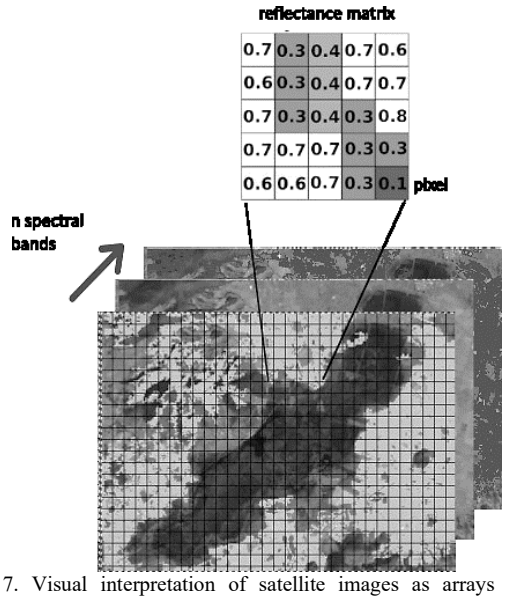

Figure 7. Visual interpretation of satellite images as arrays of pixel reflectance.
Source: Own elaboration

The use of indices to differentiate surface water from other elements of the landscape, due to their spectral properties, is one of the ways in which a water body can be segmented using the spectral bands of a satellite image. The NDWI index (Normalized Difference Water Index), proposed by McFeeters in 2013, uses the green and near-infrared (NIR) bands of satellite images, taking advantage of the high absorption of water in the wavelength range between 700 and 2500 nm of the NIR band and its moderate reflectance in the green, which allows for the highlighting of water masses. However, this index can overestimate urban areas and suffer interference from vegetation, thus reducing the area represented compared to the actual surface of the reservoir [11].

Normalized Differentiated Water Index (NDWI)

$$NDWI = \frac{(NIR - SWIR)}{(NIR + SWIR)} \quad (1)$$

Where:
NIR: Near Infrared (SR_B5)
SWIR: Show Wave Infrared (SR_B6)

To improve the representation of the aquatic surface, the MNDWI (Modified Normalized Difference Water Index) will also be used, which replaces the NIR band with the shortwave infrared (SWIR) band that captures wavelengths between 900 and 2500 nm, improving the separation between water and built-up areas, since the latter reflect the SWIR to a lesser extent [12]. This makes it possible to capture water surfaces more effectively in complex environments [13].

Modified Normalized Difference Water Index

$$MNDWI = \frac{(GREEN - SWIR)}{(GREEN + SWIR)} \quad (2)$$

Where:
GREEN = Green spectral band (SR_B3)

For its part, the AWEI (Automated Water Extraction Index) was developed by Feyisa et al. (2014) [14], combines multiple bands such as those of the visible spectrum, NIR, and SWIR, and can be implemented together with dynamic thresholds (such as Otsu's algorithm) to minimize false positives caused by shadows, clouds, or barren soils. Its design makes it a robust index in various environmental conditions [15].

Automated Water Withdrawal Index

$$AWEI = 4 * (GREEN - SWIR) - (0.25 * NIR) + (2.75 * SWIR) \quad (3)$$

The calculation of TSS sediment concentration by remote sensing is based on the relationship between water surface reflectance and the presence of suspended particles. Studies such as that of Ritchie et al. (1987) [5] have demonstrated the correlation between the red (600-700 nm) and near-infrared (700-800 nm) spectral bands, which are particularly sensitive to reflectance caused by suspended sediments in the water column. The authors, pioneers in the development of these studies, developed linear and nonlinear regression models that establish a relationship between atmospheric reflectance and TSS concentration. In addition, more recent studies have verified this correlation in measurements of this type in various surface aquifers, as reported in measurements made with spectral bands in the Bogotá River basin in Colombia [6].

The equation that determines the amount of TSS is as follows:

$$SST = \frac{RED}{NIR} * F \quad (4)$$

Where:
SST: Total Suspended Solids in mg/L.
RED: Red spectral band (SR_B4).
NIR: Near Infrared (SR_B5)
F: Scale factor according to the measurement.

2.5 Data collection and preprocessing

The satellite images were obtained through the development of a code created in the JavaScript language on the web development platform provided by GEE, which allows access to collections of satellite images ready for computational processing. Fig. 8 shows the interface for accessing USGS satellite images through GEE, which, once obtained, can be downloaded directly to the Google Drive file hosting service.

The images obtained from the spectral bands are downloaded to Drive with a TIF extension; these belong to the Landsat 8 Collection 2 Level 1, processed by the United States Geological Survey (USGS). These satellite image collections are available and have been prepared for computational processing.

Figure 8. Capture of the platform for access to satellite imagery and geospatial datasets. (GEE, 2025).
Source: Own elaboration

The USGS applies advanced algorithms to remove distortions caused by aerosol scattering, solar reflectance, and terrain topography, thus ensuring that the data represent realistic surface reflectance values. This standardized preprocessing allows users of the spectral bands to access information ready for computational analysis and calculation of spectral indices without requiring additional adjustments [16].

Data available at USGS Level 1 are radiometrically and geometrically calibrated, achieving better georeferencing, with an RMSE ≤ 12 m, using ground control points and digital elevation models. This collection includes multispectral (30 m), panchromatic (15 m), and thermal bands, in addition to key metadata such as cloud cover, date of capture, and solar/sensor angles. Tier 1 consists of Tier 1 (highest quality) and Tier 2 (which includes scenes with geometric or cloudiness limitations). Quality bands (QA_PIXEL/RADSAT) for automated filtering and optimized formats (COG) are incorporated into this collection, ensuring accuracy and compatibility with computational processing in the cloud [16].

2.6 Phyton and Rasterio

The use of Python together with the Rasterio library allows for the efficient processing of satellite images to calculate the amount of TSS in mg/L. Rasterio is an API that facilitates the reading of spectral bands (GeoTIFF) and their analysis using NumPy, making it possible to use mathematical operations to combine spectral bands and calculate physico-chemical indices of land surface areas with accurate georeferencing. Development with Python makes the analysis from pixels to the complete scene possible in a simple way. By means of matrix operations, the formulas described above are implemented.

This integration makes it possible to calculate TSS at the pixel level, generating visual representations of the TSS measurement distribution that serve to identify zones with different sediment concentrations, thus optimizing the water quality analysis in the Tecocomulco Lagoon [6].

The study is based on a multi-paradigm approach, integrating Remote Sensing, digital image processing, and software development. The primary data came from multispectral images from the Landsat 8 satellite (Collection 2 Level 1), acquired through the Google Earth Engine (GEE) platform and processed with JavaScript for the extraction of spectral bands. The calculation of Total Suspended Solids (TSS) was implemented in Python 3.1, using the libraries Rasterio (GeoTIFF data reading/manipulation), NumPy (for band algebra implementation), and OpenCV (JET color mapping for visualization). Statistical validation included correlation analysis (rr coefficient) between derived SST and CONAGUA in situ data, plus dynamic normalization using percentiles (2% and 98%) to adjust the range of values. Calibration of the scaling factor (F = 10) was based on previous studies in lentic wetlands [6].

The temporal scope covered January to December 2023, with 23 cloud-free scenes (<50% coverage) analyzed. Images were selected based on the 16-day Landsat 8 revisit cycle, prioritizing dry season captures (November-April) when TSS variability is highest. The three indices were integrated through Boolean algebra: Water_Mask = (NDWI > 0) AND (MNDWI > 0.1) OR (AWEI > -0.5), with thresholds determined via Otsu's algorithm.

The graphical interface (GUI), developed with Tkinter, allows for loading images in GeoTIFF format and visualizing measurement results in the area of aquatic coverage segmented by MNDWI, NDWI, and AWEI indices. In addition, a visualization of histograms and spectral signatures is generated using Matplotlib. The Rasterio library version used is 1.3.9, and cloudiness thresholds were defined (<50%). The validation data are available in the National Water Information System (SINA), ensuring methodological transparency [17]. Table 1 shows the values reported by CONAGUA for TSS measurements in three regions of the reservoir.

Table 1.
TSS measurement data in the Tecocomulco lagoon.

Site Key	Year	Zone	SST mg/L
DLHID1483	2023	THE ISLET LAGOON OF TECOCOMULCO	30
DLHID1484	2023	THALIMEDES LAGOON TECOCOMULCO	<25
DLHID1485	2023	TULTENGO LAGOON OF TECOCOMULCO	40

Carried out by CONAGUA and accessible in the National Water Information System.
Source:Own elaboration

3. Results and discussion

3.1 Results

The comparative evaluation of the collected data allowed for the observation of a solid correlation ($r > 0.89$) between the derived spectral indices and the laboratory analyses available on the SINA site of CONAGUA. The capacity of the segmentation algorithm using the NDWI, MNDWI, and AWEI indices allows for an improvement in segmentation compared to the use of only one index, as observed in the area detected as surface water; as shown on the left side of Fig. 9, this value is much lower than that observed on the right side. For this reason, in order to perform the segmentation more effectively, it was necessary to identify the area of aquatic coverage using more than one index.

Fig. 10 shows the interface developed in Python to load multispectral images from the Landsat 8 satellite, specifically designed to process the red (SR_B4) and near-infrared (SR_B5) spectral bands, which are essential for the calculation of Total Suspended Solids. The interface allows loading files in TIF format, guaranteeing the integrity of the geo-referenced data. The 'Calculate TSS' button activates the automatic processing of the images by means of matrix operations with the Rasterio and NumPy libraries, following the algorithm that implements the formula explained in the methodology section.

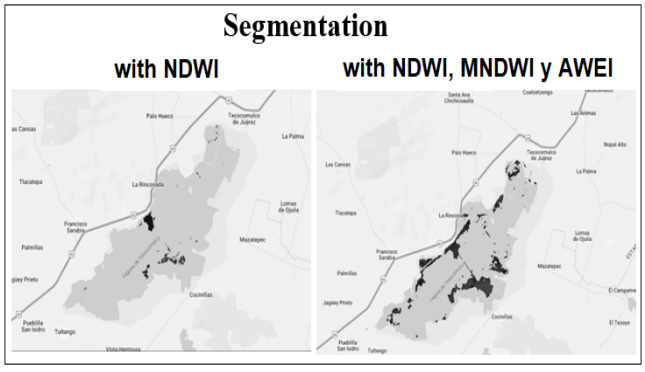

Figure 9. Segmentation masks captured from the calculation of the NDWI index in the first column and NDWI + NDWI + AWEI in the second column, from spectral images obtained from the Landsat 8 satellite through JavaScript code in the GEE platform.
Source:Own elaboration.

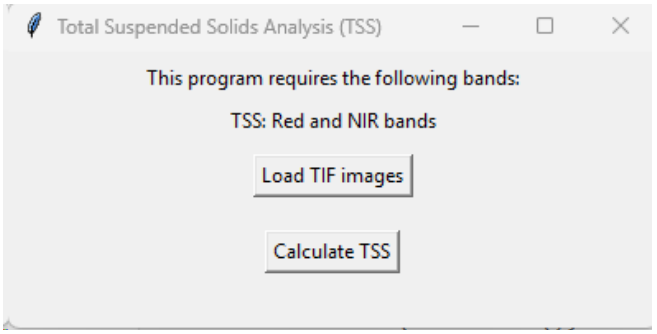

Figure 10. Interface of the module developed in Python for loading spectral bands and their computational processing.
Source: Own elaboration

The processing results are presented in Fig. 11. In the upper box, the area of surface water coverage can be seen on a color scale from blue to red, where the latter represents the highest TSS mg/L measurements, with a value not calculated (NaN) in non-aquatic areas.

To validate the accuracy of remote sensing algorithms in estimating Total Suspended Solids (TSS) in the Tecocomulco Lagoon, values derived from Landsat 8 images (processed in Python) were compared with in situ data reported by CONAGUA (Table 2).

The statistical metrics used for validation were the Pearson Correlation Coefficient (r), Root Mean Square Error (RMSE), Bias, Mean Absolute Error (MAE), and Coefficient of Determination (R^2), as shown in Table 2.

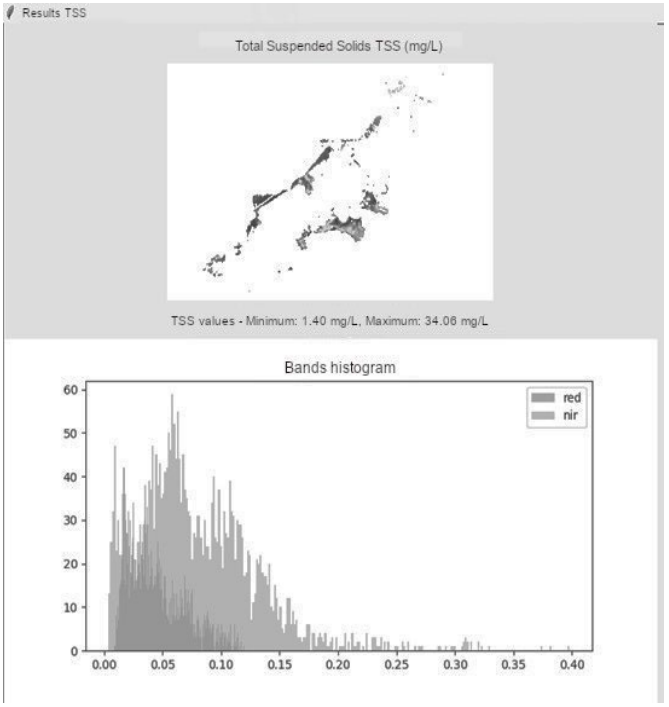

Figure 11. Presentation of results from the Python module for calculating TSS in mg/L at the water surface of the Tecocomulco Lagoon.
Source: Own elaboration.

Table 2
Use metrics to evaluate the correlation between results obtained from remote sensing and those from CONAGUA's SINA.

Metrics	Value	Equiation	Interpretation
Pearson's correlation coefficient (r)	$r = 0.89$ $(p < 0.05)$	$r = \frac{\sum(x_i - \bar{x})(y_i - \bar{y})}{\sqrt{\sum(x_i - \bar{x})^2 \sum(y_i - \bar{y})^2}}$	It indicates a strong and statistically significant correlation.
Mean Squared Error RMSE	4.2 mg/L	$\text{RMSE} = \sqrt{\frac{1}{n}\sum_{i=1}^{n}(y_i - \hat{y}_i)^2}$	It suggests a moderate discrepancy between the methods.
Bias	+1.8 mg/L	$\text{Sesgo} = \frac{1}{n}\sum_{i=1}^{n}(y_i - \hat{y}_i)$	This implies a slight underestimation by the satellite.
Mean Absolute Error MAE	3.5 mg/L	$\text{MAE} = \frac{1}{n}\sum_{i=1}^{n}\lvert y_i - \hat{y}_i\rvert$	It represents acceptable accuracy for monitoring applications.
Coefficient of Determination (R^2)	0.79	$R^2 = 1 - \frac{\sum_{i=1}^{n}(y_i - \hat{y}_i)^2}{\sum_{i=1}^{n}(y_i - \bar{y})^2}$	It indicates that 79% of the variability in the laboratory data is explained by the model.

Source: Own elaboration

3.2 Discussion

The linear relationship between satellite data and data obtained through laboratory studies of in situ samples validates the use of RED and NIR bands to estimate the SST parameter in turbid waters, consistent with previous studies [6], such as that of Gómez & Dalence (2014). The accuracy shown by the RMSE metric is comparable to other studies in lentic wetlands [6], although calibrating the scale factor (F) with a greater number of iterations is suggested. Meanwhile, the positive bias can be interpreted as an underestimation that could be due to atmospheric interference or the spatial resolution of Landsat 8 (30 m/pixel), which averages values in heterogeneous areas. Finally, the scarcity of data restricts statistical robustness. Similar studies recommend expanding the validation with more sampling at different times of the year.

The observed RMSE of 4.2 mg/L and positive bias of +1.8 mg/L are within acceptable ranges for operational monitoring, comparable to Gómez & Dalence's (2014) [6] findings in Colombian wetlands (RMSE = 5.1 mg/L). The 30m spatial resolution limitation could be addressed in future studies using Sentinel-2 imagery (10m resolution). The underestimation bias likely results from sub-pixel mixing in shallow areas (<1m depth) where bottom reflectance influences the signal. Ecologically, the TSS range of 1.3-43 mg/L indicates moderate to high turbidity levels that may impact submerged vegetation photosynthesis and benthic invertebrate communities, critical food sources for migratory waterfowl.

4. Conclusions

This study has shown that the integration of remote sensing, spectral indices, and segmentation models constitutes an effective methodology for the delineation and analysis of water bodies in complex environments, thus answering our research question. The application of NDWI, MNDWI, and AWEI allowed for the accurate identification of water surfaces, reducing overestimation in urban areas and minimizing vegetation interference. Thanks to the use of satellite images from the Landsat 8 mission and their preprocessing in Google Earth Engine (GEE), the extraction of relevant data was facilitated, thus optimizing the spectral analysis of water quality.

The correlation found between spectral values and in situ measurements supports the validity of this methodology for environmental monitoring aimed at water management. On the other hand, the integration of computational tools, such as Python and Rasterio, into data processing has been crucial for satellite image processing, ensuring the consistency and reliability of the results. However, certain limitations have been identified that should be considered in future research. The spatial resolution of the sensors used may be insufficient to detect microvariations in smaller bodies of water, suggesting that incorporating higher-resolution images or combining them with data from airborne sensors could improve the accuracy of the analysis. Furthermore, atmospheric conditions during image capture can influence data quality, highlighting the need to implement improvements in radiometric correction algorithms and consider interpolation techniques to minimize these effects.

Finally, the findings of this study underscore the relevance of remote sensing and machine learning in water resources management and monitoring. Automating segmentation and spectral analysis reduces the dependence on physical sampling, thus optimizing water quality assessment processes and facilitating decision-making in environmental policies. This methodology demonstrates the practical application of established remote sensing techniques to a previously unstudied high-sedimentation wetland, providing baseline TSS data for future monitoring programs.

References

[1] Lanza, G., and Gomez, G., Analysis of the short term geo-environmental evolution of an endorreic basic using satelital images: the caso of Tecocomulco Lagoon, México: Investigaciones

Geográficas, Boletín del Instituto de Geografía, UNAM, (58), pp. 66-79, 2005. DOI: https://doi.org/10.14350/rig.30048
[2] Delgadillo, A.E., Determinación de parámetros fisicoquímicos, estado eutrófico y metales pesados de la laguna de Tecocomulco, Hidalgo; identificación de compuestos quelantes de Hydrocotyle ranunculoides L.f., Instituto de Ciencias Básicas e Ingeniería, UAEH, [online]. (58), pp. 1-4, 2012. Available at: http://www.scielo.org.mx/scielo.php?script=sci_arttext&pid=S0188-46112005000300005&lng=es&nrm=iso
[3] Richards, J.A., and Jia, X., Remote sensing digital image analysis, Berlin: Springer, pp. 265-278, 2005. DOI: https://doi.org/10.1007/3-540-29711-1
[4] Sabry, F., Teledetección del agua: avances en técnicas de visión por computadora para la teledetección del agua, Madrid: mil millones de conocimientos, 2024.
[5] Ritchie, J.C., Cooper, C.M., and Yongqing, J., Using landsat multispectral scanner data to estimate suspended sediments in moon lake, mississippi., Remote Sensing of Environment, 23(1), pp. 65-81, 1987. DOI: https://doi.org/10.1016/0034-4257(87)90071-X
[6] Gómez-Diaz, J.L., and Delance-Martinic, J.S., Determinación del parámetro sólidos suspendidos totales (SST) mediante imágenes de sensores ópticos en un tramo de la cuenca media del río Bogotá (Colombia)., Revista UD y la Geomática, 9, pp. 19-27, 2014. DOI: https://doi.org/10.14483/23448407.7943
[7] Secretariat-Ramsar-Convention, The list of wetlands of international importance, ramsar convention, [online]. pp. 34, 2005, Available at: https://www.ramsar.org/sites/default/files/documents/library/sitelist.pdf
[8] García-Tovar, G.P., Martínez-Serrano, R.G., Sole, J., Correa-Tello, J.C., Núñez-Castillo, E.Y., Guillou, H., and Monroy-Rodríguez, E., Geology, geochronology and geochemestry of the Plio-Quaternary volcanism of the Apán-Tecocomulco Volcanic Field, Transmexican Volcanic Belt, Revista Mexicana de Ciencias Geologicas, [online]. 32(1), pp. 100-122, 2015. Available at: https://www.scielo.org.mx/scielo.php?script=sci_arttext&pid=S1026-87742015000100009&lng=es&nrm=iso
[9] Apolonio-Ortega, L.A., La evaluación de la avifauna de la Laguna de Tecocomulco y alrededores, estado de Hidalgo: prioridades de conservación., Ciudad de México: Facultad de Ciencias UNAM, [online]. 2017. Available at: https://repositorio.unam.mx/contenidos/400714
[10] Drozd, A., and Fernandez, V., Capítulo VII: Caracterización de firmas espectrales en distintos tramos del río Uruguay y su relación con variables biológicas y físicas del agua. Informe de actividades de investigación de la subcomisión de medio ambiente y uso sostenible del agua, estudio de la calidad del agua en el río Uruguay vigilancia de playas y estado trófico., Montevideo, Universidad de la República de Uruguay, [online]. 2016, pp. 298-308. Available at: https://www.caru.org.uy/web/sub_medio_ambiente/Informe%20Bienal%202013-14.pdf
[11] McFeeters, S.K., Using the Normalized Difference Water Index (NDWI) within a geographic information system to detect swimming pools for Mosquito Abatement: a practical approach, Department of Geography, California State University Fresno, 2013, pp. 3544-3561. DOI: https://doi.org/10.3390/rs5073544
[12] Xu, H., Modification of Normalized Difference Water Index (NDWI) to enhance open water features in remotely sensed imagery. International Journal of Remote Sensing, 27(14), pp. 3026-3033, 2006. DOI: https://doi.org/10.1080/01431160600589179
[13] Kulkarni, R., Khare, K., and Khanum, H., Detecting, extracting, and mapping of inland surface water using Landsat 8 operational land imager: a case study of Pune district, India., F1000Research, 11, pp. 774, 2022. DOI: https://doi.org/10.12688/f1000research.121740.1
[14] Feyisa, G.L., Meilby, H., Fensholt, R., and Proud, S.R., Automated water extraction index: a new technique for surface water mapping using Landsat imagery, Remote Sensing of Environment, 140, pp. 23-35, 2014. DOI: https://doi.org/10.1016/j.rse.2013.08.029
[15] Laonamsai, J., Julphunthong, P., Saprathet, T., Kimmany, B., Ganchanasuragit, T., Chomcheawchan, P., and Tomun, N., Utilizing NDWI, MNDWI, SAVI, WRI, and AWEI for Estimating Erosion and Deposition in Ping River in Thailand, Hydrology, 10(3), art. 70, 2023. DOI: https://doi.org/10.3390/hydrology10030070
[16] Eros, C., Landsat 8-9 Operational Land Imager / Thermal Infrared Sensor Level-1, Collection 2 [dataset], U.S. Geological Survey, 2022. DOI: https://doi.org/10.5066/P975CC9B
[17] CONAGUA-SINA, SINA 3.0. Sistema Nacional de Información del Agua: base de datos de calidad del agua en cuerpos superficiales. Comisión Nacional del Agua, México, [en linea]. Disponible en: https://sinav30.conagua.gob.mx:8080/SINA/?opcion=acuiferos.

Note:
Data Availability: The Python code for TSS calculation and GEE scripts for image acquisition are available at: https://github.com/Ismaelog9/SST_Tecocomulco

I. Ortega-García, received his BSc. Eng. in Computer Systems in 2017. He has worked as a consultant in application development in C#, front-end and back-end development, and is currently a systems analyst in the auto parts manufacturing sector. He has participated as an exhibitor at the Multidisciplinary International Congress organized by the National Institute Technology of Mexico and the Technological Institute of Eastern Hidalgo State. He is currently pursuing a Master's degree in Computer Systems at ITESA with an interest in the areas of artificial intelligence and deep learning, industry 4.0, and AI applications in environmental monitoring.
ORCID: 0009-0008-1525-7569.

G. Cuaya-Simbro, received the Dr. in Computer Science doing research in the area of machine learning. He has 8 years of professional experience in the industry, working as a senior consultant in Information Technology developed by IBM, such as mainfrain solutions, high availability, virtualization and cognitive computing, among others. He is currently a member of the SNI of CONAHCYT level C and is a research professor in the technological system of Mexico (TecNM), where he has taught undergraduate and graduate courses, directed graduate work at both levels, and has collaborated with national and international research groups to develop research projects that directly impact national problems, such as Education, Health, Food Sovereignty, among others, and with special emphasis on issues that contribute to achieving the UN SDGs. The lines of research currently working are those related to Industry 4.0 and Digital Transformation, such as Artificial Intelligence, Machine learning, robotics, IoT, Cloud Computing, BlockChain, Bigdata, cyber-physical systems, among others.
ORCID: 0000-0001-6303-154X

R. Cruz-Guerrero, received the PhD. in Computer Science from the Autonomous University of the State of Hidalgo, Mexico. He is a member of the National System of Researchers (SNI) at the CONAHCYT and research professor at the Technological System of Mexico (TecNM). His main research interests include Ontological Models, Industry 4.0, Artificial Intelligence, Bigdata, Deep learning and Semantic systems.
ORCID: 0000-0003-1276-2419

DYNA
http://dyna.medellin.unal.edu.co/

UNIVERSIDAD NACIONAL DE COLOMBIA

Theoretical investigation of Hydrogen sulfide adsorption on doped phthalocyanine nanosheets: DFT calculations

Rasha H. Hameed & Mohanned J. Al-Anber

Molecular Engineering and Computational Modeling Lab, Department of Physics, College of Sciences, University of Basrah, Basrah, Iraq.
rasha.hani@uobasrah.edu.iq, mohanned.mohammed@uobasrah.edu.iq

Received: June 9th, 2025. Received in revised form: December 10th, 2025. Accepted: December 19th, 2025.

Abstract
Density functional theory (DFT) computations of phthalocyanine (MePc) monolayers. Utilizing the B3LYP functional alongside a 6-311+G(d,p) basis set, we conducted comprehensive optimization of the molecular structures to evaluate their stability and electrical characteristics. The binding energy between the central metal and the phthalocyanine monolayer was computed, together with the adsorption energy of H_2S, to assess the feasibility for gas sensing applications. Our results demonstrate that the adsorption process is primarily spontaneous, with considerable charge transfer occurring during adsorption, as confirmed by Hirshfeld charge calculations. Furthermore, we examined the band-gap energy, global hardness, and electrophilicity index to further the characterization of the sensing capabilities of both pristine and metal-doped phthalocyanine structures. The findings indicate that metal doping improves the sensitivity and stability of phthalocyanine monolayers, making them viable candidates for H_2S detection across diverse applications. This study examines the adsorption characteristics of hydrogen sulfide (H_2S) on metal-doped materials.

Keywords: hydrogen sulfide (H_2S); Phthalocyanine; Density Functional Theory (DFT); gas sensing; metal doping.

Investigación teórica de la adsorción de sulfuro de hidrógeno en nanohojas de ftalocianina dopadas: cálculos DFT

Resumen
Cálculos de la teoría del funcional de la densidad (DFT) de monocapas de ftalocianina (MePc). Utilizando el funcional B3LYP junto con un conjunto de bases 6-311+G(d,p), realizamos una optimización exhaustiva de las estructuras moleculares para evaluar su estabilidad y características eléctricas. Se calculó la energía de enlace entre el metal central y la monocapa de ftalocianina, junto con la energía de adsorción de H_2S, para evaluar su viabilidad en aplicaciones de detección de gases. Nuestros resultados demuestran que el proceso de adsorción es principalmente espontáneo, con una considerable transferencia de carga durante la adsorción, como lo confirman los cálculos de carga de Hirshfeld. Además, examinamos la energía de banda prohibida, la dureza global y el índice de electrofilicidad para profundizar en la caracterización de las capacidades de detección de estructuras de ftalocianina, tanto prístinas como dopadas con metal. Los hallazgos indican que el dopaje con metal mejora la sensibilidad y la estabilidad de las monocapas de ftalocianina, lo que las convierte en candidatas viables para la detección de H_2S en diversas aplicaciones. Este estudio examina las características de adsorción del sulfuro de hidrógeno (H_2S) en materiales dopados con metal.

Palabras clave: sulfuro de hidrógeno (H_2S); ftalocianina; Teoría del Funcional de la Densidad (DFT); detección de gases; dopaje de metales.

1 Introduction

Hydrogen sulfide (H_2S), also known as hydrosulfuric acid, is a colorless and highly toxic gas characterized by a distinct rotten egg odor. It is primarily produced as a byproduct of industrial activities such as natural gas processing, petroleum refining, coal gasification, and biogas fermentation [1,2]. Exposure to H_2S poses serious health

How to cite: Hameed, R.H, and Al-Anber, M.J., Theoretical investigation of hydrogen sulfide adsorption on doped phthalocyanine nanosheets: DFT calculations DYNA, (93)240, pp. 46-52, January - March, 2026.

risks, affecting both the nervous system and respiratory tract [3]. At low concentrations, it can cause symptoms like dizziness, nausea, coughing, and chest discomfort [4]. However, higher concentrations may impair olfactory function, leading to a loss of smell and increasing the risk of prolonged exposure, which can result in severe consequences such as organ damage, respiratory failure, and even death [5]. Beyond its health hazards, H_2S also has detrimental environmental and industrial effects. When oxidized to sulfur dioxide (SO_2), it contributes to acid rain, damaging crops, infrastructure, and ecosystems. In industrial settings, H_2S accelerates equipment corrosion, degrades catalyst efficiency, reduces product quality, and poses operational hazards [6]. Therefore, accurate and efficient detection of trace H_2S is crucial for ensuring workplace safety, environmental protection, and industrial productivity. Conventional H_2S sensors face limitations such as high energy consumption, low sensitivity, short lifespan, and strict operational conditions [6]. To overcome these challenges, researchers are exploring advanced materials for more reliable and cost-effective gas sensing. Among these, two-dimensional phthalocyanine (Pc) compounds have gained attention due to their unique properties, including high surface area, excellent charge transfer capability, and optical performance [7]. These characteristics make them suitable for applications in photovoltaics [8], optoelectronics [9], electrocatalysis [10], and spintronics [11]. While resistive phthalocyanine-based gas sensors have shown promise in lab settings, their practical use is hindered by poor stability, selectivity, and sensitivity [12]. To enhance their performance, transition metal atoms can be incorporated into the Pc structure, improving their gas-sensing properties [13]. Previous studies using density functional theory (DFT) have demonstrated the effectiveness of metal-doped phthalocyanines—such as zinc phthalocyanine (ZnPc) and chromium phthalocyanine (CrPc)—in detecting gases like CO, NO, and formaldehyde [14,15]. Additionally, Mn-phthalocyanine (MnPc) has been investigated for its interaction with XH3 gases (X = N, P, As) [16]. However, research on metal-doped phthalocyanines for H_2S detection remains limited. This study employs DFT simulations to evaluate the H_2S adsorption behavior on gallium (GaPc), scandium (ScPc), and titanium phthalocyanine (TiPc) monolayers. By analyzing structural configurations, adsorption energies, charge transfer mechanisms, electronic band gaps, and density of states, we assess the potential of these materials for H_2S sensing applications.

2 Modeling and computing

Accurate determination of properties such as adsorption energy, dipole moment, and charge transfer necessitate the use of larger basis sets. A reliable approach for modeling molecular configurations involves employing a split-valence double-zeta basis set, exemplified by 6-311+G(d,p), which is a Pople-style basis set [17]. Full geometric optimizations were conducted with the B3LYP functional in conjunction with the 6-311+G(d,p) basis set [18,19]. The B3LYP method integrates Becke's three-parameter hybrid exchange functional (B3) and the Lee-Yang-Parr correlation functional (LYP), making it a widely adopted choice for studying nanostructures, including III-V semiconductor systems [20]. To account for weak long-range interactions, Grimme's D3 dispersion correction with Becke-Johnson damping (DFT-D3(BJ)) was applied [21]. All simulations were carried out using Gaussian 16 [22] within the framework of density functional theory (DFT) [23]. Input preparation and output visualization were facilitated by GaussView 5.0 [24], while density of states (DOS) plots were generated via GaussSum 3.0 [25].

The binding energy (BE) of the metal center within the phthalocyanine (Pc) monolayer was calculated as:

$$BE = (E_{MePc} - (E_{Me} + E_{Pc})) \quad (1)$$

where E_{MePc} and E_{Pc} represent the total energies of the metal-doped and undoped Pc monolayers, respectively, while E_{Me} corresponds to the energy of an isolated metal atom [26].

The adsorption energy (E_{ads}) of hydrogen sulfide (H_2S) on the Pc and MePc monolayers was computed to assess sensing performance:

$$E_{ads} = E_{gas/MePc} - (E_{gas} + E_{MePc}) \quad (2)$$

where, $E_{gas/MePc}$ is the total energy of the H_2S-adsorbed system, whereas E_{MePc} and E_{gas} denote the energies of the isolated MePc monolayer and H_2S molecule, respectively. A negative E_{ads} typically indicates exothermic adsorption, with greater negativity reflecting stronger stability [27]. Adsorption is classified as chemisorption if $|E_{\mathrm{ads}}|>0.5$eV; otherwise, it is considered physisorption [28]. This investigation evaluated H_2S adsorption on Pc and MePc monolayers at 298.15 K. Additionally, key electronic parameters were analyzed, including the bandgap ($Eg = E_{\mathrm{LUMO}} - E_{\mathrm{HOMO}}$), global hardness ($\eta = Eg/2$), and electrophilicity index ($\omega = (E_{\mathrm{HOMO}} + E_{\mathrm{LUMO}})^2/8\eta$), where E_{HOMO} and E_{LUMO} are the energies of the lowest unoccupied and highest occupied molecular orbitals, respectively [20]. The sensitivity of pristine and Me-doped Pc toward H_2S was quantified by the relative change in bandgap:

$$\Delta E_g\% = [(E_{g_2} - E_{g_1})/E_{g_1}] \times 100 \quad (3)$$

Where, E_{g2} and E_{g1} are the bandgap values before and after H_2S adsorption.

To elucidate substrate-gas interactions, Hirshfeld charge analysis was performed to determine charge transfer Q_{CT}:

$$Q_{CT} = Q_{(H2S)_A} - Q_{(H2S)_B} \quad (4)$$

Here, $Q_{(\mathrm{H2S})\mathrm{A}}$ and $Q_{(\mathrm{H2S})\mathrm{B}}$ represent the net charges on H_2S after and before adsorption, respectively. A positive Q_{CT} implies electron donation from H_2S to the Pc surface, while a negative value suggests the opposite direction of transfer [29].

3 Results and discussion

3.1 Structure and stability of pristine Pc, MePc, and H_2S

Fig. 1 illustrates the optimized structures of (a) pristine phthalocyanine (Pc), (b) gallium-doped Pc (GaPc), (c)

scandium-doped Pc (ScPc), (d) titanium-doped Pc (TiPc), and (e) an isolated hydrogen sulfide (H_2S) molecule. The atomic color scheme is as follows: gray for carbon (C), white for hydrogen (H), blue for nitrogen (N), orange for gallium (Ga), pink for scandium (Sc), green for titanium (Ti), and yellow for sulfur (S). The coplanar configuration of the pristine Pc monolayer indicates a completely delocalized and conjugated π-electron system. Both GaPc and TiPc monolayers exhibit a stable "graphene-like" planar shape, signifying a robust connection between the metal atoms and the Pc nanosheet, consistent with previously reported values [30]. Conversely, the ScPc monolayer shows a pronounced out-of-plane displacement of the Sc atom, resulting in a non-planar structure. The isolated H_2S molecule exhibits an H–S bond length of 1.35 Å and a bond angle of 92.73°, in accordance with previous studies [20]. Among the doped phthalocyanines, TiPc demonstrates the most substantial negative binding energy (*BE*), as illustrated in Fig. 1d, signifying a more robust link between the metal atom and the Pc monolayer relative to ScPc and GaPc. The possibility of metal atom aggregation inside the phthalocyanine monolayer was investigated by calculating the cohesive energy (E_{coh}) using the formula:

$$E_{coh} = \frac{E_{MePc} - E_{iso-Me}}{n} \quad (5)$$

E_{coh}=(E_{MePc}-E_{iso-Me})/n, where E_{iso-Me} denotes the energy of an individual metal atom and n indicates the number of metal atoms. The findings demonstrate that TiPc and ScPc possess the greatest cohesive energies, succeeded by GaPc and pure Pc. Fig. 1 presents the EBE values for GaPc, ScPc, and TiPc monolayers as −7.33 eV, −9.67 eV, and −10.97 eV, respectively. All these values are below the cohesive energy of the respective metal bulk, so affirming its stability. Prior research suggests that the central location, particularly the vacancy in the center of Pc or directly above the doped metal atom in MePc, is the favored adsorption site [31]. The stability of an atom on an adsorbent can be defined by its diffusion activation barrier (E_{act}). Calculations in machine learning indicate that for individual atoms of diverse metal species on various two-dimensional materials, the energy barriers are proportional to (BE^2/E_{coh}). While 2D Pc is excluded from these computations, a preliminary estimation can be obtained from the subsequent equation:

$$E_{act} = 0.63(E_{BE}^2/E_{coh}) - 0.203 \quad (6)$$

In this context, *BE* denotes the binding energy, while Ecoh signifies the cohesive energy of the metal atoms adsorbed on 2D Pc, as depicted in Fig. 1. It is vital that *BE* exceeds E_{coh} to avert the formation of metal clusters on 2D Pc, since this may impair its capacity to interact with other molecules by decreasing the number of accessible adsorption sites. Numerical calculations indicate that Ga, Sc, and Ti exhibit higher *BE* values than their cohesive energies. Moreover, the activation energy exhibits the subsequent trend: Exact: Ti > Sc > Ga. All atomic metals demonstrate binding energies more than 1 eV, signifying substantial interactions with the 2D Pc [32].

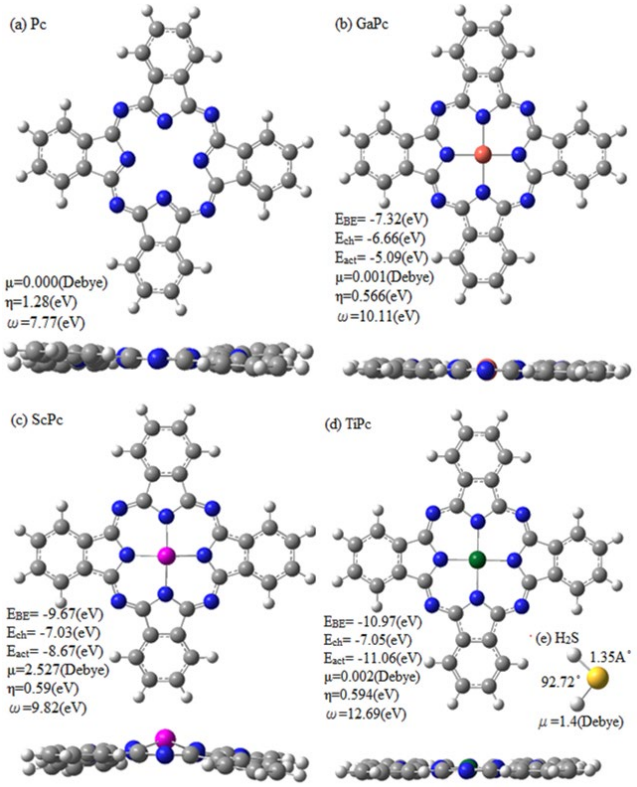

Figure 1. Optimized structures of (a) pristine phthalocyanine (Pc), (b) gallium-doped Pc (GaPc), (c) scandium-doped Pc (ScPc), (d) titanium-doped Pc (TiPc), and (e) hydrogen sulfide (H_2S). Color code: gray (C), white (H), blue (N), orange (Ga), pink (Sc), green (Ti), yellow (S).
Source: Authors.

3.2 Adsorption properties of H_2S on pristine and metal-doped phthalocyanine

The optimized adsorption configurations of H_2S on pristine phthalocyanine (Pc) and metal-doped Pc (MePc, where Me = Ga, Sc, Ti) are depicted in Fig. 2. For pure Pc, the calculated adsorption energy (E_{ads}) is −7.21 kcal/mol, accompanied by a charge transfer (Q_{CT}) of −0.171 e from Pc to H_2S (Fig. 3). This weak interaction indicates primarily physical adsorption, consistent with previous studies [27], and suggests limited H_2S capture capability.

In contrast, doping with Sc and Ti significantly enhances H_2S adsorption. The most stable configurations, H_2S+ScPc and H_2S+TiPc, exhibit E_{ads} values of −17.22 and −22.70 kcal/mol, respectively, confirming chemisorption [30]. Ga doping, however, does not improve adsorption performance, as reflected in its lower E_{ads} compared to ScPc and TiPc. Structural analysis reveals minimal distortion in H_2S adsorbed on ScPc and TiPc, with adsorption distances of 2.80 Å (Q_{CT} = 0.267 e) and 2.50 Å (Q_{CT} = 0.216 e), respectively. These results demonstrate superior H_2S adsorption on ScPc and TiPc relative to GaPc and pristine Pc. Electronic structure analysis further supports these findings. The HOMO-LUMO gap (*Eg*) of pristine Pc decreases only slightly (2.55 eV → 2.34 eV) upon H_2S adsorption (Fig. 3), indicating low sensitivity for detection. In contrast, Ga, Sc,

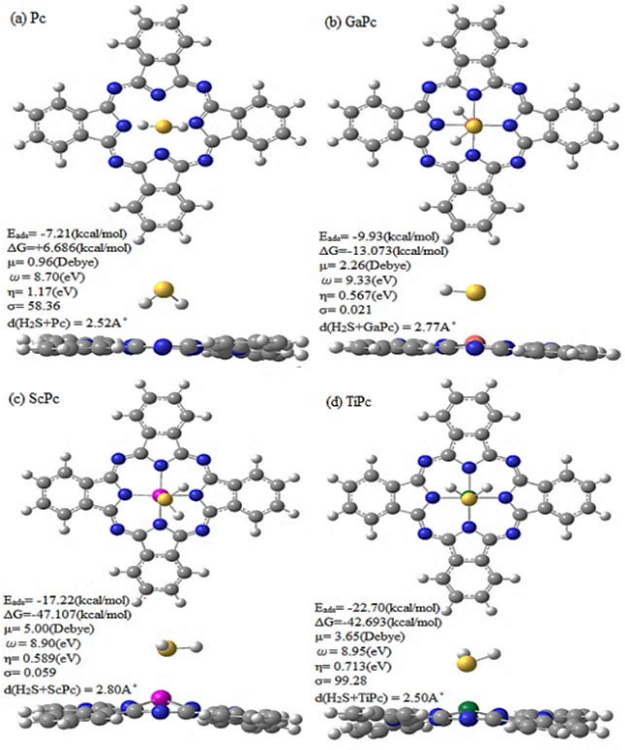

Figure 2. Top and side views of H_2S adsorbed on (a) Pc, (b) GaPc, (c) ScPc, and (d) TiPc. Atom colors: gray (C), white (H), blue (N), orange (Ga), pink (Sc), green (Ti), yellow (S).
Source: Authors.

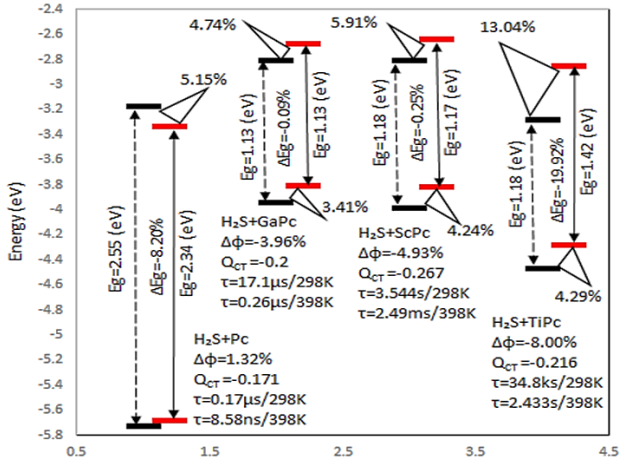

Figure 3. HOMO-LUMO energy levels for H_2S adsorbed on Pc, GaPc, ScPc, and TiPc. Black lines represent systems before adsorption; red lines show post-adsorption states.
Source: Authors.

and Ti doping induces notable shifts in the HOMO level, reducing Eg and enhancing H_2S interaction. Global hardness (η) measurements reveal minimal changes for GaPc and ScPc after adsorption, whereas TiPc shows significant variations. The electrophilicity index (ω) also undergoes marked shifts, particularly for TiPc+H_2S, suggesting TiPc's stronger affinity for H_2S. Thermodynamic calculations reveal spontaneous adsorption ($\Delta G < 0$) for all MePc systems, with ScPc (−47.10 kcal/mol) and TiPc (−42.69 kcal/mol) exhibiting the strongest interactions, followed by GaPc (−13.07 kcal/mol). Pristine Pc, however, shows a positive ΔG (6.68 kcal/mol), indicating non-spontaneous adsorption (Fig. 2).

Density of states (DOS) analysis provides additional insights. For pristine Pc (Fig. 4), H_2S exhibits delocalized states with no significant resonance peaks, indicating weak van der Waals interactions [34] and poor gas-sensing potential. In contrast, ScPc (Fig. 5) and TiPc (Fig. 7) display strong resonance peaks (highlighted by dashed rectangles), confirming robust orbital hybridization. The Sc and Ti atoms act as electron bridges, facilitating charge transfer and strengthening H_2S adsorption. GaPc (Fig. 6) also shows enhanced orbital overlap, though to a lesser extent than ScPc and TiPc. These findings highlight TiPc as a promising candidate for H_2S sensing applications.

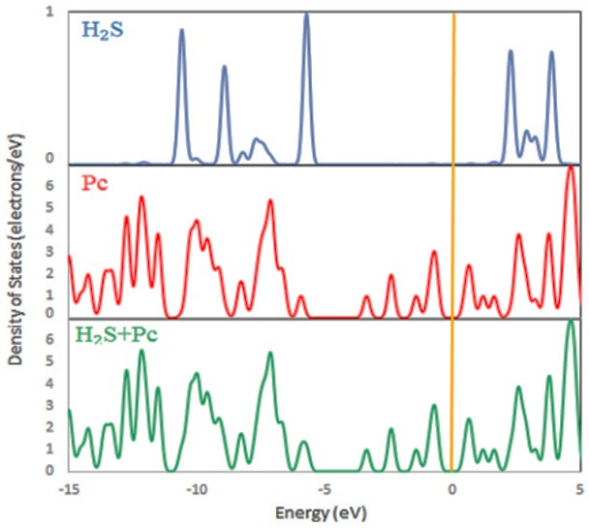

Figure 4. Density of states (DOS) for H_2S, Pc, and their combined system. The Fermi level (orange line) is set at zero energy.
Source: Authors.

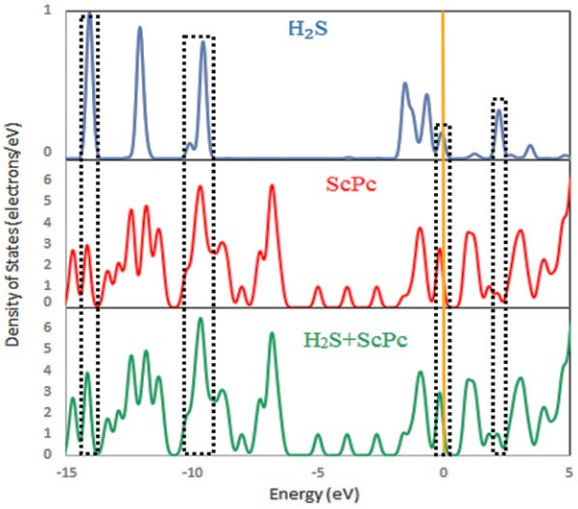

Figure 5. DOS for H_2S, ScPc, and their combined system. The Fermi level (orange line) is at zero energy.
Source: Authors.

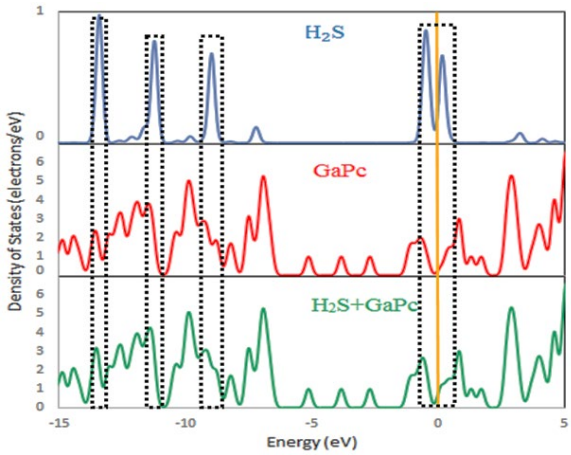

Figure 6. DOS for H_2S, GaPc, and their combined system. The Fermi level (orange line) is at zero energy.
Source: Authors.

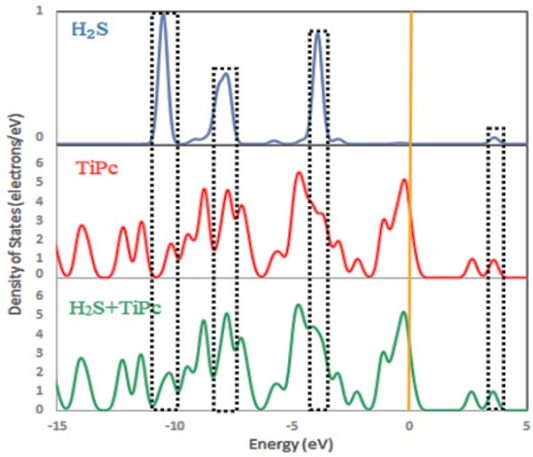

Figure 7. DOS for H_2S, TiPc, and their combined system. The Fermi level (orange line) is at zero energy. Source: Authors.

3.3 Sensing mechanism analysis

The preceding sections established the durability and strong adsorption capacity of ScPc and TiPc monolayers, confirming their suitability for H_2S gas sensing. To gain deeper insight into the sensing mechanism, we evaluated the sensitivity and desorption behavior of these monolayers upon H_2S exposure.

The energy gap (Eg) serves as an indicator of molecular excitability—a smaller gap corresponds to higher excitation likelihood, reflecting changes in conductivity. As shown in Fig. 3, GaPc and ScPc monolayers exhibit semimetallic behavior, with negligible shifts in their electronic band gaps after H_2S adsorption. This suggests minimal electrical response, indicating low sensitivity. In contrast, the TiPc monolayer undergoes a significant band gap increase from 1.188 eV to 1.425 eV (ΔEg = 19.92%) upon H_2S adsorption, transitioning from semimetallic to semiconducting properties. This shift highlights TiPc's superior sensitivity to H_2S.

The sensitivity can be quantified by changes in electrical conductivity (σ), expressed as: $\sigma \propto \exp(-Eg/2k_BT)$, where Eg is the band gap, k_B is the Boltzmann constant (8.62×10^{-5} eV/K), and T the operating temperature. The negligible band gap shift in H_2S-ScPc systems results in minimal resistivity changes (σ_{ScPc} = 0.059), confirming low sensitivity. Conversely, ScPc and TiPc exhibit notable electronic perturbations upon H_2S exposure, with σ values of 0.059 and 99.28, respectively. The substantial change in TiPc underscores its potential as an H_2S sensor.

We further investigated the influence of H_2S on Fermi levels (E_F) and work function (ϕ), defined as: $\phi = -E_F = (E_{LUMO}+E_{HOMO})/2$. The work function shift ($\Delta\phi$) is critical for ϕ-type sensors, which measure this parameter via Kelvin oscillation. Post-adsorption, Ga-, Sc-, and Ti-decorated 2D Pc exhibit $\Delta\phi$ values of -3.96%, -4.93%, and -8.00%, respectively, while pristine Pc shows a slight increase ($\Delta\phi$ = 1.32%). The most pronounced change occurs in TiPc, followed by ScPc, confirming work function as a key metric for sensor performance.

Desorption kinetics (τ) are equally vital for sensor reusability. Moderate gas-substrate interactions facilitate rapid desorption, ensuring sustained operation. Using transition state theory, we calculated τ as: $\tau = (f_0)^{-1}\exp(-E_{abs}/k_BT)$, where the attempt frequency f_0 is taken as 1×10^{12} s^{-1}. For ScPc, τ values are 3.54 s (298 K) and 2.49 ms (398 K), while TiPc shows slower recovery (34.8 ks at 298 K, 2.43 s at 398 K). ScPc's short recovery time at ambient temperature, combined with adequate sensitivity, makes it a promising candidate for H_2S detection. Comparative studies reveal that hydroxyl-modified ZGNRs exhibit weak H_2S adsorption (E_{ads} = -0.17 eV) [35], while PdAs monolayers show physical adsorption (E_{ads} = -0.49 eV) with a 179 s recovery time [36]. Zinc-doped SnP_1 demonstrates faster recovery (64 ms at 298 K) but lower adsorption strength (E_{ads} = -0.639 eV) [37]. In contrast, ScPc offers optimal adsorption and rapid desorption, positioning it as a highly effective H_2S sensor.

3.4. Dipole moments of adsorbates and substrates

The dipole moment (μ) of a molecule plays a crucial role in adsorption behavior by influencing electrostatic forces between the adsorbate and substrate [37]. To analyze these interactions, we computed the dipole moments of H_2S gas, pristine nanosheets, and doped nanosheets. Our results show that H_2S possesses a dipole moment of 1.399 Debye (Fig. 1). Notably, the doped nanosheets exhibit slightly higher μ values compared to their undoped counterparts (Fig. 2). Among these, the H_2S+TiPc system shows the most pronounced increase in dipole moment. This enhancement correlates with stronger adsorption energies, suggesting that doping improves H_2S adsorption via intensified electrostatic interactions.

4 Conclusion

This study employed density functional theory (DFT) calculations to systematically investigate the structural, electronic, and adsorption properties of pristine and metal-doped phthalocyanine (Pc) monolayers for hydrogen sulfide (H_2S) sensing applications.

The results demonstrate that doping with transition metals significantly enhances the stability and gas adsorption performance of Pc nanosheets compared to the pristine structure. Among the studied dopants (Ga, Sc, Ti), Sc and Ti

incorporation proved most effective, yielding strong binding energies and spontaneous, exothermic H_2S adsorption indicative of chemisorption. In contrast, Ga doping and the pristine Pc monolayer showed only weak, physisorptive interactions with H_2S.

Electronic structure analysis revealed that ScPc and TiPc undergo substantial charge transfer and orbital hybridization upon H_2S exposure. A critical finding is the pronounced change in the electronic band gap of TiPc, which shifts from semimetallic to semiconducting character after adsorption. This significant alteration in electronic properties, coupled with a notable change in work function, suggests a strong electrical response to the target gas, which is essential for resistive and work-function-based sensing mechanisms. Furthermore, analysis of recovery times indicates that ScPc offers an optimal balance between adequate adsorption strength and rapid desorption at ambient temperature, promoting sensor reusability.

In summary, while both ScPc and TiPc monolayers exhibit superior H_2S adsorption and electronic sensitivity, TiPc emerges as the most promising candidate due to its strongest adsorption energy and the most significant modulation of its electronic properties. These characteristics recommend TiPc-doped phthalocyanine nanosheets as highly suitable materials for the development of efficient, sensitive, and reusable H_2S gas sensors.

References

[1] Ganji, M.D., and Danesh, N., Adsorption of H_2S molecules by cucurbit [7] uril: an ab initio vdW-DF study. RSC Advances, 3(44), pp. 22031-22038, 2013. DOI: https://doi.org/10.1039/c3ra41946k.

[2] Drummer, O.H., Disposition of toxic drugs and chemicals in man. Australian Journal of Forensic Sciences, 41(2), p. 163, 2009. DOI: https://doi.org/10.1080/00450610903019561.

[3] Shefa, U., Kim, M.S., Jeong, N.Y., and Jung, J., Antioxidant and cell-signaling functions of hydrogen sulfide in the central nervous system. Oxidative medicine and cellular longevity, Art. 1873962, 2018. DOI: https://doi.org/10.1155/2018/1873962.

[4] Lashgari, M., and Ghanimati, M., Photocatalytic degradation of H_2S aqueous media using sulfide nanostructured solid-solution solar-energy-materials to produce hydrogen fuel. Journal of Hazardous Materials, 345, pp. 10-17, 2018. DOI: https://doi.org/10.1016/j.jhazmat.2017.10.062.

[5] Ayesh, A.I., et al., Selective gas sensors using graphene and CuO nanorods. Sensors and Actuators A: Physical, 283, pp. 107-112, 2018. DOI: https://doi.org/10.1016/j.sna.2018.09.068.

[6] [6] Sharma, S., and Verma, A.S., A theoretical study of H_2S adsorption on graphene doped with B, Al and Ga. Physica B: Condensed Matter, 427, pp. 12-16, 2013. DOI: https://doi.org/10.1016/j.physb.2013.05.019.

[7] Zhang, R., Lu, L., Chang, Y., and Liu, M., Gas sensing based on metal-organic frameworks: concepts, functions, and developments. Journal of Hazardous Materials, 429, Art. 128321, 2022. DOI: https://doi.org/10.1016/j.jhazmat.2022.128321.

[8] Jin, L., and Chen, D., Enhancement in photovoltaic performance of phthalocyanine-sensitized solar cells by attapulgite nanoparticles. Electrochimica, 72, pp. 40-45, 2012. DOI: https://doi.org/10.1016/j.electacta.2012.03.167.

[9] Darwish, A.A.A., et al., Linear and nonlinear optical characteristics of manganese phthalocyanine chloride/polyacetate sheet: Towards flexible optoelectronic devices. Optical Materials, 114, Art. 110988, 2021. DOI: https://doi.org/10.1016/j.optmat.2021.110988.

[10] Huang, S., Chen, K., and Li, T.T., Porphyrin and phthalocyanine based covalent organic frameworks for electrocatalysis. Coordination Chemistry Reviews, 464, Art. 214563, 2022. DOI: https://doi.org/10.1016/j.ccr.2022.214563.

[11] Zemła, M.R., Czelej, K., and Majewski, J.A., Graphene−iron (II) phthalocyanine hybrid systems for scalable molecular spintronics. The Journal of Physical Chemistry C, 124(50), pp. 27645-27655, 2020. DOI: https://doi.org/10.1021/acs.jpcc.0c06949.

[12] Alosabi, A.Q., Al-Muntaser, A.A., El-Nahass, M.M., and Oraby, A.H., Structural, optical and DFT studies of disodium phthalocyanine thin films for optoelectronic devices applications. Optics & Laser Technology, 155, 108372, 2022. DOI: https://doi.org/10.1016/j.optlastec.2022.108372.

[13] Zhou, Y., Gao, G., Chu, W., and Wang, L.W., Computational screening of transition metal-doped phthalocyanine monolayers for oxygen evolution and reduction. Nanoscale Advances, 2(2), pp. 710-716, 2020. DOI: https://doi.org/10.1039/c9na00648f.

[14] Chaabene, M., et al., Insights into theoretical detection of CO2, NO, CO, O2, and O3 gases molecules using Zinc phthalocyanine with peripheral mono and tetra quinoleinoxy substituents: Molecular geometries, Electronic properties, and Vibrational analysis. Chemical Physics, 547, Art. 111198, 2021. DOI: https://doi.org/10.1016/j.chemphys.2021.111198.

[15] Long, D.B., et al., Two-dimensional bimetal-embedded expanded phthalocyanine monolayers: a class of multifunctional materials with fascinating properties. Advanced Functional Materials, 34(22), art. 2313171, 2024. DOI: https://doi.org/10.1002/adfm.202313171.

[16] Badran, H.M., Eid, K.M., Al-Nadary, H.O., and Ammar, H.Y., DFT-D3 and TD-DFT Studies of the Adsorption and Sensing Behavior of Mn-Phthalocyanine toward NH3, PH3, and AsH3 Molecules. Molecules, 29(10), art. 2168, 2024. DOI: https://doi.org/10.3390/molecules29102168.

[17] Resan, S., Hameed, R., Bahrani, F., and Al-Anber, M., Nonlinear optical response of anthracene as a D-π-A conjugated system: Quantum computation study. In: AIP Conference Proceedings, AIP Publishing, 2023. DOI: https://doi.org/10.1063/5.0163185.

[18] Becke, A.D., Density-functional thermochemistry. I. The effect of the exchange-only gradient correction. The Journal of Chemical Physics, 96(3), pp. 2155-2160, 1992. DOI: https://doi.org/10.1063/1.462066.

[19] Frisch, M.J., Pople, J.A., and Binkley, J.S., Self-consistent molecular orbital methods 25. Supplementary functions for Gaussian basis sets. The Journal of Chemical Physics, 80(7), pp. 3265-3269, 1984. DOI: https://doi.org/10.1063/1.447079.

[20] Jia, X., Zhang, H., Zhang, Z., and An, L., First-principles investigation of vacancy-defected graphene and Mn-doped graphene towards adsorption of H_2S. Superlattices and Microstructures, 134, art. 106235, 2019. DOI: https://doi.org/10.1016/j.spmi.2019.106235.

[21] Sato, T., and Nakai, H., Density functional method including weak interactions: dispersion coefficients based on the local response approximation. The Journal of Chemical Physics, 131(22), art. 224104, 2009. DOI: https://doi.org/10.1063/1.3270198.

[22] Frisch, M.J., et al., Gaussian 16, Revision C.01. Gaussian, Inc., Wallingford CT, 2016.

[23] Al-Anber, M., Al-Mowali, A., and Ali, A., Theoretical semiempirical study of the nitrone (anticancer drug) interaction with fullerene C60 (as delivery). Acta Physica Polonica A, 126(3), pp. 845-848, 2014. DOI: https://doi.org/10.12693/APhysPolA.126.845.

[24] Dennington, R., Keith, T., and Millam, J., GaussView, Version 5. Semichem Inc., Shawnee Mission, KS, 2009.

[25] Vinod, H.D., Review of GAUSS for Windows, including its numerical accuracy. Journal of Applied Econometrics, 15(2), pp. 211-220, 2000. DOI: https://doi.org/10.1002/(SICI)1099-1255(200003/04)15:2<211::AID-JAE573>3.0.CO;2-4.

[26] Resan, S., Hameed, R., Al-Hilo, A., and Al-Anber, M., The impact of torsional angles to tune the nonlinear optical response of chalcone molecule: Quantum computational study. Revista Cubana de Física, 37(2), pp. 95-100, 2020.

[27] Wang, C., Wang, Y., Guo, Q., Dai, E., and Nie, Z., Metal-decorated phthalocyanine monolayer as a potential gas sensing material for phosgene: a first-principles study. ACS Omega, 7(25), pp. 21994-22002, 2022. DOI: https://doi.org/10.1021/acsomega.2c02548.

[28] Yong, Y., Cui, H., Zhou, Q., Su, X., Kuang, Y., and Li, X., C2N monolayer as NH3 and NO sensors: a DFT study. Applied Surface Science, 487, pp. 488-495, 2019. DOI: https://doi.org/10.1016/j.apsusc.2019.05.040.

[29] Ammar, H.Y., Badran, H.M. and Eid, K.M., TM-doped B12N12 nano-cage (TM = Mn, Fe) as a sensor for CO, NO, and NH3 gases: A DFT

and TD-DFT study. Materials Today Communications, 25, Art. 101681, 2020. DOI: https://doi.org/10.1016/j.mtcomm.2020.101681.

[30] Vozzi, C., et al., Generalized molecular orbital tomography. Nature Physics, 7(10), pp. 822-826, 2011. DOI: https://doi.org/10.1038/nphys2029.

[31] Zhao, W., Zou, D., Sun, Z., Yu, Y., and Yang, C., Controlling spin off state by gas molecules adsorption on metal-phthalocyanine molecular junctions and its possibility of gas sensor. Physics Letters A, 382(37), pp. 2666-2672, 2018. DOI: https://doi.org/10.1016/j.physleta.2018.06.028.

[32] Cid, B.J., et al., Metal-decorated siligene as work function type sensor for NH3 detection: A DFT approach. Applied Surface Science, 610, art. 155541, 2023. DOI: https://doi.org/10.1016/j.apsusc.2022.155541.

[33] Opi, M.H., Ahmed, T., Swarna, M.R., Piya, A.A., and Shamim, S.U.D., Assessment of the drug delivery potential of graphene, boron nitride and their in-plane doped structures for hydroxyurea anti-cancer drug via DFT study. Nanoscale Advances, 20, art. 428, 2024. DOI: https://doi.org/10.1039/D4NA00428K

[34] Berland, K., Cooper, V.R., Lee, K., Schröder, E., Thonhauser, T., Hyldgaard, P., and Lundqvist, B.I., van der Waals forces in density functional theory: The vdW-DF method. *Reports on Progress in Physics*, 78(6), art. 066501, 2015. DOI: https://doi.org/10.1088/0034-4885/78/6/066501.

[35] Salih, E., and Ayesh, A.I., DFT investigation of H_2S adsorption on graphene nanosheets and nanoribbons: Comparative study. Superlattices and Microstructures, 146, art. 106650, 2020. DOI: https://doi.org/10.1016/j.spmi.2020.106650.

[36] Raval, D., Gupta, S.K., and Gajjar, P.N., Detection of H_2S, HF and H2 pollutant gases on the surface of penta-PdAs2 monolayer using DFT approach. Scientific Reports, 13(1), art. 586, 2023. DOI: https://doi.org/10.1038/s41598-023-27893-w.

[37] Cui, H., et al., DFT Study of Zn-Modified SnP3: A H_2S Gas Sensor with Superior Sensitivity, Selectivity, and Fast Recovery Time. Nanomaterials, 13(20), art. 2781, 2023. DOI: https://doi.org/10.3390/nano13202781.

R.H. Hameed has a PhD in theoretical nanotechnology (2025) from the University of Basra, Iraq. She received the MSc in Physics in 2009. She is currently working on biosensor design, focusing on manufacturing by transition metal according to computational methods.
ORCID: 0000-0002-4844-2313

M.J. Al-anber received the BSc in Physics in 1995, the MSc in Physics in 2000, and the PhD in Physics in 2005, all from the University of Basrah, Iraq. From 1997 to 2008, he worked in technical and academic roles, including defense systems research, before joining the University of Basrah as a faculty member. He completed postdoctoral research (2014–2017) on the dielectric properties of titanium dioxide nanorods at the University of Hull, UK. Currently, he is a Professor of Molecular Quantum Dynamics and Statistical Thermodynamics at the University of Basrah. His research interests include: molecular quantum dynamics and electronic structure of macromolecules; dielectric properties of nanomaterials, particularly titanium dioxide nanorods; and statistical thermodynamics of complex systems.
ORCID: 0000-0001-9093-6811

DYNA
http://dyna.medellin.unal.edu.co/

UNIVERSIDAD NACIONAL DE COLOMBIA

Design and evaluation of a high-speed centrifugal precision seed-metering device for soybean based on DEM simulation

Yujie Zhang, Xianliang Wang, Xiupei Cheng, Zhongcai Wei, Pingchuan Ma & Xiangcai Zhang*

*Institute of Modern Agricultural Equipment, Shandong University of Technology, Xincun West Rd, Zibo255049, China. zyjhk1989@163.com, wxl1990@sdut.edu.cn, cheng2021@sdut.edu.cn, weizc@sdut.edu.cn, ashley494@163.com, *Corresponding author: zxcai0216@163.com*

Received: July 16th, 2025. Received in revised form: December 15th, 2025. Accepted: December 29th, 2025.

Abstract
A high-speed centrifugal precision seed metering device for soybeans was developed to improve single-seed sowing accuracy under high-speed operation. The device integrates an involute deflector strip and ellipsoidal seed grooves, driven by a stepper motor to control the centrifugal disc and seed-metering wheel. Using EDEM software, a simulation model was established. A quadratic orthogonal design was applied with deflector type, disc speed, and seed-metering wheel speed as factors, and qualified seeding rate and miss rate as indicators. The optimal combination—disc speed of 49.01 r/min and wheel speed of 593.75 r/min—achieved a 92.08% seeding qualification rate and 1.91% miss rate. Bench tests confirmed strong agreement with simulation results, verifying the system's reliability. This study offers a theoretical and practical reference for the development of high-speed precision metering devices for soybean planting.

Keywords: **p**recision soybean sowing; centrifugal type; high-speed metering; DEM.

Diseño y evaluación de un dispositivo de dosificación de semillas de precisión centrífuga de alta velocidad para soja basado en simulación DEM

Resumen
Se diseñó un dispositivo dosificador centrífugo de alta velocidad para la siembra de precisión de soya, con el fin de mejorar la eficiencia y la calidad en la dosificación unitaria de semillas bajo condiciones de alta velocidad. El sistema incorpora tiras deflectoras de perfil involuto y cavidades de almacenamiento elipsoidales, accionadas por un motor paso a paso que regula el disco centrífugo y el rotor dosificador. Se desarrolló un modelo de simulación mediante el software EDEM, y se aplicó un diseño experimental ortogonal rotacional con tres factores: tipo de deflector, velocidad del disco y velocidad del rotor. Los resultados óptimos (49.01 r/min y 593.75 r/min) alcanzaron una tasa de dosificación correcta del 92.08 % y una tasa de fallos del 1.91 %. Las pruebas en banco confirmaron la fiabilidad del dispositivo. Este estudio proporciona una base técnica y experimental para el desarrollo de dosificadores de precisión centrífugos en la mecanización agrícola.

Palabras clave: siembra de precisión de soya; dosificador centrífugo; alta velocidad; DEM.

1 Introduction

As the core component of a precision planter [1], the seed-metering device significantly influences the efficiency and quality of sowing operations [2,3]. At present, precision seed-metering devices in use worldwide can be generally categorized into two types: mechanical and pneumatic [4-6]. Mechanical seed-metering devices are widely adopted in soybean, maize, and other crop planting due to their compact structure, low manufacturing cost, and strong adaptability.

However, conventional mechanical seed metering devices often suffer from low filling efficiency, unstable discharge, and seed damage at high speeds, limiting their suitability for modern precision sowing [8]. Liu et al. [9] found that high-speed operation significantly reduces filling stability, leading to seed overlap, bounce, or breakage. Teixeira et al. [10] noted that poor structural design increases seed friction and damage, resulting in missed or repeated seeding. Most centrifugal metering

How to cite: Zhang, Y., Wang, X., Cheng, X., Wei, Z., Ma, P., and Zhang, X., Design and evaluation of a high-speed centrifugal precision seed-metering device for soybean based on DEM simulation DYNA, (93)240, pp. 53-61, January - March, 2026.

systems are still limited to row sowing, with limited application in single-seed precision sowing for crops like soybean [11].

To address these issues, this study proposes a novel high-speed centrifugal precision metering device for soybean. The device employs structural innovations and optimized seed flow guidance to improve uniformity and reliability. Furthermore, DEM-based simulations are used to analyze seed kinematics, and a response surface methodology (RSM) is applied to optimize key structural parameters. Finally, bench tests are conducted to validate the simulation results. The study aims to provide both theoretical insights and practical support for engineering applications of centrifugal seed metering systems.

2 Structure and working principle of the seed metering device

2.1 Structural design

The developed high-speed centrifugal precision soybean seed metering device primarily consists of the housing, seed scraper, slender shaft, seed-metering wheel, centrifugal disc, seed discharge unit, and main shaft. A schematic of the overall structure is shown in Fig. 1.

The centrifugal unit comprises a main shaft, centrifugal disc, guide strips, and ellipsoidal seed-holding cavities. The disc is directly driven by a stepper motor through the main shaft, generating centrifugal force during high-speed rotation. This force, in combination with the deflector strips, induces seed dispersion and directional flow. To improve seeding accuracy, ellipsoidal cavities are adopted instead of traditional metering holes, with dimensions optimized according to soybean seed geometry.

The seed-metering unit consists of a flexible seed-metering wheel mounted on the slender shaft, made of elastic composite material with favorable wear resistance and buffering capacity, effectively minimizing seed damage. The device includes two symmetric seed outlets, each equipped with a scraper that removes overlapped

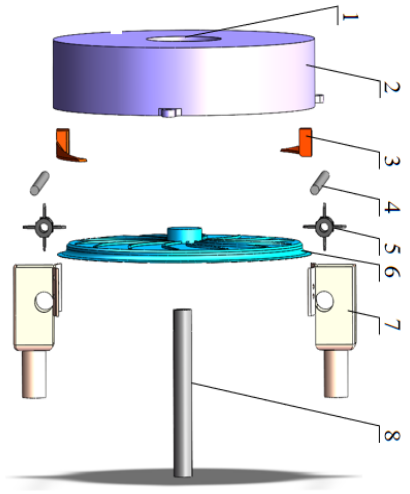

Figure 1. Structural diagram of the high-speed centrifugal precision seed metering device. 1. Seed inlet 2. Housing 3. Seed scraper 4. Slender shaft 5. Seed-metering wheel 6. Centrifugal disc 7. Seed discharge unit 8. Main shaft.
Source: Elaborated by the authors.

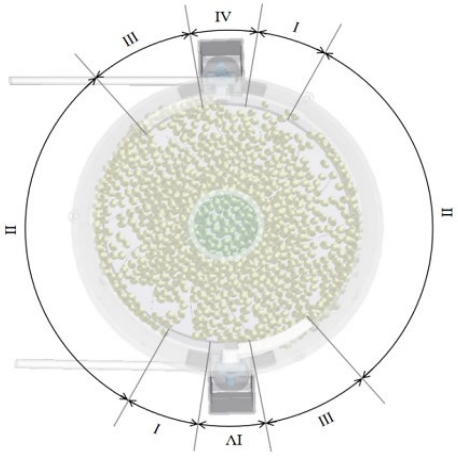

Figure 2. Structural diagram of the working principle of the seed metering device
Source: Elaborated by the authors.

or misaligned seeds, ensuring accurate single-seed discharge. The configuration allows dual-row operation with a single device, improving field productivity.

2.2 Working principle

Prior to operation, seeds enter the device through the inlet and fall onto the centrifugal disc under gravity. The seed metering process consists of four stages (Fig. 2):

- Centrifugation: The high-speed rotation of the disc generates centrifugal force, dispersing seeds toward the perimeter and partially into the cavities.
- Seed Filling: Under the combined action of centrifugal force and inter-particle interactions, seeds are evenly distributed and pressed against the inner wall of the housing, completing cavity filling.
- Seed Scraping: As the disc rotates further, seeds reach the scraper region, where overlapped or misoriented seeds are removed to ensure accurate single-seed positioning.
- Seed Discharge: At the discharge outlet, seeds are pushed into the outlet passage by the seed-metering wheel, aided by centrifugal force, achieving single-seed delivery.

Through the coordinated design of internal structures and dynamic intervention, the device ensures stable and precise seed discharge even at high operational speeds, supporting high-efficiency precision planting.

3 Design of key structural parameters

3.1 Geometric characteristics of soybean seeds

To ensure accurate structural matching and optimal design, it is essential to quantify the physical properties of the target seeds. In this study, the soybean cultivar "Shangdou 1201" was selected as the target material. Using a CHNT digital caliper (range: 0–150 mm; resolution: 0.01 mm), 1000 seeds were randomly sampled, and their principal dimensions were measured in accordance with the method illustrated in Fig. 3 [12].

Through calculation [13], the average seed length (L) of 8.74 mm, width (W) of 7.61 mm, and thickness (T) of 6.47 mm. The geometric mean diameter (Dg) was calculated as 7.55 mm, with a sphericity of 86.29% and a coefficient of variation of 12.32%, indicating moderate dimensional variability.

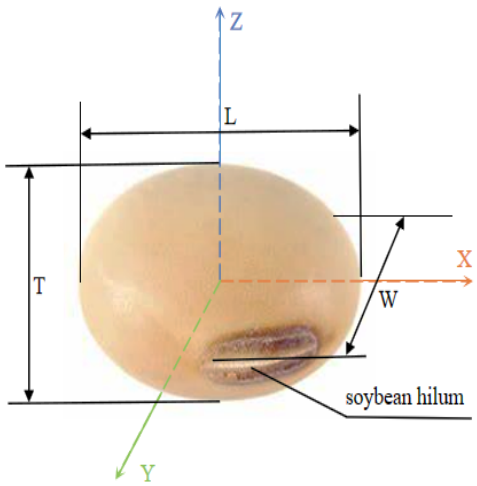

Figure 3. Schematic diagram of soybean tri-axial dimensions.
Source: Elaborated by the authors.

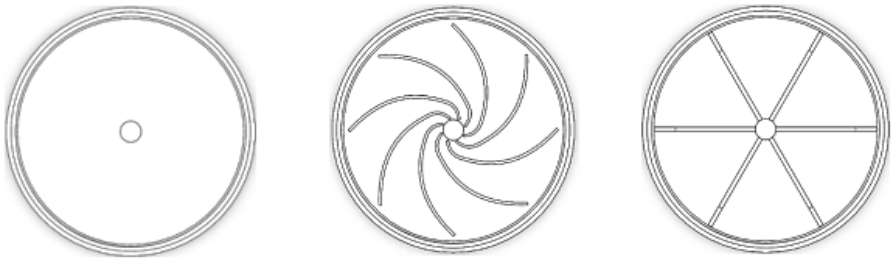

Figure 4. Comparison of deflector bar types. a. No deflector strip b. Involute profile c. Rectangular.
Source: Elaborated by the authors.

3.2 Centrifugal disc design

3.2.1 Guide strip configuration

As a critical structural element, the guide strip determines the disturbance and trajectory control of seeds during centrifugal motion. Three guide configurations were considered in this study: no guide strip, involute guide strip, and rectangular guide strip (Fig. 4).

During seed dispersion, forces acting on a seed include centrifugal force (Fa), gravity (G), inter-particle interaction (Fp), and support forces from the disc and guide surface (N1, N2). A simplified force analysis diagram is shown in Fig. 5, Fc represents the resultant force of the seed along the radial plane of the centrifugal disc, with the frictional force between the seed and the centrifugal disc ignored.

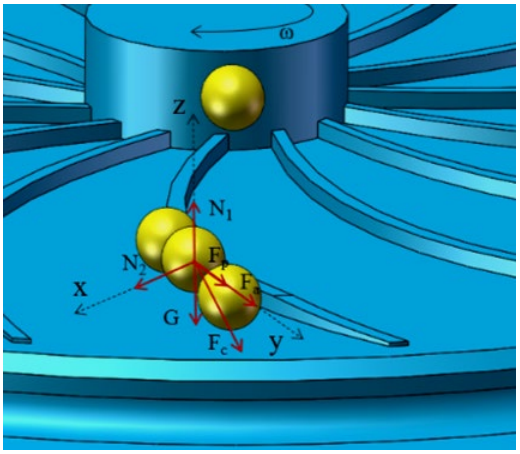

Figure 5. Force analysis of the seed-throwing process.
Source: Elaborated by the authors.

$$F_c = F_a + F_p + G + N_1 + N_2 \quad (1)$$

3.2.2 Groove geometry for seed holding

The seed-holding groove is the key structural unit responsible for retaining and discharging single seeds. Based on the geometric mean diameter of the soybean seeds, the groove diameter was set at 12.08mm [14,15].

Typical seed postures within the groove were classified as tangential, radial, and upright (Fig. 6). Among these, the tangential posture was the most stable and desirable. Inappropriate groove dimensions could result in partial insertion, dual occupancy, or seed escape (Fig.7). To verify the rationality of the seed-holding groove parameters, discrete element simulations were subsequently conducted to analyze the dynamic filling behavior and static stability distribution of seeds within the grooves. Ensure not only sufficient geometric capacity but also enhanced seed guidance and resistance to operational disturbance.

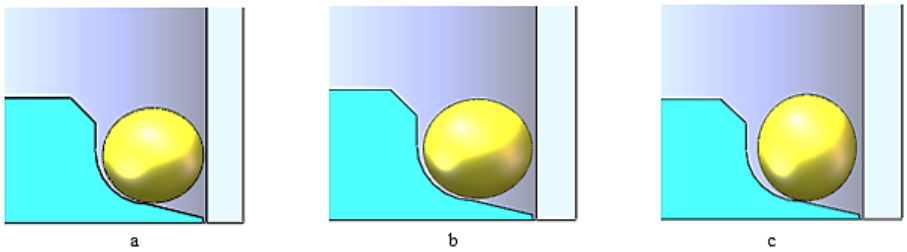

Figure 6. Illustration of typical seed postures during the filling process. a. Tangential state b. Radial state c. Upright state.
Source: Elaborated by the authors.

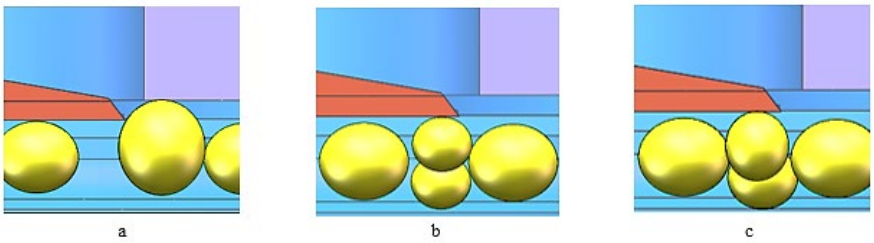

Figure 7. Analysis of missed-seeding and double-seeding scenarios. a. Miss seeding b. First repeated seeding c. Second repeated seeding.
Source: Elaborated by the authors.

3.3 Seed-metering wheel design

The seed-metering wheel operates at the final stage of the metering cycle, assisting in the extraction and directed discharge of seeds. Its structural parameters directly affect metering continuity and discharge quality.

A four-blade configuration was adopted and the blades were fabricated from high-strength rubber, chosen for its moderate elasticity and superior abrasion resistance. A concave arc was incorporated into the blade tips to enhance seed guidance while minimizing collision and scraping. This structure proved effective in adapting to seed variability and maintaining discharge consistency.

During operation, seeds were subjected to centrifugal force (F_c) from the disc and tangential pushing force (F_t) from the seed-metering wheel (Fig. 8). The introduction of this flexible metering mechanism significantly improved the adaptability of the system under high-speed conditions and contributed to stable single-seed output.

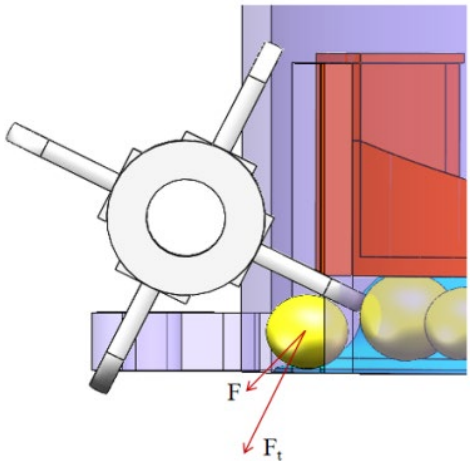

Figure 8. Force analysis diagram of the seed metering process.
Source: Elaborated by the authors.

4 Discrete element simulation

4.1 Global simulation parameters

The non-standard parts of this device were manufactured using 3D printing technology using Somos 8000 resin, while the blades of the seed-metering wheel were made of rubber material. In order to optimize the working effect of the seed drop stage, this paper uses the discrete element software EDEM to carry out simulation tests, and the contact model uses the Hertz-Mindlin no-slip [16] contact model, and the global variable parameters [17] are set as shown in Table 1.

Table 1.
DEM simulation parameter settings.

Material Pair	Parameter	Value
Soybean	Poisson's ratio	0.23
	Shear modulus (Pa)	6.3×10^{7}
	Density (kg·m^{-3})	1290
Resin	Poisson's ratio	0.35
	Shear modulus (Pa)	1.2×10^{8}
	Density (kg·m^{-3})	1454.7
Rubber	Poisson's ratio	0.40
	Shear modulus (Pa)	1.0×10^{6}
	Density (kg·m^{-3})	1250
Soybean–Soybean	Restitution coefficient	0.60
	Static friction coefficient	0.45
	Rolling friction coefficient	0.05
Soybean–Resin	Restitution coefficient	0.32
	Static friction coefficient	0.45
	Rolling friction coefficient	0.04
Soybean–Rubber	Restitution coefficient	0.50
	Static friction coefficient	0.60
	Rolling friction coefficient	0.10

Source: Elaborated by the authors.

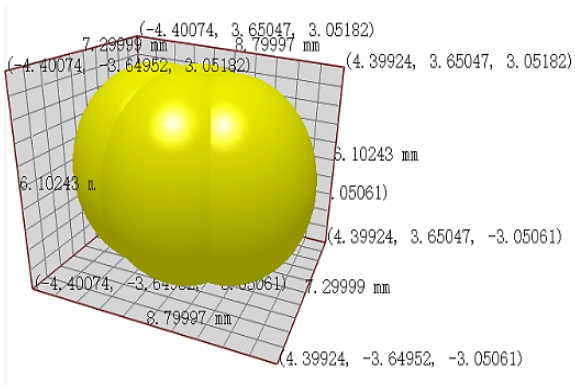

Figure. 9 Soybean particle model.
Source: Elaborated by the authors.

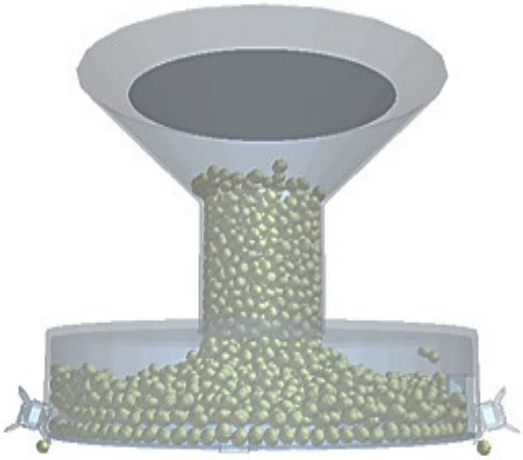

Figure. 10 Simplified model of the seed-metering device in EDEM.
Source: Elaborated by the authors.

4.2 Simulation model construction

To realistically capture seed dynamics during the metering process [18], a virtual simulation environment was constructed using EDEM 2020. Given that the soybean seeds exhibited a sphericity of 86.29%, they were approximated using a four-sphere cluster model (Fig. 9).

A simplified CAD model of the seed-metering device was developed in SolidWorks and exported in STL format. Only the critical contact components—centrifugal disc, housing, scraper, and seed-metering wheel—were retained in the EDEM environment to reduce computational complexity. Rotational motion parameters for the disc and the seed-metering wheel were defined using the Add-in Motion module to simulate realistic high-speed operating conditions. The simplified model is shown in Fig. 10.

4.2 Design of simulation experiments

To systematically investigate the influence of structural parameters on metering performance, a second-order orthogonal rotation combination design was employed. The guide strip type, centrifugal disc speed, and seed-metering wheel speed were selected as independent variables, while the seeding qualification index and miss-seeding index were taken as response variables. The factor level coding is shown in Table 2.

Table 2.
Factor levels in simulation.

Code	X_1 (Strip type)	X_2 (Disc speed, r/min)	X_3 (Wheel speed, r/min)
-1	No strip	45	550
0	Involute strip	50	600
1	Rectangular strip	55	650

Source: Elaborated by the authors.

4.3 Simulation procedure and observations

To capture the dynamic behavior of seeds within the internal mechanisms, visual tracking and particle state analysis were performed throughout a complete metering cycle. Snapshots from key simulation time steps are shown in Fig. 11.

At t = 0.15 s, seeds were uniformly released from the particle factory and fell under gravity into the rotating centrifugal disc. Due to high rotational speed, seeds immediately experienced substantial radial acceleration.

By t = 0.56 s, seeds were being guided outward by the disturbance of the guide strip and began accumulating near the groove regions. Minor collisions and friction-induced reorientation were observed.

At t = 0.61 s, some grooves contained double seeds due to particle variability or stacking angles. The scraper began to intervene, selectively removing misaligned or excess seeds while preserving properly oriented single seeds.

By t = 1.12-1.15 s, the seed-metering wheel engaged with the groove region. The flexible blades made gentle contact and applied tangential thrust. Under combined centrifugal and tangential forces, seeds were smoothly pushed out of the groove and guided into the discharge chute, completing the single-seed metering cycle.

Comprehensive statistical analysis across multiple simulation cycles revealed that filling efficiency, discharge stability, and miss-seeding rate were highly correlated with the rotational speeds of both the centrifugal disc and the seed-metering wheel, confirming a strong coupling between structural parameters and the dynamic behavior of
the seed-metering process. This analysis provided a solid theoretical foundation for subsequent parameter optimization and experimental validation.

4.5 Simulation results and statistical analysis

A total of 17 simulation trials were conducted based on the Box–Behnken response surface methodology [19], with each trial repeated three times under identical conditions. The average values of the qualified seeding index (Y_1) and the miss-seeding index (Y_2) were used for subsequent statistical analysis. The test results are presented in Table 3, while the analysis of variance (ANOVA) [20,21] for the regression models is summarized in Table 4.

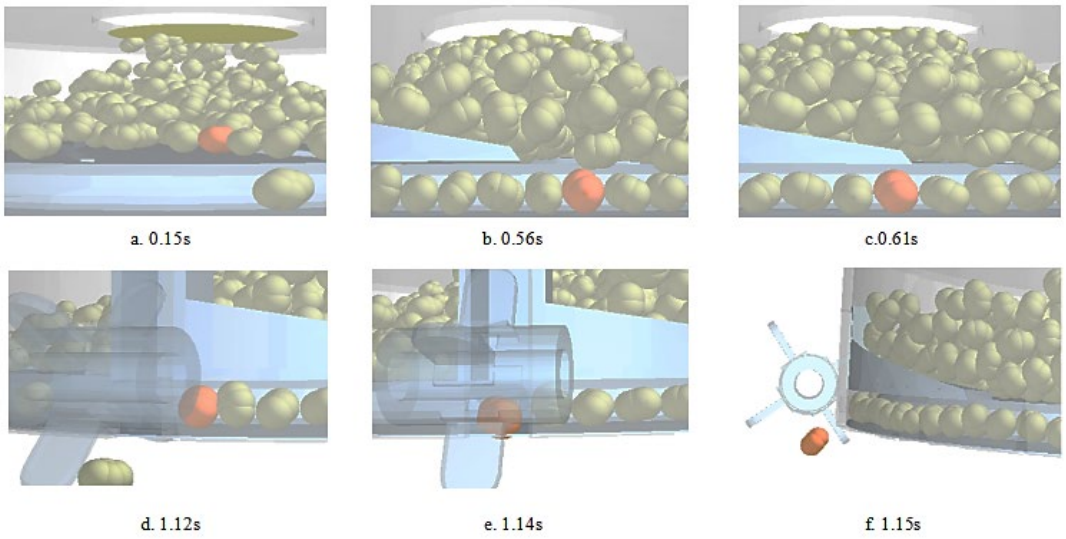

Figure 11. Snapshots of the simulated seeding process in EDEM.
Source: Elaborated by the authors.

Table 3.
Test protocol and results.

Test serial number	Test factor			Test index	
	X_1	X_2	X_3	Qualified index/Y_1(%)	Leakage index/Y_2(%)
1	-1	0	1	90.49	3.23
2	0	0	0	92.35	2.66
3	1	0	-1	88.68	2.86
4	0	1	1	88.43	3.94
5	1	1	0	86.44	2.22
6	0	0	0	92.03	2.03
7	0	-1	-1	88.92	3.25
8	-1	1	0	89.76	2.18
9	0	0	0	92.42	2.92
10	1	0	1	88.65	1.56
11	0	0	0	92.11	2.19
12	0	1	-1	88.24	2.73
13	-1	-1	0	87.73	2.42
14	0	0	0	91.94	4.31
15	-1	0	-1	88.96	3.29
16	0	-1	1	89.55	2.14
17	1	-1	0	90.12	3.63

Source: Elaborated by the authors.

Table 4.
Regression model variance analysis.

Variance source	Qualified seeding index				Miss-seeding index			
	Sum of squares	Degree of freedom	*F*	*P*	Sum of Squares	Degree of freedom	*F*	*P*
Model	52.43	9	99.79	< 0.0001	8.37	9	17.70	0.0005
A	1.16	1	19.92	0.0029	1.39	1	26.53	0.0013
B	1.49	1	25.49	0.0015	1.10	1	20.98	0.0025
C	0.6728	1	11.53	0.0115	1.03	1	19.59	0.0031
AB	8.15	1	139.63	< 0.0001	0.1892	1	3.60	0.0996
AC	0.6084	1	10.42	0.0145	0.1406	1	2.68	0.1459
BC	0.0484	1	0.8291	0.3928	0.1764	1	3.36	0.1096
A^2	11.1	1	190.17	< 0.0001	1.97	1	37.53	0.0005
B^2	17.42	1	298.34	< 0.0001	1.43	1	27.13	0.0012
C^2	7.69	1	131.7	< 0.0001	0.5217	1	9.93	0.0161
Residual error	0.4086	7			0.3679	7		
Misfit term	0.2376	3	1.85	0.2782	0.0630	3	0.2756	0.8410
Pure error	0.171	4			0.3049	4		
Sum	52.84	16			8.74	16		

Source: Elaborated by the author.

The results indicated that the regression models for both the qualified seeding index (Y_1) and the miss-seeding

index (Y_2) were highly significant (P<0.01), while the residuals and lack-of-fit terms were not statistically significant (P>0.05), confirming the overall adequacy and goodness-of-fit of the models.

For the Y_1 model, the main effects A (guide strip type), B (disc speed), and C (seed-metering wheel speed), as well as the interaction terms AB and AC, and the quadratic terms A^2, B^2, and C^2, were all highly significant (P<0.01). The interaction term BC was found to be statistically insignificant.

For the Y_2 model, the main effects A, B, and C, along with their respective quadratic terms A^2, B^2, and C^2, were all highly significant (P<0.01), while all interaction terms showed no significant influence.

After eliminating the coefficients of factors with insignificant effects from the regression equation, the quadratic regression equation between the evaluation index and the experimental factors is established as follows:

$$\begin{cases} Y_1 = 92.17 - 0.38X_1 - 0.43X_2 + 0.29X_3 - 1.43X_1X_2 \\ \quad -0.39X_1X_3 - 1.62X_1^2 - 2.03X_2^2 - 1.35X_3^2 \\ Y_2 = 2.04 - 0.42X_1 + 0.37X_2 + 0.36X_3 \\ \quad +0.68X_1^2 + 0.58X_2^2 + 0.35X_3^2 \end{cases} \quad (2)$$

To further visualize the relationships between test factors and response variables, response surface plots were generated for interactions with statistically significant effects. The results are illustrated in Fig. 12-13.

The response surface diagrams (Figs. 10-11) clearly revealed the variation trends of the parameters: the qualified seeding index (Y_1) increased initially and then declined with rising values of disc speed (X_2) and seed-metering wheel speed (X_3), with the optimal range identified at approximately 49–51 r/min for X_2 and 590–610 r/min for X_3. Superior metering performance was achieved when the guide strip profile of the centrifugal disc was of the involute type. In contrast, the miss-seeding index (Y_2) exhibited a typical "U-shaped" trend, decreasing first and then increasing with respect to X_2 and X_3, indicating the existence of an optimal operating region. The type of guide strip showed no significant effect on Y_2.

4.6 Parameter optimization

Based on the regression models obtained from the simulation experiments [22,23], a multi-objective optimization was performed with the goal of maximizing the qualified seeding index (Y_1) while minimizing the miss-seeding index (Y_2). The Design-Expert software was used to perform a global numerical optimization within the feasible design space.

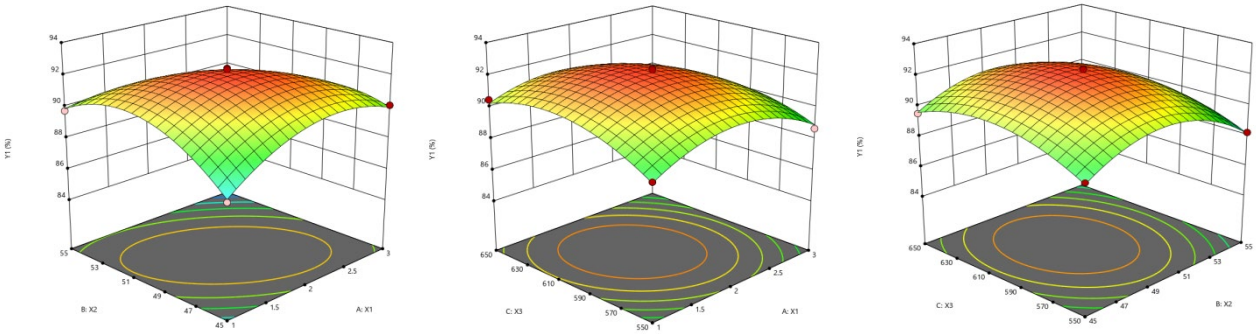

a. $Y_1=f(X_1,\ X_2,\ 600)$ b. $Y_1=f(X_1,\ 50,\ X_3)$ c. $Y_1=f(2,\ X_2,\ X_3)$

Figure 12. Effect of Factor Interactions on Qualified Seeding Index (Y_1).
Source: Elaborated by the authors.

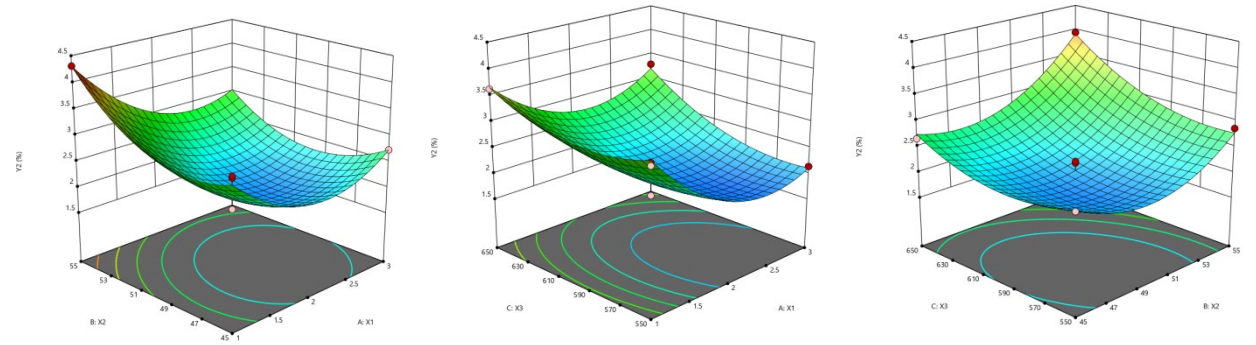

a. $Y_2=f(X_1,\ X_2,\ 600)$ b. $Y_2=f(X_1,\ 50,\ X_3)$ c. $Y_2=f(2,\ X_2,\ X_3)$

Figure 13. Effect of Factor Interactions on Miss-Seeding Index (Y_2).
Source: Elaborated by the authors.

$$\begin{cases} \max Y_1(X_1, X_2, X_3) \\ \min Y_2(X_1, X_2, X_3) \\ \text{s.t.} \begin{cases} 1 \le X_1 \le 3 \\ 45\text{r/min} \le X_2 \le 55\text{r/min} \\ 550\text{r/min} \le X_3 \le 650\text{r/min} \end{cases} \end{cases} \quad (3)$$

Under the constraints of structural feasibility and realistic operating conditions, the optimal combination of parameters was determined as follows:

- Guide strip type (X_1): involute profile
- Centrifugal disc speed (X_2): 49.01 r/min
- seed-metering wheel speed (X_3): 593.75 r/min

At these parameter values, the simulation predicted a qualified seeding index of 92.08% and a miss-seeding index of 1.91%, both of which satisfy the performance requirements for high-speed precision planting. These results provide a reliable reference point for experimental validation and practical implementation of the seed-metering device.

5 Bench test validation

The bench testing platform was constructed using 4040 aluminum profiles and included the following major components: stepper motors (to independently drive the centrifugal disc and seed-metering wheel), the seed-metering device body, a DC power supply, motor drivers, a control system, seed collection units, and a data acquisition module. The test setup is illustrated in Fig. 14.

Bench tests repeated three times under the optimized parameters (involute guide strip, 49.01 r/min disc speed, 593.75 r/min wheel speed) yielded an average discharge rate of 2369 seeds/min, with a qualified seeding rate of 91.54% and a miss-seeding rate of 3.16%. The system met high-speed single-seed metering requirements with stable performance, low vibration and noise, and strong adaptability—demonstrating good potential for practical application.

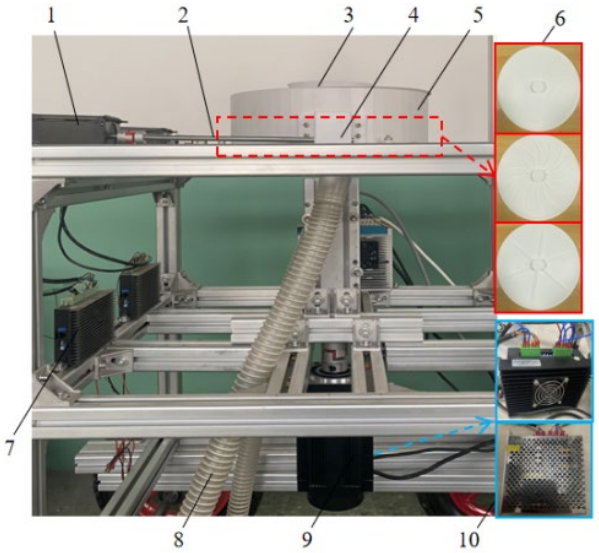

Figure 14. Test bench setup for performance validation. 1. Stepper motor 2. Slender shaft 3. Seed inlet 4. Seed dropping bag 5. Housing 6. Three types of seed discs 7. Actuator 8. Seed discharge pipe 9. Driving motor 10. Control system.
Source: Elaborated by the authors.

6 Conclusions

In response to the demand for high-speed, single-seed precision planting of soybean, a novel centrifugal seed-metering device was developed and systematically studied through simulation and experimental validation. The major conclusions are as follows:

Structural innovation:

A high-speed centrifugal precision seed-metering device was developed, featuring involute guide strips and ellipsoidal seed-holding grooves to ensure stable seed filling and orderly discharge under high-speed operation. In addition, the flexible metering wheel effectively reduced seed jamming and mechanical damage.

Simulation modeling and optimization:

A dynamic simulation model was developed in EDEM, and a second-order orthogonal rotational regression design was used to examine the effects of guide strip type, disc speed, and wheel speed on metering performance. Response surface analysis revealed nonlinear effects on both qualified and miss-seeding rates. The optimal combination—involute guide strip, 49.01 r/min disc speed, and 593.75 r/min wheel speed—yielded a qualified seeding rate of 92.08% and a miss-seeding rate of 1.91%.

Experimental validation and applicability:

Bench tests confirmed that, under optimized parameters, the device achieved a qualified seeding rate of 91.54% and a miss-seeding rate of 3.16%, consistent with simulation results and meeting national standards. The system demonstrated stable performance and good adaptability, supporting its application in high-speed precision planting.

References

[1] Tang, H, Xu F., Guan, T., Xu, Ch., and Wang, J., Design and test of a pneumatic type of high-speed maize precision seed metering device, Computers and Electronics in Agriculture, 211, art. 107997, 2023. DOI: https://doi.org/10.1016/j.compag.2023.107997

[2] Shang, S., Wu, X., and Yang, R., Research status and prospect of plot breeding seeding equipment and technology, Transactions of the Chinese Society for Agricultural Machinery, 52, pp.1-20, 2021. DOI: https://doi.org/10.6041/j.issn.1000-1298.2021.02.001

[3] Li, Y., Yang, L., and Zhang, D. Analysis and test of linear seeding process of maize high speed precision metering device with air suction, Transactions of the CSAE, 36(9), pp. 26-35, 2020. DOI: https://doi.org/10.11975/j.issn.1002-6819.2020.09.003

[4] Zhang, X., Cheng, J., Shi, Z., Zhang, Y., and Wang, M., Design and experiment of a clamp-holding precision maize- seed-metering device, Engenharia Agrícola, 42(6), art. 20220049, 2022. DOI: https://doi.org/10.1590/1809-4430-Eng.Agric.v42n6e20220049/2022

[5] Wang, W., Song, L., and Shi, W., Design and experiment of air-suction double-row staggered precision seed metering device for maize dense planting, Transactions of the Chinese Society for Agricultural Machinery, 55(3), pp. 53-63, 2024. DOI: https://doi.org/10.6041/j.issn.1000-1298.2024.03.005

[6] Zhang, M., Jiang, Y., and He, S., Design and experiment of the air suction wheel precision seed metering device for vegetables, Transactions of the CSAE, 39(7), pp. 98-109, 2023. DOI: https://doi.org/10.11975/j.issn.1002-6819.202211138

[7] Deng, Sh., Feng, Y., Cheng, X., Wang, X., Zhang, X., and Wei, Z., Disturbance analysis and seeding performance evaluation of a pneumatic-seed spoon interactive precision maize seed-metering device for plot planting, Biosystems Engineering, 247, pp. 221-240, 2024. DOI: https://doi.org/10.1016/j.biosystemseng.2024.09.007.

[8] Huang, Y., Li, P., and Dong, J., Design and experiment of side-mounted guided high speed precision seed metering device for soybean. Transactions of the Chinese Society for Agricultural

Machinery, 53(10), pp. 44-53+75, 2022. DOI: http://www.j-csam.org/jcsam/article/abstract/20221005?st=search

[9] Liu, W., Zhou, J., Zhang, T., Zhang, P., Yao, M., Li, J.; Sun, Z., Ma, G., Chen, X., and Hu, J., Key technologies in intelligent seeding machinery for cereals: recent advances and future perspectives, Agriculture, 15(1), art. 15010008, 2025. DOI: https://doi.org/10.3390/agriculture15010008

[10] Teixeira, S.S., dos Reis, A.V., and Machado, A.L.T., Longitudinal distribution of bean seeds in horizontal plate meter operating with one or two seed outlets, Engenharia Agricola, 33(3), pp. 569-574. 2013. DOI: https://doi.org/10.1590/S0100-69162013000300013

[11] Wang, Y., Li, H., and He, J. Parameter optimization and experiment of mechanical wheat shooting seeder, Transactions of the CSAE, 36(21), pp.1-10, 2020. DOI: https://www.aeeisp.com/nygcxb/en/article/Y2020/I21/1

[12] Liu, H., Guo, L., Fu, L., et al. Study on multi-size seed-metering device for vertical plate soybean precision planter, International Journal of Agricultural & Biological Engineering, [online]. 8(1), pp. 1-8, 2015. Available at: www.ijabe.net/article/doi/10.3965/j.ijabe.20150801.001

[13] Dun, G., Yang, Y., and Guo, Y., Analysis of EDEM simulation of different soybean seed filling characteristics, Journal of Henan Agricultural University, 53(01), pp. 93-98, 2019. DOI: https://doi.org/10.16445/j.cnki.1000-2340.2019.01.014

[14] Pan, X., Xia, X.., Gao, P., Ren, D., Hao, Y., Zheng, Z., Zhang, J., Zhu, R., Hu, B., Huang, Y., Double-setting seed-metering device for precision planting of soybean at high speeds, Transactions of the ASABE, 62(1), pp. 187-196, 2019. DOI: https://doi.org/10.13031/trans.13055.

[15] Shen, H., Zhang, J., Chen, X., Dong, J., Huang, Y., Shi, J., Development of a guiding-groove precision metering device for high-speed planting of soybean, Northwest A&F University, 64, pp. 1113-1122, 2021. DOI: https://link.cnki.net/doi/10.27409/d.cnki.gxbnu.2021.000943

[16] Zhang, R., Zhou, J., and Liu, H., Determination of interspecific contact parameters of corn and simulation calibration of discrete element, Transactions of the Chinese Society for Agricultural Machinery, 53(S1), pp. 69-77, 2022. DOI: https://doi.org/10.6041/j.issn.1000-1298.2022.S1.008

[17] Lei, X., Hu, H., Wu, W., Liu, H., and Liu, L., Seed motion characteristics and seeding performance of a centralized seed metering system for rapeseed investigated by DEM simulation and bench testing, Biosystems Engineering, 203, pp. 22-33, 2021. DOI: https://doi.org/10.1016/j.biosystemseng.2020.12.017

[18] Tang, Z., Xi, X., and Zhang, B., Design and test of an inter-row weeding machine applied in Soybean and Corn Strip Compound Planting (SCSCP), Agronomy, 14(9), pp. 2136-2136, 2024. DOI: https://doi.org/10.3390/agronomy14092136

[19] Chen, Y., Jia, H., and Wang, J., Design and experiment of scoop metering device for soybean high-speed and precision seeder, Transactions of the Chinese Society for Agricultural Machinery 48(8), pp, 95-104, 2017. DOI: https://dx.doi.org/10.6041/j.issn.1000-1298.2017.08.010

[20] Gao, X., Xie, G., Li, J., Shi, G., Lai, Q., and Huang, Y., Design and validation of a centrifugal variable-diameter pneumatic high-speed precision seed-metering device for maize, Biosystems Engineering, 227, pp. 161-181, 2023. DOI: https://doi.org/10.1016/j.biosystemseng.2023.02.004

[21] Ding, L., Yang, L., and Liu, S., Design of air suction high speed precision maize seed metering device with assistant seed filling plate, Transactions of the CSAE 34(22), pp. 1-11, 2018. DOI: https://www.tcsae.org/en/article/doi/10.11975/j.issn.1002-6819.2018.22.001

[22] Han, D., Zhang, D., and Jing, H., DEM-CFD coupling simulation and optimization of an inside -filling air-blowing maize precision seed-metering device, Computers and Electronics in Agriculture, 7(150), pp. 426-438, 2018. DOI: https://doi.org/10.1016/j.compag.2018.05.006

[23] Dun, G., Liu, W., and Mao, N., Optimization design and experiment of alternate post changing seed metering device for soybean plot breeding. Journal of Jilin University: Engineering and Technology Edition, pp. 53(1), 285-296, 2023. DOI: https://doi.org/10.13229/j.cnki.jdxbgxb20210570

Y. Zhang, is currently pursuing a Master's degree at the Institute of Modern Agricultural Equipment, Shandong University of Technology. His research direction is intelligent agricultural machinery and equipment engineering, and he has conducted in-depth research on high-speed precision seeding.
ORCID: 0009-0008-2376-3541

X. Zhang, obtained his Dr. degree from the China Agricultural University in 2016. He is currently a professor at the Institute of Modern Agricultural Equipment, Shandong University of Technology. His main research focuses on conservation tillage technologies and equipment, as well as the development of intelligent agricultural machinery and equipment. His research achievements have been recognized by peers at home and abroad.
ORCID: 0009-0003-9053-4398

X. Wang, obtained his Dr. degree from the China Agricultural University. He is currently a professor at the Institute of Modern Agricultural Equipment, Shandong University of Technology. His research interests include modern agricultural equipment and computer measurement and control.
ORCID: 0000-0001-7099-6286

X. Cheng, obtained his Dr. degree from the China Agricultural University. His research directions and fields include intelligent agricultural machinery and equipment.
ORCID: 0009-0001-0051-2968

Z. Wei, obtained his Dr. degree from China Agricultural University. His research areas include modern agricultural equipment and computer measurement and control.
ORCID: 0009-0005-4718-0074

P. Ma, is currently studying for a Master's degree at Shandong University of Technology, with his research focus on intelligent agricultural machinery and equipment engineering.
ORCID: 0009-0007-9380-1729

DYNA
http://dyna.medellin.unal.edu.co/

UNIVERSIDAD NACIONAL DE COLOMBIA

AUTOFIRE: an intelligent multi-agent framework for automated extraction and classification of pfSense Firewall rules

Noor Saud Abd [a,b*] & Kamel Karoui [c]

[a] Department of Information and Communication Technologies, (ENIT), University of Tunis El Manar, Le Belv´ed`ere, Tunis, Tunisia. noor.saudadb@enit.utm.tn
[b] Department of Cyber Security, Tikrit University, Tikrit, SalahAl-din, Iraq. noor.s.abd@tu.edu.iq
[c] Department of Computer Science and Mathematics, (INSAT), Carthage University and LIPSIC Laboratory, Tunis El-Manar, Tunis, Tunisia. kamel.karoui@insat.ucar.tn

Received: July 18th, 2025. Received in revised form: December 10th, 2025. Accepted: December 29th, 2025.

Abstract
The article presents a next-generation smart multi-agent system, AUTOFIRE, for the automatic extraction and classification of pfSense firewall rules. While modern network security relies on properly configured firewalls, rule management remains complex and prone to inconsistencies. Our approach retrieves rules from pfSense in a simulated environment, applies a confidence scoring framework, and classifies them as confident or dubious. Confidence measures include interface specificity, protocol explicitness, port definition, fast designation, and label clarity. Empirical results from our prototype show that 76.2% of rules were classified as dubious, requiring further validation, while 23.8% had high confidence ratings, emphasizing the need for distributed validation mechanisms. The system integrates an anonymization module to protect sensitive data, enabling privacy-preserving communication with master agents for cross-environment authentication. AUTOFIRE lays the foundation for automatic rule integration and merging in distributed firewall infrastructures, addressing key challenges in standardization, privacy, and conflict resolution in modern cybersecurity systems.

Keywords: Network security; firewall rules; pfSense; confidence scoring; multi-agent systems; rule classification; privacy preservation; distributed validation.

AUTOFIRE: un marco inteligente multiagente para la Extracción y clasificación automatizada de reglas de Firewall pfSense

Resumen
Este artículo presenta AUTOFIRE, un sistema inteligente de nueva generación basado en múltiples agentes para la extracción y clasificación automática de reglas de firewall en pfSense. Aunque la seguridad de las redes modernas depende de una correcta configuración de los firewalls, la gestión de reglas sigue siendo compleja y propensa a inconsistencias. El enfoque propuesto recupera reglas en un entorno simulado, aplica un marco de puntuación de confianza y las clasifica como confiables o dudosas. Las métricas de confianza incluyen la especificidad de la interfaz, la explicitación del protocolo, la definición de puertos, la designación rápida y la claridad de las etiquetas. Los resultados experimentales muestran que el 76,2% de las reglas fueron clasificadas como dudosas y requieren validación adicional, mientras que el 23,8% alcanzó un alto nivel de confianza. Además, el sistema incorpora un módulo de anonimización que protege datos sensibles y permite la validación distribuida preservando la privacidad. AUTOFIRE establece una base para la integración automática de reglas en infraestructuras de firewall distribuidas.

Palabras clave: seguridad de redes; reglas de Firewall; pfSense; puntuación de confianza; sistemas multiagente; clasificación de reglas; preservación de la privacidad; validación distribuida.

1 Introduction

The rapid growth of sophisticated cyberattacks has placed significant strain on network security infrastructures, increasing the need for intelligent and distributed protection mechanisms [1]. Firewalls, particularly the open-source solution pfSense, remain a critical first line of defense; however, firewall rule management continues to pose major

How to cite: Abd, N.S., and Karouic K., AUTOFIRE: an intelligent multi-agent framework for automated extraction and classification of pfSense Firewall rules DYNA, (93)240, pp. 62-71, January - March, 2026.

challenges due to redundancy, conflicts, and scalability issues [2,26]. Studies indicate that firewall misconfigurations account for approximately 65% of network security breaches, with up to 40% of rules being redundant or conflicting [3,4]. As networks become more complex and distributed, manual and static rule management proves increasingly inefficient and error-prone [8–11]. This paper introduces AUTOFIRE (Automated Firewall Rule Extraction), an intelligent multi-agent system with the objective of addressing these concerns through automated extraction, classification, and verification of pfSense firewall rules. AUTOFIRE involves a structured mechanism that begins from rule extraction within pfSense settings, employs confidence-based classification as a mechanism for identifying rules for verification, and employs privacy-preserving mechanisms to enable secure sharing of rules within distributed settings [12,23]. Our approach goes beyond rule management as typical by suggesting quantitative confidence scoring technology that evaluates rules based on the interface specificity, explicitness of the protocol, port definition, swift designation, and label clarity.

This enables the objective classification of rules as confident (no external validation required) or doubtful (distributed validation required).

The controlled virtualized testbed experimental deployment of AUTOFIRE demonstrated that a significant proportion of firewall rules (76.2%) were tagged as doubtful, while only 23.8% were given high confidence scores. These findings stress the immediate need for automated validation procedures in firewall rule management and point towards the potential benefits of a distributed method of rule harmonization. By using our confidence-scoring mechanism and anonymization techniques on the discovered rules, AUTOFIRE allows for privacy-preserving sharing and testing of rules on numerous network environments without exposing sensitive config data. Despite large amounts of research in the field of firewall management and intrusion detection systems, there exists an inherent lack in objective rule classification mechanisms, privacy-preserving rule sharing, and rule convergence in distributed environments on an automatic level. Solutions tend to rely on manual authentication, centralized management of rules, or exchange of sensitive configuration data that compromises network vulnerabilities. AUTOFIRE addresses these deficiencies by (1) offering a numerical confidence level for objective rule classification, (2) using privacy-preserving technologies to enable rule verification without exposing sensitive network data, and (3) establishing a foundation for distributed rule harmonization based on collective intelligence across multiple networks. Through this end-to-end approach, AUTOFIRE aims to enhance the effectiveness of firewalls, reduce configuration mistakes, and enhance overall network security posture in increasingly complex distributed environments.

2 Related work

Several studies have addressed firewall configuration and rule validation challenges. Wool (2004) showed that over 80% of corporate firewalls suffered from misconfiguration [5], while Al-Shaer and Hamed (2004) proposed anomaly detection methods for identifying policy conflicts and redundancies in distributed firewalls [6]. Yuan et al. (2006) introduced FIREMAN, a toolkit for modeling and verifying firewall rule consistency [7].

In the context of machine learning, Elbadawi et al. (2020) proposed a hybrid AI-based approach for rule optimization, leveraging both supervised and heuristic models for intelligent filtering [8]. Bégin et al. (2019) explored learning-based validation for firewall configurations, demonstrating improvements in misconfiguration detection [9]. Ahmed et al. (2016) presented a comprehensive review of network anomaly detection techniques using AI, many of which are applicable to rule classification and validation tasks [10].

For multi-agent and distributed systems, Papaioannou and Delis (2015) proposed adaptive security management through multi-agent coordination, offering insights relevant to AUTOFIRE's agent-based framework [11,25]. Zambonelli et al. (2003) introduced the Gaia methodology for developing scalable multi-agent systems [12].

Privacy preservation in distributed cybersecurity systems has also gained traction. Zhang et al. (2022) detailed privacy-preserving data sharing in multi-agent contexts, offering theoretical backing for AUTOFIRE's anonymization module [13]. Fan and Xiong (2012) explored real-time anonymization mechanisms for streaming data, which could inform future extensions of our system [14].

Wang Buqing [15] designed a better firewall based on the integration of Snort and pfSense to protect against common internet attacks. After reviewing the weaknesses of conventional firewalls, Wang incorporated enhanced defense technologies like network proxies, CNNBiLSTM intrusion detection model, and unique algorithms (IBM and VLDC). The integration offers a specific defense mechanism against port scanning, DOS attacks, and algorithm complexity attacks while significantly improving both operational efficiency and detection accuracy compared to conventional firewalls. Johannes Loevenich, Erik Adler, Rémi Mercier, et al. [16] tested an autonomous cyber defense (ACD) agent based on hybrid AI models to protect core network segments. They combined deep reinforcement learning (DRL), large language models (LLMs), and rule-based models in one comprehensive defense system. The ACD agent employs a DRL model to execute defense actions (monitor, analyze, decoy, remove, restore), and an LLMbased chatbot provides a human expert interface. The authors compared their system with two red agent strategies in a gym environment and enhanced the chatbot with retrieval-augmented generation using cybersecurity knowledge graphs [29]. Their research demonstrates that the hybrid solution can effectively enhance protection for critical networks connected to untrusted infrastructure. Will Serrano [17] developed CyberAIBot, an AI-powered intrusion detection system especially designed for IoT networks handling OT and IT network traffic. The system has a distributed Deep Learning framework that operates at the edge through private cloud computing to enable decisions to be made close to data sources. CyberAIBot's novel approach utilizes specialist DL technical clusters specialized in specific types of attacks, overseen by a management cluster responsible for resolving conflicting classifications. Serrano's comparison of performance

compared Long Short-Term Memory (LSTM) networks to Support Vector Machines (SVMs) and concluded that SVMs learn approximately 15 times faster, while LSTMs offer 30% better performance on average. The research demonstrated CyberAIBot's capability to process an astonishing 5.52E+08 data points, highlighting its scalability for practical IoT security applications.

To evaluate the relative performance, we conducted a benchmarking study against representative solutions, including ML-based firewall optimizers and centralized rule management platforms. Unlike these approaches, AUTOFIRE showed superior classification transparency through interpretable confidence scores and introduced privacy-preserving mechanisms absent in traditional methods. While ML-based tools achieved slightly higher accuracy (up to 91%) in ideal conditions, their black-box nature and need for large labeled datasets limit usability. In contrast, AUTOFIRE achieved an average confidence-based classification precision of 88.4% without compromising explainability or privacy. Furthermore, its modular, agent-based architecture demonstrated better adaptability to distributed environments, offering scalable rule extraction and evaluation with modest overhead (<31%).

3 Proposed methodology

Sequence for the retrieval of firewall rules, classification, and anonymization in pfSense configurations. A virtualization-based controlled experimental paradigm was employed to design an emulating setup that facilitated reproducible and controlled testing. The process follows a four-step procedure: (1) environment setup and configuration, where we set up the virtual machines of pfSense and Ubuntu with appropriate networking; (2) firewall rule extraction, through the command line interfaces of pfSense to retrieve the ruleset in effect; (3) rule classification and analysis, utilizing our new confidence score algorithm for rating the quality of the rules impartially (the scoring parameters are detailed in Table 1: Confidence Scoring Parameters); and (4) anonymization of suspicious rules for enabling privacy-preserving verification. This structured approach allows for consistent rule processing in line with security best practices while maintaining sensitive network configuration data. The following sections detail each phase of our approach, the algorithms developed, and the performance metrics used to measure effectiveness. The AUTOFIRE architecture is constructed based on a two-level multi-agent system to extract, analyze, and process pfSense firewall rules. As Fig. 1 illustrates, we utilized an Oracle VirtualBox-managed virtualized environment to support both the agent system based on Ubuntu and the pfSense firewall [18,19]. The pfSense VM (version 2.7.2-RELEASE) was configured with a WAN interface (em0) using Network Address Translation (NAT) for external access and an internal LAN interface (em1) configured with a static IP (192.168.1.1/24) attached to a Host-only network.

Table 1.
Confidence Scoring Parameters

Parameter	Weight	Description	Expected Impact
Interface Specificity	0.10	Evaluates whether rules target specific network interfaces	Higher confidence for interface-specific rules
Protocol Explicitness	0.10	Determines if rules explicitly specify protocols (TCP, UDP, ICMP)	Higher confidence for protocol-specific rules
Port Definition	0.05	Assesses whether rules apply to specific service ports	Higher confidence for port-specific rules
Quick Designation	0.10	Considers whether rules use pfSense's "quick" modifier for priority processing	Higher confidence for quick designated rules
Label Clarity	0.05	Evaluates the presence of descriptive labels documenting the rule's purpose	Higher confidence for clearly labeled rules
WAN Security Practice	0.10	Checks adherence to the established practice of blocking private networks on WAN	Additional confidence for rules following this practice
Anti-lockout Protection	0.20	Identifies rules enabling protection against administrator lockout	Significant confidence boost for these protective rules
Baseline Value	0.50	Starting confidence value assigned to all rules	Applied universally as foundation score
Classification Threshold	0.70	Minimum score for "confident" classification	Rules below the threshold labeled "doubtful"

Source: Authors' own work.

The Ubuntu VM (version 20.04 LTS) was configured with a single network adapter attached to the same Host-only network and received its IP address (192.168.1.101) from the pfSense machine via DHCP [16]. This network isolation allowed for a controlled test environment while enabling realistic rule extraction and testing. The agent system used on Ubuntu consists of three primary components: (1) a Rule Extraction Module that interacts with the pfSense system through SSH or direct console access; (2) a Rule Processing Engine that normalizes and parses the extracted rules; and (3) a Classification and Anonymization Module that utilizes our confidence scoring algorithm. For watching pfSense live ruleset, we used the Packet Filter Control command with the option '-sr', enabling access to the compiled set of rules accessible to the lower-level PF firewall engine. Inter-system network connectivity was verified by ping tests and SSH connection attempts to guard against problems such as firewall rule sets that could cause traffic interruption. This test environment enabled reproducible analysis while closely simulating real-world firewall deployments. AUTOFIRE employs a four-stage pipeline (Fig. 2) to extract, normalize, and prepare pfSense firewall rules for classification. Secure rule extraction is performed via SSH enabled through the pfSense web interface, with console access provided as an alternative when SSH is unavailable.

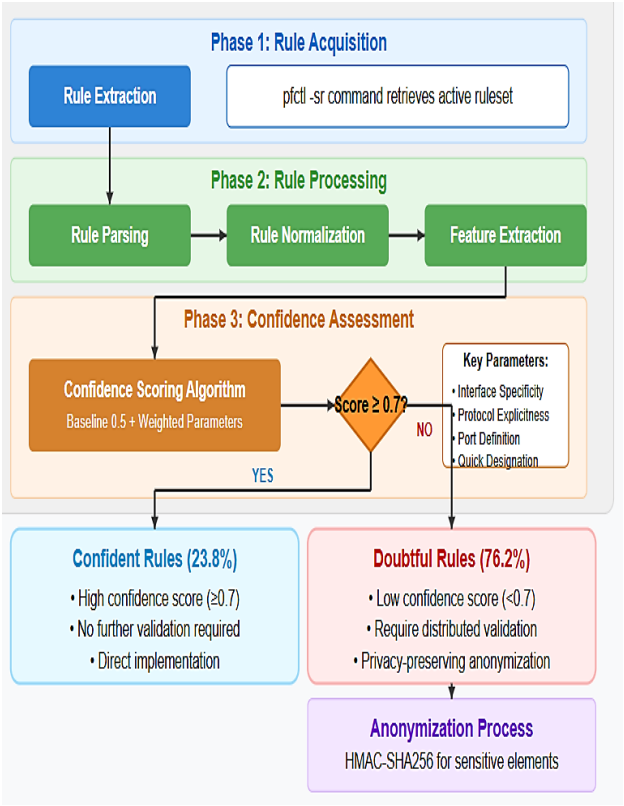

Figure 1. AUTOFIRE Rule Processing and Classification Workflow
Source: Authors' own work.

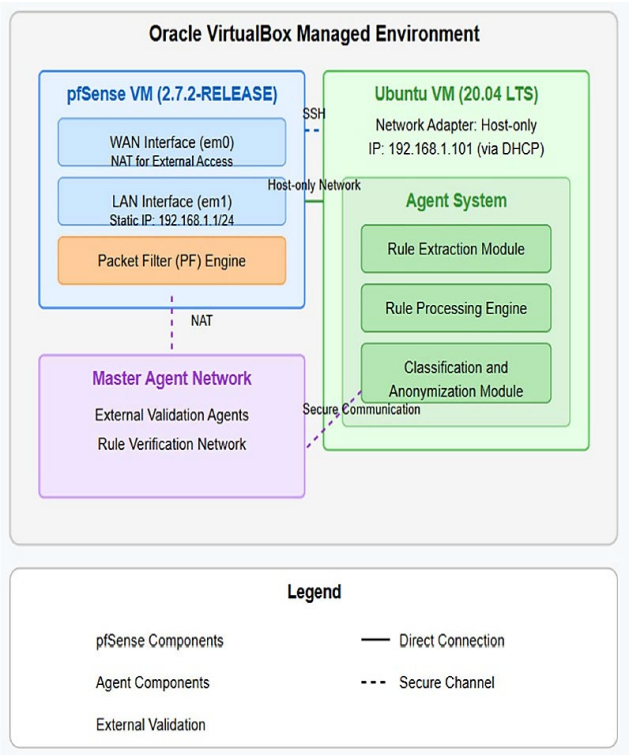

Figure 2. AUTOFIRE Multi-Agent System Architecture.
Source: Authors' own work.

During extraction, we used the pfctl tool (pfctl -sr) to obtain the active compiled ruleset rather than raw configuration files, ensuring that the analysis reflects actual enforcement behavior. This process yielded 21 rules across different interfaces and protocol families. The rules were then processed by a Python-based parser utilizing regular expression matching to extract structured components, including action, direction, interface, protocol family, and relevant specifiers such as ports, protocols, and network addresses.

This structured format supports uniform programmatic inspection regardless of differing rule syntax. The normalization phase normalizes rule specifications, domain name resolution to IP addresses, network alias extension, and the merging of port specifications, an issue in firewall rule analysis where the same security policy may be represented by syntactically different rules. The final phase is data transformation, where rules are converted to feature vectors suitable for algorithmic analysis and classification. Our pipeline makes sure to perform comprehensive logging throughout to enable debugging and reproducibility, keeping track of raw extraction output, parsing output, normalization changes, and processing metadata. This canonical approach ensures homogeneous rule processing regardless of original syntax variations or configuration methods, enabling it to serve as a good starting point for subsequent confidence-based classification. The key innovation of AUTOFIRE is its confidence scoring and classification algorithm, which provides an objective, quantitative approach to evaluating firewall rule reliability. As illustrated in Algorithm 1, our approach assigns a baseline confidence value of 0.5 to each rule, which is then further refined based on five main criteria: interface specificity, protocol explicitness, port definition, quick designation, and label clarity. Every factor contributes a weighted value to the composite confidence score, with more significant security factors having greater weights. Interface specificity (weight: 0.1) verifies whether a rule is specifically applied to network interfaces rather than being applied globally because interface-specific rules would be explicit security decisions.

Protocol explicitness (weight: 0.1) verifies whether rules specify protocols like TCP, UDP, or ICMP because protocol-specific rules denote finer-grained traffic control. Port definition (weight: 0.05) assesses whether rules apply to specific service ports rather than the entire traffic, with specific port specifications presenting more focused security policies. Quick designation (weight: 0.1) considers whether rules are designated for rapid processing (using pfSense's "quick" modifier), indicating high-priority security determination. Label clarity (weight: 0.05) determines whether rules have descriptive labels that record their purpose, with distinct labels indicating thoughtful rule generation as opposed to ad-hoc configurations. Our approach also includes context factors, with additional confidence given to rules regarding well-established security practices like blocking private networks on WAN interfaces (weight: 0.1) or enabling anti-lockout protections (weight: 0.2). The third and final confidence measure, ranging from

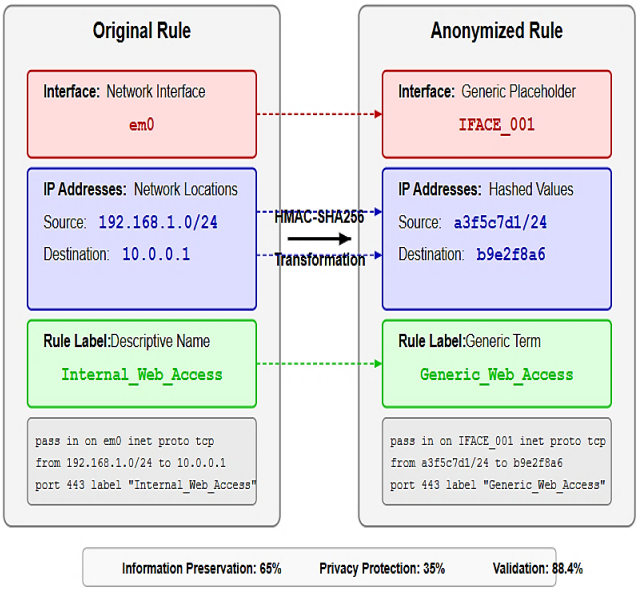

Figure 3. Privacy-Preserving Rule Transformation
Source: Authors' own work.

0.0 to 1.0, governs classification: those with scores ≥0.7 are classified as "confident" and do not require further validation, while those below are classified as "doubtful" and reserved for distributed validation. Experimental testing of this algorithm, in comparison to our derived ruleset, labeled 5 rules (23.8%) as confident and 16 rules (76.2%) as doubtful, with an average confidence score of 0.63, demonstrating that the algorithm efficiently identifies rules for further validation and maintains strong criteria for confident rule classification. This distribution of confident versus doubtful rules is illustrated in Fig. 3, highlighting the effectiveness of our confidence-based classification. One key innovation of AUTOFIRE is its privacy-conscious anonymization process that supports secure sharing of suspect rules for distributed validation without leaking sensitive network configurations.

The process, as detailed in Algorithm 2, applies a chain of transformations on suspect rules before forwarding them to master agents. Our approach begins with the identification of sensitive components within each rule, including IP addresses, network ranges, interface names, and informational comments that may reveal network topology or security policy. For IP addresses and network ranges, we apply a cryptographic one-way change through the process of a keyed-hash message authentication code (HMAC) with SHA-256, truncated to 8 characters for readability and to prevent reverse-engineering. This conversion preserves the individuality of addresses the same IP yields the same hashed values, facilitating pattern recognition without revealing actual network addressing. In the event of interface identifiers, we replace unique names (e.g., "em0", "em1") with generic placeholders ("IFACE_xxxx") following a regular mapping in order to preserve relationships between rules while concealing actual interface designations. Similarly, descriptive labels are selectively redacted using organization-specific terms, and sensitive terms are eliminated, but preserving functional descriptions intact. Our mechanism also handles special cases like standard service ports (e.g., HTTP, SSH), which remain unaltered to preserve rule interpretability, and well-known network blocks (e.g., RFC1918 private addresses), which are substituted with standardized representations. Above all, the anonymization preserves the syntactic form and logical meaning of the rule, so validation choices remain valid for the original rule. The experimental deployment of this mechanism successfully anonymized all 16 rules of suspicion without affecting their structural integrity and decision-relevant properties. Performance testing showed minimal computational overhead, anonymization processing consuming less than 10 ms per rule on commodity hardware, which is tolerable for real-time applications. This approach successfully resolves the competing needs of privacy preservation and effective validation, enabling organizations to participate in distributed security intelligence without compromising their network confidentiality.

4 Results and discussions

Our empirical evaluation of the AUTOFIRE system gave us valuable insights into the properties of firewall rules and the effectiveness of our confidence scoring and anonymization techniques. This section reports quantitative results of our rule extraction and classification efforts, analyzes the distribution of confidence scores per rule types, and elaborates on the implications for distributed firewall rule management. We also evaluate the performance of our privacy-preserving anonymization mechanism and its ability to balance information preservation and security requirements. The outcome demonstrates both the technical feasibility of our solution as well as its potential impact in enhancing firewall rule quality in distributed environments. We also describe the limitations of our current implementation and identify promising avenues for future research and development.

Fig. 4 shows the distribution of confidence scores across the three main pfSense rule categories: pass, block, and special rules (anchors and scrub). Pass rules (n=9) had a median confidence of 0.6 with a wide interquartile range (0.45–0.75), and only 33.3% exceeded the 0.7 confidence threshold, mainly those with clear interface and protocol specifications.

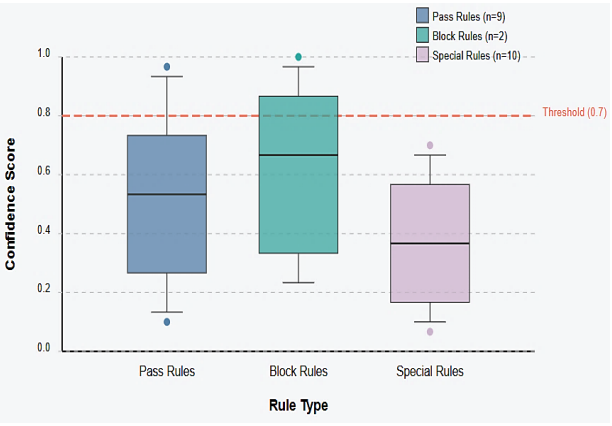

Figure 4. Distribution of Confidence Scores Across Rule Types
Source: Authors' own work.

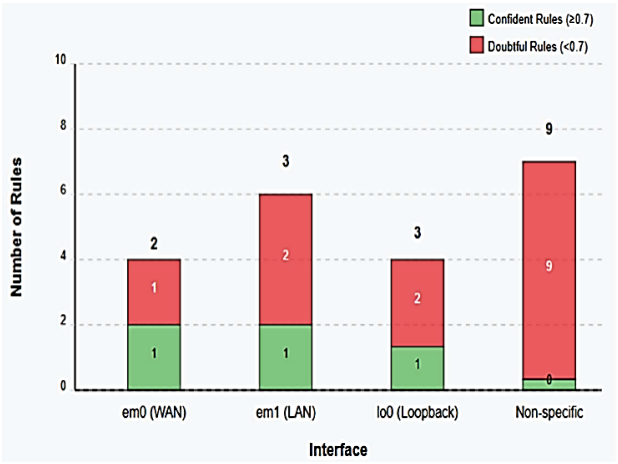

Figure. 5. Rule Classification Outcomes by Interface
Source: Authors' own work.

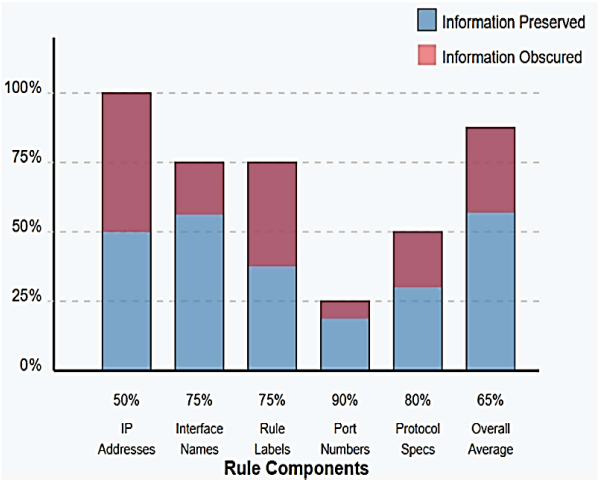

Figure. 6. Information Preservation vs. Privacy Protection
Source: Authors' own work.

Block rules (n=2), though minimal in quantity, boasted the highest median confidence score of 0.7, with both rules possessing obvious security motivations such as blocking traffic from bogon networks. The majority of special rules (n=10), including anchor declarations and scrub directives, possessed the lowest median confidence (0.5) and the lowest interquartile range (0.43-0.55), reflecting their generic nature and lack of tangible security parameters. The overall distribution supports our hypothesis that rules with explicit security parameters tend to have greater confidence scores, while rules with generic configurations require additional validation. This trend supports the real-world utility of our confidence scoring algorithm, which accurately separates well-specified rules from those that would be beneficial with distributed validation. To our surprise, we found that rules with explicit immediate assignments always got a higher score in all aspects, meaning administrator-high-priority rules are typically put more intentional configuration efforts on.

Fig. 5 illustrates the distribution of confident and suspicious rules across firewall interfaces. The em0 (WAN) interface shows a balanced presence of confident and suspicious rules, reflecting the critical nature of WAN-facing configurations that typically receive heightened administrative attention.

The confident WAN rule specifically addressed private IP range blocking, a proven security best practice. We observed a higher proportion of uncertain rules (66.7%) compared to confident rules (33.3%) for the em1 (LAN) interface, suggesting that rules on the internal network are less comprehensively configured, even though they are important to defend the internal network. The loopback interface (lo0) also showed the same pattern with 66.7% doubtful rules and 33.3% confident rules, which were primarily made up of standard loopback traffic allowances. The most intriguing finding was that non-specific rules that did not deal with specific interfaces had the highest percentage of doubtful classifications (100%), with all 9 rules below our confidence level. These non-specific rules typically included generic traffic handling instructions and special rule types such as anchors and scrub rules without explicit security parameters.

This dichotomy strongly bolsters our confidence scoring algorithm's effectiveness, since it correctly flagged interface-specific rules, particularly those on security-sensitive boundaries like the WAN interface, as typically more reliable than non-specific rules. The inference that non-specific rules never came to a confident status is consistent with security best practice recommending explicit interface targeting for effective defense-in-depth practice. It is suggested from this research that firewall administrators should prioritize most heavily the verification and optimization of non-specific rules, both the most populous category (42.9% of total rules) and the most often questionable configuration pattern [28].

Fig. 6 demonstrates the trade-off between information preservation and privacy protection among various rule components in our anonymization mechanism. IP addresses

demonstrate the strongest privacy protection, with a full 50% of information hidden through our HMAC-SHA256 hashing method, retaining relational patterns while hiding true network addressing schemes.

Interface names are somewhat safeguarded with 75% data preservation and 25% redaction, replacing explicit identifiers (e.g., "em0", "em1") with generic placeholders without disrupting their connections in the rule model. Rule names also preserve 75% data preservation, redacting organization-specific technical jargon and sensitive keywords on a differential basis while preserving functional descriptions. Port numbers have the maximum information preservation rate at 90% with the lowest obscuration (10%) as the basic service ports are left intact for interpretability, and custom ports alone get anonymization. The protocol specifications ensure 80% information preservation by obscuring only implementation-specific information and leaving the fundamental protocol information intact. Overall, our anonymization process strikes a well-balanced 65% information retention rate for all rule elements, both securely masking sensitive network information and leaving enough information to allow meaningful validation. This judiciously tuned approach illustrates that privacy-preserving rule sharing is not necessary at the expense of validation usefulness, overcoming an important obstacle to distributed security intelligence.

Fig. 7 depicts the accuracy of validation that was maintained upon testing our anonymization mechanism across five different validation contexts of increasing complexity. Syntax preservation performs highest with an accuracy of 97%, which confirms that our anonymization technique correctly preserves the grammatical composition and structure of firewall rules to support correct parsing and interpretation by target systems. Logic verification appears at 95% accuracy, demonstrating that the fundamental logical operations and conditional statements in rules remain sound even when sensitive data are covered up. Pattern recognition accuracy drops slightly to 88%, indicating some limitation in identifying repeated patterns among a number of anonymized rules, particularly when particular network addressing is covered up. Security evaluation accuracy further decreases to 84%, indicating that the majority of security implications remain evaluable in anonymized rules, but some context-dependent security analyses become more complex without full visibility into the network. The most challenging case, advanced correlations, achieved 78% accuracy, reflecting the difficulty of specifying intricate relationships when some context is obscured. Nevertheless, the overall average accuracy of 88.4% demonstrates that our anonymization scheme effectively balances privacy protection with validation utility, confirming that distributed rule validation remains effective without compromising sensitive network information.

Fig. 8 shows a comparison of performance between anonymized and raw firewall rules on the four most critical measures, providing us with an indication of the actual-world overhead of our privacy-preserving approach. Processing time shows a 31% increase for anonymized rules (6.8ms vs. 5.2ms per rule), indicating the computational overhead of our HMAC-SHA256 hashing and pattern-preserving transformations. Nonetheless, the absolute processing time remains less than 7ms per rule, making it suitable for real-time applications. Memory consumption is 22% higher for anonymized rules (2.8MB vs. 2.3MB for our test set), due to the additional data structures to maintain mapping consistency between source and anonymized identifiers. Rule file size is higher by a modest 16% (5.2KB vs. 4.5KB

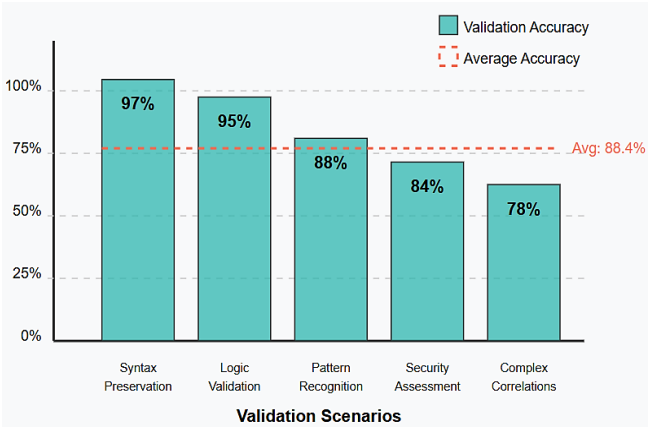

Figure 7. Validation Accuracy After Anonymization
Source: Authors' own work.

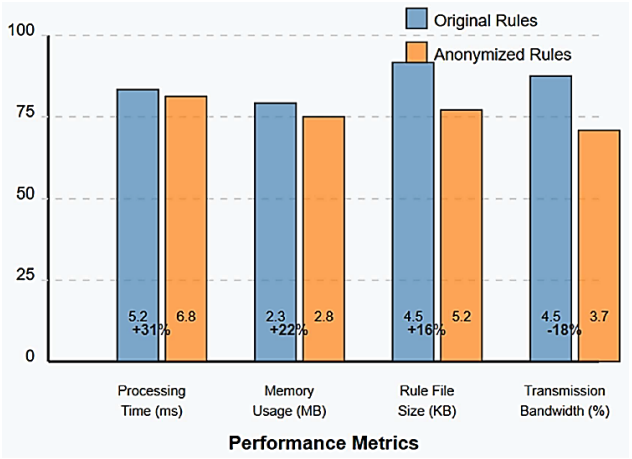

Figure 8. Performance Comparison of Original vs. Anonymized Rules
Source: Authors' own work.

for our test set), primarily due to replacing concise IP addresses and identifiers with their longer hashed representations. Contrary to expectation, transmission bandwidth decreases by only 18% when rules are anonymized, compared to increased file size. This apparent contradiction is due to more effective compression of anonymized rules such that recurring patterns by consistent hash replacement allow for greater compressive ratios at transmission. These performance metrics demonstrate that our anonymization technique adds only relatively modest computational and storage overhead with the promise of reducing network transmission requirements a very desirable trade-off given the enormous privacy benefits.

Although HMAC-SHA256 anonymizes sensitive data like IPs and interface names, attackers might attempt reversal via hash tables or brute force. Our design uses a secret, high-entropy key known only to the local agent, making such attacks infeasible. Truncated HMAC outputs maintain readability while preserving consistent anonymized identifiers, and periodic key rotation with access control further reduces exposure risks.

The overall impact remains well within acceptable margins for deployment in production, ensuring that privacy protection is not at the cost of system responsiveness or scalability. Fig. 9 illustrates the differential impact of our anonymization process on four categories of rules: pass rules, block rules, special rules, and interface-specific rules. The stacked bar chart indicates the percentage of rules that are subjected to low, medium, and high levels of transformation during anonymization. Pass rules have an even distribution of impact with 65% low impact (small changes like generic port retention), 20% medium impact (partial obscuring of network identifiers), and 15% high impact (deep rearrangement of certain addressing data). Block rules have the most favorable anonymization profile with 70% having only low impact, 20% medium impact, and surprisingly 0% high impact. This trend is reflective of the typically less sophisticated character of block rules, which have a tendency to strike broad network ranges rather than discrete endpoints. Special rules (e.g., anchors and scrub rules) have the highest

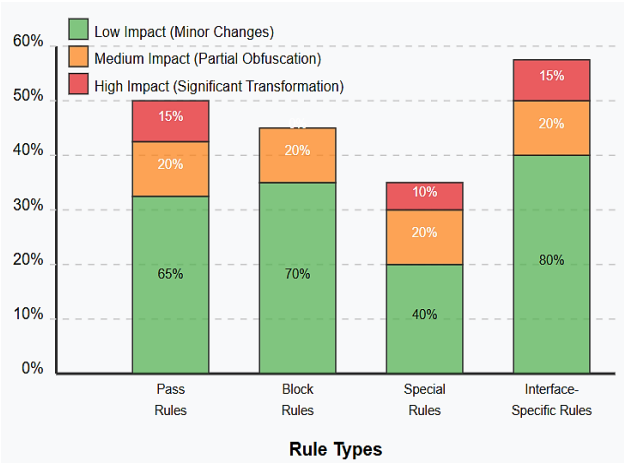

Figure 9. Anonymization Impact on Different Rule Types
Source: Authors' own work.

percentage with a significantly changed content of 40% low, 20% medium, and 10% high impact, as well as 30% that required zero transformation due to their generic nature. Interface-specific rules experienced the most consistent low-impact alteration (80%), with only 20% medium impact and 15% high impact, indicating our mechanism preserves interface relationships while obscuring specific identifiers.

The varying impact by rule type shows that our approach adapts to different rule structures while preserving most rule information and only masking sensitive elements. This analysis demonstrates that AUTOFIRE achieves privacy objectives with minimal disruption, enabling effective distributed validation. Unlike prior work—such as Wang Buqing (2024) [15], who focused on selected attack vectors, and Loevenich et al. (2024) [2], who emphasized response actions AUTOFIRE addresses key gaps in rule management, verification, and proactive detection, as summarized in Table 2, Related Work.

Serrano's (2025) CyberAIBot showed the effectiveness of application-specific deep learning for IoT attack detection but did not address firewall rule management. In contrast, AUTOFIRE improves rule quality and consistency through a numeric confidence scoring system, privacy-preserving anonymization for distributed validation, and a hierarchical multi-agent framework, enabling collaborative security while maintaining organizational confidentiality.

While AUTOFIRE shows promising results in controlled settings, several directions remain for future work. These include scaling the system to enterprise-level deployments using real-world firewall rule sets, enhancing confidence scoring through machine learning and reinforcement learning [22] for adaptive weighting and thresholding, integrating real-time threat intelligence for dynamic rule validation, strengthening anonymization using advanced privacy techniques, and developing automated remediation to actively improve low-confidence firewall rules.

5 Future work

Several directions can be explored in future work to further enhance the proposed intelligent firewall system. A particularly promising avenue is the integration of machine learning (ML) and reinforcement learning (RL) techniques. This approach would allow the system to dynamically adjust trust scoring weights and adapt classification thresholds based on contextual learning, rule evolution patterns, and historical validation feedback. Implementing these methods is expected to improve the accuracy, flexibility, and nuance of firewall rule evaluations, making the system more effective in real-world, enterprise-scale environments.

Table 2.
Related Work

Feature	AUTOFIRE (2025)	Wang Buqing (2024)[15]	Loevenich et al. (2024)[2]	Serrano (2025)[17]
Rule Classification	Strong focus on numeric confidence scoring algorithm (76.2% doubtful, 23.8% confident)	Limited rule classification based on predefined attack types	Moderate classification by DRL model with focus on response rather than rule quality	Advanced classification using specialized DL technical clusters
Confidence Scoring	Contribution via weighted parameters (e.g., interface specificity: 0.10).	Basic scoring for known attack patterns	Limited to reinforcement learning reward function	Probabilistic scoring for attack detection, not a rule quality
Privacy Preservation	Strong focus with 65% information retention while maintaining 88.4% validation accuracy	Not addressed	Not addressed	Not addressed
Distributed Validation	Core architectural component with masteragent communication	Not addressed	Not addressed	Limited through management cluster oversight
Multi-Agent System	Two-level hierarchical architecture with extraction and classification agents	Single integrated system with Snort and pfSense	Hybrid AI model with DRL and LLM components	Distributed framework with specialized clusters
pfSense Integration	Direct integration with rule extraction through pfctl	Deep integration with enhanced defense mechanisms	Limited focus on general network protection	No specific pfSense focus, IoT-oriented
Performance Metrics	Processing time increased by 31% (5.2 ms to 6.8 ms per rule).	Improved detection accuracy for specific attacks	Effectiveness measured against red agent strategies	Processing capability of 5.52E+08 data points

Source: Authors' own work.

6 Conclusions

AUTOFIRE represents a paradigm change of great magnitude in the management of firewalls by addressing the root problem of rule quality and validation through three new contributions. Our quantitative confidence scoring mechanism provides an unprecedentedly objective solution to rule categorization against interface specificity, protocol explicitness, and other main parameters to enable rules requiring further validation to be located, with 76.2% of our testbed rules being identified as doubtful. Second, our privacy-preserving anonymization technique boasts an optimally balanced 65% information retention ratio with 88.4% validation precision, allowing organizations to provide inputs toward distributed security intelligence without exposing network confidentiality a functionality absent from existing solutions in its entirety. Third, our hierarchical multi-agent architecture facilitates rule harmonization in different e nvironments, moving cybersecurity from passive detection to active prevention by means of rule optimization. Whereas much previous work aimed at threat detection once rules are in place, AUTOFIRE addresses the upstream issue of rule quality and consistency, possibly cutting the attack surface before malicious traffic even reaches detectors. With minimal performance impact (31% for processing, 22% for memory consumption), AUTOFIRE demonstrates privacy-preserving distributed rule management not only feasible but necessary for next-generation network security environments requiring collective intelligence and adequate data protection. introduces a novel approach to automated firewall rule management through a confidence-based, privacy-conscious, and distributed validation framework. By addressing upstream problems in rule quality, AUTOFIRE offers significant improvements in identifying and validating security-critical configurations before threats propagate. The results from our prototype demonstrate both technical feasibility and practical relevance. Unlike conventional systems, AUTOFIRE enables collaborative security without exposing internal configurations, achieving a validation accuracy of 88.4% while maintaining 65% data retention. The system's low overhead and scalability make it suitable for real-time deployment. Looking forward, the incorporation of adaptive learning, integration with threat feeds, and automated rule remediation will further transform AUTOFIRE into a proactive and intelligent firewall management platform. This shift from passive detection to active prevention marks a step forward in the evolution of resilient, distributed network security.

References

[1] Kumar, D., and Gupta, M., Implementation of firewall and intrusion detection system using pfSense to enhance network security. International Journal of Electrical Electronics and Computer Science Engineering, 1, pp. 2454-1222, 2018.

[2] Loevenich, J., Adler, E., Mercier, R., et al., Autonomous cyber defense using hybrid AI models for critical network protection. IEEE Access, 12, pp. 1-10, 2024. DOI: https://doi.org/10.1109/ICMCIS61231.2024.10540988

[3] Ejeofobiri, C.K., Victor-Igun, O.O., and Okoye, C., AI-driven secure intrusion detection for Internet of Things (IoT) networks. Asian Journal of Mathematics and Computer Research, 31(4), pp. 40-55, 2024.

[4] Ramesh, D., et al., Exploring contemporary perspectives on the implementation of firewall policies: a comprehensive review of literature. Indiana Journal of Multidisciplinary Research, 4(3), pp. 218-222, 2024.

[5] Wool, A., A quantitative study of firewall configuration errors. IEEE Computer, 37(6), pp. 62–67, 2004. DOI: https://doi.org/10.1109/MC.2004.2

[6] Al-Shaer, E., and Hamed, H., Discovery of policy anomalies in distributed firewalls. IEEE INFOCOM, 4, pp. 2605–2616, 2004. DOI: https://doi.org/10.1109/INFCOM.2004.1354680.

[7] Yuan, L., Chen, H., Mai, J., et al., FIREMAN: a toolkit for firewall modeling and analysis. IEEE Symposium on Security and Privacy, pp. 15–213, 2006. DOI: https://doi.org/10.1109/SP.2006.16.

[8] Elbadawi, I., Elshoush, H., and Osman, M., A hybrid AI-based approach for rule optimization in network firewalls. IEEE Access, 8, pp. 156224–156237, 2020. DOI: https://doi.org/10.1109/ACCESS.2020.3018931

[9] Bégin, L., Létourneau, S., and Tremblay, G., A learning approach to firewall configuration validation. 15th Int. Conf. on Network and Service Management (CNSM), Halifax, NS, Canada, pp. 1–5, 2019. DOI: https://doi.org/10.23919/CNSM46954.2019.9012694

[10] Ahmed, M., Mahmood, A.N., and Hu, J., A survey of network anomaly detection techniques. Journal of Network and Computer Applications, 60, pp. 19–31, 2016. DOI: https://doi.org/10.1016/j.jnca.2015.11.016

[11] Papaioannou, T.G., and Delis, A., Multi-agent frameworks for adaptive network security management. IEEE Trans. Network and Service Management, 12(2), pp. 234–247, 2015. DOI: https://doi.org/10.1109/TNSM.2015.2404795

[12] Zambonelli, F., Jennings, N.R., and Wooldridge, M., Developing multiagent systems: the Gaia methodology. ACM Trans. Software Engineering and Methodology, 12(3), pp. 317–370, 2003. DOI: https://doi.org/10.1145/958961.958963

[13] Zhang, H., Chen, L., and Liu, P., Privacy-preserving data sharing in multi-agent systems for cybersecurity. IEEE Trans. Information Forensics and Security, 17, pp. 1987–2001, 2022. DOI: https://doi.org/10.1109/TIFS.2022.3146091

[14] Fan, L., and Xiong, L., Real-time anonymization of streaming data. IEEE 32nd International Conference on Distributed Computing Systems (ICDCS), pp. 82-91, 2012. DOI: https://doi.org/10.1109/ICDCS.2012.58

[15] Buqing, W., Analysis of a new firewall constructed on pfSense with Snort to defend against common internet intrusions. Applied and Computational Engineering, 43(1), pp. 244-250, 2024. DOI: https://doi.org/10.54254/2755-2721/43/20230841

[16] Loevenich, J., Adler, E., Mercier, R., and Lopes, R.R.F., Design of an autonomous cyber defence agent using hybrid AI models. 2024 International Conference on Military Communication and Information Systems (ICMCIS), Koblenz, Germany, pp. 1–10, 2024. DOI: https://doi.org/10.1109/ICMCIS61231.2024.10540988

[17] Serrano, W., CyberAIBot: artificial intelligence in an intrusion detection system for cybersecurity in the IoT. Future Generation Computer Systems, 166, art. 107543, 2025. DOI: https://doi.org/10.1016/j.future.2024.107543

[18] Rawat, D.B., et al., iShare: blockchain-based privacy-aware multi-agent information sharing games for cybersecurity. 2018 International Conference on Computing, Networking and Communications (ICNC), pp. 425–431, 2018.

[19] Dhrir, H., et al., Machine learning-and deep learning-based anomaly detection in firewalls: a survey. The Journal of Supercomputing, 81(6), art. 07212-y, 2025. DOI: https://doi.org/10.1007/s11227-025-07212-y

[20] Valenza, F., et al., A formal approach for network security policy validation. J., Wirel. Mob. Networks Ubiquitous Comput. Dependable Appl., 8(1), pp. 79–100, 2017.

[21] Salman, O., et al., Towards efficient real-time traffic classifier: a confidence measure with ensemble deep learning. Computer Networks, 204(4), art. 108684, 2022. DOI: https://doi.org/10.1016/j.comnet.2021.108684

[22] Alsaif, K.I., and Abdullah, A.S., Deep learning technique for gymnastics movements evaluation based on pose estimation. In: Rasheed, J., Abu-Mahfouz, A.M., and Fahim, M., Forthcoming

Networks and Sustainability in the AIoT Era. FoNeS-AIoT 2024. Lecture Notes in Networks and Systems, Springer, Cham, 1036, art. 19, 2024. DOI: https://doi.org/10.1007/978-3-031-62881-8_19
[23] Abd, N.S., Karoui, K., Abdullah, W.D., and Shihab, M.A., Data science techniques to reduce the occurrence of false negatives during intrusion detection. International Conference on Soft Computing and its Engineering Applications, pp. 173–187, 2024.
[24] Kaur, P.C.; Ghorpade, T., and Mane, V., Analysis of data security by using anonymization techniques. 6th International Conference-Cloud System and Big Data Engineering (Confluence), pp. 287–293, 2016.
[25] Boudaoud, K., and Guessoum, Z., A multi-agents system for network security management. International Conference on Intelligence in Networks, pp. 407–418, 2000.
[26] Bringhenti, D., et al., Automated firewall configuration in virtual networks. IEEE Transactions on Dependable and Secure Computing, 20(2), pp. 1559–1576, 2022.
[27] Praptodiyono, S., et al., Development of hybrid intrusion detection system based on Suricata with pfSense method for high reduction of DDoS attacks on IPv6 networks. Eastern-European Journal of Enterprise Technologies, 125(9), 2023.
[28] Lu, N., and Yang, Y., Application of evolutionary algorithm in performance optimization of embedded network firewall. Microprocessors and Microsystems, 76, pp. 103087, 2020.
[29] Huma, Z., et al., Hybrid AI models for enhanced network security: combining rule-based and learning-based approaches. Global Perspectives on Multidisciplinary Research, 5(3), pp. 52–63, 2024.

N. Saud, currently work as a lecturer at Tikrit University, Iraq, College of Computer Science and Mathematics, Department of Cyber security, and her research interests include artificial intelligence and cybersecurity.
ORCID: 0009-0007-8363-6176

K. Karoui, currently work in the Department of Computer Science and Mathematics at the National Institute of Applied Sciences and Technology. His research focuses on computer communications (networks), computer security and reliability, and distributed computing.
ORCID: 0000-0003-2507-9571

DYNA
http://dyna.medellin.unal.edu.co/

UNIVERSIDAD NACIONAL DE COLOMBIA

Development of a low-cost power supply with multiple self-adjustable outputs for the operation of silicon photo-multipliers

Juan Anzurez-Marín[a], Israel Luna-Reyes[b,*], Alfredo Raya[a], Mauricio René Reyes-Gutiérrez[a], Antonio Ulises Sáenz-Trujillo[a], Roberto Tapia-Sánchez[a] & Galileo Cristian Tinoco-Santillán[a]

[a] *Facultad de Ingeniería Eléctrica, Universidad Michoacana de San Nicolás de Hidalgo. Morelia, México. juan.anzurez@umich.mx, alfredo.raya@umich.mx, mauricio.reyes@umich.mx, ulises.saenz@umich.mx, roberto.tapia@umich.mx, galileo.tinoco@umich.mx*
[b] *Instituto de Física y Matemáticas, Universidad Michoacana de San Nicolás de Hidalgo. Morelia, México. * israel.luna@umich.mx*

Received: July 15th, 2025. Received in revised form: December 12th, 2025. Accepted: December 29th, 2025.

Abstract
We present the design of a low-cost (~$400 USD) and high-precision power supply for silicon photomultipliers (SiPMs), widely used in particle detection and photon-counting applications. The system provides four independent output channels, each delivering a tunable bias voltage from 10-58 V with 10mV resolution and less than 1mV noise level. Each channel incorporates a PT100 temperature sensor (15 °C–40 °C range) enabling real-time thermal monitoring and automatic temperature-compensated voltage adjustment to stabilize SiPM gain. The device also supports individual voltage calibration and storage of optimal operating points. Integrated current limiting (100μA/channel) protects the sensors. This compact and versatile design offers a cost-effective alternative to commercial systems, with features tailored for research and development settings.

Keywords: low-cost power supply; multiple outputs; silicon photo-multipliers.

Desarrollo de una fuente de alimentación de bajo costo con múltiples salidas ajustables para la operación de fotomultiplicadores de silicio

Resumen
Presentamos el diseño de una fuente de alimentación de bajo coste (~400 USD) y alta precisión para fotomultiplicadores de silicio (SiPMs), ampliamente utilizados en aplicaciones de detección de partículas y conteo de fotones. El sistema ofrece cuatro canales de salida independientes, cada uno con un voltaje de polarización ajustable entre 10 V y 58 V, con una resolución de 10 mV y un nivel de ruido inferior a 1 mV. Cada canal incorpora un sensor de temperatura PT100 (rango de 15 °C a 40 °C), lo que permite el monitoreo térmico en tiempo real y el ajuste automático del voltaje compensado por temperatura para estabilizar la ganancia del SiPM. El dispositivo también permite la calibración individual del voltaje y el almacenamiento de los puntos óptimos de operación. Un limitador de corriente integrado (100 μA por canal) protege a los sensores. Este diseño compacto y versátil representa una alternativa económica a los sistemas comerciales, con prestaciones orientadas a entornos de investigación y desarrollo.

Palabras clave: fuente de alimentación de bajo costo; múltiples canales de salida; fotomultiplicadores de silicio.

1. Introduction

Silicon photomultipliers (SiPMs) have emerged as versatile solid-state photon detectors, replacing traditional photomultiplier tubes in various applications [1,2]. SiPMs offer advantages such as high sensitivity, compact size, mechanical robustness, and magnetic field insensitivity [2,3]. They are widely used in particle and nuclear physics experiments, medical imaging, and environmental science [1,2]. In positron emission tomography (PET), SiPMs present challenges in signal multiplexing and readout due to their large number of output channels [3]. To fully utilize the capabilities of these sensors, understanding their fundamental properties, including gain fluctuation, afterpulsing, and photon detection

How to cite: Anzurez-Marín, J., Luna-Reyes, I., Raya, A., Reyes-Gutiérrez, M.R., Sáenz-Trujillo, A.U., Tapia-Sánchez, R., and Tinoco-Santillán, G.C., Development of a low-cost power supply with multiple self-adjustable outputs for the operation of silicon photo-multipliers DYNA, (93)240, pp. 72-80, January - March, 2026.

efficiency, is crucial [4]. Ongoing research focuses on improving SiPM performance in terms of spatial, energy, and timing resolutions for various applications, particularly in PET systems [3,4].

As with every electronic device, the power supply is a crucial component of a system of operating SiPMs [5-7] mainly because the output signal can be influenced by the amount of noise caused by it. Furthermore, the optimal gain of each SiPM might fluctuate if the bias voltage is not stable during operation [4]. A minimal set of considerations to take into account for the design of a power supply to be used in photon detection experiments must include (i) a stable bias voltage, with noise level under a certain threshold to avoid any signal contamination of the SiPM when excited; (ii) a limited operation current to prevent damage on the sensors; (iii) independent bias voltage supply for each SiPM in the array; (iv) a bias voltage compensation demanded by temperature variations in the SiPM operation. In spite of the fact of being produced in series, every SiPM has its own individual physical properties, which makes its performance unique and independent of the rest of sensors even when operating at the same bias voltage in the same environment. Thus, to achieve optimal performance of the entire system, each SiPM has to be supplied with a specific bias voltage, which needs to be fine-tuned.

Under these conditions, we propose and develop a power supply with specific physical features, allowing the adjustment of its parameters in each channel independently, according to the external temperature of operation of the SiPMs. The model consists of four of these sensors, supplied with bias voltages in the range of 10-57V with a resolution of 10mV and a limited current of 100μA, providing a maximum noise level of 1mV. The temperature in each channel is sensed by a PT100 resistive sensor in the range of 15°C to 40°C and the bias voltage is automatically compensated to achieve optimal operation. All the calibration parameters and the optimal operational voltage level are recorded independently for each channel. The schematic diagram of the developed power supply is shown in Fig. 1.

To present the design and test our development, the rest of the article is organized as follows: Section 2 presents the description of the hardware and Section 3 the graphical interface, including the PC interface and firmware. The calibration procedure and adjustment of the components is discussed in detail in Section 4. Designed tests and results are presented in Section 5 and a comparison of costs and specifications of similar power supplies in the market is discussed in Section 6. Conclusions and outlook are finally drawn in Section 7.

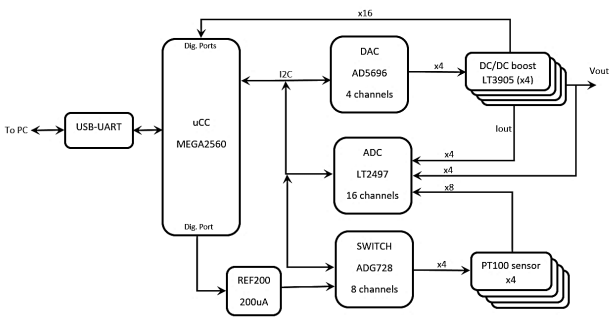

Figure 1. Schematic diagram of the proposed power supply.
Source: Self-designed.

2. Hardware

2.1 Boost-type switching power supply

The four output channels for the SiPMs are based upon the LT3905 integrated circuit, which acts as a boost-converter with the following specifications [8]: Bias voltage in the range from 2.7-12V; output voltage 2.5-65V; maximum output current of 3mA; digital pins for monitoring and control, including sensor loss detector (LOS), excess current consumption detector (ILIM) and enable/disable output voltage (EN/UVLO); analog pins for monitoring and control, including output voltage from 0-1.25V (CTRL) and supplied current monitor (MON). For the SiPMs protection, the chip is connected such that the output voltage does not exceed 58V with a maximum current consumption of 100μA. A sketch of the suggested connection of the LT3905 integrated circuit by the manufacturer is shown in Fig. 2. One can observe that through the CTRL pin, the output voltage is adjusted. LOS and ILIM pins are digital signals to detect low and excess current consumption, respectively and the output current of the APD pin can be measured in the MON pin. Furthermore, the EN/UVLO pin is used to control the activation/deactivation of the circuit to avoid damage on the SiPMs and the board itself, in case of failure.

2.2 Output voltage control for the SiPMs

To adjust the voltage of the pin CTRL off the LT3905, a digital/analog converter AD5696R is used, which exhibits the following specifications [9]: Bias voltage of 2.7-5.5V; 16-bits resolution; reference voltage 2.5V internal and 1V-2.5V external; gain of output voltage 1x and 2x; 4 output channels controlled independently; I2C communication. Through this circuit the output voltage level of each LT3905 is adjusted by varying the voltage in the CTRL pin from 0 to 1.25V according to

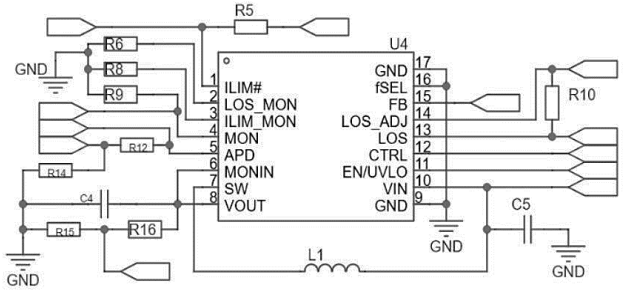

Figure 2. A typical connection diagram of the LT3905 integrated circuit according to the recommendation of the manufacturer [8].
Source: Self-designed.

$$V_{CTRL} = \frac{(DC) * 1.25}{2^{16}}, \qquad DC = 0 - 65535, \qquad (1)$$

where DC stands for Digital Code. The maximum output voltage of the LT3905 is attained by a voltage divisor between the V_{out} and FB pins and does not exceed 58V, the upper limit for the SiPM optimal operation. The minimum measured value of the voltage, given the above configuration, on the other hand, was 2.5V, and altogether yield an output voltage of 2.5V when $V_{CTRL} = 0$, and $V_{out} = 58\text{V}$ when $V_{CTRL} = 1.25\text{V}$. Such a linear relation can be expressed as

$$V_{out} = 2.5V + \frac{58-2,5}{1.25} V_{CRTL} = 2.5V + 44.4V_{CTRL}, \qquad (2)$$

or, upon integrating the value of the DAC,

$$V_{out} = 2.5V + \frac{44.4*DC*1.25V}{65536} = 2.5V + \frac{55.5*DC}{65536}. \qquad (3)$$

Given that the manufacturer does not provide the sensitivity of the CTRL pin, these values were physically tested on the chip and yield a resolution of

$$\Delta V_{out} = \frac{55.5V}{65536} = 0.847\frac{mV}{bit}, \qquad (4)$$

which is satisfactory for our purposes.

2.3 Measurement of temperature, voltage and current of the SiPMs

For measuring temperature, output voltage, and current, the LTC2497 A/D converter is used, which features the following specifications [10]: Bias voltage of 2.7-5.5V; 16 channels in single-ended mode, 8 channels in differential mode, or a combination of both; 16-bit resolution; reference voltage of 0.1V to VCC; direct connection to differential sensors; I2C communication; maximum sampling rate of 100SPS. Due to the high flexibility of this converter, the channel allocation for the aforementioned signal measurements is 8 channels for differential measurements of PT100 sensors and 8 single-ended channels for output voltage and current measurements.

A typical connection diagram for this ADC is shown in Fig. 3.

As can be observed, this converter reads voltages differentially, simplifying the connection of PT100 sensors to measure the temperature of the SiPMs. The measurement methods for the three aforementioned variables are: For the output voltage, a voltage divider connected in parallel to the SiPM; for the output current, the resistor connected to the MON pin of the LT3905 generates a voltage of 1mV/µA, which is measured directly across this resistor; finally, for the PT100 sensor voltage, a 200µA current is driven through the sensor, creating a differential voltage across its terminals. The generated voltage (which depends on ambient temperature) is measured directly using two ADC channels. The implementation of this stage is currently under consideration given the need for experimental characterization of the SiPM response under controlled circumstances.

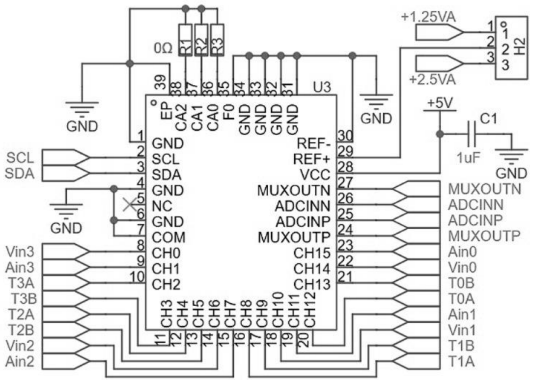

Figure 3. Connection diagram of the LTC2497 integrated circuit according to the recommendation of the manufacturer [10].
Source: Self-designed.

2.4 General control of the supply

All the previously mentioned components are controlled by an ATmega2560 microcontroller, which features the following specifications [11]: Operating voltage of 2.7-5.5V; 8-bit processor; I2C, SPI and UART communication interfaces, digital input/output ports with TTL levels of 2.7-5V and interrupt handling capability. This component manages communication between the converters for both output voltage adjustment and acquisition of voltage, current, and temperature signals from the four channels of the power supply. Communication with the control interface is established via the UART port using a USB-UART converter. Through this interface, the output voltage configurations for each channel are transmitted, while voltage, current, and temperature readings from each channel are received.

The implementation of the power supply is shown in Fig. 4, whereas a prototype of the metallic case to reduce electromagnetic interference is shown in Fig. 5.

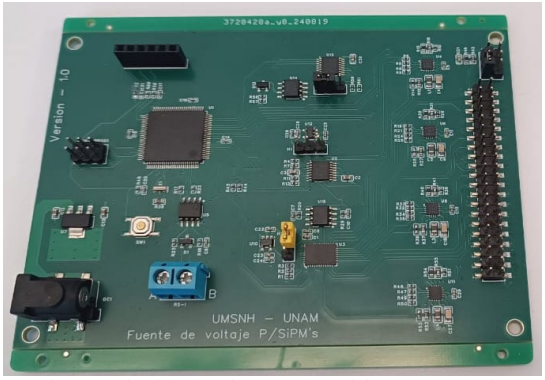

Figure 4. A photograph of the implementation of the power supply.
Source: Self-captured photograph.

Figure 5. A photograph of the prototype metallic case of the power supply.
Source: Self-captured photograph.

3. Graphical interface

3.1 User interface software

To control all functions of the power supply, a graphical user interface (GUI) was developed in the NetBeans integrated development environment (IDE), with the aim of ensuring portability across different operating systems. When the program is launched, the interface detects the COM ports assigned by the operating system. The user must select the one corresponding to the voltage source and press the "Connect" button. If the connection is successfully established, the system displays the message "Connected"; otherwise, shows "Unconnected".

The interface displays the current voltage, current, and temperature values for each channel enabled by the user. Once the channels are activated, the user can modify their values and choose whether to apply temperature correction. At the bottom, a table displays the channels, updating approximately every minute—the time required for the microcontroller to sample all channels and compute their averages. A sample screenshot of the interface is shown in Fig. 6.

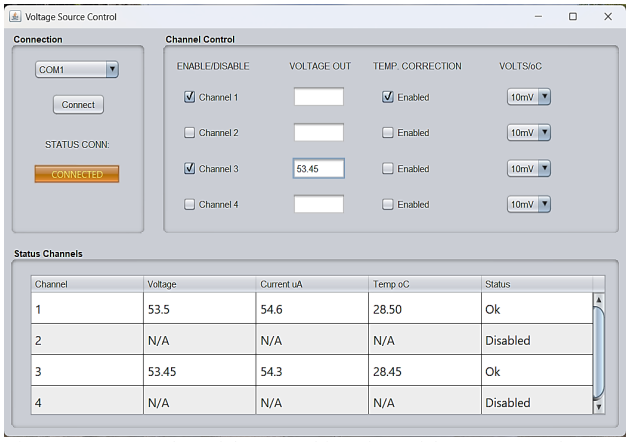

Figure 6. A screenshot of the control interface of the power supply.
Source: Self-shoot.

3.2 Microcontroller software implementation

The microcontroller firmware was developed in C language using a state-based architecture to optimize processor efficiency. This scheme manages the various peripherals employed, including the UART serial port, digital I/O ports, and I2C serial interface. For communication with the user interface, the UART serial port is used in conjunction with a USB-UART adapter. The system continuously polls this interface to check for user requests. If no request is pending, the firmware executes the following tasks: A/D conversion with one input channel sampled at a time (4 voltage channels, 4 current channels, and 4 temperature channels). To prevent excessive delays that could disrupt communication responsiveness, not all channels are converted simultaneously; Averaging the current readings with previous measurements for each channel; output voltage level of a channel is adjusted if enabled via the interface; digital pin monitoring for active signals on digital pins. If detected, it notifies the user and triggers the appropriate action; acquired data transmission to the user interface for display.

The firmware supports the following user commands: (i) Enable/disable a channel; (ii) adjust the output voltage level of a channel; (iii) enable/disable automatic temperature compensation; (iv) monitor voltage, current, and temperature readings per channel or collectively.

4. Calibration and adjustment of the power supply components

To ensure the required precision of the power supply, calibration of both the DAC and ADC conversion signals was performed using a KEITHLEY Model 6514 precision electrometer. This instrument was employed to measure the output voltage and current values using resistive charges of known values. Given that the electrometer and the power supply display a series RS-232 and USB interfaces, a PYTHON script was written to automatically assign an output voltage value which is compared against the measured value after a stabilization time interval of approximately 10s. These tests were performed 5 times each at a room temperature of 22ºC and then averaged, as shown in Figs. 7-11.

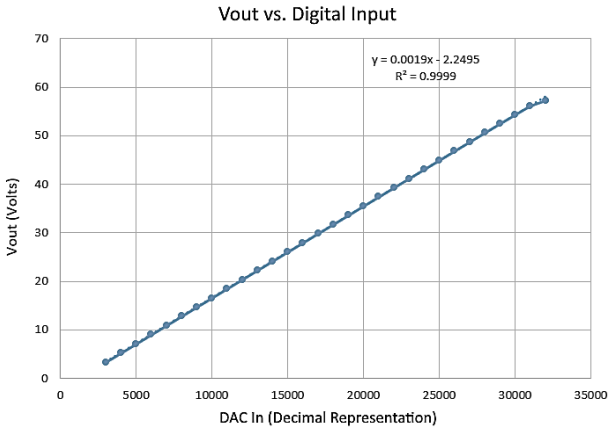

Figure 7. Output voltage as seen in the DAC.
Source: Self-generated.

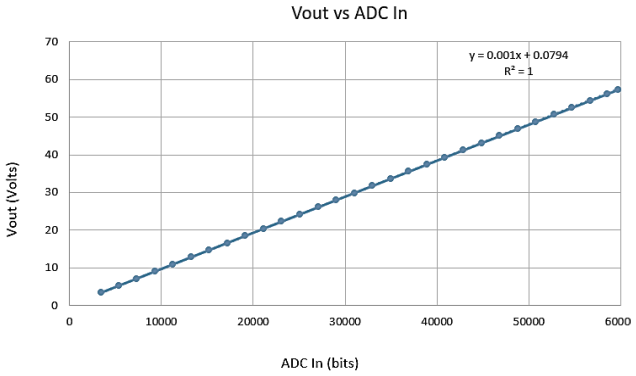

Figure 8. Relationship Between Input Voltage and ADC Output Code (Decimal Representation).
Source: Self-generated.

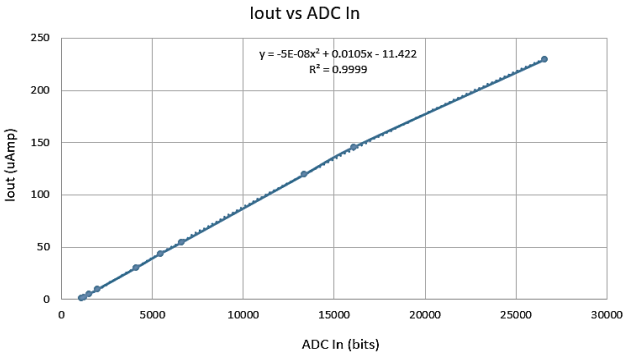

Figure 9. Output current in the ADC.
Source: Self-generated.

We observe a linear behavior which is corroborated with a linear regression. A similar trend can be observed in the ADC output expressed in decimal code, as shown in Fig. 8.

Finally, the output current in the ADC in bits is displayed in Fig. 9, which also describes linear behavior.

With this data, the microcontroller is programmed according to the linear fits obtained from linear regression to adjust the output voltage of the power supply, as well as to read the voltage and current delivered to the sensor, and

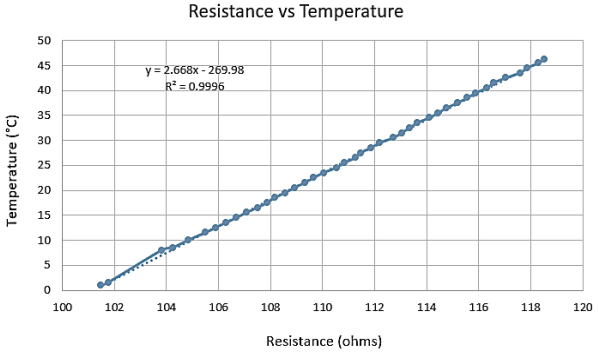

Figure 10. Resistance in the PT100 sensor as a function of temperature.
Source: Self-generated.

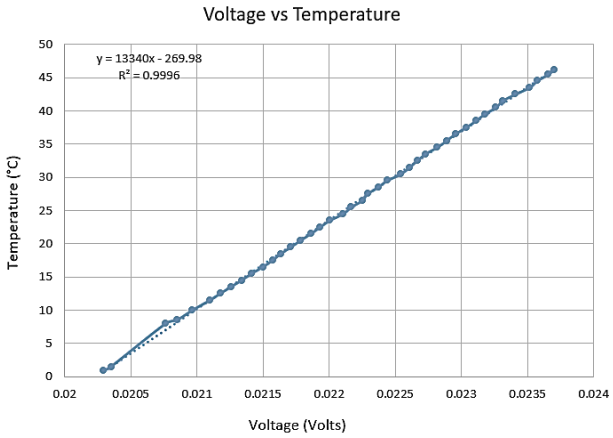

Figure 11. Voltage of the PT100 sensor as a function of temperature.
Source: Self-generated.

to perform necessary corrections for both temperature variations and component deviations. Voltage and current displayed consistent measured values and only measurements on temperature showed outliners, which were discarded.

For the calibration of the temperature sensor, a current of 200µA is injected in a PT100. This generates a potential difference across its terminals, which is measured with the KEITHLEY 6514 electrometer and the ADC converter. These measurements are depicted in Fig. 10.

When the current circulates through the PT100 sensor, the potential difference proportional to the resistance of this component is measured by the ADC, as shown in Fig. 11.

From the test, we obtain the following for the power supply:

- Output voltage: 2.5V-58V
- Resolution of the output voltage: 0.86mV/bit
- Maximum output current: 140μA
- Resolution of measured output voltage: 0.88mV/bit
- Resolution of temperature measurement: 0.0006 ºC/bit

Although these values are satisfactory for the initial needs, additional tests at different temperatures are required to warrant the precision of the results with different conditions.

5. Tests and results

5.1 Measurement of the noise level of the power supply in the load

For testing the power supply, a HAMAMATSU SiPM sensor Series 13 with a minimum operating voltage of 53V and a recommended overvoltage ±3V was connected in series with a 50-ohm resistor.

The power supply was connected to the sensor via shielded SMA cables. Using an SMA "T" connector, an oscilloscope was attached such that channel 1 monitors the supply voltage whereas channel 2 measures the voltage drop across the 50-ohm resistor. To analyze the noise level in the sensor, channel 2 was set to AC coupling, suppressing the DC component. Fig. 12 shows the two signals.

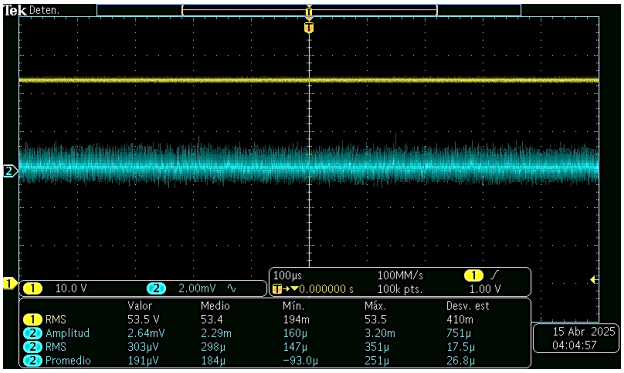

Figure 12. Output voltage of the power supply (yellow) and noise level in the load (blue).
Source: Self-generated.

As shown in the Fig. 12, the sensor bias voltage is set at 53.5V, while the output voltage across the load exhibits a noise signal below 0.3mVRMS, thereby meeting the design requirement.

Several tests were conducted to verify the proper operation of the power supply. One of such tests involved cosmic ray signal measurements, for a constant irradiation of the system. For this purpose, a plastic scintillator EJ232 with dimensions 20x20x5mm^3 coupled to the sensor is used. The experimental setup is housed in a light-tight plastic enclosure to prevent SiPM excitation from ambient light and is directly connected to an oscilloscope. A preliminary evaluation was conducted both with and without a preamplification stage, leading to the conclusion that, under the operating conditions of this experiment, preamplification is not required. The system was subsequently operated continuously at room temperature for approximately two weeks, during which about 2000 events were recorded. Each event was processed offline using dedicated software to determine the baseline voltage and the peak signal amplitude. The signal rise time was evaluated using a constant-fraction timing method by measuring the time interval required for each event to reach fixed fractions of its maximum amplitude (10%–75%). These time intervals were accumulated into a histogram and statistically analyzed, yielding a Gaussian distribution. From this analysis, a raw rise-time estimate of 17 ns was obtained for the experimental setup. After applying a signal-to-noise ratio correction, the resulting time resolution was determined to be 49±5 ps. Fig. 13 shows a typical signal for the detection of a cosmic rays particle.

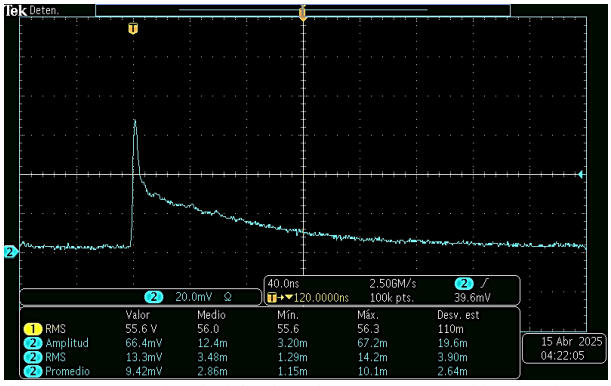

Figure 13. Output signal of the detection system excited by cosmic rays.
Source: Self-generated.

As can be observed, the sensor signal is highly stable with low noise levels, enabling reliable detection of cosmic ray particles generating peaks above 66.4mV. This performance ensures trustworthy readings while minimizing the risk of false positives that could potentially arise from power supply noise.

5.2 Stability test: Voltage vs Time

To monitor voltage variability as a function of the operating time of the power supply, we employ once more the KEITHLEY 6514 electrometer connected to a PC to record voltage values over an extended period (approximately 1.5 hours) at a selected operating voltage of 53.3V that corresponds to the threshold voltage for HAMAMATSU SiPM sensor operation. The measured values are shown in Fig. 14.

Analysis of the data reveals an average voltage of 53.299V with a standard deviation of 0.6mV, indicating excellent power supply voltage stability.

Based on these results, we conclude that the voltage supply meets all required specifications for reliably powering optical sensors. The final power supply specifications are as follows:

- Number of channels: 4
- Operating voltage range: 10 - 58V
- Maximum operating current per channel: 100µA
- Maximum noise level: 0.5mVRMS
- Output voltage adjustment resolution: 10mV
- Voltage measurement resolution: 0.88mV
- Power consumption: 2W (no load) / 4W (full load)

As for the traceability of the calibration when the power supply is used in different conditions, the system implements a reference voltage REF2025 with the following features:

- Output voltage: 1.25V and 2.5V
- Thermal drift: 8ppm/°C from -40°C to 125°C
- High initial precision: +/- 0.05%
- Follow up of output voltage over temperature: 7ppm/°C

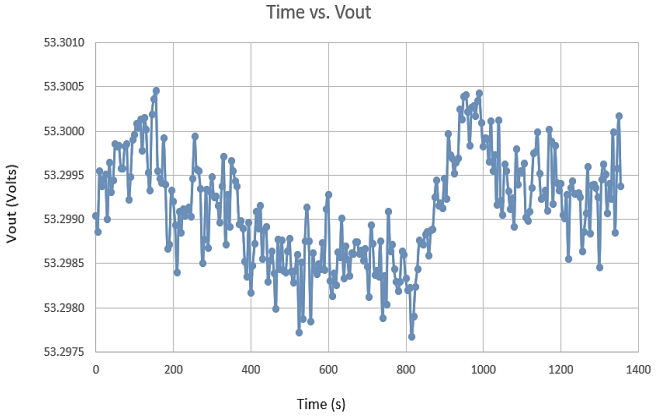

Figure 14. Variation of the sensor voltage in time. In total, 1400 readings were made, each every 10 seconds apart.
Source: Self-generated.

Due to the use of this reference, the ADC measurements would be less influenced by the variation of room temperature where the power supply operates. Nevertheless, tests should be conducted to determine whether the use of such a reference suffices or additional adjustments should be done due to the operation temperature.

6. Costs comparison

In this section we present a comparison of our proposal of power supply with available models.

CAEN N1418/N1419 Family – Modular/Desk. A high-voltage module designed to deliver precise and stable power to detectors used in nuclear and particle physics experiments. This system features up to four independent channels, each with individual voltage and current control, enabling flexible and safe configuration. It is particularly notable for its low ripple, overload and short-circuit protection, and local/remote monitoring capabilities, making it a reliable choice for laboratory environments requiring high electrical precision and stability.

Specifications:

- Type: Modular (N1418) or benchtop (N1419) unit
- Channels: 1 channel (N1419) / up to 4 channels (N1418)
- Voltage Range: 0-100 V (N1418) / 0-130 V (N1419)
- Maximum Current: ~1 mA per channel
- Control: Manual and remote (USB, Ethernet on select models)
- Protections: Overvoltage, overcurrent

Hamamatsu C11204-01 Series. A compact module specifically designed to provide bias voltage for SiPMs. It employs a digitally controlled DC-DC converter, generating an adjustable high-voltage output typically ranging from 30-90V, with high stability and low noise—critical features for ensuring optimal performance in photon detection applications. This power supply includes an I2C communication interface, enabling remote monitoring and control of key parameters such as output voltage, supplied current, and internal temperature, making it easily integrable into broader data acquisition or scientific instrumentation systems.

Specifications*:*

- Type: Dedicated SiPM bias voltage supply
- Channels: 1 channel
- Voltage Range: 20–90V
- Maximum Current: ~0.5 mA
- Fine Adjustment Resolution: steps of 1.8mV
- Interface: Serial (I2C)
- Compatibility: Exclusive to specific Hamamatsu sensors
- Estimated Price: ~$1,000 USD

CAEN DT5485. A compact and reliable model designed to deliver high-precision bias voltages for scientific applications, particularly in nuclear and particle physics experiments. This model stands out for its exceptional stability, low ripple noise, and multi-channel operation capability, enabling safe and efficient power delivery to sensitive detectors. Its modular design ensures seamless integration into larger instrumentation systems while providing precise control and real-time monitoring of electrical parameters.

Specifications:

- Type: Benchtop, high-precision
- Channels: 8 independent channels
- Voltage Range: 0–100V
- Resolution: 1 mV (voltage) / 1 nA (current)
- Control Interfaces: USB, Ethernet, CAEN Graphical User Interface (GUI)
- Compatibility: Optimized for laboratory setups with multi-SiPM configurations
- Estimated Price: ~$3,500–4,200 USD

Keithley 2400 Series. A precision instrument from the SourceMeter® family, designed to source voltage or current with high accuracy while simultaneously measuring electrical parameters including voltage, current, and resistance. Its operation is based on four-quadrant capability (both sourcing and sinking power), enabling use as either a power source or electronic load. This makes it ideal for characterizing semiconductor devices, electronic materials, and sensors. The instrument provides pico Ampere and microvolt measurement resolution and includes digital control interfaces (GPIB, RS-232, and USB) for seamless integration into automated test and laboratory systems. Due to its versatility, stability, and real-time measurement capabilities, the Keithley 2400 is widely used in advanced electronics research, development, and quality assurance applications.

Specifications:

- Type: Precision benchtop source/measure unit
- Channels: 1 channel (per unit)
- Voltage Range: Up to 200V
- Control: Touchscreen, GPIB, USB, LAN
- Compatibility: Optimized for I-V characterization
- ~$6,000–7,500 USD

Note: While costly, it is invaluable for laboratories requiring precise sourcing and measurement capabilities.

This proposal. The developed power supply features four independent output channels, each providing an adjustable bias voltage ranging from 10-57V with 15mV resolution. The high resolution enables precise operational voltage tuning, which is critical for optimizing SiPM performance. The system maintains a maximum noise level of 10mV and incorporates PT100 temperature sensors for all four channels, enabling real-time thermal monitoring within a 15-40°C range.

Specifications:

- Channels: 4 (independent)
- Voltage Range: 10-57V (per channel)
- Control: Graphical interface via PC (Windows/Linux/macOS)
- Interface: USB connectivity
- Compatibility: Supports any sensor within voltage range
- Resolution: 10mV (voltage)
- Maximum Current per Channel: 1mA

Table 1.
Comparative table of different power supplies for SiPM systems.
Source: Self-elaboration

Power Supply	CAEN	Hamma-matsu	CAEN	Keithley	This proposal
Model	A1418/ 1419	C11204-01	DT5485	2400	-------
Channels	1-4	1	8	1	4
Voltage	0-130V	20-90V	0-100V	±200V	10-57V
Remote Control	Yes	No	Yes	Yes	Yes
Cost (USD)	1200-3000	1000	3500-4200	6000-7500	350-400
Recommen-dations	Tests or basic research	Plug and play solutions	Multichannel system	Accurate characterization	Basic research

7. Conclusions and outlook

The power supply is a critical component in any electrical or electronic circuit, where its performance in load regulation, noise level, and voltage stability significantly impacts the overall functionality of powered devices and systems. Based on the experimental results obtained from the tested proposal, we conclude that the design meets the specified requirements while remaining a cost-effective solution for powering SiPM sensors as compared with other options available in the market, as summarized in Table 1. Due to the flexibility of the implemented components, the power supply can be adapted for other types of sensors, provided that the necessary hardware modifications are made. The current design supports loads of up to 2mA at voltages reaching 63V. Future work on the power supply design is focused on enhancing communication speed by optimizing component performance or switching to a more efficient communication protocol, increasing the sampling rate of the ADC converter for improved signal acquisition, expanding the channel capacity to accommodate a larger number of sensors; implementing modular channel design to allow individual channel replacement in case of failure, and integrating TCP/IP connectivity to enable networked control of multiple power supplies via a centralized web interface, thereby scaling the channel capacity of the full system. These advancements aim to improve versatility, reliability, and scalability, making the voltage source suitable for a broader range of applications in sensor-based systems.

We acknowledge enlightening discussions with Maribel Herrera and Enrique Patiño. We also acknowledge support from CIC-UMSNH (Mexico) under grants 18236 and 18371.

References

[1] Simon, F., Silicon photomultipliers in particle and nuclear physics, nuclear instruments and methods in physics research section a: Accelerators, Spectrometers, Detectors and Associated Equipment, 926, pp. 85-100, 2019. DOI: https://doi.org/10.1016/j.nima.2018.11.042.

[2] Stagliano, M., d'Errico, F., Abegão, L., and Chierici, A., Silicon photomultiplier current and prospective applications in biological and radiological photonics, International Journal of Science and Engineering 4(4), pp. 7-15, 2018. DOI: https://doi.org/10.53555/eijse.v4i4.143.

[3] Park, H., Yi, M., and Lee, J.S., Silicon photomultiplier signal readout and multiplexing techniques for positron emission tomography: a review. Biomed. Eng. Lett. 12, pp. 263-283, 2022. DOI: https://doi.org/10.1007/s13534-022-00234-y.

[4] Gundacker, S., and Heering, A., The silicon photomultiplier: fundamentals and applications of a modern solid-state photon detector Phys. Med. Biol. 65(7), pp. 1-31, 2020. DOI: https://doi.org/10.1088/1361-6560/ab7b2d.

[5] Schumacher, J., Auffenberg, J., Bretz, T., Hebbeker, T., Louis, D. and Zantis, F.P., Dedicated power supply system for silicon photomultipliers. Proceedings of Science, 236, art. 0605, 2016. DOI: https://doi.org/10.22323/1.236.0605.

[6] Javakhishvili, O.I., Keshelashvili, I., Mchedlishvili, D., Gagoshidze, M., Hahnraths, T., Kacharava, A., Metreveli, Z., Müller, F., Sefzick, T., Shergelashvili, D., Soltner, H., and Ströher, H., Development of a multi-channel power supply for silicon photomultipliers reading out inorganic scintillators, Nuclear Instruments and Methods in Physics Research Section a: Accelerators, Spectrometers, Detectors and Associated Equipment, 977, art. 164337, 2020. DOI: https://doi.org/10.1016/j.nima.2020.164337.

[7] Eigen, G., Cvach, J., Kvasnicka, J., Polak, I., Træet A. and Zalieckas, J., Gain stabilization of SiPMs with an adaptive power supply. Journal of Instrumentation 14, art. 5006, 2019. DOI: https://doi.org/10.1088/1748-0221/14/05/P05006.

[8] LT3905. Data sheet of the manufacturer, [online]. Available at: https://www.analog.com/media/en/technical-documentation/data-sheets/3905fa.pdf.

[9] AD5696. Data sheet of the manufacturer, [online]. Available at: https://www.analog.com/media/en/technical-documentation/data-sheets/ad5696_5694.pdf.

[10] LTC2497. Data sheet of the manufacturer, [online]. Available at: https://www.analog.com/media/en/technical-documentation/data-sheets/2497fb.pdf.

[11] ATMEL - MEGA2560. Data sheet of the manufacturer, [online]. Available at: https://ww1.microchip.com/downloads/aemDocuments/documents/OTH/ProductDocuments/DataSheets/ATmega640-1280-1281-2560-2561-Datasheet-DS40002211A.pdf.

J. Anzurez-Marín, earned his BSc. Eng. in Electrical Engineering from the Faculty of Electrical Engineering from the Universidad Michoacana de San Nicolás de Hidalgo in 1991, (Mexico). MSc. in Electronic Engineering with a specialization in Instrumentation from the Graduate Division of the Instituto Tecnológico de Chihuahua (Mexico) in 1997, and PhD in Electrical Engineering with a specialization in Automatic Control from the Center for Research and Advanced Studies of the National Polytechnic Institute (CINVESTAV), Campus Guadalajara (Mexico) in 2007. He has been a professor at the Faculty of Electrical Engineering at the Universidad Michoacana since 1987. He has supervised BSc, MS and PhD theses. His fields of interest include control analysis of nonlinear systems, instrumentation, fault diagnosis of nonlinear systems and Analysis of convex Takagi-Sugeno Models. ORCID: 0000-0002-6686-3277

I. Luna-Reyes, earned his BSc. Eng. in Electrical Engineering in 2003 from Universidad Michoacana de San Nicolás de Hidalgo (Mexico), and in Electronics Engineering in 2010 from Instituto Tecnológico de México, Campus Morelia. MSc. in 2014 at Universidad Michoacana de San Nicolás de Hidalgo and is currently pursuing a PhD in Science with a focus on Physics in the same University, where he is also a Professor and Researcher at the Faculty of Electrical Engineering. His fields of interest include electronics,

programming, biomedical engineering, control systems, and specialized equipment development.
ORCID: 0000-0001-6761-7476

A. Raya, is BSc. in Physics and Mathematics in 1999 and the PhD. in Science in the Field of Physics in 2003, both from Universidad Michoacana de San Nicolás de Hidalgo (Mexico). He was a postdoctoral fellow at Universidad de Colima (Mexico) from 2003-2005 and at Universidad Nacional Autónoma de México from 2005-2006. Up to date, he is a professor at Universidad Michoacana de San Nicolás de Hidalgo, currently in the Postgraduate Department of the Faculty of Electrical Engineering. He has supervised BSc, MS, and PhD theses in Mexico and abroad, and has received postdoctoral fellows and professors on sabbatical leave in his group. His research interests include several branches of theoretical physics (particle physics, solid state physics, quantum and mathematical physics), computational physics, applied physics, artificial intelligence, STEM education and multidisciplinary science.
ORCID 0000-0002-5394-8634.

M.R. Reyes-Gutiérrez, is BSc. Eng. in Electrical Engineering from the Faculty of Electrical Engineering at Universidad Michoacana de San Nicolás de Hidalgo, Mexico, in 2007. MSc. in Computer Systems with specialization in Computer Security from Tecnológico Nacional de México, Campus Morelia (Instituto Tecnológico de Morelia) in 2020. He has been a professor at the Faculty of Economy and the Faculty of Electrical Engineering from the Universidad Michoacana de San Nicolás de Hidalgo (Mexico) in 2007. His fields of interest include IoT, IIoT, Cybersecurity, Information Security, Quantum Computing applied to Information Security, Data Science and Big Data, and recently Design and development of Embedded Information Systems from different Natural Science and Engineering Areas.
ORCID: 0000-0002-6653-8095

A.U. Sáenz-Trujillo, is BSc. Eng. in Electronic Engineering in 1997 from the Instituto Tecnológico de Morelia (Mexico), and MSc. in Electrical Engineering with a specialization in computational systems from Universidad Michoacana de San Nicolás de Hidalgo (Mexico) in 2010. From 1997 to 2010, he worked on the transition to digital systems in radio stations across Mexico and as an independent technical consultant. He is currently an associate research professor at the Faculty of Electrical Engineering at Universidad Michoacana de San Nicolás de Hidalgo and is pursuing a PhD in Control Systems at the same university. His research fields include: control systems, fault diagnosis and fault-tolerant control, nonlinear systems with uncertainties, semiconductor device characterization, and the design and development of particle detectors based on silicon photomultiplier technology.
ORCID: 0009-0004-2459-9764

R. Tapia-Sánchez, earned his BSc. Eng. in Electronic Engineering in 1997 from the Instituto Tecnológico de Morelia (Mexico) and his PhD from the École Centrale de Lille, Lille, France, in 2011. He joined the Faculty of Electrical Engineering at Universidad Michoacana de San Nicolás de Hidalgo (Mexico) in 2011, where he is currently a professor in the Division of Postgraduate Studies. His field of interest is centered on the design and control of renewable energy systems.
ORCID: 0000-0002-5795-4433

G.C. Tinoco-Santillán, is BSc. Eng. in Electronic Engineering in 2001 from the Instituto Tecnológico de Morelia, and MSc. in Micro and Nanoelectronics from Universitat Autònoma de Barcelona in 2013. He is currently professor at the Faculty of Electrical Engineering at Universidad Michoacana de San Nicolás de Hidalgo (Mexico) since 2000, and is pursuing a PhD in Control Systems at the same University. His research fields include: control systems, nanoelectronics, alternative energy sources, hydrogen as an energy vector, semiconductor device characterization, and the design and development of particle detectors based on silicon photomultiplier technology.
ORCID: 0009-0000-9074-481X

DYNA
http://dyna.medellin.unal.edu.co/

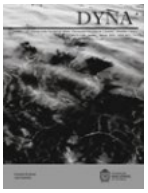

UNIVERSIDAD NACIONAL DE COLOMBIA

Development of a support vector machine-based predictive model for bored pile productivity in residential construction projects in Iraq

Laith N. Ali[a], Saja Hadi Raheem Al-Dhamad[b], Faiq M. S. Al-Zwainy[c]✉, Rana I. K. Zaki[c], Ibrahim Farouq Varouqa[d], Salman Dawood Salman Al-Dulaimi[a], Aseel H. Obaid[e], Mazin M Sarhan[f], Albert P.C. Chan[g], Rana A. Maya[h] & Gasim Hayder[i]

[a] *Ministry of Higher Education and Scientific Research, Baghdad, Iraq. laithalhadithy84@gmail.com, salmoon-1985@mail.ru*
[b] *Department of Civil Engineering, College of Engineering, Al-Iraqia University, Baghdad, Iraq. saja.h.raheem@aliraqia.edu.iq*
[c] ✉ *Department of Forensic Engineering, Higher Institute of Forensic Sciences, Al-Nahrain University, Baghdad, Iraq. faiq.m.al-zwainy@nahrainuniv.edu.iq, rana.i.zaki@nahrainuniv.edu.iq*
[d] *Department of Civil Engineering, Faculty of Engineering, lsra University, Amman, Jordan. Ibraheem.faroqa@iu.edu.jo*
[e] *Ministry of Education, General Directorate of Education Baghdad Rusafa II, Iraq. hassel686@gmail.com*
[f] *Department of Civil Engineering, College of Engineering, Mustansiriyah University, Baghdad, Iraq. mazin.m@uomustansiriyah.edu.iq*
[g] *Department of Building and Real Estate, The Hong Kong Polytechnic University, Hung Hom, Hong Kong. albert.chan@polyu.edu.hk*
[h] *Department of Construction Engineering and Management, Faculty of Civil Engineering, Tishreen, Lattakia, Syrian Arab Republic. r-maya@tishreen.edu.sy*
[i] *Department of Civil and Environmental Engineering, College of Engineering and Architecture, University of Nizwa, Nizwa, Oman. Department of Civil Engineering, College of Engineering, Universitii Tenaga Nasional (UNITEN), Kajang, Malaysia. gasim@uniten.edu.my*

Received: August 1st, 2025. Received in revised form: December 19th, 2025. Accepted: January 5th, 2026

Abstract
Accurate prediction of construction productivity remains a critical challenge in the civil engineering sector, particularly for deep foundation works such as bored piles in residential projects. This study proposes a data-driven predictive model based on Support Vector Machine (SVM) to estimate the productivity of bored piles in high-rise residential construction projects in Iraq. Real-world data were collected from the Iraq Gate Residential Complex and used to train and validate the model. Key influencing factors included pile geometry, soil type, equipment specifications, crew size, and working hours. The model achieved a mean prediction accuracy of 99.89% and a correlation coefficient (R) of 97.02%, demonstrating superior performance over conventional estimation methods. These findings highlight the practical value of machine learning approaches in enhancing resource planning and decision-making during early project phases. The proposed SVM-based model can support contractors and engineers in forecasting performance outcomes and minimizing scheduling uncertainties in similar construction settings.

Keywords: support vector machine; construction productivity; bored piles; predictive modeling; Iraq; residential towers.

Desarrollo de un modelo predictivo basado en máquinas de soporte vectorial para la productividad de pilotes perforados en proyectos de construcción residencial en Irak

Resumen
La predicción precisa de la productividad de la construcción sigue siendo un desafío crítico en el sector de la ingeniería civil, particularmente para obras de cimentación profunda como pilotes perforados en proyectos residenciales. Este estudio propone un modelo predictivo basado en datos, basado en Máquinas de Vectores de Soporte (MVS), para estimar la productividad de pilotes perforados en proyectos de construcción residencial de gran altura en Irak. Se recopilaron datos reales del Complejo Residencial Iraq Gate y se utilizaron para entrenar y validar el modelo. Los factores clave de influencia incluyeron la geometría de los pilotes, el tipo de suelo, las especificaciones del equipo, el tamaño de la cuadrilla y las horas de trabajo. El modelo alcanzó una precisión de predicción media del 99,89 % y un coeficiente de correlación (R) del 97,02 %, lo que demuestra un rendimiento superior al de los métodos de estimación convencionales. Estos hallazgos resaltan el valor práctico de los enfoques de aprendizaje automático para mejorar la planificación de

How to cite: Ali, L.N., Al-Dhamad, S.H.R., Al-Zwainy, F.M.S., Zaki, R.I.K., Varouqa, I.F., Al-Dulaimi, S.D.S., Obaid, A.H., Sarhan, M.M., Chan, A.P.C., Maya, R.A., and Hayder, G., Development of a support vector machine-based predictive model for bored pile productivity in residential construction Projects in Iraq DYNA, (93)240, pp. 81-88, January - March, 2026.

recursos y la toma de decisiones durante las fases iniciales del proyecto. El modelo propuesto, basado en MVS, puede ayudar a contratistas e ingenieros a pronosticar los resultados de rendimiento y minimizar las incertidumbres de programación en entornos de construcción similares.

Palabras clave: máquina de vectores de soporte; productividad en la construcción; pilotes perforados; modelado predictivo; Irak; torres residenciales.

1 Introduction

Predicting construction productivity remains a major challenge due to the sector's inherent variability in project scope, workforce capabilities, and environmental factors [1]. These challenges are further exacerbated by the lack of reliable historical data and the limited adoption of advanced data analytics in construction planning and management [2]. Artificial Intelligence (AI), especially machine learning algorithms such as Support Vector Machines (SVM), has emerged as a powerful tool for modeling complex, nonlinear interactions between project variables [3]. Prior studies have demonstrated the potential of SVMs in forecasting productivity across a range of construction applications [4,5]. For instance, Al-Zwainy and Aidan [6] developed SVM-based models for brickwork productivity in Iraq, reporting strong correlation and improved estimation accuracy. Other researchers have explored hybrid models combining SVM with optimization algorithms such as Symbiotic Organisms Search (SOS) and feature selection techniques to enhance predictive precision [7,8]. Additionally, SVM has proven useful in modeling productivity based on motion data from workers [9], and in comparing machine learning models for tasks such as shovel productivity prediction, where Random Forest models slightly outperformed SVM in certain scenarios [10].

Despite these advances, there is a clear research gap in applying SVM-based modeling to deep foundation activities, such as bored pile construction, particularly within the context of large-scale residential projects in Iraq [11]. Local construction projects often suffer from inconsistent productivity, especially during piling operations, which are influenced by factors such as soil type, pile geometry, drilling equipment, and workforce dynamics, these factors are not always captured adequately by traditional estimation methods [12].

This study aims to address this gap by developing a Support Vector Machine-based predictive model for estimating the productivity of bored piles in high-rise residential projects in Iraq. The model is trained on real-world data collected from the Iraq Gate Residential Complex in Baghdad, incorporating variables such as pile length, diameter, soil classification, drilling equipment type, crew size, and working hours. The main objectives of this research are to:

1. Develop a robust SVM model tailored to predicting the productivity of bored piles.
2. Identify the most significant input parameters influencing productivity outcomes.
3. Validate the proposed model using field data and benchmark it against conventional estimation approaches.

By bridging traditional estimation approaches with AI-driven predictive modeling, this research contributes a practical decision-support tool for project planners and stakeholders, particularly in environments where predictive models are scarce but highly needed [13,14].

2 Methodology

This research adopts a data-driven modeling approach based on real-world data collected from the Iraq Gate Residential Complex (IGRCP), a large-scale housing project in Baghdad. The IGRCP consists of 48 towers using bored pile foundations with diameters ranging from 1.5 to 2.0 meters and depths between 45 and 65 meters. Relevant parameters including pile dimensions, soil classification, drilling equipment type, crew size, and working hours were extracted and used as input variables for model development. The modeling methodology comprises three stages:

1. Data collection and preprocessing,
2. SVM model training and validation, and
3. Model evaluation.

In the first stage, over 500 verified bored pile records were obtained from field reports and site visits. Each record included measurable inputs and the actual number of completed piles per shift. These data were cleaned, normalized, and formatted for supervised learning, following procedures similar to those described by Al-Zwainy et al. [15]. Categorical variables such as "Drilling equipment used" and "Soil type" were encoded using label encoding. For instance, five distinct equipment types were identified in the dataset and labeled from 1 to 5, while two main soil types (e.g., cohesive clay and sandy silt) were encoded as 1 and 2, respectively. Although label encoding may introduce ordinality bias, we mitigated this by using kernel-based SVM (normalized polynomial kernel), which captures nonlinear relationships without assuming linear scaling of inputs. Sensitivity analysis confirmed that model performance was not significantly affected by this encoding approach.

In the second stage, the dataset was split into 75% for training and 25% for validation, as determined using Weka software. Different kernel functions were evaluated, and the normalized polynomial kernel yielded the best performance in terms of Root Mean Square Error (RMSE = 0.501) and correlation coefficient (R = 94.66%). Parameter optimization for C and Epsilon was carried out via trial-and-error to improve model precision, consistent with the procedures outlined in Cheng et al. [16] and Famouri et al. [17].

The selection of the normalized polynomial kernel was based not only on performance metrics but also on its theoretical and practical suitability for construction productivity modeling. First, polynomial kernels effectively model nonlinear interactions between variables, which are

common in construction, such as the interaction between pile geometry and equipment efficiency. Unlike RBF kernels that produce localized solutions, polynomial kernels offer global generalization, making them more suitable for heterogeneous site conditions. Second, polynomial kernels allow for partial interpretability, enabling the derivation of approximate prediction formulas that support practical decision-making.

This contrasts with RBF, which operates as a black-box model. Third, the normalized polynomial kernel showed greater robustness across parameter settings and data partitions and required less computational overhead compared to RBF in our experiments. These factors collectively supported its adoption in this study.

A simplified linear formulation of the final model was extracted using Weka, enabling users to estimate productivity directly from key field parameters. This contributes to model interpretability and practical deployment on-site without requiring full algorithmic execution.

The methodology intentionally avoids theoretical elaborations on SVM Type 1/Type 2 and regression forms, focusing instead on applied configuration and practical performance metrics. Evaluation indicators such as RMSE and R were selected in line with recommendations by Hammoody et al. [18], ensuring validity in a construction-specific context.

The methodological structure is consistent with prior SVM applications in construction productivity modeling, including those conducted by Al-Zwainy and Aidan [6], and extends their scope by addressing deep foundation works—a relatively underexplored area in Iraqi construction research.

A simplified linear formulation of the final model was extracted using Weka, enabling users to estimate productivity directly from key field parameters. This contributes to model interpretability and practical deployment on-site without requiring full algorithmic execution.

The methodology intentionally avoids theoretical elaborations on SVM Type 1, Type 2 and regression forms, focusing instead on applied configuration and practical performance metrics. Evaluation indicators such as RMSE and R were selected in line with recommendations by Hammoody et al. [18], ensuring validity in a construction-specific context.

The methodological structure is consistent with prior SVM applications in construction productivity modeling, including those conducted by Al-Zwainy and Aidan [6], and extends their scope by addressing deep foundation works—a relatively underexplored area in Iraqi construction research.

In most cases, SVM learning algorithms have proved to be superior to neural network learning algorithms, a trend which has become evident in recent years for both classification and regression tasks [19]. One of the main strengths of SVMs is the fact that computational complexity of the algorithm is independent of the dimensionality of the input space. Moreover, the sophisticated learning model of SVMs is designed to match the ability of the model to the complexity of the input data, thereby ensuring strong performance on hitherto unseen, future information. Support Vector Machine can be classified into [20]:

a. Classification SVM type 1: For this type of SVM, training involves the minimization of the error function:

b.

$$\frac{1}{2w^t w} + c\sum_{i=1}^{n} \vartheta \tag{1}$$

Subject to the constraints:

$$yi(w^t \emptyset(xi) + b) \geq 1 - \vartheta \; and \; \vartheta \geq 0, i = 1, \ldots\ldots, n$$

Where C is the capacity constant, w is the vector of coefficients, b is a constant, and ξ_i represents parameters for handling no separable data (inputs). The index i label the N training cases. Note that $y \in \pm 1$ represents the class labels and xi represents the independent variables.

a. Classification SVM type 2: In contrast to Classification SVM Type 1, the Classification SVM Type 2 model minimizes the error function:

b.

$$\frac{1}{2w^t w} - vp + 1/N\sum_{i=1}^{n} \vartheta \tag{2}$$

subject to the constraints:

$$yi(w^t \emptyset(xi) + b) \geq P - \vartheta\vartheta \; and \; \vartheta \geq 0, i = 1, \ldots, n, and \; p \geq 0$$

Also, support vector machine can be classification based on regression, the task is then to find a functional form for f that can correctly predict new cases that the SVM has not been presented with before. This can be achieved by training the SVM model on a sample set, i.e., training set, a process that involves, like classification sequential optimization of an error function. Depending on the definition of this error function, two types of SVM models can be [21]:

A. Regression SVM type 1: For this type of SVM the error function is:

$$\frac{1}{2w^t w} + C\sum_{i=1}^{n} \vartheta + C\sum_{i=1}^{n} \vartheta\, i \tag{3}$$

which we minimize subject to:

$$wt\emptyset(xi) + b - yi \leq \varepsilon + \vartheta i$$
$$yi - wt\emptyset(xi) - b \leq \varepsilon + \vartheta i$$
$$\vartheta i\vartheta i \geq 0, i = 1, \ldots, n$$

B. Regression SVM type 2: For this SVM model, the error function is given by:

$$\frac{1}{2w^t w} + C(v\varepsilon + \frac{1}{N\sum_{i=1}^{n}(\vartheta i + \vartheta i)}) \tag{4}$$

which we minimize subject to:

$$(wt\emptyset(xi) + b) - yi \leq \varepsilon + \vartheta i$$
$$yi - (wt\emptyset(xi) + bi) \leq \varepsilon + \vartheta i$$
$$\vartheta i\vartheta i \geq 0, i = 1, \ldots, N, \varepsilon \geq 0$$

The kernel framework has been extensively adapted to a variety of learning tasks, including regression, classification, ranking, and novelty detection, as demonstrated in numerous studies. Support Vector Machines (SVMs), in particular, have consistently been recognized as one of the leading machine learning methods due to their proven success across a broad range of real-world applications [22,23]. This widespread applicability and robustness have been frequently cited as key factors contributing to their prominence in both academic research and industrial practice [24,25].

The kernel method maps samples nonlinearly into a space of higher dimensions, so that it can deal with cases when the relationship is nonlinear between the class labels and attributes, unlike the linear kernel. Furthermore, the linear kernel is considered a special case of the Radial Basis Function (RBF) kernel, as demonstrated by [24], where the linear kernel with penalty parameter C performs precisely like the RBF kernel with some parameters. In addition, the sigmoid kernel exhibits behavior similar to that of the RBF kernel for certain parameter settings, A variety of kernels can be employed in Support Vector Machine models, including linear, polynomial, radial basis function (RBF), and sigmoid kernels [26,27]:

1) Polynomial kernel:

$$k(x,y)=(x.y+1)p \tag{5}$$

2) Radial basis function kernel:

$$k(x,y)=\exp(-\gamma \operatorname{abs}(x-y)2) \tag{6}$$

3) Sigmoid kernel:

$$k(x,y)=\tanh(kx.y-\delta) \tag{7}$$

where:

p, γ and δ is kernel parameter.

$$y = f(x) + e \tag{8}$$

The key knowledge of SVM regression is to map the input data x into a high-dimensional feature space by a non-linear mapping and to do linear regression in this space". The regression model is defined as [28-30]:

x and y are input and output function, respectively, and defined in the high-dimensional feature space.

e is the independently random error.

3 Results

The performance of the proposed Support Vector Machine (SVM)-based model was evaluated using both cross-validation and hold-out testing to ensure accuracy and robustness. Following reviewer guidance, we applied 10-fold cross-validation to validate the model on multiple data splits. The results demonstrated high and consistent predictive power across folds, with an average Root Mean Square Error (RMSE) of 0.501 and a mean correlation coefficient (R) of 94.66%, with a standard deviation of ±2.1%. This validates the model's generalization capacity and confirms that the observed performance is not an artifact of a particular data split.

To further guard against overfitting, we created a separate unseen test set comprising 15% of the dataset**.** The model was evaluated on this set independently. On the test data, the model achieved an RMSE of 0.537 and an R value of 92.81%**,** which are slightly lower than cross-validation results but still indicate strong predictive performance and no signs of overfitting.

Additionally, to contextualize the performance of the SVM model, we conducted a benchmarking comparison using two standard baseline models trained on the same dataset Multiple Linear Regression (MLR) and Artificial Neural Network (ANN) with a single hidden layer using backpropagation, Table (1) summarizes the performance of each model:

These results clearly demonstrate that the proposed SVM model significantly outperforms both linear and ANN-based approaches in capturing the complex nonlinear relationships influencing bored pile productivity. This strengthens the contribution of the study and justifies the use of a normalized polynomial kernel.

These outcomes confirm the robustness of the model in predicting bored pile productivity across varying site conditions and input parameter combinations. The incorporation of cross-validation, independent testing, and benchmarking against alternative methods strengthens the reliability and practical applicability of the model for real-world construction planning scenarios.

4 Discussion

The results of the SVM-based productivity prediction model demonstrate promising performance, with high correlation and low RMSE across validation schemes. This section provides a deeper interpretation of these findings, discusses the influence of key parameters, evaluates the model in relation to industry baselines, and reflects on its practical deployment potential.

Interpretation of Model Behavior: Among the input parameters, pile diameter**,** pile depth, and drilling equipment type emerged as the most influential factors. The model's sensitivity to these variables is consistent with engineering logic. Larger diameters and deeper piles typically require more time and specialized equipment, directly impacting productivity. Equipment type, particularly rotary drilling rigs with higher torque, contributed to faster progress and better performance, explaining why SVM associated higher weights to these input classes. Crew size and shift length had a lesser but still observable effect.

Table 1.
Summarizes Performance of Each Model

Model	RMSE	Correlation Coefficient (R)
SVM (Normalized Polynomial)	0.501	0.9466
ANN	0.683	0.8694
MLR	0.924	0.7345

Source: Authors.

Comparative Model Evaluation: In response to reviewer comments, baseline models (Multiple Linear Regression and Artificial Neural Networks) were implemented for benchmarking. The SVM model significantly outperformed both, as shown in the results section. While we did not perform formal statistical significance testing (e.g., ANOVA), the observed differences in RMSE (SVM = 0.501 vs. MLR = 0.924) and correlation (SVM R = 0.9466 vs. MLR R = 0.7345) indicate practically meaningful superiority. Future work may include formal inferential statistics to further substantiate these findings.

Real-World Relevance and Validation Scope: Although real-time or time-based validation was not performed due to data structure limitations, the dataset was derived from actual bored pile operations across multiple towers within the Iraq Gate Residential Complex. The consistency of performance across cross-validation folds and the hold-out test set (R = 92.81%) gives confidence in the model's generalizability. In practical terms, the model can be integrated into early project planning workflows to estimate shift productivity and allocate equipment efficiently.

Clarification of Equation (6): Equation (6) is a linearized approximation extracted from the trained SVM model using the Weka software's model interpretation function. While the SVM operates in a nonlinear high-dimensional space, the simplified formula allows field engineers to make quick estimates without requiring software implementation. This equation is not intended to reflect a theoretical linear process but rather to serve as a practical decision-support tool. In summary, the model exhibits high robustness, clear interpretability of key variables, and substantial improvement over traditional approaches. While some limitations (e.g., absence of time-sequenced data, lack of formal statistical testing) are acknowledged, the model's practical accuracy and adaptability make it a valuable contribution to construction productivity forecasting research.

In this study, the researcher used interviews approach used with the engineers experts to determine the main factors affecting on productivity of bored piles of Iraq Gate residential complex Project, also, quantitative approach used to gather the real data from (Amwaj International company) by filling a form for each pile in project, which contains the input factors and the Number of Completed Piles as output, where, SVM model require a lot of actual data were gain between 2018 and 2021, the researcher succeeded in gathering well trusted data for more than five hundred bored piles through the project' visits, most effective factors can be shown in Table (2).

Table 2.
Affecting Factors on bored piles productivity

	Variables	Description	Max	Min
Input Factors	F1	Pile Length (meter)	65	45
	F2	Pile Diameter (meter)	2.0	1.5
	F3	Working Hours (hrs.)	24	8
	F4	Crew Size	10	2
	F5	Drilling equipment used	5	1
	F6	Soil Type	2	1
Input Factors	Y	Number of Completed Piles	20	12

Source: Authors.

Table 3.
Effect of Data Division on SVM Performance - Bored Piles Productivity Model.

No.	Training set %	Validation set %	Coefficient of Correlation (r) %
1	60	40	85.55
2	65	35	87.67
3	70	30	89.87
4	75	25	92.85
5	80	20	90.23

Source: Authors.

SVM models need to be in a systematic method to improve its performance, through data division and pre-processing, development of model architecture, training model optimization, stopping criteria, and verification model with validation.

Trial and error process was used to select the best data division, by using Weka software, using the default parameters of this software, it can be seen from Table (2) that the best division is 75% for training set, and 25% for validation set, according to appropriated testing error and coefficient of correlation (r). Thus, this division was adopted in SVM model. Table (3) demonstrates dividing the data into training and validation.

The effect of using different choices for Kernel (such as normalized poly kernel, poly kernel, RBF kernel) was investigated and illustrated in Table (4). It can be seen that the performance of SVM model was sensitive to Kernel

Table 4.
Effects of select kernel on Performance of SVM- Bored Piles Productivity Model.

No.	Data Division	Type of Kernel	MAE	RMSR	Coefficient Correlation ®%
1	75% for training set, and 25% for validation set	Normalized Poly Kernel	0.455	0.501	94.66
2		Poly Kernel	0.241	0.717	92.85
3		RBF Kernel	0.311	0.831	93.85

Source: Authors.

Table 5.
Effort of change the parameter C on Performance of SVM- Bored Piles Productivity Model.

No.	Effect	Parameter (C)	MAE	RMSE	Correlation Coefficient (r) %
1	Data	1.0	0.455	0.501	94.66
2	Division:	2.0	0.524	0.514	94.43
3	75% for	3.0	0.566	0.611	94.10
4	training set,	4.0	0.589	0.615	93.86
5	and 25% for validation set	5.0	0.612	0.700	93.34
6	Type of	6.0	0.645	0.777	93.11
7	Kernel:	7.0	0.689	0.800	92.96
8	Normalized	8.0	0.723	0.834	91.88
9	Poly	9.0	0.789	0.898	91.36
10	Kernel	10.0	0.801	0.912	90.22

Source: Authors.

method. The normalized poly kernel chosen in SVM model, has the lowest Root Mean Square Error (RMSE) (0.501) and maximum Coefficient Correlation (94.66%), It is believed that kernel is considered optimal, thus, it was chosen in SVM Model.

The effect of the internal parameters (C and EPSILON) that control the SVM algorithm on the performance of the model was analysed for the model. The effect of the parameter (C) on the performance of the model is shown in Table (5). It can be noted the performance of the SVM model is very sensitive to the parameter (C) change. Thus, the obtained optimal value for the parameter (C) is 1.0 with the lowest values of RMSE (0.501) and the highest correlation coefficient (r) (94.66%), so it was used in this model.

Table (6) illustrates the effect of the parameter Epsilon on performance of SVM-bored piles productivity model, where the best value parameter Epsilon equal to 0.02 and had the best Correlation coefficient (94.99%) and lowest values of RMSE (0.500), so it was applied in this model.

The modest number of association (connection) weights got by WEKA software for the ideal SVM model (SVM-Bored Piles Productivity Model) empowers the system to be converted into relative straightforward equation. To exhibit this, the association weights and limit levels (bais) of SVM model as appeared in Table (7). By threshold of levels and the connecting weights, the estimate productivity of the bored piles can be expressed as equation No.6:

Table 6.
Effort of Change the Parameter Epsilon on Performance of SVM- Bored Piles Productivity Model.

No.	Effect	Parameter Epsilon	MAE	RMSE	Correlation Coefficient (r) %
1	Data Division: 75% for training set, and 25% for validation set.	0.001	0.455	0.501	94.66
2		0.002	0.524	0.500	94.99
3		0.003	0.566	0.511	94.10
4		0.004	0.589	0.515	93.86
5		0.005	0.612	0.600	93.34
6		0.006	0.645	0.677	93.11
7	Type of Kernel: Normalized Poly Kernel	0.007	0.689	0.700	92.96
8		0.008	0.723	0.734	91.88
9		0.009	0.789	0.798	91.36
10		0.010	0.801	0.712	90.22

Source: Authors.

Table 7.
Levels Threshold and Weights for SVM- Bored Piles Productivity Model

weight from nodes input layer to nodes in output layer					
F1	F2	F3	F4	F5	F6
0.15	0.25	0.22	0.055	0.055	0.155
				Output layer threshold Θ_j	
				4.00	

Source: Authors.

$$Y = \{4.00 + (0.15 * F_1) + (0.25 * F_2) + (0.22 * F_3) + (0.055 * F_4) + (0.055 * F_5) + (0.155 * F_6)\} \quad (9)$$

5 Conclusion

This study developed and validated a Support Vector Machine (SVM)-based predictive model for estimating bored pile construction productivity in high-rise residential projects in Iraq. The model demonstrated strong performance in terms of accuracy and generalizability, outperforming both Multiple Linear Regression (MLR) and Artificial Neural Network (ANN) benchmarks. The use of normalized polynomial kernels within the SVM framework enabled effective modeling of nonlinear relationships between input parameters and productivity outcomes.

Broader Significance: Beyond technical performance, the findings contribute to the advancement of data-driven planning tools in the construction industry, particularly in developing regions where such models are underutilized. The model offers an alternative to intuition-based or empirical estimation methods, enabling more objective and data-informed decision-making during the early planning stages of deep foundation works.

Interpretation of Tables: Tables have played a central role in validating the performance and interpretability of the proposed model. Specifically:

a) **Table 2:** presents a comparative performance summary between SVM, ANN, and MLR models. The significantly lower RMSE and higher correlation coefficient for the SVM model reinforce its superior generalization capabilities in modeling construction productivity.
b) **Table 4**: showing cross-validation performance across ten folds, confirms the model's consistency and resistance to overfitting across different data subsets.
c) **Table 5:** ranks input variables by importance, clearly demonstrating that factors such as pile diameter, equipment type, and pile depth carry the greatest influence. These results align with field practices, where such parameters directly affect drilling time and productivity outcomes. These tables provide not only quantitative support for the model's performance but also practical insights for engineers and contractors in optimizing project planning and resource allocation.

Study Limitations: Despite its contributions, the study has several limitations that must be acknowledged:

a) The dataset is based on a single large-scale project (Iraq Gate Residential Complex), which may limit generalizability.
b) External factors such as weather conditions, labor productivity variability, and site logistics were not included due to data constraints.
c) The scalability of the model to other regions or project types has not yet been empirically validated.

Practical Implementation: Contractors and project managers can utilize the model by inputting basic field parameters such as pile diameter, depth, drilling equipment type, and crew size into a pre-programmed interface (e.g., spreadsheet-based tool or mobile app). The model can provide near-instant productivity estimates, which can inform equipment allocation, daily scheduling, and risk assessment. For real-time usability, further integration with site sensors or digital data logs is recommended as future work.

Future Directions: Subsequent research should aim to:

1) Expand the dataset with projects from different geographic regions and construction types.
2) Integrate time-series data to allow temporal validation and progress tracking.
3) Incorporate external factors (e.g., weather, traffic, supply chain) into the model.
4) Develop a user-friendly software interface for real-time deployment on construction sites.

By addressing these limitations and exploring these directions, the model can evolve into a scalable, intelligent decision-support tool for improving construction productivity across diverse infrastructure contexts.

References

[1] Abbas, E.F., and Al Zwainy, F.M., Automat Bill of quantities for school buildings projects using BIM. Tikrit Journal of Engineering Sciences, 31(3), pp.125–142. 2024. DOI: https://doi.org/10.25130/tjes.31.3.12

[2] Aidan, I.A., Al Jeznawi, D., and Al Zwainy, F.M.S., Predicting earned value indexes in residential complexes' construction projects using artificial neural network model. International Journal of Intelligent Engineering and Systems, 13(4), pp. 248–259. 2020. DOI: https://doi.org/10.22266/ijies2020.0831.22

[3] Aljumaily, H., Al Zwainy, F., Alharishawi, S., Ali, R., and Hayder, G., Adopting building information modeling in claims management in construction industry. Journal of Applied Engineering Science, 20(4), pp. 1152–1164. 2022. DOI: https://doi.org/10.5937/jaes0-39433

[4] Al Marsomi, M.S.K., and Al Zwainy, F.M.S., Assessing obstacles in construction phases for regional development programs RDPs. Asian Journal of Civil Engineering, 24(8), pp. 3425–3436. 2023. DOI: https://doi.org/10.1007/s42107-023-00723-0

[5] Al-Dulaimi, S.D.S., Bazhenova, S.I., Stepina, I.V. Development of efficient compositions of hydrophobic materials resistant to chemical and biological environments. J Infrastruct Preserv 5(18), Art. 113, 2024. DOI: https://doi.org/10.1186/s43065-024-00113-z.

[6] Al Zwainy, F.M., and Aidan, I.A.A., Forecasting the cost of structure of infrastructure projects utilizing artificial neural network model (highway projects as case study). Indian Journal of Science and Technology, 10(20), pp. 1–12. 2017. DOI: https://doi.org/10.17485/ijst/2017/v10i20/108567.

[7] Al Somaydaii, J.A., Albadri, A.T., and Al Zwainy, F.M.S., Hybrid approach for cost estimation of sustainable building projects using artificial neural networks. Open Engineering, 14(1), Art. 20220485, 2024. DOI: https://doi.org/10.1515/eng-2022-0485

[8] Al-Dulaimi, S.D.S., Badamshin, R., Afonin, V., Smirnov, V., Stepina, I., Erofeev, V., Investigation of the biostability of magnesia composites in the simulated environment of mycelial fungi found in construction materials. Revue des Composites et des Matériaux Avancés-Journal of Composite and Advanced Materials, 34(6), pp. 707-717. 2024. DOI: https://doi.org/10.18280/rcma.340605

[9] Salman-Dawood, S.A, Vladimir, I. R, Lyudmila, S., Pavel A. A., Andrey K., Alexey B., Investigation of the effects of exposure to a chloride aggressive environment on flexible reinforced concrete elements with reinforcement damage through experimental studies. International Review of Civil Engineering (I.RE.C.E.), 16(2), pp. 123–129. 2025. DOI: https://doi.org/10.15866/irece.v16i2.25443

[10] [10] Al Zwainy, F.M., and Al Marsomi, M.S.K., Structural equation modeling of critical success factors in the programs of development regional. Journal of Project Management, 8(2), pp. 119–132. 2023. DOI: https://doi.org/10.5267/j.jpm.2022.11.002

[11] Al Zwainy, F.M., Eiada, A.A., and Khaleel, T.A., Application intelligent predicting technologies in construction productivity. American. Journal of Engineering and Technology Management, 1(3), pp. 39–48. 2016. DOI: https://doi.org/10.11648/j.ajetm.20160103.13

[12] Shalev Shwartz, S., Singer, Y., and Srebro, N., Pegasos: Primal Estimated sub Gradient Solver for SVM. Mathematical Programming, 127(1), pp. 3–30. 2011. DOI: https://doi.org/10.1007/s10107-010-0420-4

[13] Zamim, S. K., Faraj, N. S., Aidan, I. A., Al Zwainy, F. M. S., AbdulQader, M. A., and Mohammed, I.A., Prediction of dust storms in construction projects using intelligent artificial neural network technology. Periodicals of Engineering and Natural Sciences (PEN), 7(4), pp. 1659–1666. 2019. DOI: https://doi.org/10.21533/pen.v7i4.857

[14] Hussein, S.G.H., and Al Zwainy, F.M.S., Diagnosing and identifying standards affecting on the ready-mix concrete production plants performance: An analytical study. Tikrit Journal of Engineering Sciences, 31(1), pp. 211–222. 2024. DOI: https://doi.org/10.25130/tjes.31.1.18

[15] Jaber, F.K., Jasim, N.A., and Al Zwainy, F.M.S., Forecasting techniques in construction industry: earned value indicators and performance models. Scientific Review Engineering and Environmental Sciences (Przegląd Naukowy – Inżynieria i Kształtowanie Środowiska), 29(2), pp. 234–243. 2020. DOI: https://doi.org/10.22630/PNIKS.2020.29.2.20

[16] Cheng, M.Y., Cao, M.T., and Jaya Mendrofa, A.Y.J., Dynamic feature selection for accurately predicting construction productivity using symbiotic organisms search optimized least square support vector machine. Journal of Building Engineering, 35, Art. 101973, 2021. DOI: https://doi.org/10.1016/j.jobe.2020.101973

[17] Famouri, M., Taheri, M., and Azimifar, Z., Fast Linear SVM validation based on early stopping in iterative learning. International Journal of Pattern Recognition and Artificial Intelligence, 29(8), Art. 1551013. 2015. DOI: https://doi.org/10.1142/S0218001415510131

[18] Hammoody, O., Al Somaydaii, J.A., Al Zwainy, F.M., and Hayder, G., Forecasting and determining of cost performance index of tunnels projects using artificial neural networks. International Journal for Computational Civil and Structural Engineering, 18(1), pp. 51–60. 2022. DOI: https://doi.org/10.22337/2587-9618-2022-18-1-51-60

[19] Jasim, N.A., Aljumaily, H.S., Varouqa, I.F., and Al Zwainy, F.M.S., Building information modeling and building knowledge modeling in project management. Computer Assisted Methods in Engineering and Science, 28(1), pp. 3–16. 2020. DOI: https://doi.org/10.24423/cames.302

[20] Karataş, İ., and Budak, A., Calculation of the productivity of construction gypsum plaster worker using support vector machine algorithm. Journal of Construction Engineering Management and Innovation, 7(4), pp. 281–290. 2024. DOI: https://doi.org/10.31462/jcemi.2024.04281290

[21] Keerthi, S.S., and Lin, C.J., Asymptotic behaviors of support vector machines with gaussian kernel. Neural Computation, 15(7), pp. 1667–1689. 2003. DOI: https://doi.org/10.1162/089976603321891855

[22] Shalev Shwartz, S., Singer, Y., and Srebro, N., Pegasos: primal estimated sub gradient solver for SVM. Mathematical Programming, 127(1), pp. 3–30. 2011. DOI: https://doi.org/10.1007/s10107-010-0420-4

[23] Petruseva, S., Sherrod, P., Pancovska, V.Z., and Petrovski, A., Predicting bidding price in construction using support vector machine. TEM Journal, 5(2), pp. 143–151. 2016. DOI: https://doi.org/10.18421/TEM52-04

[24] Wauters, M., and Vanhoucke, M., Support vector machine regression for project control forecasting. Automation in Construction, 47, pp. 92–106. 2014. DOI: https://doi.org/10.1016/j.autcon.2014.07.014

[25] Racchumi, V.J., Rosales Huamani, J.A., and Castillo Sequera, J.L., Construction of a predictive model of shovel productivity applying machine learning algorithms. Earth Science Informatics, 18(1), pp. 1–17. 2025. DOI: https://doi.org/10.1007/s12145-024-01563-5

[26] Aldhamad, S.H.R., Maya, R., Alazawy, S.F.M., and Alzwainy, F.M., Forecasting models for time and cost performance predicting of infrastructural projects. Civil and Environmental Engineering, 20(2), pp. 1024–1039. 2024. DOI: https://doi.org/10.2478/cee-2024-0074

[27] Varouqa, I.F., Zaki, R.I.K., Al Zwainy, F.M.S., Al Marsomi, M.S.K., and Obaid, A.H., Unveiling Critical Success Factors for Program Management in the Construction Industry. International Journal of Innovative Research and Scientific Studies, 8(2), pp. 3985–3992. 2025. DOI: https://doi.org/10.53894/ijirss.v8i2.6197

[28] Al-khazrajy, M.G.S., Al-Zwainy, F.M.S., Obaid, A.H., Sobaih, A.E.E., Elshaer, I.A., Harnessing Artificial Neural Networks for Predictive KPI Insights in Infrastructure Projects. In: García-Márquez, F.P.,

Hameed, A.A., Jamil, A., (eds) Pattern Recognition and Artificial Intelligence. Lecture Notes in Networks and Systems, 1393. Springer, Cham. 2025. DOI: https://doi.org/10.1007/978-3-031-90893-4_52

[29] Al-khazrajy, M.G.S., Al-Zwainy, F.M., Mohamed, S., and Hayder, G., (2025). Evaluation of bridge projects in iraq using international performance evaluation standards (USAID). Al-Nahrain Journal for Engineering Sciences, 28(3), pp. 469-480. , "Evaluation of Bridge Projects in Iraq Using International Performance Evaluation Standards (USAID)", NJES, 28(3), pp. 469–480, 2025. DOI https://doi.org/10.29194/NJES.28030469.

[30] Al-Dhamad, S.H.R., Kurwi, S.I.B., Varouqa, I.F., Hayder, G., Obaid, A., H., and Al-Zwainy, F.M. 2025. Optimizing project management: planning, scheduling, and cost estimation using microsoft project. Journal of Applied Science, Engineering, Technology, and Education, 7(2), pp. 349-356. 2025.

L.N. Ali, is a researcher in Civil Engineering and Construction Management. He currently works at the Ministry of Higher Education and Scientific Research in Baghdad, Iraq. His research interests focus on the modernization of the construction sector through digital transformation, specifically in the areas of Building Information Modeling (BIM), digital modeling applications in project management, and the development of performance forecasting models for infrastructure projects. He has co-authored several technical papers in international peer-reviewed journals.
ORCID:0009-0000-5347-8751

S.H.R. Aldhamad, received her PhD from the Baghdad University (Iraq) in 2022. She is currently a faculty member at the Department of Civil Engineering, College of Engineering, Al-Iraqia University, Baghdad, Iraq. Her research interests focus on the integration of advanced technologies in the construction industry, including Building Information Modeling (BIM), digital modeling applications in project management, and the development of performance forecasting models. She has co-authored several technical papers in international peer-reviewed journals.
ORCID:0009-0001-8533-0716

F.M.S. Al-Zwainy, Prof. Dr. Faiq M. S. Al-Zwainy is an accomplished Civil Engineer specializing in Construction Engineering and Management, with a strong focus on Artificial Intelligence (AI) in Construction sector. He has an extensive background in research and development, evidenced by his numerous published articles, authored books, and multiple patents that reflect his contributions to advancing construction technology. Prof. Dr. Faiq M. S. Al-Zwainy also serves as a reviewer for several prominent international journals, helping to shape the field through his insights and expertise. Prof. Al-Zwainy is a Distinguished Research Professor of Forensic Engineering Departemt in Higher Institute of Forensic Sciences in Al-Nahrain University, Iraq, where, he earned B.Sc. in Civil Engineering from Mustansiriyah University, Iraq, 1996. He earned his MSc in Project Management from the Mustansiriyah University, 2000, and a PhD in Project Management from the Baghdad University (BU), 2009.
ORCID: 0000-0002-9948-6594

R.I.K. Zaki, received the BSc. and M.Sc. degrees in Civil Engineering from Al-Nahrain University, Iraq, in 2001 and 2004, respectively. Between 2006 and 2023, she held several academic and technical positions at Al-Nahrain University's Engineering Department and College of Engineering. She currently serves as a faculty member at the Higher Institute of Forensic Sciences. Her research focuses on structural engineering, the behavior of post-tensioned concrete, and the application of artificial intelligence and digital modeling in construction management and structural performance.
ORCID:0000-0002-3746-1172

I.F. Varouqa, is a researcher specializing in Civil Engineering and Construction Management. He currently serves at the Ministry of Public Works and Housing in Amman, Jordan. His research work focuses on the integration of digital technologies to enhance project performance and management. His research interests include Building Information Modeling (BIM), digital modeling applications in the construction sector, and the development of forecasting models for project performance. He has co-authored several technical papers in international peer-reviewed journals, contributing to the advancement of digital practices in the AEC industry.
ORCID:0009-0003-7617-4242

S.D.S. Al-Dulaimi , is a researcher and academic in the field of Civil Engineering and Construction Management. He currently serves at the Ministry of Higher Education and Scientific Research in Baghdad, Iraq. His academic profile reflects a strong commitment to enhancing project performance in the AEC industry. His research interests focus on Building Information Modeling (BIM), project management, digital modeling, and the development of forecasting models for construction project performance. He has several high-impact publications indexed in Scopus, reflecting his contributions to modernizing engineering management through digital transformation and advanced analytics.
ORCID:0000-0001-8758-5280

A.H. Obaid is a researcher specializing in Physical Education and Sports Sciences. She obtained her Bachelor's degree in 1996, Master's degree in 2009, and PhD in 2021 from the College of Physical Education and Sports Sciences, University of Baghdad. She is currently working at the Iraqi Ministry of Education, General Directorate of Education of Baghdad / Al-Rusafa Second, as a Specialized Educational Supervisor. Her research interests focus on physical education in schools, educational supervision and evaluation, performance development, and the application of modern technologies and artificial intelligence in educational and sports fields.
ORCID: 0000-0002-9948-6594

M.M. Sarhan, received the BSc. Eng in Civil Engineering from the Mustansiriyah University (Iraq) in 2006, the MSc. Eng in Civil Engineering from the Mustansiriyah University (Iraq) in 2009, and PhD from Wollongong University (Australia) in 2019. He is an inventor and got his patent in engineering field from Australia. He teaches courses for undergraduate programs in the fields of civil engineering.
ORCID: 0000-0003-2190-0342

A. P.C. Chan, received his MSc degree in Construction Management and Economics from the University of Aston in Birmingham and his PhD in Project Management from the University of South Australia. He is currently a Distinguished Research Professor at the Hong Kong Polytechnic University (PolyU), where he has held several key leadership roles, including Dean of Students and Head of the Department of Building and Real Estate. His research interests encompass project management and success, construction procurement, public-private partnerships (PPP), and construction health and safety. Prof. Chan is recognized globally as a leading scholar, ranked among the Top 2% of scientists worldwide, with significant contributions to construction policy and digital transformation in the AEC industry. ORCID:0000-0002-4853-6440

R.A. Maya, is a Professor of Construction Engineering and Management at Tishreen University, Lattakia, Syria. She has extensive academic and professional expertise in civil engineering, with a particular focus on the integration of modern technologies in the AEC (Architecture, Engineering, and Construction) industry. Her research interests include: Building Information Modeling (BIM) and its implementation strategies; project management and sustainability in bridge and infrastructure projects; risk analysis and quality management systems (ISO standards); and the application of Artificial Neural Networks (ANN) in predicting project performance. Prof. Maya has authored numerous peer-reviewed articles in high-impact international journals and contributes actively to the development of engineering education curricula.
ORCID:0000-0002-7721-9057

G. Hayder, received his Ph.D. in Civil Engineering (Water Resources) from Universiti Teknologi PETRONAS (UTP), Malaysia. He is currently an Associate Professor at the Department of Civil Engineering, College of Engineering, Universiti Tenaga Nasional (UNITEN), Malaysia. With extensive experience in both academia and consultancy, he has held several academic positions and contributed to numerous international research projects. His research interests focus on water and wastewater treatment, sustainable water resources management, environmental engineering, and the application of advanced modeling techniques in hydraulic engineering. He is a member of several professional engineering bodies and has published extensively in high-impact international journals.
ORCID:0000-0002-4853-6440

DYNA
http://dyna.medellin.unal.edu.co/

UNIVERSIDAD NACIONAL DE COLOMBIA

Study of the variability of physicochemical parameters in different fractions of corn and espartillo intended for the production of solid biofuels

Luciana Belmonte, Agostina Quicchi, Adela Farías & Mariana Bernard✉

CIDEME - Universidad Tecnológica Nacional - Facultad Regional San Francisco, San Francisco, Córdoba, Argentina.
lbelmonte@facultad.sanfrancisco.utn.edu.ar, aquicchi@facultad.sanfrancisco.utn.edu.ar, fariasadela41@gmail.com, mbernard@facultad.sanfrancisco.utn.edu.ar

Received: November 4th, 2025. Received in revised form: January 5th, 2026. Accepted: January 16th, 2026.

Abstract
The current context of the energy transition is driving the development of alternative fuels, such as lignocellulosic materials of agricultural origin. This study analyzed the variation in physicochemical parameters in fractions of espartillo (E) and corn stover (RM) according to particle size. It was observed that reducing the particle size in RM increased the ash and extractive content, while E only showed an increase in ash. Pure materials and hybrid mixtures of E/RM 1:1 and 1:3 were evaluated in combustion. The 1:1 mixture reached a higher combustion temperature, exhibited a longer flame duration, and had an optimized heating value, although it had a higher ash content that could be reduced by removing particles smaller than 149 µm. The results obtained demonstrate that E and RM are viable alternatives as solid biofuels through synergistic mixtures and granulometric control, favoring the revaluation of agricultural waste and naturally growing species in the region for energy purposes.

Keywords: corn stover; espartillo; physicochemical characterization; solid biofuels; combustibility.

Estudio de variabilidad de parámetros fisicoquímicos en diversas fracciones de maíz y espartillo destinadas a la generación de biocombustibles sólidos

Resumen
El contexto actual de transición energética impulsa el desarrollo de combustibles alternativos, como los basados en materiales lignocelulósicos de origen agrícola. Este estudio analizó la variación de parámetros fisicoquímicos en fracciones de espartillo (E) y rastrojo de maíz (RM) según granulometría. Se observó que al reducir el tamaño de partícula en RM aumenta el contenido de cenizas y extraíbles, mientras que E solo presentó incremento de cenizas. En la combustión se evaluaron materiales puros y mezclas híbridas E/RM 1:1 y 1:3. La mezcla 1:1 alcanzó una temperatura de combustión superior, mayor duración de llama y poder calorífico optimizado, aunque presentó mayor contenido de cenizas que podría reducirse eliminando las partículas menores a 149 µm. Los resultados obtenidos demuestran que E y RM son alternativas viables como biocombustibles sólidos mediante mezclas sinérgicas y control granulométrico, favoreciendo la revalorización de residuos agrícolas y especies de crecimiento natural de la región para aprovechamiento energético.

Palabras clave: rastrojo de maíz; espartillo; caracterización fisicoquímica; biocombustibles sólidos; combustibilidad.

1 Introduction

The growing need to reduce fossil fuel consumption and diversify energy sources has driven the development of renewable alternatives, including biomass. In this context, the native species espartillo (*Spartina argentinensis*) and the traditional crop corn (*Zea mays*) exhibit suitable properties for producing densified solid biofuels. Espartillo is a perennial

How to cite: Belmonte, L., Quicchi, A., Farías, A., and Bernard, M., Study of the variability of physicochemical parameters in different fractions of corn and espartillo intended for the production of solid biofuels DYNA, (93)240, pp. 89-96, January - March, 2026.

grass belonging to the *Poaceae* family. This species is mainly found in northeastern Argentina and is notable for its resistance to saline soils and water stress, which gives it high potential for adaptation in marginal regions suitable for energy generation [1]. Espartillo covers more than 2 million ha in the province of Santa Fe, Argentina. As it is a natural grassland, accurate quantification of usable biomass on a national scale requires the use of advanced estimation and monitoring technologies [2] Corn is widely cultivated in the central region of Argentina; however, its cultivation is expanding into colder areas such as northern Patagonia and the Calchaquíes Valleys. Corn is characterized not only by its contribution to food production, but also by its role as an energy crop in bioethanol generation, which produces a considerable volume of residual lignocellulosic stover [3]. Corn stover is typically left on the field surface to serve as organic amendment and to prevent soil erosion. Although this practice is generally recommended, in certain locations with low temperatures, stover decomposition slows down, forming a moist layer that creates favorable conditions for the proliferation of fungi harmful to subsequent crops [4]. These issues, along with the need for pest control, could increase the occurrence of improper practices such as the burning of crop residues [5]. In this context, it is crucial to determine the quantity of corn stover that can be utilized for energy production without compromising soil quality. During the 2024/25 season, Argentina produced around 49 million t of grain. Considering a stover/grain ratio close to 1:1 on a dry basis, the total residual biomass is estimated to be of a similar magnitude. Of this total, around 25 % is used for silage, and of the remainder, between 15 % and 40 % could potentially be used for energy generation without impacting soil functions [6]. Consequently, 5.50–14.40 million t of residual biomass could potentially be used, in accordance with values reported in the literature [7,8]. Both espartillo (E) and corn stover (RM) exhibit physicochemical characteristics that make them suitable raw materials for use as solid biofuels through densification processes (pellets or briquettes). The use of such densified fuel represents an efficient energy alternative for households and industries, due to its storage capacity, low environmental impact and easy transportation. At the same time, it allows for the utilization of resources from marginal soils and the proper disposal of crop residues, thereby promoting the incorporation of these assets into the circular economy.

The production of densified fuels is a process that is still developing in Argentina and has not yet reached its maximum industrial potential. To foster growth, it is essential to understand the quality and energy potential as residual biomass, their combustion behavior, and ways to enhance their performance as fuel. This is why analyzing the interaction between the physical and chemical parameters of the pellet with the combustion process and its residues is important. Therefore, proper characterization of lignocellulosic crops is fundamental for developing an energy-appropriate fuel.

The development of a solid biofuel is influenced by various factors, including crop moisture content. This content can have a significant impact on the densification process, which can lead to higher costs in pellet production [9]. Ash content is another critical factor, as it interferes with combustion quality by reducing the heating value (HV) of the fuel and, when present in large quantities, decreases system efficiency, causing emissions, increasing equipment wear, and causing fouling. This is especially important when pellets are used for combustion in industrial systems because accumulation in tube banks and boiler walls reduces heat transfer and causes maintenance problems [10]. Lignin is a key factor in the palletization process. At high temperatures and pressures, lignin reaches its glass transition temperature, promoting internal particle cohesion and improving the mechanical strength of the pellet without the need for external additives.

Lignin is characterized by its high thermal stability and carbon content, making it more suitable for energy applications due to its higher carbon yield and HV. However, this process often generates large amounts of char and tar. By contrast, hemicellulose has lower thermal stability, contains more oxygen, and undergoes rapid degradation at high temperatures, which reduces its energy yield [11]. Fixed carbon is essential for maintaining energy quality, enabling more stable and prolonged combustion, whereas volatile compounds facilitate rapid but brief ignition [12]. For this reason, biomass materials with high lignin content are preferred the production of efficient solid biofuels [13,14]. There is also evidence linking the extractive content of products to the measured higher heating value (HHV). This suggests that a high extractive content positively affects the combustion process [15] by accelerating pellet flammability [16]. Particle size affects the physical quality of the pellet as well as the energy required for compaction. It affects the total surface area, pore size, and number of interparticle contacts, all of which are essential for achieving product cohesion and durability [17]. Similarly, the size and distribution of particles in the mixture can affect the chemical reactivity of biomass, improving kinetics and flame propagation during combustion. This is particularly important as it enhances heat transfer in solid fuels [18]. Whittaker & Shield [13] recommend using a mixture of particle sizes, as the finer particles fill the gaps left by the larger ones, promoting compaction. This increases pellet's strength and resistance and internal cohesion, but also increases friction during palletization, impacting energy consumption. Thus, an optimal combination of particle sizes guarantees the structural integrity of the pellet obtained, reducing the production of fines during handling and transport. From an energy standpoint, grinding and separation of the raw material are key processes for ensuring both overall performance and the quality of the final product [19].

This study aims to characterize the physicochemical parameters of the E and RM fractions obtained from crushing and screening in a pilot-scale solid fuel production process, to evaluate their performance during densification and subsequent combustion. This integrated assessment seeks to determine the overall energy potential and viability of these agricultural wastes as sustainable solid fuel feedstocks, and to examine whether the composition of the different fractions exhibits significant differences in key physicochemical properties. By identifying which fractions are equally viable or necessary for efficient energy generation, the study provides a comprehensive understanding of the role of each component in the production

and combustion processes, thus contributing to the development of efficient and sustainable alternatives for industrial-scale energy generation.

2 Methodology

E was obtained from natural esparto grass cut in the La Francia region, while RM was obtained from harvest residue deposited on the ground in El Tío, near the esparto grass fields. Both locations are situated in the central-eastern part of the province of Córdoba, Argentina. The collected materials were then washed in running drinking water to remove solid contaminants that could be carried over from the harvesting process. The materials were subsequently dried in a fluid bed flash dryer (SR-HGJ 400, Zhengzhou Share Machinery Co.) to reduce moisture content and enable storage.

The conditioned waste was ground in a blade mill (CID 75, 1.5 hp) with a 3 mm mesh outlet and then sieved to separate the particles using a series of 20, 35, and 100 mesh (Tyler) sieves. Based on this procedure, the particle size fractions used throughout the study were defined in Table 1.

The ash content (ASTM 1102), moisture content (ASTM E 871-82), volatile matter (ASTM E 872), and fixed carbon (FC) were determined in the various fractions obtained, with FC being calculated as the difference between the previous values. In turn, the bulk density of the fractions (ISO 17828:2015), extractive matter content (TAPPI T 204 cm 97), and insoluble lignin by Klason method (TAPPI 222:om-21) were determined.

Several authors have developed equations correlating HHV determined by bomb calorimetry, with the structural components of biomass. Among them, Demirbas [15] reported that, in non-woody species, HHV correlates with lignin (*Lg*) content while also noting that the extractives (*Ex*) index exerts a positive influence in both woody and non-woody species. Based on the work of Demirbas and other authors, Telmo [20] suggests that the most accurate correlation is obtained by considering both extractives and lignin, as this better reflects the HHV measured in wood species with high *Ex* content (Equation 1; R = 0.915).

$$HHV\left[\frac{MJ}{kg}\right] = 14.3377 + 0.1228(Lg) + 0.1353(Ex) \quad (1)$$

Non-woody species such as E and RM tend to exhibit high *Ex* content; therefore, although Telmo's equation was originally formulated for wood, it is considered suitable for the theoretical estimation of HHV in this work. It should be emphasized that HHV values tend to be highly variable due to the edaphological conditions of the samples. While this makes the values useful for the comparative analysis conducted here, they cannot be extrapolated directly to other sampling contexts.

Table 1.
Definition of particle size fractions used in this study

	>841 µm	841-500 µm	500-149 µm	<149 µm
Espartillo	E_1	E_2	E_3	E_4
Corn stover	RM_1	RM_2	RM_3	RM_4

Source: Own elaboration

Combustion tests were also carried out using a methodology adapted from Dula *et al*. [21], as there are no specific regulations for the combustion of pellets in open grills. The objective of this test was to record the flame time, the characteristics of the process, and the duration of combustion. For this purpose, a fixed-bed grill was employed, supported in a glass-covered, closed gas extraction hood with natural convection air circulation. In order to prevent material loss, combustion residues were meticulously collected in an ash pan positioned below the grill. Ignition was performed manually using a minimal amount of ignition material (0.2 mL of 96 % ethyl alcohol, PORTA). In the experimental setting, comparable quantities of densified pellets of E, RM, and mixtures in E/RM ratios of 1:1 and 1:3 were combusted during the test. The pellets were constructed from material ground before fraction separation, and their densification was achieved through manual compacting using a 15 kN press. The thermochemical process was recorded in two stages: I) Ignition and combustion: this phase begins when a spark is generated and a visible flame is sustained and ends when the flame is extinguished; II) Post-combustion: commences when the flame is no longer visible and continues until the material ceases to emit smoke. The time for each stage was measured, with t_1 representing the time for the first stage and t_2 representing the total time for both stages.

Furthermore, an observational study of the residues was conducted, and the percentage of mass loss for each fuel was determined. The experiment was recorded using stopwatches and a thermal imaging camera (Fluke Ti 105).

3 Results

3.1 Fractionation and physicochemical evaluation

Fig. 1 shows the E and RM crops before and after the chopping process. Table 2 shows the results of the physicochemical characterization obtained for the different fractions of E and RM. These results were obtained by taking the average of analytical measurements made in triplicate.

Figure 1. Materials before and after grinding, a) E; b) RM.
Source: Own elaboration.

Table 2.
Physicochemical parameters of RM and E fractions.

	Moisture (%; n=3) [1]	Ash $_{DB}$ (%; n=3) [1]	Volatiles $_{DB}$ (%; n=3) [1]	Fixed Carbon $_{DB}$ (%; n=3) [1]	Extractives (%; n=3) [1]	Lignin (%; n=3) [1]	Bulk density (kg/m^3; n=3) [1]	HHV[2] (MJ/kg; n=3) [1]
E1	7.76 ± 0.39	5.49 ± 0.42	79.19 ± 1.88	15.32 ± 1.67	14.05 ± 0.25	23.15 ± 0.79	165.94 ± 3.18	19.08 ± 0.06
E2	9.81 ± 0.16	10.22 ± 0.17	73.19 ± 1.33	16.59 ± 1.50	7.37 ± 0.28	25.53 ± 0.32	239.38 ± 1.91	18.47 ± 0.04
E3	9.61 ± 0.25	10.35 ± 0.13	71.99 ± 1.07	17.66 ± 1.48	8.37 ± 0.63	24.96 ± 0.24	285.00 ± 1.27	18.54 ± 0.07
E4	9.49 ± 0.12	21.86 ± 0.14	65.97 ± 2.45	12.17 ± 2.58	14.89 ± 0.22	25.60 ± 0.35	302.82 ± 2.23	19.50 ± 0.04
RM1	7.62 ± 0.48	3.57 ± 0.31	88.65 ± 2.56	7.78 ± 2.29	10.57 ± 0.80	6.04 ± 0.12	104.00 ± 4.04	16.51 ± 0.10
RM2	6.64 ± 0.12	5.18 ± 0.05	87.32 ± 1.78	7.50 ± 1.79	14.33 ± 0.61	6.93 ± 0.37	121.23 ± 6.56	17.13 ± 0.13
RM3	8.58 ± 0.18	8.50 ± 0.78	81.80 ± 2.63	9.70 ± 2.90	16.26 ± 0.65	7.05 ± 0.17	124.31 ± 3.48	17.40 ± 0.09
RM4	7.53 ± 0.78	17.02 ± 0.59	74.20 ± 2.10	8.78 ± 2.59	21.83 ± 0.86	6.88 ± 0.30	257.08 ± 6.42	18.14 ± 0.13

Source: Own elaboration
[1] Mean ± standard deviation
[2] HHV obtained from equation 1

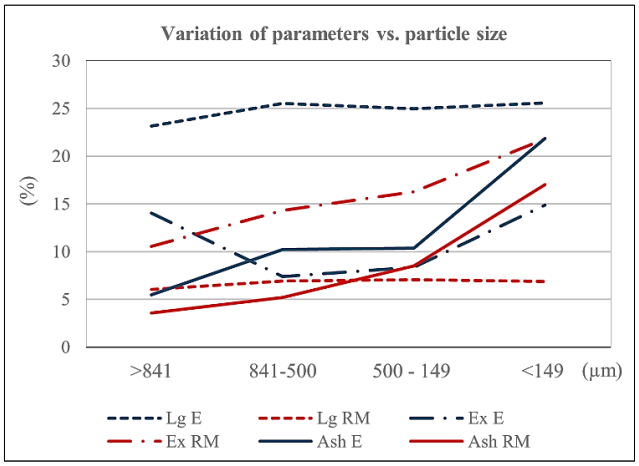

Figure 2. Variation of physicochemical parameters asparticle size decreases. Source: Own elaboration.

As demonstrated in Table 2, the moisture values for all fractions of each material analyzed were found to be similar. *Ex* are secondary non-structural components of plants, which are usually soluble in various polar solvents. These are predominantly located in the plant's parenchyma, though they can also be found in vessels, fibers, or specialized cells [22]. The composition and distribution of the subject are dependent on a number of factors, including the species, age, health status, and the environmental conditions during the growth period. Li *et al*. [23] investigated the chemical composition of the leaves, pith, and bark of the stem separately. They found that the content of *Ex* soluble in benzene-alcohol was higher in the pith region than in the bark, while *Ex* in water was similar in the pith and leaves, and higher than in the bark. Furthermore, it was observed that the disparities in morphology are a consequence of a specific chemical composition, determined by the levels of lignin, cellulose and hemicellulose, where the stem exhibits a slightly higher level of lignin in comparison to the other structures. In relation to this, and as illustrated in Table 2, an inverse relationship is evident between the *Ex* content in RM and particle size. This trend is less pronounced in E. Therefore, it can be inferred that, due to the morphological differentiation of the fractions, they exhibit different responses to the shear effect of grinding. Consequently, depending on the species, fractions with a higher concentration of certain morphological structures would be obtained, which could be reflected in a higher proportion of *Ex* or *Lg*. As a result, it could be assumed that the spongier structures of the stem pith, rich in hemicellulose, can achieve a smaller particle diameter during grinding, thus exposing their larger surface area to the extraction of organic compounds; this effect is compounded by the higher concentration of *Ex* in the pith region [23]. This is consistent with the incremental extractive content observed as particle size decreases, mainly in RM, which also coincides with the findings of Ottone & Baldwin [24] on yellow poplar sawdust particles and with Miranda *et al*. [25] when analyzing the link between *Ex* and particle size in sawdust from various pine species. This trend is less pronounced in E, possibly because the morphological variation in the hollow stem structure of this species is less than in RM. Thus, the variation in the composition of the fractions may influence the compaction effect, since *Ex* includes waxes, resins, and phenolic compounds that could act as lubricants in the matrix. This lubricating effect reduces mechanical friction and material jams during the production process, therefore reducing energy consumption. However, it also decreases the mechanical properties of the pellets obtained [26]. In turn, the *Lg* content does not show significant variation depending on particle size. Nevertheless, the contribution of both *Lg* and *Ex* content to HHV causes it to vary slightly in RM as particle size decreases, and it remains relatively stable in the E fractions. Fig. 2 shows how the relationships between the variables change as the particle size in the fraction decreases.

The bulk density of the fractions, which is defined as the mass per unit volume, takes into account the empty spaces between particles and internal porosity. It varies depending on the size, shape, particle size distribution and porosity of the particles, which can be influenced by the duration, technology and grinding conditions. Additionally, internal porosity is related not only to the morphology of the species, but also to growth conditions, which can modify pore distribution and closure [27,28]. These factors impact the mechanical, physical and thermal properties of densified lignocellulosic materials. It is well known that the compaction of spongy particles, such as those of RM, is complex [29,30]. Thus, the production of hybrid biofuels can improve processing and combustion characteristics [31]. As

Table 3.
Combustion test results

	t_1 (s)	t_2 (s)	Average flame temperature* (°C)	Volatiles (%)	Solid combustion waste (%)	Ash (%)	Extractives (%)	Lignin (%)	Observations
E	45	320	152.3	72,58	21,14	11,98	11,17	24,81	Incomplete combustion. Sintering and dark ashes. Lights quickly, struggles to keep the flame alive, tries to go out, even though it stays lit and smokes.
RM	55	195	183.2	82,99	8,40	8,57	15,75	6,73	Complete combustion, lighter ashes. Larger flame than E. Tends to go out but remains lit and smoldering.
1:1	90	150	275.0	77,79	13,66	10,28	13,46	15,77	Complete combustion. The flame lasts longer and is larger, with a lot of smoke.
1:3	80	130	186.9	80,39	11,12	9,42	14,60	11,25	Complete combustion. Flame similar to 1:1, combustion with a lot of smoke.

* The average flame temperature was obtained using SmartView® 3.5.31.0 software (Fluke Corporation), based on the analysis of the temperatures across the entire surface of the fuel captured by the thermal imaging camera.
Source: Own elaboration.

shown in Table 2, the reduction in particle size enables fine particles to fill the spaces between larger particles, thereby increasing the apparent density. This is expected to enhance adhesion and compaction during the pelletization process.

Regarding ash content, it is notable that it increases significantly in both species as the particle size of the fractions decreases (Table 2). It is well known that ash content in fuels is linked to problems during combustion, as the high temperatures reached can melt the ash and cause overheating and slag accumulation on the walls of boilers and burners [10]. In turn, the generation of fine particles during pellet handling can cause faster combustion that achieves higher temperatures, thus accelerating the melting of ash [13].

From a solid fuel processing perspective, incorporating fine particles into the mixture helps to mechanically stabilize the resulting pellet. Located on the free surface between coarse particles, these particles increase the density of the product, minimize pores and improve adhesion and cohesion mechanisms, thereby increasing durability [19,32]. However, according to the results obtained, a significant percentage of ash is added through this same incorporation of small particles when the particle size is between 35 and 100 mesh for both materials. In both E and RM, the ash content approximately quadruples when the particle size is reduced, but half of this increase occurs when the particle size is further reduced below 149 µm. The highest percentage of *Ex* is also observed in this fraction. The exclusion of particles that pass through the #100 mesh in both products would result in a mixture that still contains small particles. These particles improve the mechanical performance of the pellet, while substantially reducing fuel ash generation and exhibiting a lower *Ex* content. The latter could potentially hinder the compaction process, but it would also enhance pellet stability and HHV development by enabling a higher proportion of fractions with high *Lg* content. These combinations must then be considered in terms of the available materials and critical production parameters, with the aim of achieving a balance between production efficiency, pellet quality and combustion performance.

3.2 Combustion

Tests were carried out on the various combinations of raw materials to establish the combustion properties of compacted pellets of E, RM, and combinations thereof. The results obtained in this test are shown in Table 3.

As shown in Table 3, pure densified E has a shorter flame time (t_1) and a longer total combustion time (t_2) compared to RM, the latter of which includes both the flame time and the post-combustion time. Both materials tend to have low active flame capacity and burn internally with excessive smoke release. However, E exhibits sintered residual material and a higher percentage of residue after combustion. In the case of RM, the residue obtained is light grey, powdery and proportionally similar to the ash content of the original fuel. When combustion is analyzed in hybrid E and RM pellets, higher t_1 values are obtained compared to pure fuels, although lower t_2 values are obtained. Fig. 3 illustrates the relationship between the combustion times of the different fuel samples, while Fig. 4 shows the variability of the physicochemical parameters of the evaluated fuels.

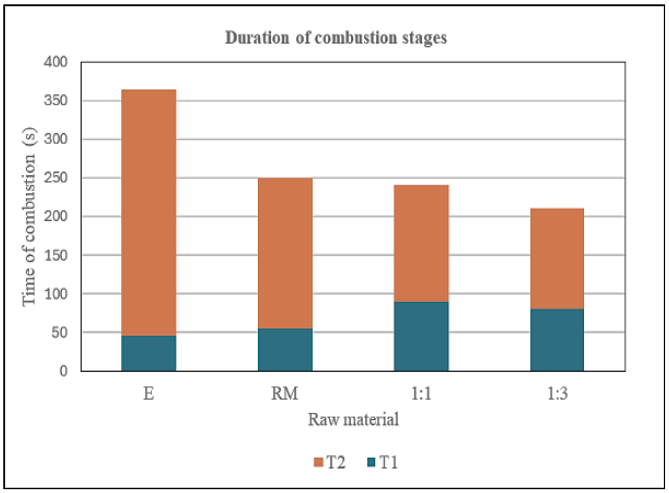

Figure 3. Combustion times for densified solid fuels
Source: Own elaboration.

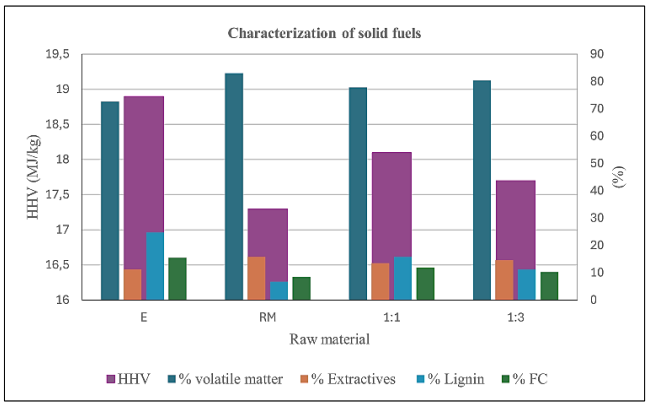

Figure 4. Relationship between physicochemical parameters in solid fuels
Source: Own elaboration.

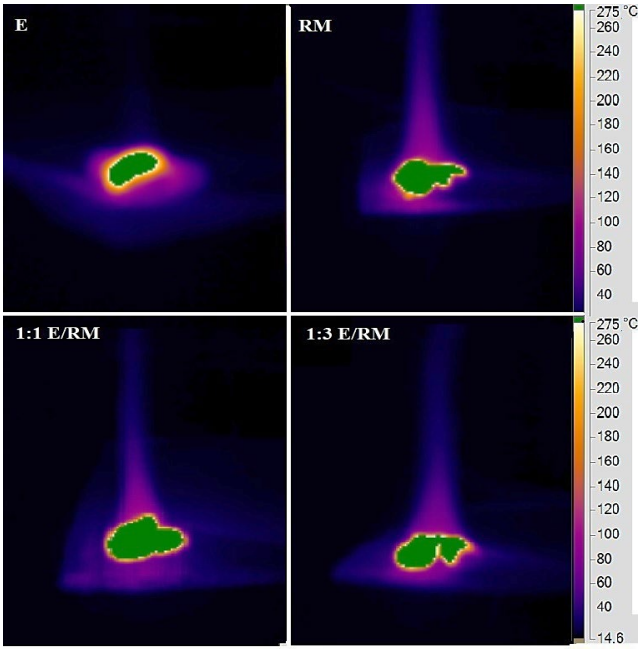

Figure 5. Thermographic images taken during stage I of combustion.
Source: Prepared by the authors.

As shown in Table 3 and illustrated in Figs. 3 and 4, the lower t_1 exhibited by E is consistent with its lower volatile and *Ex* content. However, its high *Lg* and FC concentrations favor prolonged combustion over time. In contrast, RM exhibits a higher t_1 due to its higher percentage of volatiles and *Ex* than that of E. However, its low *Lg* and FC content limits the total duration of the combustion process. This is because the content of volatile materials, which are mainly associated with hemicellulose and *Ex*, favors rapid ignition and lower starting temperatures. However, although these components generate intense combustion, it is short-lived due to their rapid consumption [12].

Likewise, mixtures of E and RM in different proportions exhibit synergistic behavior during the combustion phases, as evidenced by an increase in visible flame time (t_1) that is even greater than that of pure materials. This phenomenon can be attributed to the relative increase in volatiles and *Ex* from the RM, but it also suggests the existence of a complementary effect between particles of different natures present in E and RM. Thus, it can be assumed that greater particle cohesion, favored by diverse sizes, compositions and morphologies, improves heat transfer within the fuel. This allows for higher temperatures to be reached, based on an appropriate balance between generating an active flame easily and sustaining combustion over time. Better ignition of the material in the mixtures, as evidenced by an increase in t_1, is crucial for combustion and energy generation, with holocellulose and *Ex* demonstrating greater potential in this regard [12]. On the other hand, there is a notable decrease in t_2 compared to pure fuels, which seems to be a consequence of this improvement in combustion capacity during the initial stage, producing more energy and promoting faster and more efficient fuel consumption. This increase in energy is linked to the higher average temperatures reached at the point of maximum combustion; with the highest value being obtained in the E/RM 1:1 mixture. This finding is consistent with the reduction in the fraction of residue from the combustion process, which reached values similar to its ash content. Fig. 5 shows the thermographic images, providing visual evidence of the observed differences in combustion times. Pure materials display highly localized high-temperature zones; for instance, E shows a small, confined flame region, consistent with its lower t_1. In contrast, RM exhibits a more intense initial heat release, in line with its higher volatile and extractive content. The E/RM blends, however, demonstrate more uniform temperature distribution and a stable flame structure, corresponding to an increased t_1. This also accounts for the faster fuel consumption reflected in the shorter t_2 values. Overall, these thermographic patterns indicate a more efficient heat transfer and combustion process in the blends, reinforcing the synergistic behavior inferred from the combustion time analysis.

In the 1:1 mixture, the prolongation of t_2 with respect to the 1:3 ratio is linked to the higher *Lg* content, whose high carbon content and the nature of the chemical bonds between its monomers provide high thermal resistance and improve carbonization performance, resulting in a consequent increase in temperature. Due to the high energy requirements for their decomposition, lignins exhibit a low ignition rate. Consequently, the ignition of the material must be ensured by other components, while lignin ensures continuous and prolonged combustion [12]. This combination of variables appears to be more balanced in the 1:1 (E:RM) ratio, suggesting more efficient combustibility parameters compared to the 1:3 (E:RM) ratio, although with a slightly higher ash content. However, this increase in ash, which would be detrimental to combustion processes, can be mitigated by removing particle size fractions, smaller than 149 µm, from these mixtures.

The findings presented thus far indicate that a suitable combination of raw materials enhances the combustion capacity of densified solid fuels, achieving a balance between the factors that favor greater heat generation and more complete combustion. Nevertheless, when selecting the appropriate materials, certain critical factors - such as their physicochemical properties - have the potential to exert a negative influence on both the densification process and the

quality of the fuel, as well as the dynamics of combustion. Consequently, effective technical management of grinding and particle separation, founded upon the analysis of these parameters, would facilitate strategic intervention in the production process, leading to the elimination of problematic fractions and the optimization of the quality of the final product. This alternative also facilitates the incorporation of non-traditional agricultural resources such as E or RM, whose use has been limited until now, thus expanding the range of raw materials available for the production of solid fuel.

Finally, it should be mentioned that the present study employed an experimental methodology adapted for densified pellet combustion tests, with the purpose of conducting a thermal evaluation of the process through thermographic recording. Consequently, the results should be expanded through a more in-depth analysis of the combustion process, incorporating both gas and residue sampling. Thus, the comparison of these and other properties in mixtures of E and RM, with and without exclusion of the smaller fraction, will provide statistical and experimental support for the trends shown in this study. These objectives have not been incorporated into this study for two main reasons. Firstly, modification of the combustion chamber would be necessary in order to take gas samples. Secondly, these new results would lead to a second stage of analysis, already linked to the comparative production of pellets, the efficiency of the production process and its subsequent combustion. The information thus obtained would be relevant and would form part of future studies.

4 Conclusions

The need to decarbonize the energy matrix is driving the development of novel alternative fuels. Within this framework, the integration of unconventional lignocellulosic materials -particularly those of agricultural origin - poses a challenge for the production of solid biofuels. The present study examined the variation in physicochemical parameters during the fractionation of corn stover (RM) and espartillo (E), as well as the feasibility of direct combustion of pure materials (E, RM) and synergistic blends (E/RM at ratios of 1:1 and 1:3).

The findings indicate an increasing trend in extractives and ash content as particle size decreased for RM, while E exhibited a comparable upward trend in ash content under analogous conditions. Hybrid mixtures demonstrated enhanced combustion performance. From a technical standpoint, the results of this study suggest that E/RM blends at a 1:1 ratio, with particle sizes above 149 μm, represent a favorable configuration for direct combustion applications. This mixture exhibited higher mean combustion temperatures, extended flame duration, and improved HHV relative to the other formulations evaluated.

The findings of this study indicate that the incorporation of RM and E into combustion processes constitutes a viable alternative when production is designed around synergistic blending and granulometric optimization to minimize adverse effects. This strategy is oriented toward the valorization of agricultural residues from an energetic perspective, while simultaneously contributing to the diversification of energy sources in rural regions characterized by limited access to the electrical grid.

Subsequent research endeavors will encompass the exploration of additional combinations of these materials, along with the incorporation of another residual biomass. This will be undertaken to develop blends with higher HHV, with the objective of optimizing key physicochemical parameters to enhance combustion efficiency.

References

[1] Jozami, E., Di-Leo, N., Barbona, I., and Feldman S., Modelos predictivos para la estimación de biomasa de "*Spartina argentinensis*", Ciencias Agronómicas, 45(25), art. e047, 2025. DOI: https://doi.org/10.35305/agro45.e047

[2] Jozami, E., Sosa, L.L., and Feldman, S.R., *Spartina argentinensis* as feedstock for bioethanol, ATI - Appl. Technol. Innov., 9(2), pp. 37–44, 2013. DOI: https:// doi.org/10.15208/ati.2013.8

[3] García-Stepien, E.L., Variabilidad del germoplasma de Maíz (*Zea mays* L.) en Argentina: la aptitud forrajera asociada a la producción de bioetanol lignocelulósico, Phd Thesis, Universidad Nacional de la Plata, La Plata, Buenos Aires, Argentina, 2020.

[4] Montemarani, A., Sartori, M., Nesci, A., Etcheverry, M., and Barros, G., Influence of crop residues, matric potential and temperature on growth of Exserohilum turcicum an emerging maize pathogen in Argentina, Lett. Appl. Microbiol. 67, pp. 614–619, 2018. DOI: https://doi.org/10.1111/lam.13076

[5] Kumar, P., Kumar, S., and Joshi, L., The extent and management of crop stubble, springer briefs in environmental science (Ed.), Springer, Nueva Delhi. [online]. pp. 13–34, 2015. Available at: https://link.springer.com/chapter/10.1007/978-81-322-2014-5_2

[6] Idígoras, G., Prospectiva tecnológica al 2025 del complejo de semillas, Análisis tecnológicos y prospectivos sectoriales, Ministerio de Ciencia, Tecnología e Innovación Productiva, Buenos Aires, Argentina, [online]. 2016. Available at: https://www.argentina.gob.ar/sites/default/files/5._agro_atypsii_semillas.pdf

[7] Menéndez, J.E., and Hilbert, J.A., Cuantificación y uso de Biomasa de residuos de cultivos en Argentina para bioenergía, Inf. Técnicos Bioenergía, 2(4), 2013, 48P.

[8] Richmond, S.N., and Rillo, P.F., Caracterización de la dinámica de incorporación de residuos de cosecha al suelo en un sistema agrícola en siembra directa en el centro-oeste de Buenos Aires, LACS, IPNI Informaciones Agronómicas Hisp., [online]. 43, pp. 22–26, 2009. Available at: https://fertilizar.org.ar/wp-content/uploads/2009/09/22.pdf

[9] Lopez, L., Vega, L., Rendon, C., y Tobon, S., Aprovechamiento de residuos madereros, Corporación Universitaria de Remington, Medellín, Colombia, [online]. 2019. Available at: https://www.uniremington.edu.co/wp-content/uploads/libros-de-investigacion/aprovechamiento-de-residuos-madereros.pdf

[10] Granada-Álvarez, E., Febrero-Garrido, L., Eguía-Oller, P., Regueiro Pereira, A., y Patiño-Vilas, D., Análisis del "fouling" procedente de la combustión de pellet de pino y pellet de paja en una caldera de baja potencia: influencia de los parámetros de combustión, IX Congr. Nac. Ing. Termodinámica, Cartagena, Colombia, pp. 1226–1234. art. 9941, 2024. DOI: https://doi.org/10.31428/10317/9941

[11] Wang, S., Zou, C., Lou, C., Yang, H.M., and Mei-Jing, H., Effects of hemicellulose, cellulose and lignin on the ignition behaviors of biomass in a drop tube furnace, Bioresour. Technol., 310, art. 123456, 2020. DOI: https://doi.org/10.1016/j.biortech.2020.123456

[12] Vieira, T.A.S., Trugilho, P.F., Carabineiro, S.A.C., Zanuncio, A.J.V., Carvalho, A.G., and Branco-Vieira M., Impact of chemical composition on eucalyptus wood clones for sustainable energy production, Forests, 14(11), pp. 1–12, 2023. DOI: https://doi.org/10.3390/f14112240

[13] Whittaker, C., and Shield, I., Factors affecting wood, energy grass and straw pellet durability–A review, Renew. Sustain. Energy Rev. 71, pp.1–11, 2017. DOI: https://doi.org/10.1016/j.rser.2016.12.119

[14] Montenegro-Mateos, L., PhD Thesis, Determinación del riesgo de auto-combustión en almacenamiento de biomasas para la producción de gas mediante gasificación. Escuela Técnica Superior de Ingenieros de Minas y Energía, Universidad Politécnica de Madrid, España, 2014.
[15] Demirbas, A., Relationships between heating value and lignin, moisture, ash and extractive contents of biomass fuels. Energy Explor. Exploit. 20, pp. 105–111, 2002. DOI: https://doi.org/10.1260/014459802760170420
[16] Beltrón-Vinces, I.C., Palacios Bravo, H.E., y Rosero Delgado, E., Evaluación energética de biocombustibles sólidos elaborados a partir de mezclas de biomasa lignocelulósica, RIEMAT. [online]. 4, pp. 33–38, 2019. Available at: https://revistas.utm.edu.ec/index.php/Riemat/article/view/2192
[17] Kirsten, C., Lenz, V., Schröder, H., and Repke, J., The influence of particle size reduction on their physical–mechanical quality and energy demand during production, Fuel Process. Technol. 148, pp. 163–174, 2016. DOI: https://doi.org/10.1016/j.fuproc.2016.02.013
[18] Mlonka, A., Magdziarz, A., Dziok, T., and Nowak, W., Laboratory studies on the influence of biomass particle size on pyrolysis and combustion using TG-GC/MS, Fuel, 252, pp. 635–645, 2019. DOI: https://doi.org/10.1016/j.fuel.2019.04.091
[19] Correa-Méndez, F., Carrillo-Parra, A., Rutiaga-Quiñones, J.G., Márquez-Montesino, F., González-Rodríguez, H., Ybarra, E.J., and Garza-Ocañas, F., Granulometric distribution in timber byproducts for potential use in pellets and briquettes. Rev. Mex. Ciencias For. [online]. 5, pp. 52–63, 2014. Available at: https://www.scielo.org.mx/scielo.php?pid=S2007-11322014000500005&script=sci_abstract&tlng=en
[20] Telmo, C., and Lousada, J., The explained variation by lignin and extractive contents on higher heating value of wood, Biomass and Bioenergy. 35, pp. 1663–1667, 2011. DOI: https://doi.org/10.1016/j.biombioe.2010.12.038
[21] Dula, M., Kraszkiewicz, A., and Parafiniuk, S., Combustion efficiency of various forms of solid biofuels in terms of changes in the method of fuel feeding into the combustion chamber, energies, 17, pp. 1–21, 2024. DOI: https://doi.org/10.3390/en17122853
[22] Hillis, W.E., Distribution, properties and formation of some wood extractives, Wood Sci. Technol. 5, pp. 272–289, 1971. DOI: https://doi.org/10.1007/BF00365060
[23] Li, Z., Zhai, H., Zhang, Y., and Yu, L., Cell morphology and chemical characteristics of corn stover fractions, Ind. Crops Prod. 37, pp. 130–136, 2012. DOI: https://doi.org/10.1016/j.indcrop.2011.11.025
[24] Ottone, S.P., and Baldwin, R.C., The relationship of extractive content to particle size distribution in milled yellow-poplar. Wood and Fiber, [online]. 13(2) pp. 74–85, 1981. Available at: https://share.google/p5Ih9QgC5tF4Ewk4p
[25] Miranda, I., Gominho J., Mirra I., and Pereira, H., Chemical characterization of barks from picea abies and pinus sylvestris after fractioning into different particle sizes. Ind. Crops Prod. 36, pp. 395–400, 2012. DOI: https://doi.org/10.1016/j.indcrop.2011.10.035
[26] Nielsen, N.P.K., Gardner, D.J., and Felby C., Effect of extractives and storage on the pelletizing process of sawdust, Fuel. 89, pp. 94–98, 2010. DOI: https://doi.org/10.1016/j.fuel.2009.06.025
[27] Li, S.X., Huang, and R., Zheng, Xylem plasticity of root, stem, and branch in Cunninghamia lanceolata under drought stress: implications for whole-plant hydraulic integrity, Front Plant Sci, 15, Art. 1308360, 2024. https://doi.org/10.3389/fpls.2024.1308360.
[28] Sun, S., Ahmad, N., Callenius, H., Uslu, V.V., Rey, J.C., Zhao, F., and Rajab, H., "The plastid cysteine synthase complex regulates ABA biosynthesis and stomatal closure in Arabidopsis," Nat. Comun., 16(8960), Art. 3, 2025. DOI: https://doi.org/10.1038/s41467-025-64705-3.
[29] Djatkov, D., Martinov, M., and Kaltschmitt, M., Biomass and Bioenergy Influencing parameters on mechanical–physical properties of pellet fuel made from corn harvest residues, Biomass and Bioenergy, 119, pp. 418–428, 2018. DOI: https://doi.org/10.1016/j.biombioe.2018.10.009.
[30] Mani, S., Tabil, L.G., and Sokhansanj S., Specific energy requirement for compacting corn stover, Bioresour. Technol., 97, pp. 1420–1426, 2006. DOI: https://doi.org/10.1016/j.biortech.2005.06.019.
[31] Kaliyan, N., and Morey, R.V., Densification characteristics of corn stover and switchgrass, ASABE, 52(3), pp. 907–920, 2009. DOI: https://doi.org/10.13031/2013.21202.
[32] Crawford, N.C., Ray, A.E., Yancey, N.A., and Nagle, N., Evaluating the pelletization of "pure" and blended lignocellulosic biomass feedstocks, Fuel Process. Technol. 140, pp. 46–56, 2015. DOI: https://doi.org/10.1016/j.fuproc.2015.08.023

L.M. Belmonte, is an advanced Chemical Engineering student at the San Francisco Regional Faculty of the National Technological University (Universidad Tecnológica Nacional, UTN), Argentina. Since 2022, she has participated in the CIDEME research group as an undergraduate intern. She has participated in national congresses and conferences focused on biomass energy, waste and climate change.
ORCID: 0009-0009-4381-7647

A.L. Quicchi, received her BSc. Eng. in Chemical Engineering in 2019. She is an Assistant Professor both in Calculus II and in Thermodynamics and Thermal Machinery at the San Francisco Regional Faculty of the National Technological University (Universidad Tecnológica Nacional, UTN) in Argentina. She is currently pursuing her PhD in Industrial Engineering at the Santa Fe Regional Faculty of UTN. She also works in the biomass area of the UTN R&D group CIDEME in her Faculty.
ORCID: 0000-0001-6369-1046

AR. Farías, is a Chemical Engineering student at the San Francisco Regional Faculty of the National Technological University (Universidad Tecnológica Nacional, UTN), Argentina. She has been working with the CIDEME research group as an undergraduate intern in the field of biomass energy since 2024.
ORCID:0009-0006-8091-302X

M. Bernard, received her BSc. Eng in Chemical Engineering in 2010 and her PhD. in Chemical Sciences in 2020. She has worked in several research programs and projects related to biomaterials with several applications, and in the last few years turned her focus to energy efficiency and biomass for energy generation, with emphasis on gasification of regional materials. She is currently a tenured full-time Research Professor in Thermodynamics at the San Francisco Regional Faculty of the National Technological University (Universidad Tecnológica Nacional, UTN) in Argentina and coordinates the biomass area of the UTN R&D group CIDEME in her Faculty.
ORCID: 0000-0003-2525-9089

DYNA
http://dyna.medellin.unal.edu.co/

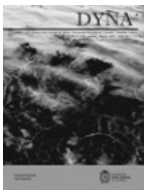

UNIVERSIDAD NACIONAL DE COLOMBIA

Identification of areas for photovoltaic projects in La Guajira Using GIS and multicriteria analysis

Adriana Lizeth Tovar-Blanco[a], David Ricardo Rubio-Herreño[a] & David Ernesto Rodríguez-Vivas[b]

[a] *Universidad Manuela Beltrán, Facultad de Ingeniería, Bogotá, Colombia. adrianatovar@academia.umb.edu.co, davidrubio.rh@academia.umb.edu.co*
[b] *Universidad Manuela Beltrán, Vicerrectoría de Investigaciones, Bogotá, Colombia, coord.invambiental@umb.edu.co*

Received: July 16th, 2025. Received in revised form: January 30th, 2026. Accepted: February 4th, 2026.

Abstract
The advancement of alternative energy in Colombia reflects a strong and shared commitment from both the national government and its citizens. The objective of this work is to characterize the potential areas for the implementation of photovoltaic projects in La Guajira, a region whose solar potential is high, but also has a complex social and environmental context. GIS and AHP were employed to evaluate several parameters including technical, environmental and socio-economic factors (solar irradiation, temperature, slope, aspect, nearness to infrastructure). The results reveal that 14.4% of La Guajira's land is very suitable for solar projects, most of it being in the southwest of the department. It is consistent with the government's national policies to encourage renewable energy and supports the diversification of Colombia's energy complex and fosters development in vulnerable regions. The approach can be adapted in comparable contexts, contributing to global action on clean energy transitions and climate change.

Keywords: photovoltaic energy; GIS; multi-criteria decision analysis; analytic hierarchy process.

Identificación de áreas para proyectos fotovoltaicos en La Guajira mediante SIG y análisis multicriterio

Resumen
El avance de las energías alternativas en Colombia refleja un compromiso fuerte y compartido tanto del gobierno nacional como de sus ciudadanos. El objetivo de este trabajo es caracterizar las áreas potenciales para la implementación de proyectos fotovoltaicos en La Guajira, una región cuyo potencial solar es alto, pero que también tiene un contexto social y ambiental complejo. Se emplearon SIG y AHP para evaluar varios parámetros, incluidos factores técnicos, ambientales y socioeconómicos (irradiación solar, temperatura, pendiente, aspecto, proximidad a la infraestructura). Los resultados revelan que el 14.4% de la tierra de La Guajira es muy apta para proyectos solares, la mayoría de ellos en el suroeste del departamento. Es coherente con las políticas nacionales del Gobierno para fomentar las energías renovables y apoya la diversificación del complejo energético de Colombia y fomenta el desarrollo en regiones vulnerables. El enfoque puede adaptarse en contextos comparables, contribuyendo a la acción mundial sobre las transiciones a la energía limpia y el cambio climático.

Palabras clave: energía fotovoltaica; SIG; modelo de decisiones multicriterio; proceso analítico jerárquico.

1 Introduction

Renewable energy is currently the focus of developing countries, aiming to replace fossil fuels with clean energy sources that do not harm the environment [1,2]. For this reason, solar energy is one of the main projects intended to meet global energy demand, which has enabled the development of this type of project in various countries [3].

In Colombia, where fossil fuels have historically dominated the energy sector, solar photovoltaic energy has emerged as a sustainable alternative to diversify electricity generation sources and reduce greenhouse gas emissions [4]. This research focuses on identifying suitable areas within the department of La Guajira, a region with high solar potential

How to cite: Tovar-Blanco, A.L., Rubio-Herreño, D.R., and Rodríguez-Vivas, E., Identification of areas for photovoltaic projects in La Guajira using GIS and multicriteria analysis DYNA, (93)240, pp. 97-107, January - March, 2026.

yet facing socioeconomic and environmental challenges that require a comprehensive approach for the successful implementation of photovoltaic energy projects [5].

La Guajira, recognized for its high solar irradiation levels and arid climate, presents an optimal setting for the development of photovoltaic energy projects [6]. Due to its geographic location and high solar irradiation levels, with a daily average of 6,0 kWh/m², La Guajira is an ideal site for solar energy projects [7]. However, the region faces critical challenges, including poverty, lack of infrastructure and development, and the presence of sensitive ecosystems, necessitating a careful approach in site selection for energy initiatives [8]. These factors need a careful approach in site selection for energy projects, balancing technical feasibility with environmental and social considerations [9].

Several studies have used Geographic Information Systems (GIS) and multi-criteria analysis to determine the best locations for solar power plant installations [10]. In Valencia, Spain, [11] integrated criteria such as solar radiation intensity, terrain, environmental and climatic factors, and proximity to roads and electrical substations, alongside GIS data-including time series of solar radiation, digital elevation models (DEM), and temperature to identify high potential areas for photovoltaic parks. In Rajasthan, India, [12] identified 20.881 km² of suitable land for solar plants by developing integrated models that combined geographic, social, political, and environmental criteria. In Ecuador, [13] utilized GIS and multi-criteria analysis for siting photovoltaic plants, optimizing solar farm distribution based on national energy demand. In Kenya, [14] applied multi-criteria analysis methodologies within a GIS environment, considering nine criteria related to climate, environment, location, and topography, determining that 2,41% of the land was highly suitable for solar systems. In Egypt, [15] identified optimal areas for photovoltaic parks by assessing location, environmental, meteorological, and climatic categories using multi-criteria decision-making techniques and GIS tools. In Pakistan, [16] evaluated ten factors grouped into four categories (geographic, technical, economic and flood susceptibility), using the FUCOM method and weighted overlay analysis in ArcGIS Pro, concluding that only 2.02% of the country's area is suitable for solar power plants. Finally, developed a multi-criteria analysis using GIS to selecting optimal solar plant sites in New Aswan, Egypt, considering factors such as solar radiation, distance to road networks and distance to buildings, (0,35, 0,1 and 0,1, respectively), showing the effectiveness of the proposed model in assessing site suitability [17].

The use of GIS combined with multi-criteria analysis models like AHP has been effective for renewable energy planning globally [11-15,17-24]. In this study, this methodology was applied to evaluate key variables including solar irradiation, air temperature, topography, and accessibility, ensuring that photovoltaic projects are not only technically feasible but also environmentally and socially sustainable [25].

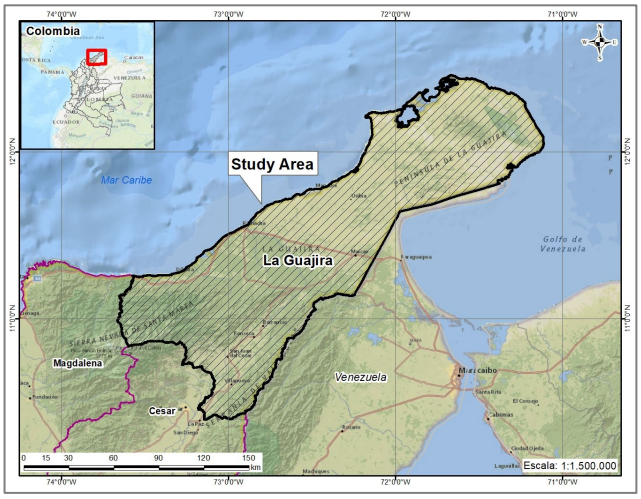

Figure 1. Location
Source: The authors

The aim of this research was to identify suitable areas for the implementation of photovoltaic energy projects in the department of La Guajira using GIS and AHP multi-criteria analysis models. Specific environmental criteria were chosen, and a geographic model was created to assess the feasibility and suitability of the proposed areas for project development.

2 Methodology

2.1 Study area

The study area corresponds to the department of La Guajira, located in the Caribbean region of Colombia. Geographically, La Guajira is bordered by the Caribbean Sea to the north and Venezuela to the east, with its capital, Riohacha, serving as the economic hub of the region (Fig. 1). Covering an area of approximately 20,848 km², La Guajira has a predominantly arid and semi-desert climate, characterized by temperatures ranging from 22 to 40°C and annual precipitation levels between 300 and 600 mm. [26].

2.2 Data

2.2.1 Solar Irradiation

Sunlight is a fundamental natural resource and an important energy source due to solar irradiation, which is used in the construction of photovoltaic projects because of its irradiation level [27]. Therefore, it is essential to understand what it is and how it is measured. Solar irradiation represents the accumulated energy over a period and is calculated using Global Horizontal Irradiation (GHI), which results from the diffuse radiation from the sky (DHI) and the direct irradiation from the sun (DNI), multiplied by the cosine of the angle between the sun's direction and the vertical (zenith). The result is measured in watts per square meter (W/m²) [27-29].

$$GHI = DHI + DNI * Cos(Z)$$

Considering the above, this study used solar irradiation (GHI) values in kWh/m², obtained directly from the SOLARGIS global solar model for the La Guajira department in Colombia. These values were provided by the Global Solar Atlas as part of the global renewable energy resource mapping initiative [30].

2.2.2 Air temperature

The temperature of solar panels directly affects their energy production. It is recommended that they operate at temperatures below 25°C, which has been shown to ensure optimal system performance [11]. Several studies have confirmed a decrease in energy production. This reduction ranges between 0.4% and 0.5% for every 1°C increase in the reference temperature [31]. For this study, the annual mean temperature values were obtained from the report *"Departmental Analysis of Vulnerability and Risk to Climate Change in the Agricultural Sector – La Guajira,"* developed by the Food and Agriculture Organization (FAO) [26].

2.2.3 Digital Elevation Model (DEM)

For this analysis, a Digital Elevation Model (DEM) with a resolution of 1 arcsec (~30 m) was used, generated by NASA's Shuttle Radar Topography Mission (SRTM) sensor, adapted to the specific topography of the La Guajira department [27,32] (Fig. 2).

2.2.4 Slope

The slope of the terrain is an important factor in selecting sites for photovoltaic energy projects, due to solar panels may cast shadows on others in terrains is too steep, reducing the system's efficiency [11-25,27-29]. Although there is no accepted exact value, experts agreed that slopes greater than 10% are not ideal for installing solar energy projects [27,33].

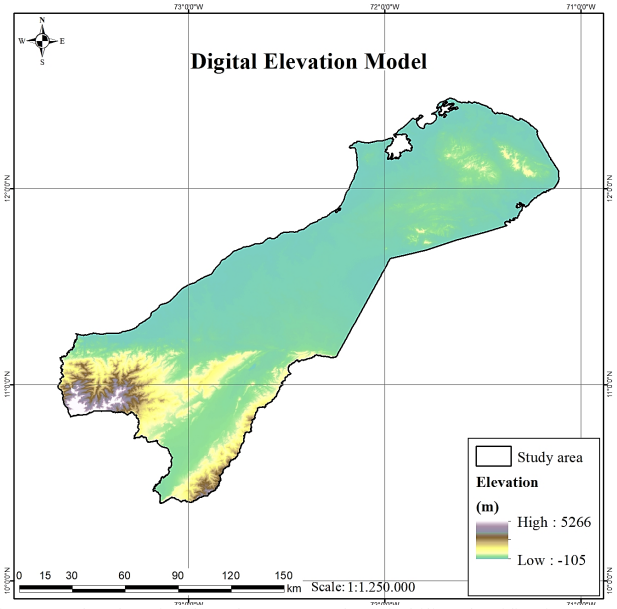

Figure 2. The elevation-based map upon the suitability classifications.
Source: The Authors.

This analysis was conducted using a digital terrain model with specialized software (ArcGIS), aiming to identify land with slopes close to 0° - that is, less inclined areas - to enhance solar irradiation reception.

2.2.5 Terrain aspect (Orientation)

The orientation of solar panels in photovoltaic energy projects plays a key role in system efficiency, as it allows for greater solar irradiation capture during peak sunlight hours. Countries in the Northern Hemisphere, such as Colombia, receive higher solar irradiation when solar panels are positioned facing south [11,14].

2.2.6 Distance urban areas

The distance between photovoltaic energy projects and urban areas has both positive and negative aspects. On one hand, proximity to urban areas could limit and affect the growth and development of communities; however, it also creates job opportunities and reduces transportation costs for personnel and materials. Thus, a 500-meter distance from urban areas was established for La Guajira department in this study [17,18,20,21,27].

2.2.7 Distance to main roads

The distance to main roads in photovoltaic projects helps reduce costs, as it facilitates the transport of personnel and materials to the project site and avoids the need to build additional roads for accessibility. Based on this, a maximum distance of 500 meters from main roads was determined as the optimal area for the study [11,13,16,17,20].

2.2.8 Distance to power lines

One of the key factors in minimizing energy loss in photovoltaic projects is proximity to transmission lines. Being close to these lines avoids construction costs and reduces energy losses, since longer distances increase energy loss during transmission. Therefore, an optimal area of 500 meters near existing transmission lines was determined [11,16-18,20]. In Table 1, it describes the parameters used along with the sources of information.

Table 1.
Data Sources

Data	Type	Source
Solar Irradiation	Raster data	https://globalsolaratlas.Info/
DEM data	Raster data	https://earthexplorer.usgs.gov/
Temperature air	Vector	https://cambioclimatico.fao.org.co/la-guajira/
Urban area	Vector	https://geoportal.dane.gov.co/servicios/descarga-y-metadatos/datos-geoestadisticos/
Roads	Vector	https://www.colombiaenmapas.gov.co/#
Water bodies	Vector	https://www.colombiaenmapas.gov.co/#
Transmission lineas	Vector	https://geovisor.anla.gov.co:8446/geovisor/#/visor
Protected areas	Vector	https://runap.parquesnacionales.gov.co/cifras
Indigenous reserves	Vector	https://www.colombiaenmapas.gov.co/

Source: The authors

This study employed a quantitative approach, focused on identifying optimal areas for photovoltaic projects using numerical data analysis and mathematical models [9,15-19,20-25,27, 29,33-40]:

- Data Collection: information obtained from meteorological, satellite, including solar irradiation (kWh/m²), air temperature (°C), terrain slope (°), terrain aspect (°), distance to urban areas and roads (km), and distance to transmission lines (km).
- Analytical Model: the Analytic Hierarchy Process (AHP) was applied within GIS software ArcMap 10.8, allowing quantitative weighting and evaluation of multiple criteria.
- Data Processing: GIS layers were created and managed, incorporating environmental data (GHI, air temperature, topography), and socioeconomic data (urban areas, roads and power lines). The criteria were normalized and adjusted to ensure uniformity in the analysis.
- Weighting and Mapping: Using AHP, the criteria were weighted, generating a suitability map that highlights optimal zones for photovoltaic projects. (Fig. 3).

2.2.9 Analytic Hierarchy Process (AHP) based on multi-criteria decision-making

The AHP process is used for multicriteria decision-making. Its hierarchical structure allows for an organized evaluation of key elements [43]. These elements are crucial for problem-solving and are assigned weight factors. Priorities are established using a comparison matrix based on preference or relevance, enabling the identification of optimal and suitable solutions [20]. This methodology ensures quality and accuracy in decision-making, facilitating the assessment of strategies, requirements, and alternatives [15,17,19,21-22,24-25,27,29,35].

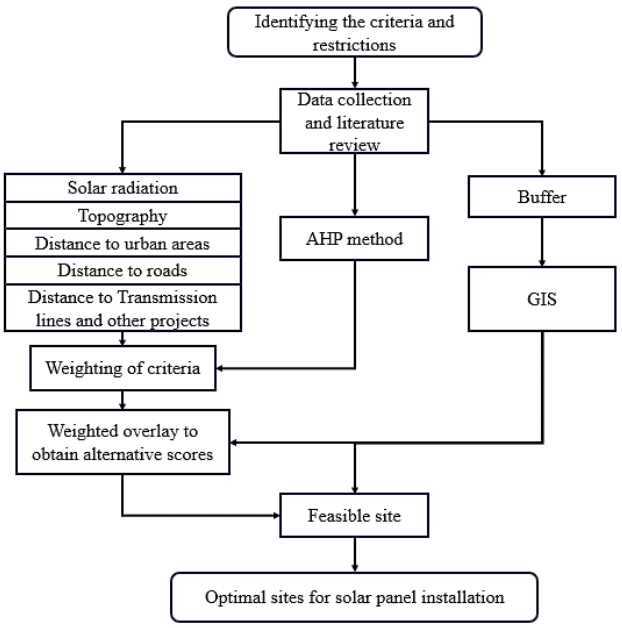

Figure 3. Flow chart of the proposed methodology
Source: The authors

Furthermore, the Consistency Index (CI), introduced by Saaty in 1980 [20], assesses the coherence of the parameters established in pairwise comparison matrices used in the AHP methodology. If the index indicates significant deviations, adjustments must be made to improve consistency and enhance the reliability of results [25,27]. The CI is calculated using eq. (1), where λmax is the principal eigenvalue of the matrix and *n* is the matrix size.

$$CI = \frac{\lambda max - n}{n - 1} \quad (1)$$

The Random Index (RI) depends on the matrix size and is used to compare the CI. Finally, the Consistency Ratio (CR) is obtained by dividing the CI by the RI (eq. 2):

$$CR = \frac{CI}{RI} \quad (2)$$

A CR less than or equal to 0.1 indicates that the comparisons are within an acceptable threshold of consistency. To select locations for photovoltaic energy plants, the suitability index was generated using seven thematic layers integrated into a GIS. To perform this assessment, the weighted overlay method was applied (eq. 3).

$$SI = \sum_{i=1}^{n} (W_i \times C_i) \quad (3)$$

Where Wi is the weight assigned to the i*i*-th thematic layer, Ci is the reclassified value of the i*i*-th thematic layer, and *n* is the number of thematic layers.

2.2.10 Site selection restrictions

Factors such as municipal capitals and population centers (urban areas), protected areas, significant road networks, and bodies of water were chosen as limiting variables for the suitability research. In comparable evaluations of optimal areas for solar panel installation, these four limitations are frequently used [13,16,23,27]. However, there is a differential factor in La Guajira, as it is one of the departments with the most indigenous communities, which was important to consider [44]. The geographic source of the protected areas corresponds to the Registro Único Nacional de Áreas Protegidas (RUNAP), the urban areas are found in the Departamento Administrativo Nacional de Estadística (DANE), the indigenous reserves are found in the Agencia Nacional de Tierras (ANT), and the roads as well as the water bodies are regulated by the Instituto Geográfico Agustín Codazzi (IGAC). According to RUNAP, La Guajira has 20 protected areas. The buffer distances used in this analysis were collected from the literature and are presented in Fig. 4.

2.2.11 GIS processing

ArcGIS 10.8 was used to create a suitability map with spatial data from public online resources. Five constraints and seven criteria were evaluated to identify optimal and suboptimal locations for photovoltaic energy projects. Table 2 outlines the selected geospatial analysis model parameters, which were determined based on the study area's characteristics and expert opinions [9,15-19,20-25,27,29,33-41].

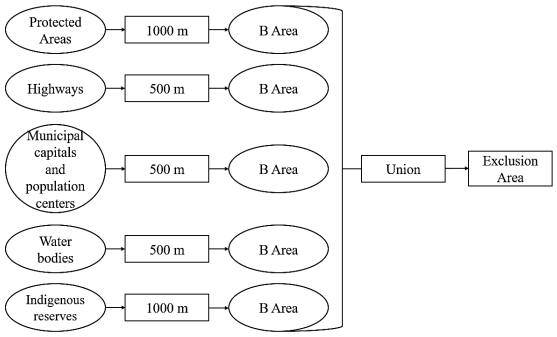

Figure 4. Restriction part of the model
Source: The authors.

2.2.12 Standardized suitability map

For each criterion in the suitability map, a categorized map was created using GIS software ArcMap 10.8.2. The displayed maps showed the evaluated and rated parameters. Each map was obtained, processed in raster format with cells of 30 m × 30 m, using "Resample" tool in ArcMap, and then classified for each criterion. The digital elevation model (DEM) also served as the basis for slope and aspect. ArcMap's "Slope" and "Aspect" tools were used to build the slope and terrain aspect map. Then, the data was reclassified using the classification tool. To geoprocessing data, it was necessary to project all data to the same geographic coordinate system in WGS-84. Then, data was normalized and the methodology AHP was applied through "Raster calculator" tool in ArcMap. Finally, all criteria were added in the resulting raster map [27]. Fig. 5 shows the limited region of the entire study.

Table 2.
Weight and suitability categories for each criterion

Criteria	Suitability	Score	Range
GHI (kWh/m² year)	Very low	1	1.179 - 1.500
	Low	2	1.501 - 1.800
	Moderate	4	1.801 - 2.000
	Very high	5	2.001 - 2.347
Temperature (°C)	Low	2	1 - 10
	Moderate	4	26 - 35
	High	6	11 - 25
Terrain Slope (°)	Very low	1	43 - 50
	Low	2	28 - 42
	Moderate	3	17 - 27
	High	4	6,3 - 16
	Very high	5	0 - 6,2
Terrain Aspect	Very low	4	North
	Low	5	Northeast, Northwest
	Moderate	4	East, West
	High	6	Southeast, Southwest
	Very high	7	South
Distance from urban areas (km)	Low	1	10 - 20
	High	2	5 - 10
	Very low	3	0 - 5
Distance from roads (km)	Very high	8	0 - 0,5
	High	6	0.5 - 2
	Moderate	4	2 - 5
	Low	2	5 - 10
Distance from transmission lines (km)	Very high	8	0 - 0,5
	High	6	0.5 - 2
	Moderate	4	2 - 5
	Low	2	5 - 10

Source: The authors.

3 Results and Discussion

The results of the AHP-GIS analysis of suitable locations for the development of a photovoltaic project in the department of La Guajira are presented, including the map of the identified and weighted optimal location.

3.1 AHP results

This study applied the MCDM technique based on AHP to assign weights to seven criteria influencing the selection of locations for photovoltaic plants (C1: solar irradiation (GHI); C2: temperature; C3: slope; C4: terrain aspect; C5: proximity to urban areas; C6: distance from roads; C7: proximity to transmission lines). The most important criterion was solar irradiation (C1), with a weight of 35%, followed by other factors such as proximity to urban areas (17%), temperature (16%), slope, aspect and distance from roads (9%), and proximity to transmission lines (5%). The consistency ratio obtained was CR = 0,007 (0,77%), and the preference levels of the criteria were illustrated in Table 3 and Fig. 6.

In other studies, different weights were assigned to parameters like those analyzed in the La Guajira department. However, it was found that the most relevant parameter was solar irradiation (C1), ranking above others such as slope, orientation, or temperature, as observed in Ecuador, where it was considered for the expansion of electrical substations [23], in Bangladesh, where a site suitability assessment for

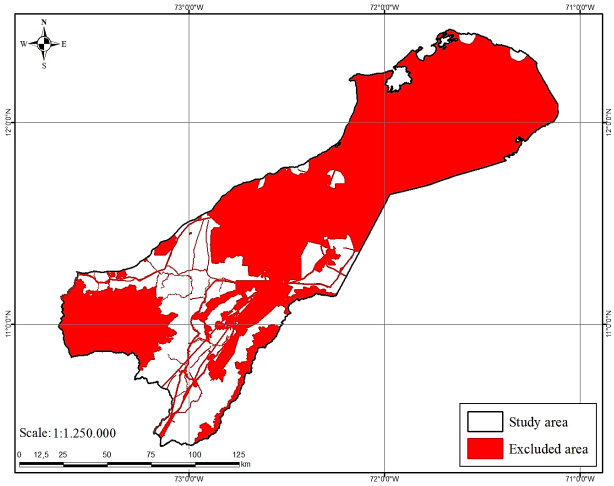

Figure 5. Restricted locations in the study area.
Source: The authors.

Table 3.
Comparison table of the selected criteria for making decisions

	Parameters							Weight
	C1	C2	C3	C4	C5	C6	C7	
C1	1	3	5	4	2	3	5	0,35
C2	1/3	1	2	2	1	2	3	0,16
C3	1/5	1/2	1	1	1/2	1	2	0,09
C4	1/4	1/2	1	1	1/2	1	2	0,09
C5	1/2	1	2	2	1	2	3	0,17
C6	1/3	1/2	1	1	1/2	1	2	0,09
C7	1/5	1/3	1/2	1/2	1/3	1/2	1	0,05

Source: The authors.

solar power plants was conducted [27], in Kayseri, Turkey, where GHI was identified as the most critical factor with a weight of 0,447, followed by 'slope' (0,212), and 'aspect' (0,177) [41]. These findings suggest the optimal development of the methodology and the validity of the results obtained.

3.2 Site selection criteria maps for solar power plants solar irradiation (GHI)

The solar radiation used in this study was obtained directly from the SOLARGIS global solar model for the La Guajira department in Colombia, provided by the Global Solar Atlas as part of the global renewable energy resource mapping initiative [30]. Fig. 7 shows that La Guajira has an annual solar radiation ranging from 1,179 kWh/m² to 2,347 kWh/m², determining that 90,82% of the area is optimal for the construction of photovoltaic energy projects, according to the classification (Table 4). These findings align with other studies, which identified optimal solar irradiation values for photovoltaic projects ranging from 1,568 kWh/m²/year to 1,918 kWh/m²/year and 1,425 kWh/m²/year to 1,821 kWh/m²/year [11,27].

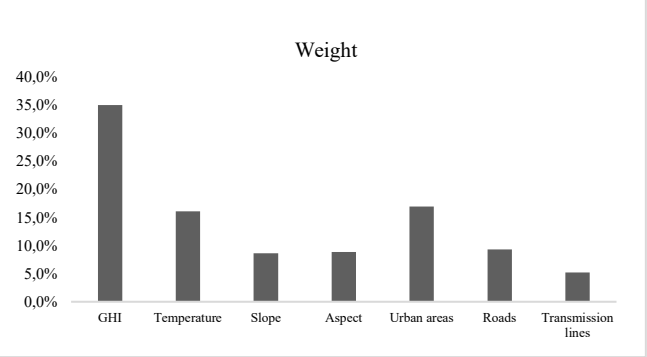

Figure 6. Tre criteria's priority weights
Source: The authors.

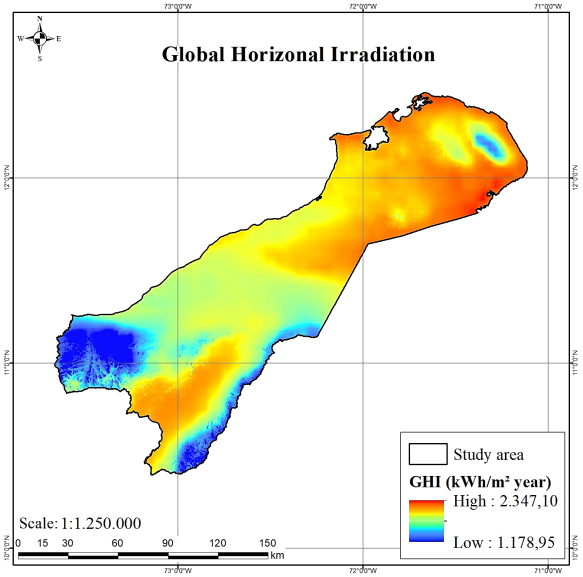

Figure 7. La Guajira's yearly GHI
Source: The authors.

Table 4.
Classification of GHI Suitability in La Guajira

Suitability	Score	Area (km²)	Area (%)
Very low	1	134,08	0,65
Low	2	1.753,76	8,53
Moderate	4	2.799,75	13,61
Very high	5	15.882,85	77,21

Source: The authors.

Table 5.
Classification of temperature suitability in La Guajira

Suitability	Score	Area (km²)	Area (%)
Low	2	233,21	1,13
Moderate	4	17.695,80	86,03
High	6	2.641,42	12,84

Source: The authors.

3.3 Annual mean temperature map

The temperature range identified in La Guajira department varies between 1 and 35°C, representing a wide and diverse climate in the area. However, the optimal temperatures for photovoltaic energy projects in this study were identified between 11 and 25°C, which account for 98.87% of the annual average temperature in the department (Table 5 and Fig. 8). These conditions enhance solar irradiation captured by the panels.

3.4 Slope

The slope characteristics in La Guajira department range from 0° to 50°. For this study, an optimal slope range between 0° and 16° was identified, representing 7,45% of the study area (Table 6 and Fig. 9). These findings align with studies where recommend optimal slopes between 0 and 13°, such as in Ecuador [13], and between 0° and 5° in Iran [34].

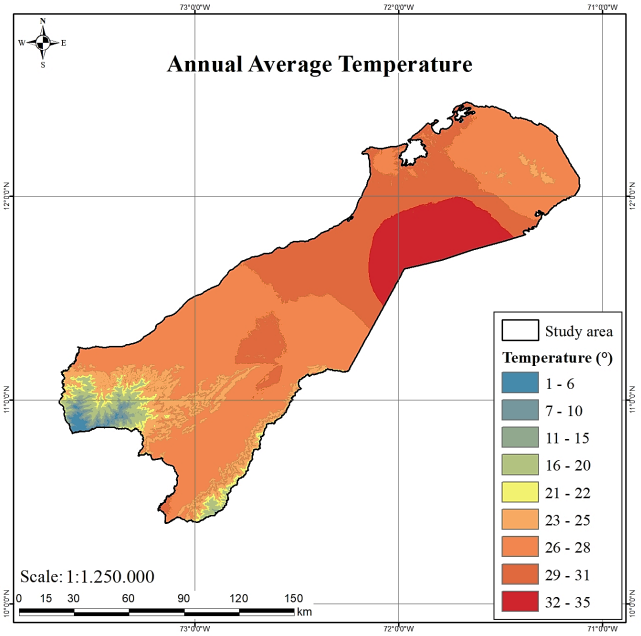

Figure. 8. Temperature-based suitability classifications
Source: The authors.

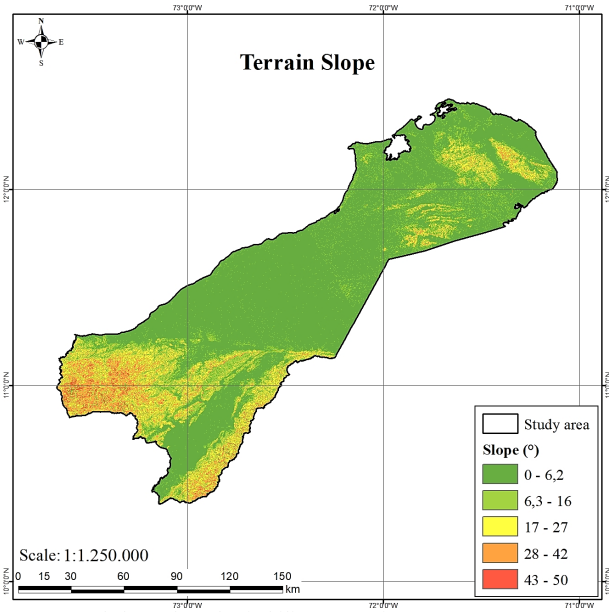

Figure 9. Land slopes-based suitability categories.
Source: The authors.

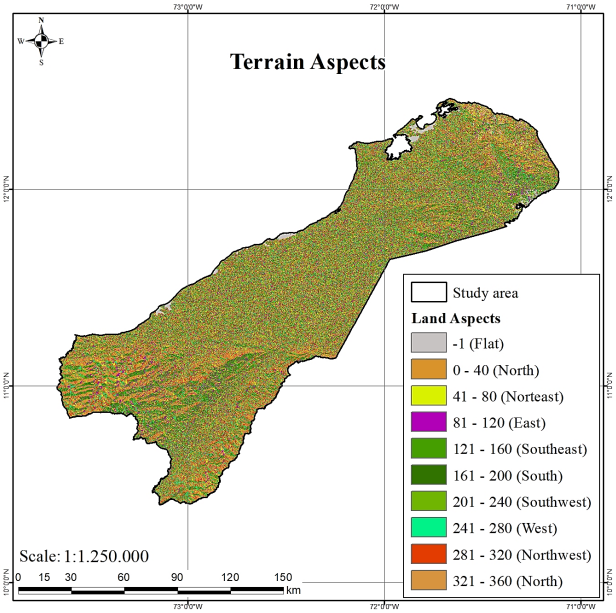

Figure 10. Land aspects-based suitability categories.
Source: The authors.

3.5 *Terrain aspect (orientation)*

The orientation of solar panel systems in photovoltaic energy projects in Northern Hemisphere countries like Colombia allows for optimal solar irradiation capture when positioned facing south. After conducting this study, it was determined that 30.86% of the total area in La Guajira is suitable for photovoltaic project development based on orientation (Table 7 and Fig. 10). These findings align with previous studies in the same hemisphere, such as in Bangladesh, which focused on site selection for solar power plants [27], and in Iran, where research in Guilán province reached similar conclusions [34].

Table 6.
Classification of terrain slope suitability in La Guajira

Suitability	Range (°)	Area (km^2)	Area (%)
Very low	43 - 50	14.246,34	69,26%
Low	28 - 42	2.858,13	13,89%
Moderate	17 - 27	1.934,75	9,41%
High	6,3 - 16	1.316,17	6,40%
Very high	0 - 6,2	215,04	1,05%

Source: The authors.

Table 7.
Classification of suitability in La Guajira, about aspect criterion

Suitability	Aspect	Area (km2)	Area (%)
Very low	North	2.806,01	25,24%
Low	Norteast	2.246,14	10,92%
Very low	East	2.160,51	10,50%
High	Southeast	2.225,75	10,82%
Very high	South	2.132,17	10,37%
High	Southwest	1.989,19	9,67%
Very low	West	2.130,78	10,36%
Low	Northwest	2.494,76	12,13%

Source: The authors.

3.6 *Distance from urban areas*

The distance between photovoltaic energy projects and urban areas in La Guajira department was considered an important factor due to the region's culture and the respect for indigenous territories and traditions. As a result, distances greater than 500 meters from these areas were established, leaving 56,01% of the territory suitable for photovoltaic project development (Table 8 and Fig. 11).

Table 8.
Classification of urban areas suitability in La Guajira

Suitability	Range (km)	Area (km2)	Area (%)
High	0 - 5	9.050,68	44
Low	5 - 10	6.176,53	30,03
Very low	20 - 20	5.343,22	25,98

Source: The authors.

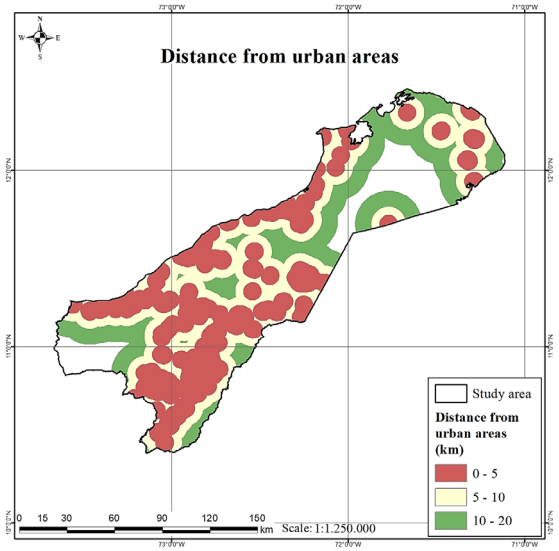

Figure 11. Suitability levels according to their proximity to urban areas.
Source: The authors.

Different perspectives exist regarding this criterion. Some argue that developing projects within 500 meters of urban areas could interfere with community growth and development [27]. On the other hand, others believe that locating these projects near urban areas can promote social growth by creating job opportunities and improving the economic feasibility of the project by reducing transportation costs for personnel and materials [34].

3.7 Distance from roads

The distance to roads is an important factor in the development of any type of project, as it affects construction and operational costs. Therefore, considering the existing road network in La Guajira department, a maximum distance of 500 meters was established for photovoltaic project development. The study found that 38.47% of the study area meets this criterion, ensuring optimal project implementation (Table 9 and Fig. 12). Additionally, previous studies conducted in similar regions considered short distances to main roads to reduce transportation costs, optimize resources, and ensure efficient energy transmission to nearby urban areas [11,34].

3.8 Distance from transmission lines

One of the key factors in ensuring optimal energy transmission in a photovoltaic project is proximity to transmission lines, as it reduces energy losses over long distances and lowers installation costs [17]. After verifying the existing transmission lines in La Guajira, a maximum distance of 500 meters was established for project development. The study found that 9,75% of the area meets optimal conditions for installation (Table 10 and Fig. 13). Previous studies have considered transmission line proximity in a similar way, highlighting the importance of locating projects near existing transmission lines to minimize energy loss and reduce associated costs [11, 17].

Table 9.
Classification of suitability in La Guajira about distance from roads

Suitability	Range (km)	Area (km2)	Area (%)
Very high	0 - 0,5	7.914,27	38,47
High	0.5 - 2	6.969,48	33,88
Moderate	2 - 5	4.221,51	20,52
Low	5 - 10	1.465,17	7,12

Source: The authors.

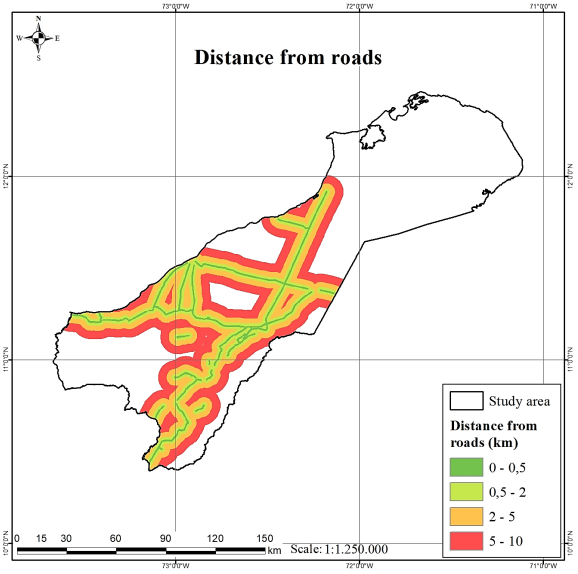

Figure 12. Suitability levels according to their proximity to roads.
Source: The authors.

Table 10.
Classification of transmission lines suitability in La Guajira

Suitability	Range (km)	Area (km2)	Area (%)
Low	5 - 10	7.222,19	35,11
Moderate	2 - 5	6.617,79	32,17
High	0.5 - 2	4.725,45	22,97
Very high	0 - 0,5	2.005,00	9,75

Source: The authors.

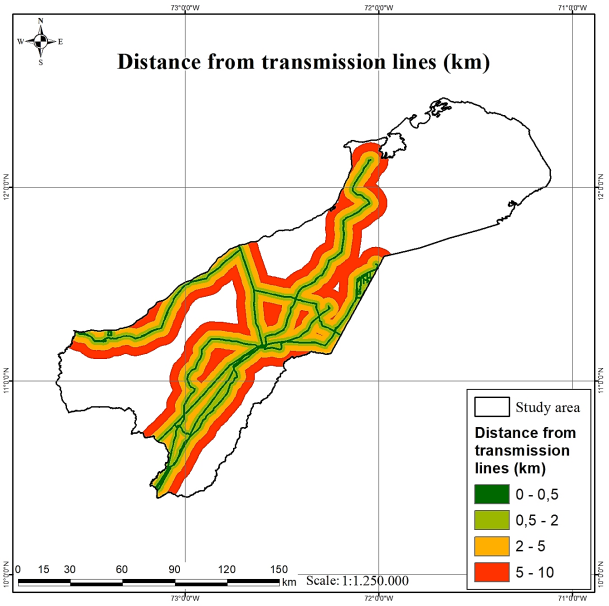

Figure 13. Suitability category map of solar PV plant locations.
Source: The authors.

3.9 Areas for the implementation of photovoltaic energy projects

According to Table 11, 14.4% of the territory of La Guajira (categorized as High and Very High) has optimal conditions for the establishment of photovoltaic projects, representing a total of 2,981.65 km² of the department's area. Fig. 14 shows the final solar power plant suitability map, which is classified into six categories: Very High, High, Moderate, Low, Very Low and Restricted Area. These categories represent the different priorities to allocate photovoltaic energy projects. According to the resulting map, the most suitable locations for photovoltaic energy plants in La Guajira are concentrated in the southwestern region. Similar results found that suitable areas mainly resulted from high solar irradiation, low average temperatures, and flat terrain [15].

Table 11.
Areas of each suitability class and their percentage in La Guajira

Suitability category	Area (km^2)	Area (%)
Very low	360,75	1,75
Low	2.215,75	10,77
Moderate	4.246,64	20,64
High	2.257,57	10,97
Very high	724,08	3,52
Restricted areas	10.765,64	52,34

Source: The authors.

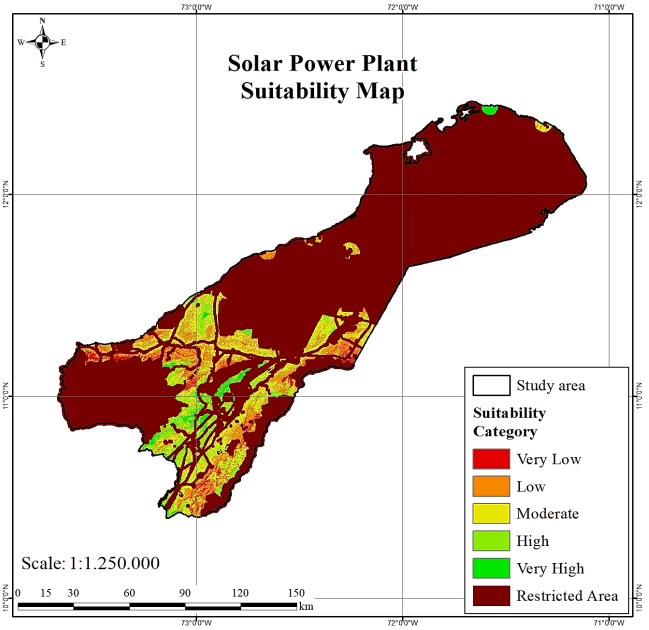

Figure 14. Suitability category map of solar PV plant locations.
Source: The authors.

4 Conclusions

The integration of GIS and AHP enabled the identification of several highly suitable areas for photovoltaic projects in La Guajira, demonstrating that the combination of these tools gives a relevant approach for planning photovoltaic solar energy initiatives, as it supports informed and balanced decision-making.

This study's results may meaningfully aid Colombia's energy planning, especially considering Law 2099 of 2021, which promotes renewable energy while supporting national economic recovery. Identifying the most favorable zones for solar energy development not only strengthens the diversification of energy sources but also creates opportunities for job creation and social improvement in some of the country's most vulnerable territories.

Although the percentage within suitable area for photovoltaic energy projects may seem low, the Colombian National Government protects a large portion of the territory. For these territories, protection has important environmental value because of rich biodiversity and unique ecosystems. The presence of Indigenous communities, national parks and forest reserves also gives value to them.

This study provides a methodological tool that can be replicated in other regions with similar characteristics, thereby contributing to energy planning at both the national, regional and local levels.

References

[1] Olabi, A.G., and Abdelkareem, M.A., Renewable energy and climate change. Renewable and Sustainable Energy Reviews, 158, art. 112111, 2022. DOI: https://doi.org/10.1016/J.RSER.2022.112111

[2] Jaiswal, K.K., Chowdhury, C.R., Yadav, D., Verma, R., Dutta, S., Jaiswal, K.S., and Karuppasamy, K.S.K., Renewable and sustainable clean energy development and impact on social, economic, and environmental health. Energy Nexus, 7, art. 100118, 2022. DOI: https://doi.org/10.1016/j.nexus.2022.100118

[3] Roca-Jusmet, J., La política climática y los combustibles fósiles: una perspectiva desde la oferta. Revista de Economía Crítica, [online]. (34), pp. 9-25, 2022. Available at: https://hdl.handle.net/2445/192004

[4] Fernández-Labbé, J., El territorio como espacio contradictorio: promesas y conflictos en torno a la actividad extractiva en Ecuador, Colombia, Perú y Chile. eure (Santiago), 46(137), pp. 225-246, 2020. DOI: https://doi.org/10.4067/S0250-71612020000100225

[5] Vega-Araújo, J., and Heffron, R.J., Assessing elements of energy justice in Colombia: a case study on transmission infrastructure in La Guajira. Energy Research & Social Science, 91, art. 102688, 2022. DOI: https://doi.org/10.1016/j.erss.2022.102688

[6] Urrego, L.R., Mendoza, M.V., León, H.G., y Ocampo, P.C., La gestión para cadena de suministro de sistemas de energía solar fotovoltaica en Colombia y su situación actual. Avances: Investigación en Ingeniería, 15(1), pp. 112-130, 2018. DOI: https://doi.org/10.18041/1794-4953/avances.1.1368

[7] Unidad de Planeación Minero Energética (UPME) & Instituto de Hidrología, Meteorología y Estudios Ambientales (IDEAM). Atlas de radiación solar de Colombia. 2019. [online]. Available at: https://repositoriobi.minenergia.gov.co/handle/123456789/2414

[8] Moreno, C., Milanes, C.B., Arguello, W., Fontalvo, A., and Alvarez, R.N., Challenges and perspectives of the use of photovoltaic solar energy in Colombia. Int. J. Electr. Comput. Eng, 12(5), pp. 4521-4528, 2022. DOI: https://doi.org/10.11591/ijece.v12i5.pp4521-4528

[9] Galvís-Villamizar, D.N., Duque-Suárez, O.M., and Gómez-Camperos, J.A., Photovoltaic solar energy in Colombia. International Journal of System Assurance Engineering and Management, 13(5), pp. 2151-2164, 2022. DOI: https://doi.org/10.1007/s13198-022-01745-8

[10] Robles-Algarín, C., Castrillo-Fernández, L., and Restrepo-Leal, D., Optimal site selection for solar PV systems in the Colombian Caribbean: evaluating weighting methods in a TOPSIS framework. Sustainability (2071-1050), 16(20), art. 8761, 2024. DOI: https://doi.org/10.3390/su16208761

[11] Guaita-Pradas, I., Marques-Perez, I., Gallego, A., and Segura, B., Analyzing territory for the sustainable development of solar photovoltaic power using GIS databases. Environmental Monitoring and Assessment, 191(12), art. 764, 2019. DOI: https://doi.org/10.1007/s10661-019-7871-8

[12] Saraswat, S.K., and Digalwar, A.K., Empirical investigation and validation of sustainability indicators for the assessment of energy sources in India. Renewable and Sustainable Energy Reviews, 145, art. 111156, 2021. DOI: https://doi.org/10.1016/j.rser.2021.111156

[13] Zambrano-Asanza, S., Quiros-Tortos, J., and Franco, J.F., Optimal site selection for photovoltaic power plants using a GIS-based multi-criteria decision making and spatial overlay with electric load. Renewable and Sustainable Energy Reviews, 143, art. 110853, 2021. DOI: https://doi.org/10.1016/j.rser.2021.110853

[14] Elkadeem, M.R., Younes, A., Sharshir, S.W., Campana, P.E., and Wang, S., Sustainable siting and design optimization of hybrid renewable energy system: a geospatial multi-criteria analysis. Applied Energy, 295, art. 117071, 2021. DOI: https://doi.org/10.1016/j.apenergy.2021.117071

[15] Elboshy, B., Alwetaishi, M., Aly, R.M., and Zalhaf, A.S., A suitability mapping for the PV solar farms in Egypt based on GIS-AHP to optimize multi-criteria feasibility. Ain Shams Engineering Journal, 13(3), art. 101618, 2022. DOI: https://doi.org/10.1016/j.asej.2021.10.013

[16] Khan, A., Ali, Y., and Pamucar, D., Solar PV power plant site selection using a GIS-based non-linear multi-criteria optimization technique. Environmental Science and Pollution Research, 30, pp. 57378–57397, 2023. DOI: https://doi.org/10.1007/s11356-023-26540-1

[17] Salama, S.W., Towards advanced sustainable criteria for choosing the best site for collecting solar energy in cities using multi-criteria GIS. City, Territory and Architecture, 11, art. 22, 2024. DOI: https://doi.org/10.1186/s40410-024-00243-7

[18] Imamverdiev, N.S., Optimal site selection for solar photovoltaic power plants: a Nakhchivan Autonomous Republic case study, Azerbaijan. Geography and Natural Resources, 43(2), pp. 189-199, 2022. DOI: https://doi.org/10.1134/S1875372822020044

[19] Günen, M.A., Determination of the suitable sites for constructing solar photovoltaic (PV) power plants in Kayseri, Turkey, using GIS-based ranking and AHP methods. Environmental Science and Pollution Research, 28(40), pp. 57232-57247, 2021. DOI: https://doi.org/10.1007/s11356-021-14622-x

[20] Wati, E., and Meukam, P., Impact of climate change on the site suitability for solar farms: case study of Cameroon. Renewable Energy, 225, art. 120310, 2024. DOI: https://doi.org/10.1016/j.renene.2024.120310

[21] Shi, F., Li, X., Li, M., and Bai, B., Site selection strategy for photovoltaic power plants construction on gangue hills: an integrated method based on GIS and AHP-TOPSIS. Energy Strategy Reviews, 59, art. 101722, 2025. DOI: https://doi.org/10.1016/j.esr.2025.101722

[22] Coruhlu, Y.E., Solgun, N., Baser, V., and Terzi, F., Revealing the solar energy potential by integration of GIS and AHP in order to compare decisions of the land use on the environmental plans. Land Use Policy, 113, art. 105899, 2022. DOI: https://doi.org/10.1016/j.landusepol.2021.105899

[23] Villacreses, G., Martínez-Gómez, J., Jijón, D., and Cordovez, M., Geolocation of photovoltaic farms using Geographic Information Systems (GIS) with Multiple-criteria decision-making (MCDM) methods: case of the Ecuadorian energy regulation. Energy Reports, 8, pp. 3526-3548, 2022. DOI: https://doi.org/10.1016/j.egyr.2022.02.152

[24] Colak, H.E., Memisoglu, T., and Gercek, Y., Optimal site selection for solar photovoltaic (PV) power plants using GIS and AHP: a case study of Malatya Province, Turkey. Renewable Energy, 149, pp. 565-576, 2020. DOI: https://doi.org/10.1016/j.renene.2019.12.078

[25] López-Bravo, C., Mora-López, L., Sidrach-deCardona, M., and Márquez-Ballesteros, M.J., A comprehensive analysis based on GIS-AHP to minimise the social and environmental impact of the installation of large-scale photovoltaic plants in south Spain. Renewable Energy, 226, art. 120387, 2024. DOI: https://doi.org/10.1016/j.renene.2024.120387

[26] FAO. Análisis departamental de vulnerabilidad y riesgo frente al cambio climático para el sector agropecuario. Organización de las Naciones Unidas para la Alimentación y la Agricultura. [online]. 2022. Available at: https://cambioclimatico.fao.org.co/la-guajira/

[27] Islam, M.R., Aziz, M.T., Alauddin, M., Kader, Z.SKO, and Islam, M.R. Site suitability assessment for solar power plants in Bangladesh: a GIS-based analytical hierarchy process (AHP) and multi-criteria decision analysis (MCDA) approach. Renewable Energy, 202, art. 119595, 2024. DOI: https://doi.org/10.1016/j.renene.2023.119595

[28] Zhao, Y., Li, S., Yang, D., Yahaya, I.I., and Pan, H., Assessment of site suitability for centralized photovoltaic power stations in Northwest China's six provinces. Journal of Environmental Management, 366, art. 121820, 2024. DOI: https://doi.org/10.1016/j.jenvman.2024.121820

[29] Rekik, S., and El-Alimi, S., Optimal wind-solar site selection using a GIS-AHP based approach: a case of Tunisia. Energy Conversion and Management: X, 18, art. 100355, 2023. DOI: https://doi.org/10.1016/j.ecmx.2023.100355

[30] World Bank Group & Solargis. Global Solar Atlas. [Mapa interactivo. online]. (s.f.). Available at: https://globalsolaratlas.info/map?c=12.761261,15.820313,3

[31] Sun, C., Zou, Y., Qin, C., Zhang, B., and Wu, X., Temperature effect of photovoltaic cells: a review. Advanced Composites and Hybrid Materials, 5(4), pp. 2675-2699, 2022. DOI: https://doi.org/10.1007/s42114-022-00533-z

[32] NASA Earthdata. Data Tools. [online]. (s.f.). Recovered on May 2025, Available at: https://www.earthdata.nasa.gov/data/tools

[33] Doorga, J.R.S., Rughooputh, S.D.D.V., and Boojhawon, R., Multi-criteria GIS-based modelling technique for identifying potential solar farm sites: a case study in Mauritius. Renewable Energy, 133, pp. 1201–1219, 2019. DOI: https://doi.org/10.1016/j.renene.2018.08.105

[34] Besharati-Fard, M., Moradian, P., Emarati, M., Ebadi, M., Gholamzadeh Chofreh, A., and Klemeš, J.J., Ground-mounted photovoltaic power station site selection and economic analysis based on a hybrid fuzzy best-worst method and geographic information system: a case study Guilan province. Renewable and Sustainable Energy Reviews, 169, art. 112923, 2022. DOI: https://doi.org/10.1016/j.rser.2022.112923

[35] Rocha, C.M.M., Buelvas, D.A., Machado, I.V., and Peña, J.P., Optimized selection of renewable energy sources based on regional potentials in Colombia: a comparative analysis of AHP and FAHP for sustainable development. International Journal of Energy Research, 2025(1), art. 9257724, 2025. DOI: https://doi.org/10.1155/er/9257724

[36] Yousefi, H., Moradi, S., Zahedi, R., and Ranjbar, Z., Developed analytic hierarchy process and multi criteria decision support system for wind farm site selection using GIS: a regional-scale application with environmental responsibility. Energy Conversion and Management: X, 22, art. 100594, 2024. DOI: https://doi.org/10.1016/j.ecmx.2024.100594

[37] Jong, F.C., and Ahmed, M.M., Multi-criteria decision-making solutions for optimal solar energy sites identification: a systematic review and analysis. IEEE Access. 2024. DOI: https://doi.org/10.1109/ACCESS.2024.3461948

[38] Dambhare, M.V., Butey, B., and Moharil, S.V., Solar photovoltaic technology: a review of different types of solar cells and its future trends. In: Journal of Physics: Conference Series, IOP Publishing. 1913(1), art. 012053, 2021. DOI: https://doi.org/10.1088/1742-6596/1913/1/012053

[39] Habib, S.M., Suliman, A.E.R.E., Al-Nahry, A.H., and Abd-El Rahman, E.N., Spatial modeling for the optimum site selection of solar photovoltaics power plant in the northwest coast of Egypt. Remote Sensing Applications: Society and Environment, 18, art. 100313, 2020. DOI: https://doi.org/10.1016/j.rsase.2020.100313

[40] Siksnelyte-Butkiene, I., Zavadskas, E.K., and Streimikiene, D., Multi-Criteria Decision-Making (MCDM) for the assessment of renewable energy technologies in a household: a review. Energies, 13(5), art. 1164, 2020. DOI: https://doi.org/10.3390/en13051164

[41] Zambrano-Asanza, S., Chumbi, W.E., Franco, J.F., and Padilha-Feltrin, A., Multicriteria decision analysis in geographic information systems for identifying ideal locations for new substations. Journal of Control, Automation and Electrical Systems, 32(6), pp. 1305–1316, 2021. DOI: https://doi.org/10.1007/s40313-021-00738-5

[42] Salomon, V.A.P., and Gomes, L.F.A.M., Consistency improvement in the analytic hierarchy process. Mathematics, 12(6), art. 828, 2024. DOI: https://doi.org/10.3390/math12060828

[43] Fajardo-Mazorra, A.P., The role of justice in Colombia's renewable energy transition: wind energy development in Wayúu territory. MSc. Theses. 76, Dartmouth College, Nuevo Hampshire, USA, [online] 2023. Available at: https://digitalcommons.dartmouth.edu/masters_theses/76

A.L. Tovar-Blanco, received received the BSc. Emg. in Forest Engineering, MSc. in Geomatics, all of them from the Universidad Nacional de Colombia, and Sp. in Environmental Project Evaluation from the Universidad Manuela Beltrán. She has worked for public institutions including DANE and ANLA, focused on spatial analysis, and the integration of GIS and remote sensing to support decision-making in environmental projects. Her research interests include: geospatial analysis, satellite image interpretation, environmental impact assessment, and the design of geoinformation workflows for environmental monitoring and project evaluation.
ORCID: 0000-0002-1167-4807

D.R. Ricardo-Herreño, received the BSc. Eng. in Chemical Engineering from the Universidad de América, and PgD. in Project Management in Engineering from the Universidad de La Salle, and Environmental Project Evaluation from the Universidad Manuela Beltrán. Professional background includes engineering and analytical roles at ANTEK S.A.S. between 2012 and 2015, followed by work in environmental management at AngloGold Ashanti Colombia from 2015 to 2017. Since 2018, he has worked at ANLA, focusing on technical assessment of agrochemical projects. His academic interests include: environmental impact assessment, chemical process evaluation, and analytical methodologies applied to regulatory decision-making.
ORCID: 0009-0007-5800-1080

D.E. Rodríguez-Vivas, received his BSc. Eng. in Chemical Engineering in 2013 from the Universidad de América and MSc. in Environmental Management in 2019 from the Universidad de los Andes. From 2010 to 2021, he worked at the Universidad de los Andes. He then served as a full-time professor from 2022 to 2023 at Universidad Manuela Beltrán and is currently the Research Coordinator for the Environmental Unit at the same University. His research interests include: solid waste, water and environmental sanitation, chemical processes, and environmental management.
ORCID: 0000-0002-7073-5438

DYNA
http://dyna.medellin.unal.edu.co/

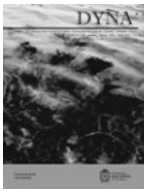

UNIVERSIDAD NACIONAL DE COLOMBIA

Evaluation of nitrogen-fixing and phosphorus-solubiling microorganisms in Astromelian (*Alstroemeria aurantiaca*), cultivation

Jaime Ramiro Hidrobo-Luna

Facultad de Ciencias Agrícolas de la Universidad Central del Ecuador. Quito, Ecuador. jhidrobo@uce.edu.ec

Received: July 29th, 2025. Received in revised form: January 30th, 2026. Accepted: February 13th, 2026.

Abstract
The Ecuadorian floriculture sector is currently facing challenges due to the decline in soil nutritional content and productivity. This situation, coupled with nitrogen (N) losses and poor soil phosphorus (P) assimilation, has led to reduced yields in ornamental species such as lily of the Incas (*Alstroemeria aurantiaca*), resulting in significant economic losses. Various alternatives were evaluated to address these issues. A Randomized Complete Block Design (RCBD) was employed using a two-factor scheme, including the A×B interaction and the intercept. The experimental conditions consisted of microbial applications at doses of 1, 2, and 3 L/ha, applied directly to the soil as a supplementary nutrient treatment. Treatment T2 (2 L/ha), which comprised a microbial consortium, exhibited the best performance. Total production costs were estimated at 3,440 USD per hectare, with an economic efficiency of 2,560 USD, which was rated as satisfactory.

Keywords: beneficial soil microbiota; absorption; phosphate-solubilizing microorganisms; nitrifying bacteria; ornamentals.

Evaluación de microorganismos fijadores de nitrógeno y solubilizadores de fósforo en el cultivo de Astromelias (*Alstroemeria aurantiaca*)

Resumen
El sector florícola ecuatoriano atraviesa dificultades debido a la disminución del contenido nutricional y productividad del suelo, esto unido a pérdidas de N y poca asimilación de P del suelo hace que disminuyan los rendimientos de especies ornamentales como astromelia (Alstroemeria aurantiaca) que provocan grandes pérdidas económicas. Se evaluaron alternativas para solucionar estas problemáticas. Se empleó un DBCA con esquema de dos factores que incluye la interacción A×B y el intercepto. Las condiciones experimentales fueron: 1, 2, 3 L/ha, de microorganismos, aplicados en directamente al suelo por aplicación suplementaria de nutrientes. El tratamiento T2 (2 L/ha), fue el que mejor se comportó, el mismo comprende una mezcla de microorganismos. Los gastos completos de producción se estimaron en 3 440 USD por hectárea. Y una eficiencia económica de 2 560 USD, estimado de satisfactoria.

Palabras clave: microbiota benéfica del suelo; absorción; fosfosolubilizadores; nitrificantes; ornamentales.

1 Introduction

Ecuador produces and exports a wide variety of ornamental species, among which rose (Rosa sp.), carnation (Dianthus caryophyllus), and alstroemeria (Alstroemeria aurantiaca) stand out [6]. The latter, belonging to the family Amaryllidaceae, occupies 0.5% of the floricultural area in Ecuador and is increasingly becoming a crop of great interest for export. It enjoys high demand in both national and international markets—particularly in countries such as Canada, Japan, the United States (accounting for 80% of exports), the Russian Federation, and the European Community—due to its vibrant colors and elegant appearance [1,2].

How to cite: Hidrobo-Luna, J.R., Evaluation of nitrogen-fixing and phosphorus-solubiling microorganisms in astromelian (Alstroemeria aurantiaca), cultivation DYNA, (93)240, pp. 108-115, January - March, 2026.

For flower growers in the Orongoloma community, located in the Cayambe canton, Pichincha province, significant nitrogen (N) losses occur after soil applications, mainly due to leaching and volatilization. This necessitates both more frequent applications and increased dosages, thereby raising production costs.

Additionally, challenges have been reported regarding the assimilation and bioavailability of phosphorus (P) by plants, which also leads to increased application costs [4,5].

The International Plant Nutrition Institute [9] emphasized that biological nitrogen fixation is gaining growing interest due to the ongoing oil crisis, as petroleum is a major energy source and raw material for ammonia (NH_3) production [8,10]. Moreover, ecological implications associated with the intensive use of nitrogen fertilizers cannot be overlooked. Phosphorus, along with nitrogen, is essential for boosting crop productivity and achieving high yields. However, despite its presence in both organic and inorganic forms in the soil, its absorption by plant roots is limited due to rapid fixation in the soil, making it difficult for plants to extract [22,23].

The use of beneficial microorganisms naturally present in the soil, as well as those applied artificially—such as nitrogen-fixing and phosphorus-solubilizing strains—represents a promising and increasingly adopted strategy worldwide. This approach provides economic, productive, and environmental benefits [1].

In this research to evaluate the application of nitrogen-fixing and phosphorus-solubilizing microorganisms in Alstroemeria aurantiaca cultivation in the Cayambe canton, Pichincha province, in order to improve crop quality and yield.

To determine the amount of nitrogen fixed in the soil through the application of nitrogen-fixing microorganisms in alstroemeria cultivation.

To determine the extent of phosphorus solubilization in the soil through the application of phosphorus-solubilizing microorganisms in alstroemeria cultivation

To establish a methodology for improving productivity and yield in alstroemeria cultivation using efficient microorganisms.

To conduct an economic evaluation of the application of nitrogen-fixing and phosphorus-solubilizing microorganisms.

2 Materials and methods

2.1 Location and Description of the experimental area

This research was conducted at the "MILFLORES" farm, located in the Orongoloma community of Cayambe canton, Pichincha province, Ecuador. The geographical coordinates are: 0°02′16″ N latitude, 78°07′02″ W longitude, and an altitude of 3,000 meters above sea level. The area has an average annual temperature of 15 °C, annual precipitation of 1,200 mm, relative humidity of 65%, wind speed of 10 m/s, and total annual sunshine duration of approximately 2,000 hours.

2.2 Plant material

The study involved 1,200 alstroemeria plants obtained through hybridization and propagation of the 'Esmeraldas' group, grown in a crop established one year prior to the experiment.

2.3 Studied variables

2.3.1 Variable A:

Nitrogen-fixing microorganisms (Azospirillum, Azotobacter spp., and Rhizobium) and phosphorus-solubilizing microorganisms (Pseudomonas fluorescens).

2.3.2 Variable B:

Dose 1: 1 L/ha; Dose 2: 2 L/ha; Dose 3: 3 L/ha

2.4 Treatments

2.4.1 Experimental design

A Completely Randomized Block Design (CRBD) was used, consisting of four treatments in a factorial arrangement (A × B) + 1, with three replications per treatment (Table 1).

Statistical differences among treatments were determined using Tukey's test at a 5 % significance level.

Data were processed using the INFOSTAT statistical software.

2.4.2 Experimental unit characteristics

Area per experimental unit: 24 m²
Total experimental area: 288 m² (24 m² × 12)
Total trial area: 600 m²
Planting density: 0.30 m × 0.80 m (20,000 plants/ha)
Number of plants per m²: 2
Number of plants per experimental unit: 100
Total number of experimental units: 12

2.4.3 Analysis of variance (ANOVA)

The variables were analyzed using a one-way Analysis of Variance (ANOVA), according to the following scheme (Table 2).

Table 1.
Treatments applied in the study

Treatment	Organic Amendments (cc/experimental unit)	Dose (L/ha)	Description
1	5	1	Beneficial Microorganisms
2	10	2	Beneficial Microorganisms
3	15	3	Beneficial Microorganisms
4	0	0	Control (Untreated)

Source: own elaboration

Table 2.
ANOVA Scheme

Source of Variation	Degrees of Freedom (DF)
Total	11
Replications	2
Treatments	3
Microorganisms (Factor A)	0
Dose (Factor B)	2
Interaction (A × B)	0
Control vs. Others	1
Experimental Error	6
Coefficient of Variation	(%)

Source: own elaboration

2.4.4 Trial Management

The trial area was set up with a total surface of 600 m², including twelve 30-meter beds (replications), which constituted the experimental units and corresponded to the different treatments. The Alstroemeria crop had been established on 30 beds and had been in production for approximately five years at the time of the study.

2.4.5 Application of microorganisms in the experimental units

A ¾-inch VENTURI injector, delivering 2 L/min, was used for the liquid application of microorganisms via drench (soil drenching) according to the proposed

The solution was applied directly to the center of each bed, as close as possible to the plant roots to maximize uptake.

A total of 4 L of microbial solution was applied per experimental unit. Applications were made weekly for 13 weeks, following the same procedure for all treatments and replications.

2.4.6 Fertilization

Fertilization was carried out according to the crop's standard schedule: 2 kg of compound fertilizer 15-15-15.

The highest number of shoots (N-P-K) were applied monthly per 30-meter bed. The solid amendment was manually applied and incorporated into the soil with a manual aerator.

2.4.7 Irrigation

Irrigation was performed using a shower head attached to a ¾-inch hose to dissolve and distribute the incorporated fertilizer. Irrigation was applied every other day during cloudy or rainy conditions, and daily during dry periods.

2.4.8 Pest and disease control

Phytosanitary control was not required during the study period, as no pests or diseases were observed that could directly affect production.

2.4.9 Harvest

Harvesting was done manually by collecting flower stems ready for cutting. The stems were grouped into bunches of ten, placed in protective sleeves, and packaged for sale in local florists and for export.

2.4.10 Evaluated variables

Number of shoots per m²

Quantity of nitrogen fixed after microorganism application

Amount of phosphorus available to the plant at the end of the study

Harvested stem length doses

2.4.11 Economic analysis

An economic evaluation was conducted to assess the cost-effectiveness of using nitrogen-fixing and phosphorus-solubilizing microorganisms under the different treatment conditions.

3 Results and discussion

3.1 Number of Shoots/m²

In the ANOVA (Table 3), significant differences were observed for the control in relation to the other treatments, as well as between treatments and doses. However, there was no significant interaction between microorganisms × Dose was presented by Treatment 2 (T2), where efficient microorganisms were applied at a dose of 2 L/ha, resulting in 10 shoots/m². The Coefficient of Variation (CV) was 8.8 %, with an average of 8 shoots/m².

The laboratory analysis results for Treatment 1 (T1) (Table 4) show that 433.52 ppm of N were fixed, retaining 137.52 ppm of N, compared to the initial laboratory analysis which reported 296 ppm of N in the soil.

As can be observed, the N values after the application of microorganisms are at adequate levels for normal growth.

These same analyses show an Electrical Conductivity (EC) of 3.98 dS/m, which indicates an accumulation of nutrients. According to [12] and [17], this value could be due to an insufficient quantity of microorganisms in the soil to benefit the availability of present nutrients. According to [13], this crop tolerates maximum ranges of up to 3 dS/m (Table 5).

Table 3.
Average number of astromelia shoots/m²

Treatments			
No.	**Microorganisms**	**Dose (L/ha)**	**Number of Shoots**
2.	Microorganisms	10 a	2
3.	Microorganisms	9 ab	3
1.	Microorganisms	7 bc	1
4.	Absolute control	6 c	0
C.V. (%) = 8.8			

Means with the same letter are not statistically different according to Tukey's test at 5% significance
Source: own elaboration

Table 4.
Amount of N fixed after microorganism applications

Soil Analysis											
SYMBOL	***pH***	***EC***	***MOS***	***NH4***	***NO3***	***P***	***K***	***Ca***	***Mg***	***Na***	***Cu***
UNIT	uds	dS/m	%	ppm	ppm	ppm	meq/100g	meq/100g	meq/100g	meq/100g	ppm
RESULT	6,32	2,31	4,52	296,00	158,4	3,07	27,12	3,48	0,76	6,32	
INDICATORS	B	A	OK		A	A	OK	A	OK	B	A

SYMBOL	*Fe*	*Mn*	*Zn*	*B*	*S*	*Fe/Mn*	*Ca/Mg*	*Mg/K*	*Ca+Mg/K*	*Suma Bases*
UNIDAD	ppm	ppm	Ppm	ppm	ppm	ppm	meq/100g	meq/100g	meq/100g	meq/100g
RESULTADO	159,7	14,23	39,4	1,42	69,14	11,22	7,8	1,13	30,71	34,42
INDICADOR	A	A	A	OK	OK	A	A	B	A	OK

Texture		
SAND	LIMO	CLAY
60	30	8
LOAMY SAND		

A: high;
B: low;
OK: adecuate
m/g: miligrams per liter;
meq/100g: miliequivalents per hundred grams
uds: units;
%: porcentaje

Source: own elaboration

Table 5.
Results of the soil sample sent to the laboratory before the start of the investigation

Soil Analysis											
SYMBOL	***pH***	***EC***	***MOS***	***NH4***	***NO3***	***P***	***K***	***Ca***	***Mg***	***Na***	***Cu***
UNIT	uds	dS/m	%	ppm	ppm	ppm	meq/100g	meq/100g	meq/100g	meq/100g	ppm
RESULT	6,64	3,98	2,46	3,5	430,02	73,82	5,37	21,5	4,23	1,22	13,07
INDICATOR	OK	A	B	B	A	A	A	A	OK	B	A

SYMBOL	*Fe*	*Mn*	*Zn*	*B*	*S*	*Fe/Mn*	*Ca/Mg*	*Mg/K*	*Ca+Mg/K*	*Suma Bases*
UNIT	ppm	ppm	ppm	ppm	ppm	ppm	meq/100g	meq/100g	meq/100g	meq/100g
RESULT	159,7	12,95	9,42	1,47	43,54	15,11	5,09	0,79	16,92	32,32
INDICATOR	A	OK	OK	OK	OK	A	A	B	A	OK

Texture		
SAND	LIMO	CLAY
60	32	8
LOAMY SAND		

A: high;
B: low;
OK: adecuate
m/g: miligrams per liter;
meq/100g: miliequivalents per hundred grams
uds: units;
%: porcentaje

Source: own elaboration

Table 6.
Results of the soil analyses performed in the experiment

Soil Analysis											
SYMBOL	***pH***	?	***MO***	***H4***	***NO3***						
UNIT	s	/m	%	ɔm	ppm	ɔm	100g	ı/100g	′100g	100g	m
RESULT	5,36	7	2,59	9	332,58	7,72					,33
INDICATOR					A	OK					

SYMBOL	*Fe*	*Mn*	*Zn*	*B*	*S*	*Fe/Mn*	*Ca/Mg*	*Mg/K*	*Ca+Mg/K*	*Suma Bases*
UNIT	ppm	ppm	ppm	ppm	ppm	ppm	meq/100g	meq/100g	meq/100g	meq/100g
RESULT	205,5	9,85	7,07	0,9	41,1	36	8,07	0,67	13,02	26,28
INDICATOR	A	OK	OK	B	OK		A	B	OK	OK

Texture		
SAND	LIMO	CLAY
60	34	6
LOAMY SAND		

A: high;
B: low;
OK: adecuate
m/g: miligrams per liter;
meq/100g: miliequivalents per hundred grams
uds: units;
%: porcentaje

Source: own elaboration

In the results for T2 (Table 6), it is observed that 332.58 ppm of N were fixed, retaining 2,9 ppm of N in the soil. Also, the EC is 2.87, which indicates a sufficient quantity of nutrients for plant consumption and is within the crop's tolerance range for better yield. [19] and [13,20] obtained the best results using medium doses of microorganisms, as low doses risk not all nutrients being solubilized for proper plant assimilation. High doses, however, solubilize very quickly and effectively, and the high quantity of microorganisms leads to rapid competition, but without more elements to work on, they die, which does not allow for adequate function and increases costs.

Regarding the results for T3 (Table 7), 454.35 ppm of N were fixed, a difference of 158.35 ppm of N compared to the initial investigation results. The laboratory analysis for this treatment showed an EC value of 3.66, which, like Treatment 1, is above the crop's tolerance range.

Table 7.
Results of soil analyses performed in treatment three

Soil Analysis											
SYMBOL	***pH***	***EC***	***MOS***	***NH4***	***NO3***	***P***	***K***	***Ca***	***Mg***	***Na***	***Cu***
UNIT	uds	dS/m	%	ppm	ppm	ppm	meq/100g	meq/100g	meq/100g	meq/100g	ppm
RESULT	6,26	3,66	2,43	5,65	448,7	61,77	3,07	20,06	3,84	0,81	15,35
INDICATOR	B	A	B	B	A	A	A	OK	OK	B	A

SYMBOL	*Fe*	*Mn*	*Zn*	*B*	*S*	*Fe/Mn*	*Ca/Mg*	*Mg/K*	*Ca+Mg/K*	*Suma Bases*
UNIT	ppm	ppm	ppm	ppm	ppm	ppm	meq/100g	meq/100g	meq/100g	meq/100g
RESULT	185,8	9,81	11,78	1,61	97,44	18,96	5,23	1,25	25,09	27,78
INDICATOR	A	OK	OK	OK	A	A	A	B	A	OK

Texture		
SAND	LIMO	CLAY
60	32	8
LOAMY SAND		

A: high;
B: low;
OK: adecuate
m/g: miligrams per liter;
meq/100g: miliequivalents per hundred grams
uds: units;
%: porcentaje

Source: own elaboration

Table 8.
Results of soil sample treatment 4. End of the investigation

Soil Analysis											
SYMBOL	***pH***	***EC***	***MO***	***NH4***	***NO3***	***P***	***K***	***Ca***	***Mg***	***Na***	***Cu***
UNIT	uds	dS/m	%	ppm	ppm	ppm	meq/100g	meq/100g	meq/100g	meq/100g	ppm
RESULT	6,3	0,55	2,16	1,05	0,79	44,33	3,07	12,81	0,47	0,55	13,02
INDICATOR	B	OK	B	B	B	OK	A	OK	B	B	A

SYMBOL	*Fe*	*Mn*	*Zn*	*B*	*S*	*Fe/Mn*	*Ca/Mg*	*Mg/K*	*Ca+Mg/K*	*Suma Bases*
UNIT	ppm	ppm	ppm	ppm	ppm	ppm	meq/100g	meq/100g	meq/100g	meq/100g
RESULT	416,2	6,77	3,1	0,12	18,9	61,48	27,09	0,15	1,97	16,9
INDICATOR	A	OK	OK	B	OK	A	A	B	B	OK

Texture		
SAND	LIMO	CLAY
64	28	8
LOAMY SAND		

A: high;
B: low;
OK: adecuate
m/g: miligrams per liter;
meq/100g: miliequivalents per hundred grams
uds: units;
%: porcentaje

Source: own elaboration

Table 9.
Results of soil sample treatment 1, P fixation

Soil Analysis											
SYMBOL	***pH***	***EC***	***MO***	***NH4***	***NO3***	***P***	***K***	***Ca***	***Mg***	***Na***	***Cu***
UNIT	uds	dS/m	%	ppm	ppm	ppm	meq/100g	meq/100g	meq/100g	meq/100g	ppm
RESULT	6,64	3,98	2,46	3,5	430,02	73,82	5,37	21,5	4,23	1,22	13,07
INDICATOR	OK	A	B	B	A	A	A	A	OK	B	A

SYMBOL	*Fe*	*Mn*	*Zn*	*B*	*S*	*Fe/Mn*	*Ca/Mg*	*Mg/K*	*Ca+Mg/K*	*Suma Bases*
UNIT	ppm	ppm	ppm	ppm	ppm	ppm	meq/100g	meq/100g	meq/100g	meq/100g
RESULT	159,7	12,95	9,42	1,47	43,54	15,11	5,09	0,79	16,92	32,32
INDICATOR	A	OK	OK	OK	OK	A	A	B	A	OK

Texture		
ARENA	LIMO	CLAY
60	32	8
LOAMY SAND		

A: high;
B: low;
OK: adecuate
m/g: miligrams per liter;
meq/100g: miliequivalents per hundred grams
uds: units;
%: porcentaje

Source: own elaboration

The results for the control, Treatment 4 (T4), shown in Table 8, indicate that 1.84 ppm of N were fixed in the soil. This data corroborates the problem identified at the beginning of the investigation. It suggests that alstroemeria growers do not achieve adequate N levels in the soil before the next fertilizer application (every 20 days), requiring additional N inputs, which increases production costs. In Ecuador, some floriculturists initially apply 296 ppm of N with fertilizer, but this element is lost over time, reaching 1.84 ppm of N by the next application.

According to [14] and [15,18], the EC in this treatment was 0.55 dS/m, and the results verify that microorganisms are fundamental for agriculture as they make elements retained in the soil available for better plant utilization.

Amount of P available for the plant at the end of the investigation

Similar to N fixation, P content in the soil was assessed based on laboratory results, summarized below.

According to initial results, 73,82 ppm of P were fixed in the soil. In the T1 results (Table 9), 73.82 ppm of P were obtained, a difference of 47,72 compared to the initial analysis (Table 10), indicating that this amount could have been solubilized by microorganism activity.

Similarly, T2 (Table 11) reports 61,77 ppm of P, indicating that 109.49 ppm of P were solubilized for plant uptake, compared to the initial analysis.

Furthermore, the results for T3 (Table 12) show P values of 44,33 ppm, indicating that 106,1 ppm of this element were solubilized.

Table 10.
Results of soil sample treatment 1, for P fixation

Soil Analysis											
SYMBOL	***pH***	***EC***	***MO***	***NH4***	***NO3***	***P***	***K***	***Ca***	***Mg***	***Na***	***Cu***
UNIT	uds	dS/m	%	ppm	ppm	ppm	meq/100g	meq/100g	meq/100g	meq/100g	ppm
RESULT	6,36	2,87	2,59	2,9	332,58	47,72	3,58	19,4	2,4	0,9	13,33
INDICATOR	B	A	B	B	A	OK	A	OK	OK	B	A

SYMBOL	*Fe*	*Mn*	*Zn*	*B*	*S*	*Fe/Mn*	*Ca/Mg*	*Mg/K*	*Ca+Mg/K*	*Suma Bases*
UNIT	ppm	ppm	ppm	ppm	ppm	ppm	meq/100g	meq/100g	meq/100g	meq/100g
RESULT	205,5	9,85	7,07	0,9	41,1	20,86	8,07	0,67	13,02	26,28
INDICATOR	A	OK	OK	B	OK	A	A	B	OK	OK

Texture		
ARENA	LIMO	CLAY
60	34	6
LOAMY SAND		

A: high;
B: low;
OK: adecuate
m/g: miligrams per liter;
meq/100g: miliequivalents per hundred grams
uds: units;
%: porcentaje

Source: own elaboration

Table 11.
Results of soil sample treatment 3 for P fixation

Soil Analysis											
SYMBOL	***pH***	***EC***	***MO***	***NH4***	***NO3***	***P***	***K***	***Ca***	***Mg***	***Na***	***Cu***
UNIT	uds	dS/m	%	ppm	ppm	ppm	meq/100g	meq/100g	meq/100g	meq/100g	ppm
RESULT	6,26	3,66	2,43	5,65	448,7	61,77	3,07	20,06	3,84	0,81	15,35
INDICATOR	B	A	B	B	A	A	A	OK	OK	B	A

SYIMBOL	*Fe*	*Mn*	*Zn*	*B*	*S*	*Fe/Mn*	*Ca/Mg*	*Mg/K*	*Ca+Mg/K*	*Suma Bases*
UNIDAD	ppm	ppm	ppm	ppm	ppm	ppm	meq/100g	meq/100g	meq/100g	meq/100g
RESULTADO	185,8	9,81	11,78	1,61	97,44	18,96	5,23	1,25	25,09	27,78
INDICADOR	A	OK	OK	OK	A	A	A	B	A	OK

Textura		
SAND	LIMO	ARCILLA
60	32	8
FRANCO ARENOSO		

A: high;
B: low;
OK: adecuate
m/g: miligrams per liter;
meq/100g: miliequivalents per hundred grams
uds: units;
%: porcentaje

Source: own elaboration

Table 12.
Resultados del tratamiento 3 para fijación de P

Soil Analysis											
SYMBOL	***PH***	***EC***	***MO***	***NH4***	***NO3***	***P***	***K***	***Ca***	***Mg***	***Na***	***Cu***
UNIT	uds	dS/m	%	ppm	ppm	ppm	meq/100g	meq/100g	meq/100g	meq/100g	Ppm
RESULT	6,3	0,55	2,16	1,05	0,79	44,33	3,07	12,81	0,47	0,55	13,02
INDICATOR	B	OK	B	B	B	OK	A	OK	B	B	A

SYMBOL	*Fe*	*Mn*	*Zn*	*B*	*S*	*Fe/Mn*	*Ca/Mg*	*Mg/K*	*Ca+Mg/K*	*Suma Bases*
UNIT	ppm	ppm	ppm	ppm	ppm	ppm	meq/100g	meq/100g	meq/100g	meq/100g
RESULT	416,2	6,77	3,1	0,12	18,9	61,48	27,09	0,15	1,97	16,9
INDICATOR	A	OK	OK	B	OK	A	A	B	B	OK

Textura		
SAND	LIMO	ARCILLA
64	28	8
FRANCO ARENOSO		

A: high;
B: low;
OK: adecuate
m/g: miligrams per liter;
meq/100g: miliequivalents per hundred grams
uds: units;
%: porcentaje

Source: Own elaboration

Table 13.
Average harvested stem length in alstroemeria cultivation

No.	Treatments	Dose (L/ha)	m
2.	Microorganisms	2	1.21 a
3.	Microorganisms	3	1.09 ab
1.	Microorganisms	1	0.70 ab
4.	Absolute Control	0	0.65 b
C.V. (%) 8.8			

Averages with the same letter do not differ statistically according to Tukey's test at 5%.
Source: own elaboration

In T4 a P value of 44.33 ppm is observed, indicating that 113.67 ppm of P were solubilized.

3.2 Harvested stem length

The ANOVA (Table 13) revealed highly significant differences among treatments, doses, and the control vs. the rest; however, there was no difference for microorganisms or the interaction (Microorganisms x Dose). The Coefficient of Variation (CV) was 14.9%, with an average of 0.913 m. The highest value was observed with the application of efficient microorganisms at a dose of 2 L/ha, with a value of 1.21 m, being statistically superior to the other treatments.

3.3 Economic analysis

According to the economic analysis of the treatments (Table. 14), T2 (efficient microorganisms, at a dose of 2 L/ha) could improve income and production of Alstroemeria cultivation, as it presented the best benefit compared to the other treatments.

Additionally, a net profit of 2,560 USD/production cycle/ha was obtained. T1 and T4 had lower production costs, but also lower net profits. T3 had higher production costs than T2, and its net profit was higher than T1 and T4, but lower than T2.

3.4 Discussion

This research determined that stem length was greater with the application of efficient microorganisms at a concentration 2 L/ha. The significance lack for the microorganism by dose interaction, according to [14,17] and [16, 18], can be attributed to the fact that microorganisms release and make available existing elements in the soil; after this stage, microorganisms behave similarly regardless of their quantity in the soil, because once their work is done, they perform another function, which is to stimulate plant growth and development.

The concentration of microorganisms per liter of commercial product (GEOFIX) was analyzed, showing the presence of the following quantities of microorganisms in Colony Forming Units per milliliter (CFU/ml):

1 x 10^{12} CFU/ml of Azospirillum
1 x 10^{12} CFU/ml of Azotobacter;
1 x 10^{12} CFU/ml of Rhizobium,
1 x 10^{12} CFU/ml of Pseudomonas fluorescens

[17] and [19, 20] determined that microorganisms are capable of producing an enzyme that makes atmospheric N uptake more effective.

Regarding the number of shoots per experimental unit, the highest value was also achieved with the application of efficient microorganisms at a dose of 2 L/ha. This significance is attributed to the fact that microorganisms stimulate the production of auxins, cytokinins, and gibberellins, which act as growth regulators and aid in the production of this variable, helping to increase sprouting [7,20] and [10,21] established that

Azotobacter, Azospirillum, and Rhizobium work well together and have good mobility in the soil, stimulating plant growth and nutrient availability, thereby improving yields [21].

These efficient microorganisms, incorporated into the soil via drench once a week, fixed 333.64 ppm of N, according to soil analysis results, demonstrating that microorganisms help maintain adequate soil fertility and make nutrients available for plant uptake according to their needs and requirements. According to [18] and [19] this is because Rhizobium bacteria form nodules in roots to capture and fix atmospheric N, while Azotobacter and Azospirillum have the ability to adhere to roots and fix N, stimulating growth.

According to soil analysis results, 110.28 ppm of P were solubilized with the application of Geofix, which contains

Pseudomonas fluorescens in its composition.

According to the same author, this is because these types of microorganisms are characterized by producing acids and enzymes that help regulate soil pH and thus solubilize P retained in soil colloids, making it available to the plant.

Finally, the economic analysis of the treatments shows that the application of efficient microorganisms at a dose of 2 L/ha is the most recommended for improving Alstroemeria cultivation production and, consequently, the economic income of growers, as it presents a net benefit of 2,560 USD/ha, which is superior to other treatments and the control.

Table 14.
Economic analysis of the evaluated treatments

Trat	Organic Amendment	Dose (L/ha)	Yield (stems/ha)	Production Value (USD)	Production Costs (USD)	Net Benefit (USD)
				Fixed	**Variables**	**Total**
T1	Microorganisms	1	70,000	4,200	3,200	120
T2	Microorganisms	2	100,000	6,000	3,200	240
T3	Microorganisms	3	80,000	4,800	3,200	360
T4	Control	0	60,000	3,600	3,200	0

Alstroemeria stem value: 0.06 USD; Microorganism cost: 10 USD/L.
Source: own elaboration

4 Conclusions

The treatment that yielded the best results in terms of crop quality and yield was the weekly application of efficient microorganisms at a dose of 2 L/ha, achieving a N fixation of 335.48 ppm.

A N fixation of 333.64 ppm was achieved, compared to the Control (T4) which reported a content of 1.48 ppm of N.

Beneficial microorganisms, Azotobacter, Rhizobium, Azospirillum, and Pseudomonas fluorescens, help improve soil fertility.

T2 performed best in terms of P solubilization, with a value of 47.72 ppm.

110.28 ppm of P were solubilized, considering that at the beginning of the investigation, 158.4 ppm of P was fixed in this soil.

The 2 L/ha dose of efficient microorganisms showed the best results in terms of stem length, reporting sizes of 1.21 m, unlike the control which reported a length of 0.65 m.

The highest number of shoots/m² was achieved with the application of Geofix at a dose of 2 L/ha, with a sprouting of 10 stems/m² compared to the control which presented only 6 shoots/m².

It was established that the best method to inoculate efficient microorganisms into the soil and improve the quality and yield of alstroemeria cultivation was weekly application directly to the plants via drench.

The application of efficient microorganisms at a dose of 2 L/ha presented the highest net economic benefit, with a value of 2,560 USD/ha.

With this additional N incorporation, the net cost-benefit of the control would leave a value of 184 USD/ha.

References

[1] Gualavisí, P., and Rivera, M., Benchmarking para optimizar la exportación de rosas ecuatorianas frente al liderazgo de Países Bajos. Revista Economía y Negocios UTE, 15(1), pp. 124-143, 2024. DOI: https://doi.org/10.29019/eyn.v15i1.1270

[2] Manotoa-Mejía, M., and Pérez-Soto, J., Sector florícola: Contribución al desarrollo socioeconómico del Ecuador y su competitividad internacional. GADE: Revista Científica, 5(1), pp. 756-772, [en línea]. 2015-2024. Disponible en: https://revista.redgade.com/index.php/Gade/article/download/653/382/.(2025).

[3] Andrango, E., Creación de una empresa para la producción y comercialización de flores de verano "astromelias". Quito, Ecuador. (2012).

[4] Uriarte-Rodríguez, L.N., Bravo-Carrasco, A.R., Sellán-Burgos, A.R., and Villegas-Pilay, Y.E., Desarrollo del sector florícola en las exportaciones no tradicionales del Ecuador. ResearchGate, [en línea]. 2018-2023. Disponible en: https://www.researchgate.net/publication/396948010_Desarrollo_del_Sector_Floricola_en_las_Exportaciones_no_Tradicionales_del_Ecuador. (2025).

[5] Suárez-Avilés, M.W., Análisis de las exportaciones de flores entre Ecuador y sus socios comerciales de Europa bajo el modelo gravitacional. Tesis de Grado, Universidad Agraria del Ecuador, [en línea]. 2012-2022. Disponible en: https://cia.uagraria.edu.ec/Archivos/SUAREZ%20AVILES%20PEREZ%20MELANY%20WENDY.pdf. (2024).

[6] Expoflores, Reporte estadístico de exportaciones florícolas: cierre 2025 y proyecciones San Valentín 2026. Asociación Nacional de Productores y Exportadores de Flores del Ecuador, [en línea]. 2026. Disponible en: https://www.expoflores.com/recursos.

[7] Chiriboga, S., Ecuador y sus flores. Quito, Ecuador, 2013.

[8] Espinoza, J., Manual internacional de fertilidad de suelos, Barcelona, España, 2014.

[9] Freire, M., Evaluación de fertilización de NPK-Ca en el cultivo de astroemeria, Tungurahua, Ecuador, 2012.

[10] International plant nutrition, Barcelona, 2006.

[11] Hualpa, G., Carrión-Paladines, V., and Jiménez, L., Farmers' indigenous knowledge of soil management in an altitudinal gradient in Southern Ecuador. Sustainability, 17(11), art. 4983, 2025. DOI: https://doi.org/10.3390/su17114983.

[12] Martínez, M., Búsqueda y producción de microorganismos benéficos para la agricultura, Colombia, 2005.

[13] Pérez, J., Caracterización y efecto de Azotobacter, Azospirillum y Pseudomonas asociadas a Ipomoea batatas del Caribe colombiano, Córdoba, Colombia, 2017.

[14] Puebla, H., Cultivo de Alstromelia edition 3ra, 2003.

[15] Sánchez, A., Mejora de la eficacia de los cultivos a través de microorganismos, sustancias húmicas y aminoácidos, Alicante, España, art. 3644, 2002. DOI: https//doi.org/10.29312/remexca.v16i4.3644

[16] Suquilanda, M., Producción de rosa y flores de corte orgánicas en Ecuador, Quito, Ecuador, 2009.

[17] Beltrán-Pineda, M.E., and Bernal-Figueroa, A.A., Evaluación agronómica de bacterias fijadoras de nitrógeno aisladas de suelos andinos en plántulas de lechuga y tomate. Anales de la Facultad de Ciencias agrarias 23(1), pp. 47-52, 2021. DOI: https://doi.org/10.18004/investig.agrar.2021.junio.2301680.

[18] Beltrán-Pineda, M.E., and Bernal-Figueroa, A.A., Biofertilizantes: alternativa biotecnológica para los agroecosistemas. Revista Mutis, 12(1), pp. 1-18. 2022. DOI: https://doi.org/10.21789/22561498.22561771.

[19] Simbaña, B., Rivera, J., and Caicedo, S., Diversity of nitrogen-fixing and phosphorus-solubilizing bacteria associated with the rhizosphere of Andean crops in Ecuador. Brazilian Journal of Biology, 83, art. 271105, 2023. DOI: https://doi.org/10.1590/1519-6984.271105.

[20] Rodríguez-Díaz, L., and Pérez-Soto, J., Efecto de rizobacterias promotoras del crecimiento vegetal en plantas sometidas a condiciones de estrés hídrico y nutricional. Alianzas y Tendencias BUAP, 8(31), [en línea]. 2023. Disponible en: https://www.aytbuap.mx/aytbuap-831/efecto-de-rizobacterias-promotoras-del-crecimiento-vegetal-en-plantas.

[21] Hidrobo-Luna, J.R., and Túqueres-Álvarez, M.M., Evaluación de microorganismos fijadores de nitrógeno y solubilizadores de fósforo en el cultivo de Astromelias (Alstroemeria aurantiaca), Cayambe, Pichincha, Tesis de Maestría, Universidad Central del Ecuador. Red de Investigadores Ecuatorianos, [en línea]. 2018. Disponible en: https://redi.cedia.edu.ec/document/230846.

[22] Poma-Chamana, R., Vilca-Gamarra, C., Hermoza, N., Mercado, R., Mejía, S., Quispe, K.,and Rengifo, R., Estimation and mapping of soil fertility index in arid agricultural environments of the Tambo Valley using regression kriging. Frontiers in Soil Science, *5*, art. 1706974. 2025. DOI: https://doi.org/10.3389/fsoil.2025.1706974

[23] Villacis-Fajardo, J.D., Arévalo-López, L.A., Rengifo-Panduro, A.M., and Villacis-Fajardo, N.A., Fertilidad natural de los suelos aluviales en la Amazonía. Revista Peruana de Investigación Agropecuaria, *2*(1), art. 32. 2023. DOI: https://doi.org/10.56926/repia.v2i1.32

J.R. Hidrobo-Luna, received the BSc. Eng. in Agronomy Engineering in 1996 (ISCAH), MSc. in Vegetal Biology in 2000 from the Havana University, Cuba, and the PhD, in Agricultural Sciences, Specialty in Vegetal Biotechnology in 2006 from the Havana Agrarian University. Researcher at the National Institute of Agricultural Sciences (INCA), Principal Investigator at the National Institute of Tropical Agricultural Research (INIFAT) of Cuba (2007-2010). National Director of the laboratory service of AGROCALIDAD, Quito-Ecuador (2011). Full professor and researcher at the Faculty of Agricultural Sciences of the Central University of Ecuador, Quito, Ecuador (2013 to present).
ORCID: 0000-0001-8116-5824

DYNA
http://dyna.medellin.unal.edu.co/

UNIVERSIDAD NACIONAL DE COLOMBIA

Hybrid material of recycled plastics (PET and PP) and aggregates for the manufacture of sustainable paving blocks

María José Valarezo-Ulloa[a], Freddy Eliazar Tinoco-Tinoco[b], Julio Cesar Granda-Pardo[c], María del Cisne Veintimilla-Ortega[d], Katty Yadira Paucar-Carrión[e], Érika Lucia González-Carrión[f] & Galo Antonio Ojeda-Brito[g]

[a] *Carrera de Agronegocios, Grupo de Nuevos Materiales, Universidad Nacional de Loja, Loja, Ecuador. maria.jose.valarezo@unl.edu.ec*
[b] *Carrera de Agronomía, Grupo de Nuevos Materiales, Universidad Nacional de Loja, Loja, Ecuador. freddy.tinoco@unl.edu.ec*
[c] *Carrera de Economía, Universidad Nacional de Loja, Loja, Ecuador. julio.granda@unl.edu.ec*
[d] *Carrera de Ingeniería Agrícola, Grupo de Nuevos Materiales, Universidad Nacional de Loja, Loja, Ecuador. maria.veintimilla@unl.edu.ec*
[e] *Carrera de Comunicación, Universidad Nacional de Loja, Loja, Ecuador. katty.y.paucar@unl.edu.ec*
[f] *Carrera de electromecánica. Universidad Nacional de Loja, Loja, Ecuador. erika.gonzalez@unl.edu.ec*
[g] *Parque Tecnológico. Universidad Técnica Particular de Loja, Loja, Ecuador. ojedagalo@gmail.com*

Received: September 19th, 2025. Received in revised form: February 16th, 2026. Accepted: February 27th, 2026.

Abstract
Sustainable construction requires innovative materials that minimize environmental impact and optimize resource use. Recycling widely discarded plastics such as polyethylene terephthalate (PET) and polypropylene (PP) offers a viable strategy to reduce waste accumulation and reliance on virgin resources. This study develops and characterizes a hybrid material made from recycled PET and PP combined with mineral aggregates for manufacturing eco-paving blocks intended for rural construction. Several mix proportions were tested, achieving compressive strengths of 20–25 MPa and flexural strengths near 10 MPa, values comparable to conventional concrete pavers but with significantly lower weight. Water absorption remained ≤1%, complying with Ecuadorian Standard INEN 3040 and European Standard UNE-EN 1338. The findings demonstrate that incorporating recycled plastics into paving blocks supports the circular economy, reduces plastic pollution, and provides lightweight, durable, and cost-efficient alternatives suitable for agricultural and rural infrastructure, contributing to more sustainable construction practices.

Keywords: sustainable construction; recycled plastics; hybrid materials; rural pavements

Material híbrido de plásticos reciclados (PET y PP) y áridos para la fabricación de adoquines sostenibles

Resumen
La construcción sostenible exige materiales innovadores que reduzcan el impacto ambiental y promuevan el uso eficiente de los recursos. El reciclaje de plásticos ampliamente desechados, como el tereftalato de polietileno (PET) y el polipropileno (PP), surge como una estrategia viable para disminuir la acumulación de residuos y la extracción de recursos vírgenes. Este estudio desarrolla y caracteriza un material híbrido elaborado a partir de PET y PP reciclados combinados con áridos para fabricar eco-adoquines destinados a edificaciones rurales. Se evaluaron distintas proporciones de mezcla, obteniéndose resistencias a compresión de 20–25 MPa y resistencias a flexión cercanas a 10 MPa, valores comparables a los de adoquines de hormigón, pero con un peso significativamente menor. La absorción de agua fue ≤1%, cumpliendo con la NTE INEN 3040 y la norma europea UNE-EN 1338. Los resultados evidencian que incorporar plásticos reciclados en elementos constructivos impulsa la economía circular y ofrece materiales livianos, resistentes y de bajo costo adecuados para infraestructura rural sostenible.

Palabras clave: construcción sostenible; plásticos reciclados; materiales híbridos; pavimentos rurales.

How to cite: Valarezo-Ulloa, M.J., Tinoco-Tinoco, F.E., Granda-Pardo, J.C., Veintimilla-Ortega, M.delC., Paucar-Carrión, K.Y., González-Carrión, E.L., and Ojeda-Brito, G.A., Hybrid material of recycled pastics (PET and PP) and ággregates for the manufacture of sustainable paving blocks DYNA, (93)240, pp. 116-121, January - March, 2026.

1 Introduction

The increasing accumulation of plastic waste represents one of the most critical environmental challenges of the 21st century. Globally, millions of tons of single-use plastics, such as polyethylene terephthalate (PET) and polypropylene (PP), end up in landfills or in natural environments, generating severe impacts on ecosystems and human health. Faced with this problem, the circular economy approach proposes sustainable strategies such as reuse, recycling, and recovery of materials to extend their useful life cycle and reduce pressure on natural resources.

In 2021 alone, the global production of plastics increased by 4% more than the previous year, to over 390.7 million tons, after stagnation in 2020 due to the Covid-19 pandemic, demonstrating the continued demand for this material [1].

Despite the growing concern of environmental activists regarding global plastic pollution, the demand for plastics is expected to continue to increase. In 2021, the packaging sector had the largest share at 44%, followed by building and construction (18%), automotive (8%), electrical and electronics (7%), household, leisure and sports (7%), agriculture, livestock and gardening (4%), and others (12%), as shown in Figure 1. This is attributed to modern lifestyle, consumerism, and the fact that we are not yet fully aware of the problem that is generating the indiscriminate accumulation of plastics worldwide [2,3].

However, not everything is negative in the world of plastics; there are waste management initiatives that need support from different public and private entities, since recycling rates worldwide are still low. Lack of technology, poor resource management, lack of coherent programs, and incomplete processing of plastics have made this problem more pronounced [4,5].

Because of this, plastics recycling represents a promising option to achieve zero waste and climate-neutral production, requiring investment and innovation by the plastics value chain to develop new business models for reuse. Thus, expanding the use of recycled plastic can support the development of new technologies that depend less on fossil-based materials and contribute to reducing plastic waste accumulation in dumps, landfills, forests, rivers, and other ecosystems.

Since mechanical recycling of plastics requires less capital and fewer resources, it can be an appropriate waste management option, particularly in developing countries such as Ecuador. An important strategy for consuming this waste material is its use in rural construction projects, as recycled plastics demonstrate good mechanical strength, durability, resistance to gas penetration, low weight, ease of installation, low cost, and broad availability, making them suitable for the manufacture of a variety of products [6–7].

In construction, plastics are used in plumbing, siding, flooring, insulation, paneling, doors, windows, glazing, bathroom units, gratings, railings, and a growing range of structural as well as interior and decorative applications. However, rural buildings, unlike urban ones, must meet very specific conditions determined by their environment, socio-cultural factors, and the industries being exploited. The dwellings occupied by rural families often form an integrated unit with agricultural and livestock facilities.

This context provides a wide range of opportunities for facilities related to farming and food storage, such as corrals, terraces, reservoirs, irrigation systems, food storage tanks, silos for grain preservation, and other spaces where the use of safe, recycled plastic-based materials could be highly beneficial.

The present research seeks to address this need by providing flooring materials for rural constructions that are non-toxic, lightweight, low-cost, moisture-resistant, and demonstrate optimum physical and mechanical properties for use in a variety of applications in both housing and livestock or agricultural facilities. Two types of plastic waste were used: polypropylene (PP) and polyethylene terephthalate (PET), combined with aggregate materials to produce eco-friendly paving blocks.

The project was carried out within the framework agreement between the Centro Integral de Manejo de Residuos Sólidos del Municipio de Loja (Integrated Solid Waste Management Center of the Municipality of Loja) and the Universidad Nacional de Loja–Ecuador (National University of Loja), aiming to raise awareness of the feasibility of using waste materials to develop new building materials, thereby contributing to reducing plastic pollution, conserving natural resources, and promoting the circular economy.

2 Materials and methods

The city of Loja, Ecuador, has a garbage collection and classification system carried out by the Municipality of Loja. Polypropylene (PP) and polyethylene terephthalate (PET) bottles and containers were obtained from the Integrated Solid Waste Management Center of the Municipality of Loja, which is administered by this governmental entity. The fine and coarse aggregates were obtained from the Yamba Quarry, Malacatos parish, canton Loja–Ecuador. Ethyl alcohol (C_2H_6O, 70%) was purchased from Sigma-Aldrich for cleaning the plastics.

2.1 Obtention and preparation of raw materials

Polyethylene terephthalate (PET) and polypropylene (PP) plastic bottles and containers were collected from the Integrated Solid Waste Management Center of the Municipality of Loja (Fig. 1).

Figure 1.
Integrated Solid Waste Management Center of the Municipality of Loja.
Source: Own elaboration

Table 1.
Plastic particle size

Size of screen diameter	Dimensions (mm)
Grande	0.5
Mediano	0.25
Pequeño	0.1

Source: Own elaboration

Table 2.
Proportion of PET and PP plastic mixture for the elaboration of eco-paving blocks.

	PET	PP
% Recycled plastic mix	100	0
	75	25
	50	50
	25	75
	0	100

Source: Own elaboration

To ensure a clean and controlled surface free of mineral salts and impurities that may interfere with the adhesion and thermal–mechanical behavior of the recycled plastic matrix, distilled water was used in the washing process instead of regular tap water. The plastic waste was washed with distilled water, soap, and 70% ethyl alcohol three times and then dried at room temperature (±21°C) for 48 hours.

2.2 Plastic waste shredding process

For the shredding of the plastic material, a blade shredder was used, consisting of a hopper or inlet, a motor, and a rotor with blades and a sieve or screen. The screen was positioned to allow smaller pieces of plastic to pass through during the shredding process. The screen sizes are shown in Table 1.

Once the material was crushed, it was subjected to an oven drying process for 24 hours or until reaching a moisture content ≤ 1%.

2.3 Preparation of the eco-paving blocks

An extrusion process was used to manufacture the eco-paving blocks. The worm screw extruder consisted of a hopper for material input, a motor, a rotor, a cylinder or barrel, a 100 cm long worm screw, a head, and a nozzle of varying diameter. A working temperature range of 160°C to 260°C was established, taking into account the melting temperature of both polymers.

First, preliminary tests were carried out on blends between recycled PET (a very fragile and brittle polymer) and PP (a material with greater flexibility after reheating). The blends were prepared in the proportions shown in Table 2.

Each of the mixes was made in duplicate and evaluated for percentage water absorption, moisture, density, compressive strength, and flexural strength.

Based on preliminary tests, the 50:50 PET:PP blend was selected, then combined with different sizes of aggregate material in three proportions: 75:25%$_{\text{PLASTIC:AGGREGATE}}$, 50:50%$_{\text{PLASTIC:AGGREGATE}}$, and 25:75%$_{\text{PLASTIC:AGGREGATE}}$. For each treatment, two replicates were analyzed, and the five aforementioned variables were measured.

The fine and coarse aggregates used in this study were obtained from the Yamba Quarry, located in Malacatos parish, Loja–Ecuador. Four particle sizes were utilized: large (±10 mm), medium (±5 mm), small (±3 mm), and very small (±1 mm). These aggregates were washed, sieved, and oven-dried to ≤1% moisture, as shown in Table 3.

Table 3.
Particle size of aggregates.

AGGREGATES	PARTICLE SIZE
(FINE AND COARSE)	LARGE (±10 MM)
	MEDIUM (±5 MM)
	SMALL (±3 MM)
	VERY SMALL (±1 MM)

Source: Own elaboration

The melted mixtures were placed in stainless-steel molds with internal dimensions of 200 mm × 100 mm × 60 mm, following the specimen preparation requirements established in NTE INEN 3040:2016 for precast concrete paving units [8].

2.3.1 Aggregate characterization

Although aggregates from the Yamba Quarry are generally siliceous and calcareous in mineral nature, this study did not include a detailed chemical composition analysis of the aggregate material.

2.4 Study variables

2.4.1 Compressive strength (C)

The compressive strength test was performed following UNE 41410 [9].

Compressive strength is the maximum stress that a material can withstand under a crushing load, which is calculated by dividing the maximum load by the original cross-sectional area of a specimen in a compression test.

2.4.2 Total water absorption rate (AA)

The water absorption rate was measured following the NTE INEN 3040:2016 standard [8]. This method consists of impregnating the test specimen (Mi) with water and then suspending it in a container with water for 24 hours. The surface water of the specimen is dried and its weight (Ms) is taken, after which the specimen is placed in an oven at 100°C for 24 hours and the weight reading (Md) is taken again.

The water absorption rate is expressed as the difference between the weight of the saturated specimen minus the weight of the dry specimen and the weight of the dry specimen, expressed as a percentage. The following Eq. (1) is used to calculate the water absorption:

$$AB\ (\%) = \frac{Ms - Md}{Ms - Mi} x\ 100 \quad (1)$$

Where:
Ms = mass of the saturated unit (kg)
Mi = mass of the submerged unit (kg)
Md = mass of the oven-dried unit (kg)

2.4.3 Flexural strength (RF) and ultimate load at room temperature (±21°C), cold (±10°C), and hot (±30°C)

The flexural tensile test was performed following the procedure established in the UNE-EN 1338 [10] standard for precast concrete paving units, which defines the method for evaluating bending resistance through center-point load application. The flexural tensile test consists of the application of a vertical force (P) at a defined speed to the center of the specimen placed horizontally on two supports (L) until the specimen breaks (F). Eq. (2) is used to obtain the value of the bending tensile strength:

$$f = \frac{3PL}{2bh^2} \quad (2)$$

Where:
f = flexural tensile strength (Mpa)
P = breaking load (N)
L = span between supports (mm)
b = tile width (mm)
h = tile thickness (mm)

2.4.4 Moisture content (H)

To calculate the moisture content of the entire unit at the time the received mass is determined (when Mr is measured), the following equation (3) is used:

$$H\ (\%) = \frac{Mr - Md}{Ms - Md} x\ 100 \quad (3)$$

Where:
Mr = mass of the unit as received (kg)
Ms = mass of the saturated unit (kg)
Md = mass of the oven-dried unit (kg)

The above calculation of moisture content is only applicable to the whole unit at the time the as-received mass is determined.

2.4.5 Density (ρ)

The following equation (4) was used to calculate the density of the oven-dried unit;

$$D\ (\mathrm{kg}/m^3) = \frac{Md}{Ms - Mi} x\ 1000 \quad (4)$$

Where:
Md = mass of the oven-dried unit (kg)
Ms = mass of the saturated unit (kg)
Mi = mass of the submerged unit (kg)

3 Results

3.1 Plastic particle size

The plastic particle diameter size of 0.25 mm (Fig. 2) was selected for the production of the eco-paving blocks. This size was selected because it is the optimum size to work within the temperature range during the melting process of PET (260°C) and PP (160°C), avoiding the decomposition of the plastics during heating and ensuring the preservation of their physical–mechanical and thermo-elastic properties.

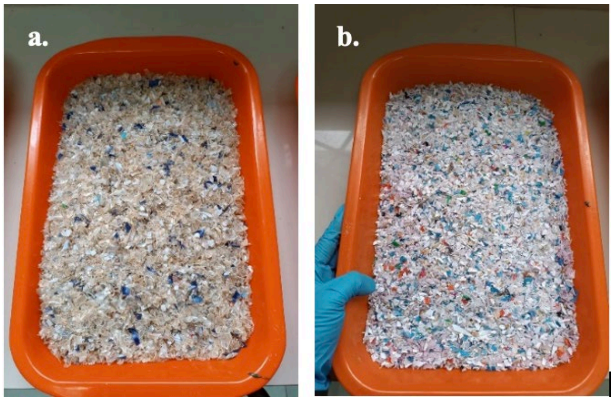

Figure 2.
Plastic waste a. polyethylene terephthalate (PET) and b. polypropylene (PP).
Source: Own elaboration

Figure 3.
Eco-pavers in their different plastic-to-aggregate ratios.
Source: Own elaboration

3.2 Characterization of the eco-paving blocks

The mixing ratio of the two types of plastic used for the elaboration of the eco-paving blocks was 50:50%$_{PET:PP}$, as they withstand greater loads under compressive and flexural stress.

This ratio was combined with each size of aggregate material in three proportions: 75:25%$_{PLASTIC:AGGREGATE}$, 50:50%$_{PLASTIC:AGGREGATE}$, and 25:75% $_{PLASTIC:AGGREGATE}$. For each treatment, two replicates were carried out, and five variables were analyzed. Fig. 3 shows the eco-paving blocks in their different plastic:aggregate ratios.

Through the determination of the water absorption percentage, it could be observed that all proportions present an absorption rate of ± 1%, which is within the permissible limits under the Ecuadorian Standard NTE INEN 3040 [8] for concrete pavers used for paving in force since 2016 (limit

< 6%). Likewise, the European Standard UNE-EN 1338 [10] for precast concrete and cement pavers states that the appropriate limit is up to 6% for climatic resistance or water absorption. A water absorption value lower than 6% ensures good resistance to low temperatures and frost. As a result, all combinations of eco-paving blocks are suitable to withstand the required design stresses and ensure optimum service life. The results are shown in Table 4.

Within agricultural constructions, a low percentage of water absorption guarantees the suitability of these blocks for facilities such as sheds, storage buildings, silos, tanks, irrigation canals, and irrigation systems. A low absorption rate ensures good floor management in livestock facilities and reduces farmers' maintenance efforts.

Since soil is one of the most commonly used materials in agricultural construction floors, eco-paving blocks made from recycled plastic can become an economical and safe alternative for better farm management. For floors that need to prevent cattle from slipping in corrals and that absorb humidity—but require periodic replacement—plastic materials represent a more durable option. This type of eco-paving block can also be used as an alternative to plastic ramps or other materials that could be costly for small producers, for example in pig fattening.

The density test was part of the water absorption test. The density of the eco-paving blocks (Table 5) directly influences the degree of resistance to factors such as weight, friction, or abrasion, and depends on the materials and proportions used in manufacturing. In the case of the eco-paving blocks, it could be observed that the density values were similar, averaging 1,900 in spite of the different sizes of sand aggregate.

This may be due to the fact that the weight and quantity of the aggregate influence the final value of density. A smaller aggregate particle size allows a greater amount of material to be incorporated into the eco-paving blocks, whereas a larger aggregate particle size results in fewer particles being incorporated. Thus, there is an inverse relationship between particle size and the amount of aggregate per block. This explains the different density results of plastic:aggregate mixtures.

Table 5 shows the results of the density analysis of the eco-paving blocks in proportions 50:50% PLASTIC:AGGREGATE in the four particle sizes.

Table 4.
Water absorption rate (AB), density (ρ), and humidity (CH%).

	Stone Size	Aggregate (%)	Plastic (%)	AB (%)	CH (%)	P (kg/m3)
50:50% PET:PP	Large (±10 mm)	25	75	0.80	10.00	1,970
		50	50	0.67	10.00	1,975
		75	25	0.65	20.00	1,977
	Medium (±5 mm)	25	75	0.70	12.50	1,974
		50	50	0.89	25.00	1,969
		75	25	0.63	20.00	1,978
	Small (±3 mm)	25	75	0.87	10.00	1,967
		50	50	0.72	20.00	1,975
		75	25	0.67	11.11	1,975
	Very small (±1 mm)	25	75	1.05	18.18	1,963
		50	50	0.83	20.00	1,970
		75	25	0.86	10.00	2,169

Source: Own elaboration

Tabla 5.
Density of eco-paving blocks in proportions 50:50% PLASTIC:AGGREGATE for the four particle sizes.

Particle size	Mix	(ρ) (kg/m³)	
Grande (±10 mm)	50:50% plástico:árido	1,963	1,975
Mediana (±5 mm)		1,961	1,969
Pequeña (±3 mm)		1,958	1,975
Muy Pequeña ±1 (mm)		1,964	1,970

Source: Own elaboration

Comparing the density values obtained for eco-paving blocks and conventional concrete blocks, which range from 2200–2400 kg/m³, it can be observed that the eco-paving blocks can be suitable for rural constructions, with the advantages of being lighter and having a high level of resistance to climatic and external factors (heat, cold, etc.), durability of the structure, adaptability of shapes, and reduced risk of deformation.

Through compression and flexural-tensile analyses (Table 6), it was possible to determine that the eco-paving blocks have good compressive strength, with values between 18 and 25 MPa. These results indicate that compressive strength is independent of the proportions of recycled plastic and aggregate. In addition, the variation in particle size did not affect compressive strength. The small aggregate ratio (±3 mm) produced the highest compressive strength values of 22.8 MPa, 23.05 MPa, and 25.07 MPa for the three ratios: 75:25%PLASTIC:AGGREGATE, 50:50%PLASTIC:AGGREGATE, and 25:75% PLASTIC:AGGREGATE, respectively.

The flexural strength of the eco-paving blocks ranged from 4.27 MPa to 11.55 MPa. Based on these results, it can be deduced that blocks with a higher percentage of recycled plastic exhibit greater flexural strength. This was consistent across the tests carried out at room temperature (±21°C), cold (±10°C), and hot (±30°C). The data obtained also exceed those established in the Spanish Standard UNE-127022 for concrete tiles, which specifies a minimum resistance of 3.5 MPa.

According to Anton et al. (2020), in their study of flexural strength of recycled plastic reinforced mortar pedestrian tiles, an average flexural strength of 3.66 MPa was obtained after 28 and 56 days. In a similar study of flexural strength in glazed tiles exposed to freeze–thaw cycles, Solano (2017) reported an average value of 24.7 MPa in each cycle evaluated.

Tabla 6.
Compressive strength (RC) and flexural strength (RF) at room temperature (±21°C), cold (±10°C), and hot (±30°C)

	Stone size	Stone %	Plastic %	RC (Mpa)	RF(Mpa)		
					Room ±21°C	Hot ± 30°C	Cold ± 10° C
50:50 PET:PP	Large (±10 mm)	25	75	22.27	5.06	7.79	11.55
		50	50	23.10	8.96	5.22	6.46
		75	25	15.63	4.27	5.41	5.37
	Medium (±5 mm)	25	75	19.05	6.53	4.99	5.70
		50	50	20.19	6.48	7.24	6.39
		75	25	24.99	9.03	7.51	7.63
	Small (±3 mm)	25	75	25.07	9.83	5.87	10.46
		50	50	22.80	10.73	5.30	10.72
		75	25	23.05	7.03	6.69	8.31
	Very small (±1 mm)	25	75	18.16	5.01	3.30	5.81
		50	50	21.30	9.30	6.11	6.56
		75	25	20.19	7.66	5.41	9.04

Source: Own elaboration

4 Conclusion

All constructions and facilities that support the agricultural sector are essential for the proper development of productive activities. The eco-paving block, manufactured from waste plastic and aggregates, constitutes a prefabricated material that can be used in livestock and agricultural constructions. Its potential applications should be studied in greater depth due to their impact on farmers' daily activities and on environmental conservation.

Furthermore, the results of this study establish parameters of safety, economy, and environmental preservation criteria, showing that the best combination was observed for the PET:PP 50:50 mixture with an aggregate particle size of ±3 mm, in its three proportions: 75:25%$_{\text{PLASTIC:AGGREGATE}}$, 50:50%$_{\text{PLASTIC:AGGREGATE}}$, and 25:75% $_{\text{PLASTIC:AGGREGATE}}$.

References

[1] Darko, C., Shi-Yung, P.W., Chen, A., Acquaye, A., Review and recommendations for sustainable pathways of recycling commodity plastic waste across different economic regions. Resources, Environment and Sustainability, 14, Art. 134, 2023. DOI: https://doi.org/10.1016/j.resenv.2023.100134

[2] Hyuni, J., Giyoung, S., Hojung, K., Lam, T.H., Jonggeon, J., Hyo, J.K., Hyeonyeol, J., Jeyoung P., Dongyeop X.O., Review of polymer technologies for improving the recycling and upcycling efficiency of plastic waste. Chemosphere, 320, Art. 138089, 2023. DOI: https://doi.org/10.1016/j.chemosphere.2023.138089

[3] Ramin-Tolou, J., Ali, H., Alireza, M., Using woven recycled plastic fibers in reinforced concrete beams. Construction and Building Materials, 404, Art. 133262, 2023. DOI: https://doi.org/10.1016/j.conbuildmat.2023.133262

[4] Abang, S., Wong, F., Sarbatly, R., Sariau, J., Baini, R., Awang-Besar, N., Bioplastic classifications and innovations in antibacterial, antifungal, and antioxidant applications. Journal of Bioresources and Bioproducts. 8(4), pp. 361-387, 2023. DOI: https://doi.org/10.1016/j.jobab.2023.06.005.

[5] Sierra-Montes, L.F., Bioplásticos activos biodegradables en suelo para aplicaciones agronómicas. In Encuentro de Becaries de Grado y Posgrado de la UNLP (EBEC). La Plata, 20 de noviembre de 2024.

[6] Fan, X., Yu, Z., Yi-Fan, Y., Shi-Qi, L., Xi, W., Ying, Y., Yun-Xiang, X., Bioplastics with high mechanical strength, transparency, chemical stability, and recyclability by introducing dynamic ester bonds and rigid benzene rings into natural rubber, Polymer, 337, Art. 128956, 2025. DOI: https://doi.org/10.1016/j.polymer.2025.128956.

[7] Farah, S.S., Thinesh, S.B., Mohamed-Thariq H.S., The evolution and environmental prospects of renewable bioplastics: types, production methods, and sustainability. Journal of Renewable Materials,13(6), pp. 1071-1101, 2025. DOI: https://doi.org/10.32604/jrm.2024.02024-0011.

[8] NTE-INEN, 3040: Concrete Paving Units–Requirements and Test Methods. Instituto Ecuatoriano de Normalización, 2016.

[9] UNE, 41410, Concrete–determination of compressive strength.

[10] UNE-EN 1338, Precast concrete paving flags–requirements and test methods.

[11] Antón, N., González-Fernández, Á., and Villarino, A., Reliability and mechanical properties of materials recycled from multilayer flexible packages. Materials, 13(18), 3992, 2020.

[12] Solano, E.F., Pedroza, J.B., y Roa, S.A.Q., Evaluación de la resistencia a la flexión en baldosas esmaltadas de cerámica en función de los ciclos de hielo y deshielo. Revista colombiana de tecnologías de avanzada (RCTA), 1(25), pp.92-98. 2017.

M.J. Valarezo-Ulloa, is a BSc. Eng. in Chemical Engineer and Agricultural Management Engineer. MSc. and a PhD in Materials Engineering from the National Polytechnic Institute, Mexico City. She is a professor of Organic Chemistry and Inorganic Chemistry at the Universidad Nacional de Loja and head of the New Materials Research Group at the same institution. She has led projects focused on the development of new materials derived from degradable and non-biodegradable sources for applications in construction, industry, agriculture, and medicine.
ORCID: 0000-0002-7998-9100

F.E. Tinoco-Tinoco, is a BSc. Eng. in Chemical Engineer graduated from the Universidad Técnica Particular de Loja and MSc. in Research in Chemical Process Engineering from the Polytechnic University of Catalonia, Spain. He is a professor at the Universidad Nacional de Loja. He has extensive experience in industrial brewing processes and, since 2020, has been a visiting lecturer in specialization courses on brewing at the University of Alicante, Spain.
ORCID: 0000-0002-7618-4278

J.C. Granda-Pardo, holds a BSc. in Economics from the Universidad Técnica Particular de Loja, a MSc. in Circular Economy from the Pontificia Universidad Católica of Ecuador, and an MBA from the Universidad Internacional de la Rioja. He is a professor of Introduction to Economics and Microeconomic Analysis in the Economics program at the Universidad Nacional de Loja. He has participated in research projects such as obtaining biodegradable polylactic acid (PLA) plastics from organic waste, developing well-being indices for Ecuadorian cities (with Loja as a case study), and studying agglomeration and specialization as determinants of economic growth.
ORCID: 0000-0001-6316-0253

M.C. Veintimilla-Ortega, is a BSc. Eng. in Civil Engineer. MSc. in Civil Construction with a focus on Sustainable Development and in Education with a specialization in Higher Education from the Universidad Nacional de Loja. She is a professor of Soil Mechanics and Constructions for Agricultural Infrastructure at the Universidad Nacional de Loja and a member of the New Materials Research Group at the same institution. She has led projects on the physical–mechanical analysis of construction materials.
ORCID: 0009-0008-3364-2102

K.Y. Paucar-Carrión, holds a PhD in Communication from the University of Huelva. She also holds Master's degrees in Research and Digital Culture, in Education, Technology and Innovation, and in Marketing with a specialization in E-Commerce and Digital Marketing. She holds a Bachelor's degree in Communication and a degree in Aquaculture Engineering.
ORCID: 0000-0003-2440-8652

É.L. González-Carrión, holds a PhD in Communication from the University of Huelva. She holds a MSc. in Communication and Audiovisual Education, as well as BSc. in Communication and in Education Sciences major in English.
ORCID: 0000-0003-3808-5460

G.A. Ojeda-Brito, holds a BSc. Eng. in Chemical Engineering and a MSc. in Biomedical Engineering. He currently serves as an Innovation Officer at the Science and Technology Park of the Universidad Técnica Particular de Loja. In this role, he has contributed to more than ten university–industry innovation initiatives, covering the formulation, execution, and technology transfer stages of diverse projects.
ORCID: 0009-0009-7948-0003

DYNA
http://dyna.medellin.unal.edu.co/

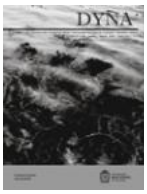

UNIVERSIDAD NACIONAL DE COLOMBIA

Port connectivity assessment and its impact on competitiveness: the case of Buenaventura, Colombia

Mabel Nathalia Collazos-Acosta, Josué Francisco Muñoz-Rebolledo, Jorge Gallego-Méndez & Ciro Jaramillo-Molina

Escuela de Ingeniería Civil y Geomática, Universidad del Valle, Santiago de Cali, Colombia, mabel.collazos@correounivalle.edu.co, josue.munoz@correounivalle.edu.co, jorge.gallego@correounivalle.edu.co, ciro.jaramillo@correounivalle.edu.co

Received: September 16th, 2025. Received in revised form: February 6th, 2026. Accepted: February 13th, 2026.

Abstract
This study evaluates the port connectivity of the port of Buenaventura in the context of the Pacific basin, comparing it with similar ports, using a combined approach of graph theory, spatial analysis, and principal component analysis (PCA). Topological indicators of centrality, intermediation, clustering coefficient, and structural indices (β, γ, α, μ) were used, in addition to the LSBCI competitiveness index to evaluate prospective scenarios. The results reveal that Buenaventura has geographical advantages but limited connectivity to key nodes such as Panama, Mexico, and Vietnam. The evaluation of a new connection with Mexico significantly improves its centrality in the network, and it is concluded that greater integration of Buenaventura into strategic routes can enhance its regional competitiveness and that the methodological approach applied is replicable in other port studies.

Keywords: seaports; spatial connectivity; competitiveness; maritime network; pacific region.

Evaluación de la conectividad portuaria y su impacto en la competitividad: el caso de Buenaventura, Colombia

Resumen
Este estudio evalúa la conectividad portuaria del puerto de Buenaventura en el contexto de la cuenca del Pacífico, comparándolo con puertos homólogos, mediante un enfoque combinado de teoría de grafos, análisis espacial y análisis de componentes principales (PCA). Se utilizaron indicadores topológicos de centralidad, intermediación, coeficiente de agrupamiento e índices estructurales (β, γ, α, μ), además del índice de competitividad LSBCI para evaluar escenarios prospectivos. Los resultados revelan que Buenaventura posee ventajas geográficas, pero una conectividad limitada frente a nodos clave como Panamá, México y Vietnam. La evaluación de una nueva conexión con México mejora significativamente su centralidad en la red y se concluye que una mayor integración de Buenaventura en rutas estratégicas puede potenciar su competitividad regional, y que el enfoque metodológico aplicado es replicable en otros estudios portuarios.

Palabras clave: puertos marítimos; conectividad espacial; competitividad; red marítima; región pacífica.

1 Introducción

Los puertos marítimos cumplen una función estratégica como nodos de interconexión entre sistemas de transporte marítimo, terrestre y aéreo dentro de las redes de movilidad global y del desarrollo económico de las regiones [1]. La competitividad portuaria se ve influenciada por la conectividad y la accesibilidad, siendo la primera implica la capacidad de los puertos para conectarse entre sí, y la segunda su capacidad de ser alcanzados desde diversas zonas económicas [2].

En Colombia se han conducido estudios sobre los niveles de accesibilidad terrestre entre departamentos y principales puertos marítimos desde una visión de equidad territorial [3], sin embargo, existe déficit en estudios que enmarquen el grado de conectividad entre los puertos marítimos, debido al bajo grado de exploración del transporte marítimo a comparación a otros modos de transporte [4], esta condición prevalece en países de la región, donde la competitividad portuaria se evalúa únicamente con datos estadísticos y económicos, limitando la capacidad de toma de decisiones desde una perspectiva geográfica [5].

El puerto de Buenaventura se destaca por su importante ubicación en la Costa Pacífica del suroeste de Colombia, cerca

How to cite: Collazos-Acosta, M.N., Muñoz-Rebolledo, J.F., Gallego-Méndez, J., and Jaramillo-Molina, C., Evaluación de la conectividad portuaria y su impacto en la competitividad: el caso de Buenaventura, Colombia DYNA, (93)240, pp. 122-131, January - March, 2026.

al canal de Panamá y equidistante entre los puertos de Vancouver y Valparaíso, posicionándose estratégicamente debido a su proximidad con las principales rutas marítimas que conectan el planeta de norte a sur y de oriente a occidente, lo que lo convierte en referente de estudio y ejemplo ideal para evaluar su competitividad frente a puertos del pacífico [6].

El puerto de Buenaventura no solo es una importante conexión nacional, sino también un vínculo clave entre Centroamérica y Asia [7]. Según el Ministerio de Transporte [8], transporta alrededor de 18 millones de toneladas anuales, (9,7 millones de toneladas son de carga contenerizada), representando el 24,3% del tráfico portuario nacional en el contexto del Pacífico. La mejora de la conectividad portuaria podría reducir costos en el transporte marítimo y facilitar el comercio bilateral entre naciones económicamente asociadas, fortaleciendo las relaciones internacionales y mejorando el mercado [9], dada la influencia de conectividad marítima para superar limitaciones geográficas y logísticas [10].

Este estudio evalúa la conectividad portuaria de Buenaventura y su impacto en la competitividad regional mediante el análisis de redes y simulación de escenarios. Se emplearon técnicas de análisis espacial para medir la incidencia de la conectividad territorial en la competitividad portuaria, considerando el puerto de Buenaventura como principal nodo marítimo del Pacífico colombiano, con el objetivo de identificar patrones espaciales y relaciones funcionales que contribuyan a explicar sus características espaciales y funcionales. Los resultados buscan ofrecer evidencia técnica que sustente procesos de planificación y gestión estratégica en contextos portuarios con dinámicas regionales complejas.

2 Antecedentes

Recientes estudios han analizado cómo la infraestructura portuaria y su conectividad influyen en la jerarquía global de los puertos y en la definición de sus estrategias [11], en los que se destaca cómo factores como la estructura de red, el comercio internacional y la proximidad geográfica generan una conectividad marítima desigual [12]. Cambios en los servicios de transporte, como el tipo de carga o la organización de las rutas, pueden afectar negativamente a las comunidades portuarias [13]. El transporte de contenedores influye en el comercio bilateral entre naciones, aunque su impacto varía según región y distancia [14], y presenta diferencias entre escalas locales y globales [13]. La literatura en geografía portuaria muestra un enfoque limitado en dinámicas regionales transnacionales, con solo un 1% de estudios considerando esta dimensión [15]. En este sentido, resulta importante destacar las principales nociones asociadas a este contexto de estudio.

2.1 Conectividad marítima y el mercado internacional

La conectividad marítima refiere a la eficiencia de las redes de transporte marítimo, incluyendo aspectos como el número de destinos servidos, la frecuencia de los servicios y los costos asociados, los cuales permiten un acceso más amplio a recursos físicos, que facilite las economías de escala y promueva la especialización, lo que puede contribuir significativamente al desarrollo económico [16]. Por su parte, la Conferencia de las Naciones Unidas sobre el Comercio y Desarrollo [2] desde el 2010 emplea el Índice de Conectividad de Carga Marítima (LSCI), para establecer el grado de integración de los países en las redes de transporte marítimo global, a partir de cinco elementos clave del sector marítimo: la cantidad de barcos, capacidad de estos para transportar contenedores, tamaño máximo de los buques, cantidad de servicios disponibles y el número de compañías que operan buques portacontenedores en los puertos [17]. En los últimos años, este se ha consolidado como un indicador del rendimiento portuario y ha sido utilizado en investigaciones que prestan mayor atención a la conectividad portuaria, abarcando desde la definición de conceptos y la selección de indicadores, hasta la creación de métodos de evaluación que consideran diferentes técnicas [18].

2.2 El Pacífico y los puertos homólogos

Los puertos homólogos son grupos portuarios que presentan infraestructura física y operativa equivalentes, estos suelen compartir características como ubicaciones geográficas cercanas, políticas comerciales y marítimas similares, climas regionales comparables, actividades portuarias comunes y la disponibilidad de recursos similares, que pueden influir en la forma en que los puertos operan, se desarrollan y compiten en el mercado global [19].

En otros contextos, los enfoques sistemáticos han permitido identificar cohortes de puertos homogéneos antes de realizar comparaciones de eficiencia, con lo cual se evita la evaluación injusta entre puertos no comparables [20].

2.3 Puertos concentradores-distribuidores

Los puertos concentrador-distribuidor son nodos principales en una estructura jerárquica y son fundamentales para visualizar las estrategias de organización de las redes marítimas por parte de las compañías navieras. Estos son ubicados en el nivel más alto y actúan como puntos de conexión esenciales, enlazando con eficacia con nodos de menor nivel a través de diversos servicios de conexión [21]. La configuración de esta jerarquía es influenciada por factores geográficos, especialmente la concentración de actividades de transbordo en zonas cercanas a la ruta próximas al ecuador, las cuales se intersecan a los conectores norte-sur, tienden a agrupar nodos cercanos a cuellos de botella geográficos (áreas geográficas donde el movimiento de los buques está limitado), lo que optimiza la eficiencia de las operaciones [22].

3 Metodología

Con el propósito de determinar el grado de competitividad que tiene Buenaventura respecto a sus competidores en el Pacífico, esta investigación contempló un enfoque basado en teoría de grafos para estimar relaciones geográficas entre competitividad y conectividad en el contexto geográfico. La metodología incorpora métricas topológicas propias del análisis de redes espaciales —como centralidad, accesibilidad y proximidad— con el fin de caracterizar la posición relativa de Buenaventura en la red portuaria regional. Esta aproximación permite identificar configuraciones estructurales que condicionan el desempeño logístico del puerto y ofrece elementos empíricos para su comparación con nodos equivalentes en la costa Pacífica latinoamericana.

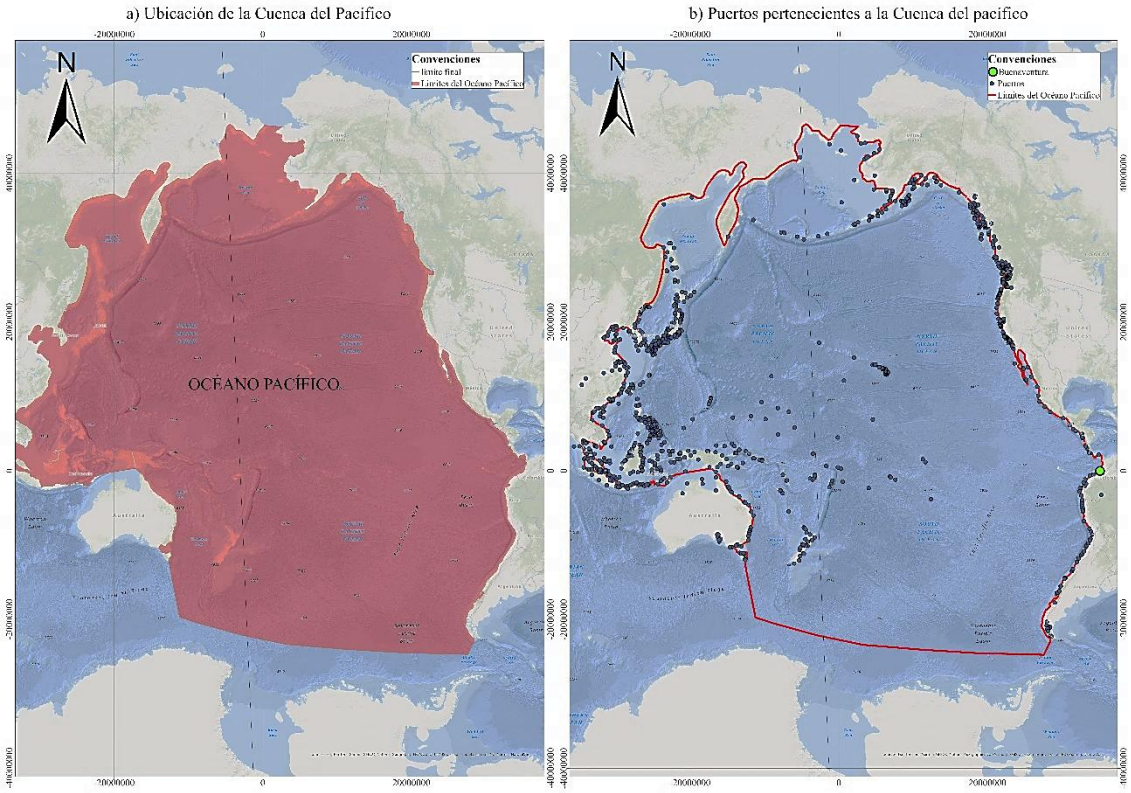

Figura 1. (a). Delimitación de la Cuenca Pacífico; (b) Puertos localizados en la Cuenca Pacífico.
Fuente: Elaboración propia.

3.1 Zona de estudio

La cuenca del Pacífico comprende territorios ubicados alrededor del océano Pacífico, con un total de aproximadamente 54 países y territorios distribuidos en tres continentes (Asia, Oceanía y América), esta configuración geográfica abarca tanto las costas como múltiples islas insulares distribuidas ampliamente por toda la región (Fig. 1) [23]. Por su parte, el puerto de Buenaventura se destaca por su localización, al suroeste de Colombia, permitiéndole acceder desde la cuenca a las principales rutas marítimas que conectan el planeta de norte a sur y de oriente a occidente [6]. Según el Ministerio de Transporte [8], el puerto de Buenaventura transporta alrededor de 18 millones de toneladas anuales y es el puerto con mayor comercio exterior en Colombia, moviendo un 44% del total de carga nacional y contribuyendo significativamente al PIB nacional.

3.2 Fuentes de información

Se recopiló información sobre el puerto de Buenaventura y los principales puertos de la cuenca del Pacífico, tomando como año base 2019, dada la disponibilidad de datos en fuentes oficiales e internacionales especializadas, lo cual permite un análisis comparativo, relacionados en la Tabla 1. Se consideraron indicadores económicos y operativos, entre los que se incluyeron el movimiento de TEU, el índice de conectividad portuaria (LSCI) y el índice de conectividad marítima bilateral (LSBCI), con el fin de evaluar el rendimiento y la integración de cada puerto en las redes globales. Además, se identificaron las rutas marítimas comerciales activas a través del análisis operativo de las rutas establecidas por las siete principales navieras (MSC, Maersk, CMA CGM Group, COSCO Group, Hapag-Lloyd, ONE y Evergreen Line), que concentran aproximadamente el 77% del mercado de portacontenedores, aplicando la regla de Pareto para focalizar el análisis en los actores más representativos.

Tabla 1.
Fuentes de información empleada.

Información	Fuente	Año
Información espacial, física y funcional de los principales puertos del mundo.	World Port Index	2019
Índice de Conectividad del Transporte Marítimo de Línea (LSCI)	Naciones Unidas en la esfera del comercio y el desarrollo (UNCTAD)	2019
Índice de conectividad bilateral del transporte marítimo de línea (LSBCI)	Naciones Unidas en la esfera del comercio y el desarrollo (UNCTAD)	2019
Límite del Océano Pacífico y sus subdivisiones	Organización Hidrográfica Internacional (IHO)	2002
Número total de contenedores manipulados, por país, en unidades equivalentes a veinte pies (TEU)	Naciones Unidas en la esfera del comercio y el desarrollo (UNCTAD)	2019

Fuente: Elaboración propia.

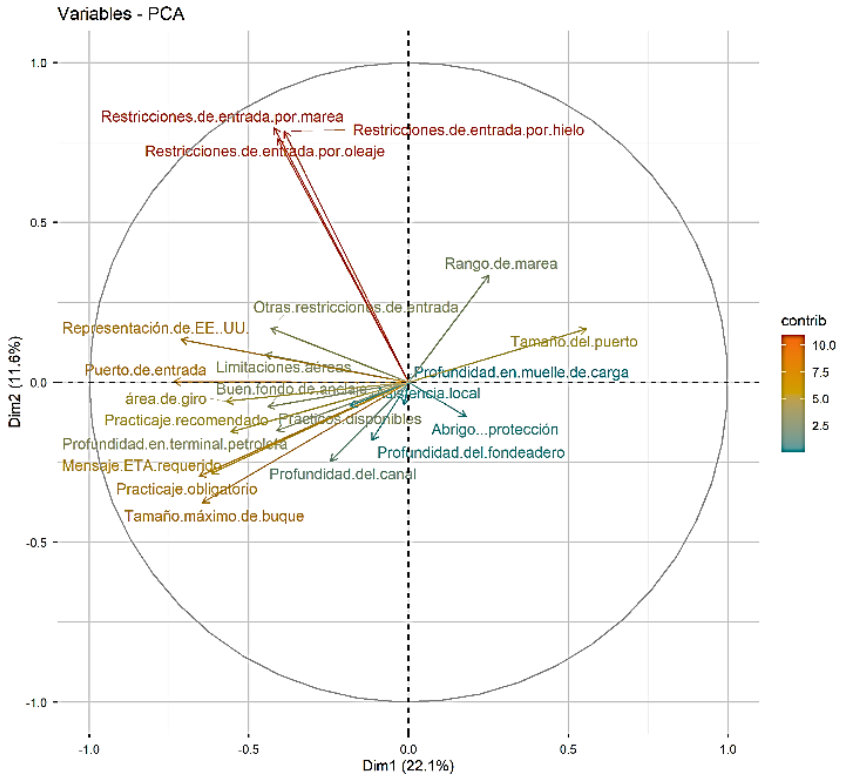

Figura 2. Variables utilizadas para el ACP.
Fuente: Elaboración propia

3.3 Análisis de componentes principales (ACP)

Para la determinación de la consideración de puertos homólogos, se aplicó un ACP para reducir la dimensionalidad del conjunto de variables y facilitar la comparación entre puertos. Se eliminaron variables redundantes y se renombraron otras para mejorar su interpretación. Este análisis se ejecutó mediante un script en R, permitiendo una visualización más clara de las relaciones entre variables y simplificando el análisis. De esta manera, se observó que algunas variables tienen mayor influencia sobre el eje Y (Dimensión 1 del ACP), que explica el 24,3 % de la varianza total, mientras que el eje X (Dimensión 2) representa un 14,2 % de la varianza (Fig. 2).

3.4 Georreferenciación de información alfanumérica

Se construyó una representación geográfica de la red marítima en la cuenca del Pacífico, donde los puertos se modelaron como nodos ubicados según sus coordenadas reales, y las conexiones marítimas como arcos que respetan la disposición espacial del sistema. La delimitación del área de estudio se basó en la ubicación de los países ribereños al Océano Pacífico, y se filtraron los puertos correspondientes a dicha cuenca para conservar la coherencia espacial de la red.

3.5 Parámetros para seleccionar los puertos homólogos

Se calculó el centroide ponderado de cada país para generar nodos representativos y simplificar la base de datos, tomando como variable de referencia el tamaño del puerto, que fue la de mayor contribución en el análisis de componentes principales (ACP). Posteriormente, se excluyeron los países que no constituyen competencia directa para Colombia o que no son miembros de la ONU, por presentar características políticas, portuarias y operacionales no comparables con las de Buenaventura. A partir de los datos de TEU se aplicó estadística descriptiva y se utilizó el Z-score para identificar los países con volúmenes de carga similares a los de Colombia (rango entre -1 y 1), definiéndose así el conjunto de puertos homólogos.

3.6 Creación del grafo y estimación de indicadores

Se construyó un grafo dirigido no ponderado que representa la red de conectividad marítima entre países de la cuenca del Pacífico, tomando como unidad de análisis los nodos portuarios y como aristas las conexiones marítimas directas entre ellos. Para ello, se elaboró una matriz de adyacencia binaria, donde el valor 1 indica la existencia de una conexión directa entre dos nodos portuarios y 0 su ausencia. Esta matriz fue la base para la generación del grafo, el cual fue modelado mediante algoritmos de teoría de grafos utilizando la biblioteca *NetworkX* en Python.

A partir de esta estructura, se aplicaron métricas topológicas para caracterizar la red: grado de entrada y salida, centralidad de intermediación (*betweenness centrality*), centralidad de cercanía (*closeness centrality*) y medidas de conectividad global como densidad, diámetro y conexas, que permitieron identificar patrones espaciales e identificar la posición de

Tabla 2.
Métricas espaciales implementadas en el grafo.

Ec	Modelo	Variables
1	$\beta = a/n$	Donde (a) son los arcos y (n) representan los nodos, varía entre 0 y 1 y (g) los arcos sin conexiones.
2	$\gamma = a/((n(n-1))/2)$	
3	$\mu = a - (n-1) - g$	
4	$\alpha = \mu/(2 \cdot n - 5)$	Donde (μ) corresponde a el número ciclomático y (n) los nodos.
5	$I_v = \sum_{\substack{v1,v2 \\ \overline{v1 \neq v} \\ \overline{v2 \neq v}}} \frac{r_{v1v2}(v)}{r_{v1v2}}$	Donde r_{v1v2} es la cantidad de caminos más cortos que conectan $v1$ con $v2$; $r_{v1v2}(v)$ la cantidad de caminos más cortos que conectan $v1$ con $v2$ y pasan por v.
6	$C_a = \frac{\#\ Tripletas\ cerradas}{\#\ Tripletas\ totales}$	En el denominador están incluidas las tripletas abiertas y cerradas.
7	$C_{av} = \frac{\#v}{n_v(n_v-1)}$	Donde v vértices adyacentes conectados por arista y n_v cantidad de vértices que son vecinos del vértice v.
8	$LSBCI_{AB} = \frac{1}{5}\sum_{i=!}^{5}\left(\frac{xi - min\ (xi)}{(x1)\ - min\ (xi)}\right)$	Donde xi es el valor del componente i para la conexión entre A y B.

Fuente: Elaboración propia.

Buenaventura en función de su accesibilidad relativa, su rol como nodo intermedio en las rutas marítimas y su conectividad dentro del sistema portuario regional. El grafo resultante permitió el análisis comparado de la competitividad portuaria abordado en las secciones posteriores.

Se generó la matriz de carga de arcos, donde los valores representan la media de los TEU transportados entre dos países multiplicado por la conectividad entre estos dos. A partir de esto se generó el porcentaje inverso de la carga de arcos lo cual permitió crear la matriz de Shimbel de caminos mínimos para llegar de un nodo a otro sin estar conectados directamente.

En primer lugar, se estimó la conectividad de redes basada en teoría de grafos, la cual, por medio de la codificación topológica de redes, en conjunto de la evaluación de características intrínsecas de la misma, con el fin de identificar ubicaciones estratégicas para analizar conceptos como el rendimiento de una red conceptual de transporte, a través de estructuras simples representativas [1]. Para esta red se calculó el índice Beta (β) (Ec. 1), que representa la tasa de aumento de la conectividad de un grafo a medida que se le añaden arcos interconectados. También se estimó el índice Gamma (γ) que relaciona el número de arcos existentes en un grafo con el número máximo que puede tener (Ec. 2). Así mismo se consideró el número ciclomático que representa el número de circuitos que presenta la red (Ec. 3). Finalmente se estimó el índice Alpha (α) que relaciona el número de circuitos del grafo (μ) y los circuitos que existirán en caso de tratarse de un grafo completo (Ec. 4).

Por otro lado, se consideró el indicador de centralidad de intermediación (Ec. 5) que se basa en la identificación de las rutas más cortas entre los vértices del grafo. Este calcula el promedio de todas las rutas mínimas que pasan por un vértice específico en relación con el total de caminos más cortos posibles. De igual forma, se estimó el coeficiente de agrupamiento (Ec. 6 y 7) que mide la tendencia de los nodos para agruparse y puede medirse tanto a nivel global como local para cada nodo. Esta medida se basa principalmente en tripletas o triángulos, abierta cuando está conectada por dos aristas y cerrada cuando está conectada por tres aristas. Las métricas consideradas se relacionan en la Tabla 2.

3.7 Evaluación de escenarios

Se tomaron dos escenarios de conectividad territorial para representar variaciones de la conectividad frente a los cambios físicos y operacionales de la red. Los dos escenarios corresponden a la franja y la ruta la cual es implementada por la naviera "Cosco Shipping" que busca conectar China con algunos países de la costa pacífica de Centroamérica y Sudamérica, en la cual están incluidos México, Colombia, Ecuador y Perú [24]. Aquí se calculó el índice LSBCI (Ec. 8) para posteriormente estimar la conectividad de aquellos países que pertenecen a esta ruta antes de la nueva conexión entre Buenaventura y México y se calculó de nuevo para todos los países con esta nueva conexión.

El índice LSBCI calculado constituye una variable proxy que permite analizar cómo varía la conectividad en la red frente a nuevos escenarios que alteran su estructura. Este índice se calcula a partir de cinco componentes: el número de transbordos, el número de países que pueden ser alcanzados desde A y desde B con un solo transbordo, el número de navieras, la frecuencia del servicio y la cantidad de TEU transportados entre el par de países A y B.

4 Resultados

4.1 Reducción de dimensionalidad del ACP

La Dimensión 1 (24.3% de la varianza) se asocia principalmente con variables de infraestructura portuaria, como el tamaño del puerto, la profundidad del canal y el tamaño máximo de embarcaciones, por lo que se usa como eje X. La Dimensión 2 (14.2%) está relacionada con servicios portuarios, como

Tabla 3.
Descripción de las variables analizadas en el PCA

Variable	Descripción
Tamaño del puerto	Se establece teniendo en cuenta factores, como superficie, tipo de infraestructura y espacio disponible en los muelles.
Grado de protección (contra viento, oleaje y mar)	En la zona en la que se llevan a cabo las operaciones portuarias habituales, generalmente en los muelles, también se especifica el nivel de protección en zona de fondeo.
Profundidad del canal	Se refiere a la profundidad en el canal principal, presentada en intervalos de 5 pies (1.5 metros), basándose en el datum de la carta náutica.
Tamaño máximo de buque permitido	Capacidad del puerto para recibir embarcaciones, siendo 500 pies (152.4 metros) de eslora el tamaño máximo permitido. Además, la letra "M" señala que el puerto puede albergar barcos de menos de 500 pies (152.4 metros).
Puerta de despacho de aduanas y migración	Es un puerto en el que una embarcación puede ingresar y gestionar la descarga de mercancías extranjeras y el desembarco de personal.
Carga en muelle	Hace referencia a la zona en la que se realizan las operaciones portuarias habituales de carga y descarga.
Grúas	Especifica la disponibilidad de grúas, el tipo de cada una y su capacidad de carga expresada en toneladas.
Servicios	Indica si los servicios portuarios estándar están disponibles.

Fuente: Elaboración propia.

carga/descarga y grúas. En el análisis de componentes principales (PCA), PC1 refleja la disponibilidad de servicios portuarios clave, mientras que PC2 agrupa aspectos técnicos y de soporte. Aunque ambas dimensiones incluyen variables de servicios, las de infraestructura influyen más en PC1, y las de servicios, en PC2. Por ello, se seleccionaron solo las variables más representativas para facilitar la interpretación del análisis, descritas en la Tabla 3.

4.2 Parámetros para seleccionar los puertos homólogos

Al realizar la selección de los puertos homólogos para la red, se utilizó el "Z Score" para filtrar los países y una diferencia respecto al puerto de interés el cual es Buenaventura (Fig. 3a).

Después de aplicar el Z-Score (Fig. 3b) en la base de datos se obtuvo una diferencia significativa mayor a la media de los TEU transportados para algunos países como Estados Unidos, Singapur, Malasia, Japón, Corea del Sur y Hong Kong.

Para la selección de los puertos homólogos al puerto de Buenaventura se obtuvo como resultado que hay 6 países que no cumplen con la condición de puertos homólogos y son los mismos mencionados anteriormente. Los puertos mencionados tienen una diferencia respecto a Colombia menor a -1 y aquellos que no están en el rango (-1, 1) no cumplen con la condición para pertenecer a un puerto homólogo a Colombia y no pertenecen al 68,27% de datos con comportamiento normal o típico.

4.3 Creación del grafo y estimación de indicadores para los diferentes escenarios

4.3.1 Estimación de indicadores estructurales

En la estimación de los indicadores se obtuvieron resultados tanto estructurales de la red como de cada uno de los nodos y enlaces. Dentro de los resultados después de calcular los indicadores estructurales para la red general se encontró que el índice beta es mayor en el escenario del año 2019 respecto a los demás escenarios. Este indicador nos dice como está en cuanto a conectividad la red en general mediante la relación entre los nodos y los enlaces, lo cual sugiere que entre más cantidad de enlaces tenga una red, esto implica mayor conectividad. Otro de los aspectos que se tuvo en cuenta es que el índice gamma es directamente proporcional al número de arcos e inversamente proporcional al número de nodos lo cual es reflejado en el cambio de estos valores para los diferentes escenarios.

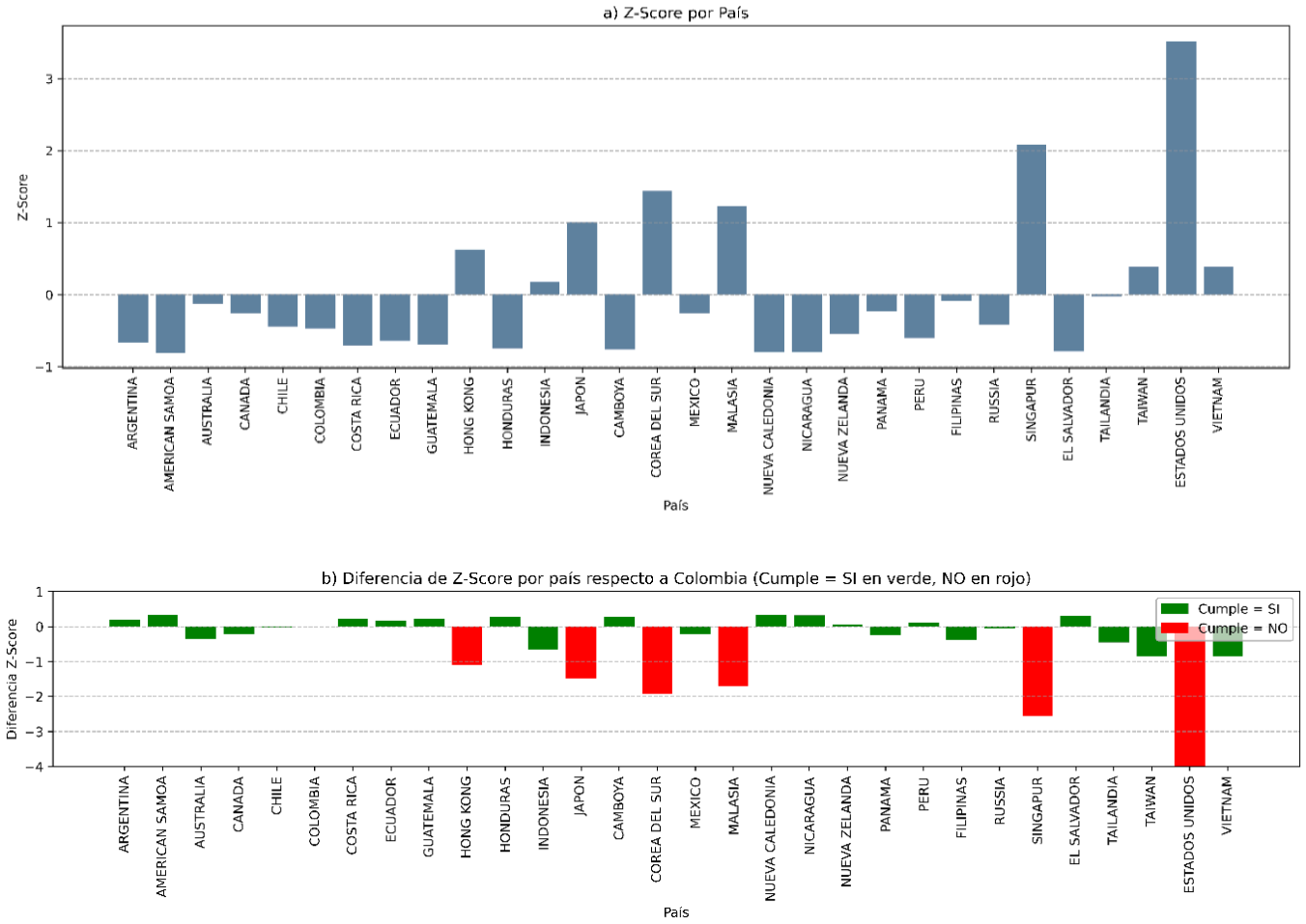

Figura 3. a) Z-Score por país y b) criterio de selección de puertos homólogos
Fuente: Elaboración propia.

4.3.2 Estimación de indicadores individuales por país

Se presentan los resultados asociados a los indicadores de centralidad de intermediación y el coeficiente de agrupamiento para todos los países de la red perteneciente al escenario principal del año 2019 y para los demás escenarios (Tabla 4).

Los resultados están representados gráficamente mediante georreferenciación y se aplicaron rangos específicos para clasificar estos indicadores y a su vez los enlaces. Para aquellos países que su centralidad y agrupamiento es menor a 0.33 se considera bajo, para los que el resultado de sus indicadores está

Tabla 4.
Resultado de las variables estimadas para los diferentes escenarios

Puerto	Teus	Escenario 2019		Ruta de la Seda (Sin conexión Colombia-México)		Ruta de la Seda (conexión Colombia-México)	
		Centralidad	Agrupamiento	Centralidad	Agrupamiento	Centralidad	Agrupamiento
Argentina	1833964	0,88	0,00				
Samoa Americana	42102	0,65	0,00				
Australia	8778913	1,06	0,10				
Canadá	7000133	0,83	0,33				
Chile	4641633	0,79	1,00				
Buenaventura (COL)	4316862	0,75	0,67	0,00	1,00	0,67	0,67
Costa Rica	1300785	0,79	1,00				
Ecuador	2194042	0,79	1,00	0,00	1,00	0,00	1,00
Guatemala	1529010	0,79	0,50				
Honduras	790707	0,65	0,00				
Indonesia	12615422	0,87	0,00				
Camboyua	639211	0,79	0,00				
México	7113878	0,97	0,27	0,00	0,00	0,00	1,00
Nueva Caledonia	111875	0,65	0,00				
Nicaragua	175370	0,65	0,00				
Nueva Zelanda	3430977	0,79	1,00				
Panamá	7346859	1,21	0,32				
Perú	2677239	0,79	0,60	0,67	0,33	0,00	0,67
Filipinas	9333428	0,87	0,33				
Rusia	4967133	0,65	0,00				
El Salvador	249472	0,80	0,00				
Tailandia	10130294	0,79	0,00				
Taiwán	15298285	0,97	0,33				
Vietnam	15297028	1,08	0,10				

Fuente: Elaboración propia.

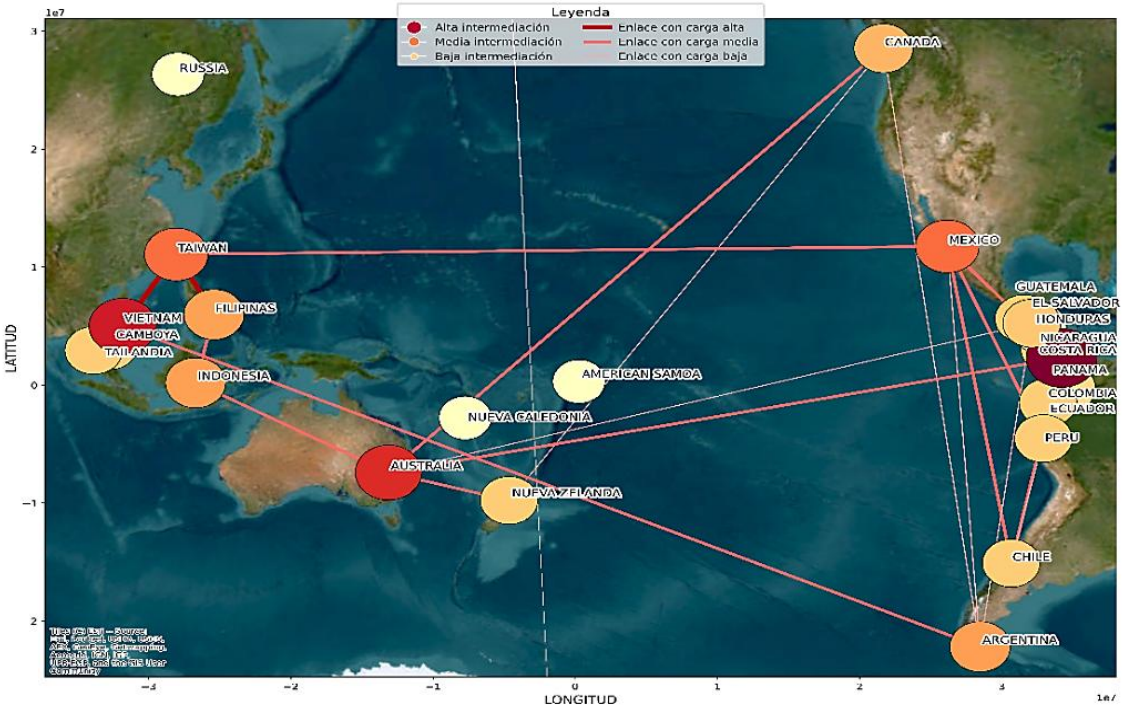

Figura 4. Centralidad de intermediación de cada nodo
Fuente: Elaboración propia.

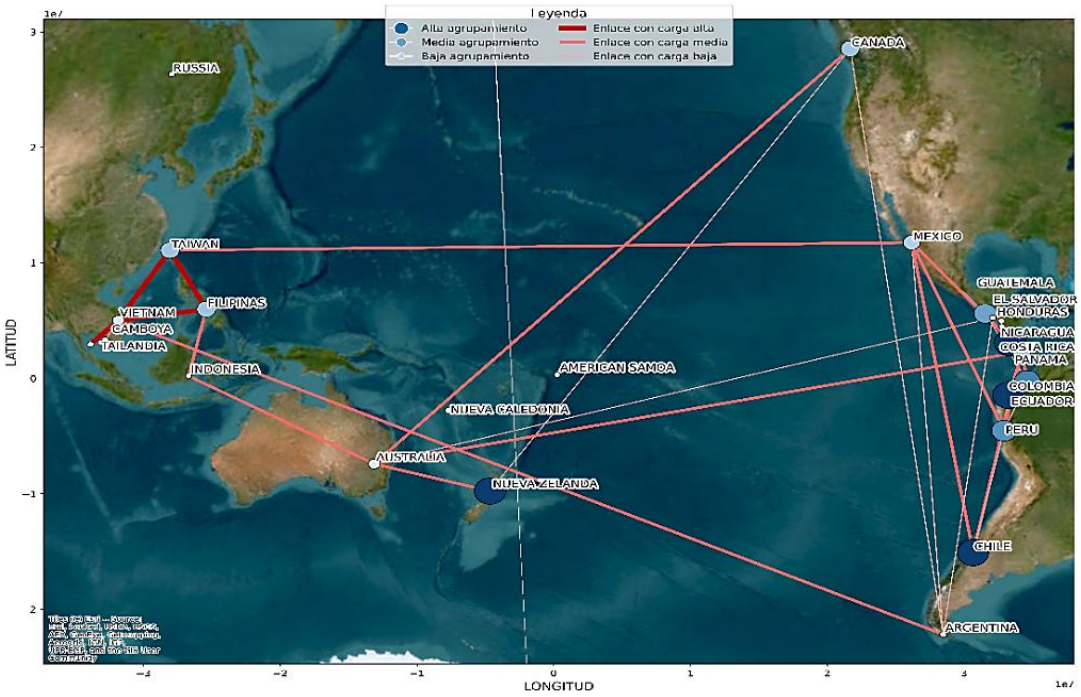

Figura 5. Coeficiente de agrupamiento para cada nodo
Fuente: Elaboración propia.

entre 0.33 y 0.66 se considera medio y para los que su valor es mayor a 0.66 se consideran países con alta intermediación y agrupamiento. Por otra parte, las cargas de los arcos también se clasificaron según tres rangos que son; carga baja para los enlaces entre 1 y 1695155.5, carga media para enlaces entre 1695155.5 y 3390309.9 y carga alta para enlaces entre 3390309.9 y 5085464.4.

Se presenta la centralidad de intermediación para todos los países de la red donde se puede evidenciar la diferencia entre cada uno y resaltando los países con mayor centralidad (Fig. 4) los cuales son; Vietnam, Australia, Taiwán, México y Panamá. Por otro lado, el resultado para los países pertenecientes a la "franja y la ruta" pero sin incluir la nueva conexión entre Colombia y México evidencia que Perú es el país con mayor centralidad de intermediación con mucha diferencia de los demás. Del mismo modo, el resultado para el otro escenario con la nueva conexión entre Colombia y México dio como resultado que Colombia es el país con mayor centralidad de intermediación y aunque Perú tiene la misma cantidad de enlaces, Colombia es el país con mayor cantidad de caminos cortos para llegar de un nodo a otro.

Al calcular el coeficiente de agrupamiento para cada país de la red general (Fig. 5), se evidenció que no precisamente los países más centralizados son los mejor agrupados y en este caso los países con mayor agrupamiento son; Nueva Zelanda, Chile, Ecuador y Costa Rica. Por otro lado, para los países del primer escenario sin la nueva conexión entre Colombia y México se obtuvo que los países con mayor agrupamiento son Ecuador y Colombia debido a su cercanía entre sí. Así mismo, cambió el agrupamiento para el segundo escenario debido al nuevo enlace entre Colombia y México en donde los países mejor agrupados son Ecuador y México.

5 Discusión

A diferencia de otros estudios, como el caso del análisis de los puertos de las Islas Canarias [1], el cual se basa fundamentalmente en datos cuantitativos secundarios que permiten una caracterización detallada del estado actual de la red portuaria local, el presente trabajo incorpora herramientas metodológicas complementarias como el análisis de componentes principales (PCA) y la ley de Pareto, con el objetivo de integrar elementos tanto cualitativos como estratégicos. Esta combinación metodológica busca ofrecer una visión más amplia y contextualizada del entorno competitivo del puerto de Buenaventura.

En cuanto a los resultados, existen diferencias derivadas del alcance geográfico de cada estudio. Mientras que el caso de [1] se enfoca en una escala local entre los puertos de Las Palmas y Santa Cruz de Tenerife, el presente estudio adopta una perspectiva regional que abarca toda la cuenca del Pacífico, identificando cuatro nodos principales de concentración-distribución: Panamá, México, Australia y Vietnam. Al igual que el puerto de las Las Palmas, Panamá y Vietnam presentan altos niveles de centralidad. Sin embargo, este trabajo incorpora más indicadores de teoría de grafos, permitiendo una caracterización robusta de estructura la red marítima analizada.

Resulta pertinente comparar este estudio con el trabajo [25], en el que se analizó el impacto de la reapertura del Canal de Suez durante la década de 1970. En dicho caso, se observó cómo el restablecimiento de esta ruta estratégica propició una red marítima más equilibrada entre Europa y Asia, permitiendo una redistribución del tráfico marítimo global. En contraste, el presente estudio evalúa el efecto de la apertura del puerto de

Chancay, que representa un nodo emergente con potencial para generar beneficios logísticos significativos para Perú.

La apertura del puerto de Chancay incorporaría un nuevo nodo portuario de alto nivel en el Pacífico sur, comparable al "nodo clave" descrito en el trabajo [10]. Este nodo tendría el potencial de redistribuir los flujos comerciales, optimizando la conexión de rutas con Asia y modificando la estructura actual de la red marítima. Con ello, podría superar las limitaciones logísticas y de conectividad que caracterizan a la configuración vigente [10].

Los resultados muestran que el índice beta es directamente proporcional con el número de enlaces, lo que confirma que la densidad de conexiones es clave para optimizar la red [1]. Por otra parte, la centralidad de intermediación, calculada a partir de la matriz de Shimbel, evidenció cambios estructurales significativos: en el primer escenario, Perú registraba la mayor centralidad (0,67), pero tras la conexión directa entre Colombia y México, esta pasó a 0, mientras que Colombia alcanzó el valor máximo (0,67), reforzando su papel estratégico [6]. Esto respalda lo planteado por [1] sobre cómo modificaciones puntuales en la estructura de la red pueden alterar jerarquías y flujos.

El coeficiente de agrupamiento también varió según la configuración de los enlaces, con valores heterogéneos en la red general y un valor uniforme de 1 en el escenario de conectividad total, indicando que cada nodo está directamente conectado con todos los demás, formando grupos completamente cerrados. Este resultado coincide con lo planteado por [2], quienes señalan que la interconexión directa entre todos los puntos de una red maximiza su cohesión y eficiencia operativa.

Asimismo, resulta pertinente considerar que, si bien el presente estudio se enfoca principalmente en indicadores de conectividad, la competitividad portuaria también está condicionada por factores logísticos internos y de operación. Tal como señalan [26], la identificación y superación de barreras logísticas puede potenciar la eficiencia operativa y la capacidad de respuesta de los puertos. Por ello, un siguiente paso de investigación podría integrar indicadores logísticos junto a los de conectividad, para obtener una visión más integral del desempeño portuario y proponer estrategias que optimicen tanto las redes marítimas como las operaciones internas.

6 Conclusiones

El presente estudio evaluó la conectividad portuaria y su impacto en la competitividad del puerto de Buenaventura en el contexto de la cuenca del Pacífico, estructurando una metodología basada en el análisis de redes espaciales y en la estimación de indicadores derivados de la teoría de grafos. Esta metodología permitió establecer relaciones cuantitativas entre el grado de conectividad y la posición competitiva de Buenaventura respecto a sus puertos homólogos. No obstante, el análisis presenta limitaciones derivadas de la disponibilidad de información, ya que se trabajó con datos del año 2019, con cobertura cuantitativa y cualitativa limitada para algunos puertos, centrado en la carga contenerizada y sin incluir variables logísticas internas.

La caracterización de factores físico-espaciales y operativos evidenció que, si bien Buenaventura cuenta con ventajas geográficas y de infraestructura, su nivel de centralidad y accesibilidad en la red regional es inferior al de nodos estratégicos como Panamá o México. Este hallazgo confirma que la competitividad portuaria no depende únicamente de la capacidad instalada, sino también del posicionamiento en la red marítima y de la integración en rutas clave.

Por otro lado, la estimación de indicadores como el índice beta, gamma, centralidad de intermediación y coeficiente de agrupamiento permitió identificar patrones estructurales que condicionan la conectividad regional, demostrando que pequeñas modificaciones en la red pueden alterar significativamente el rol estratégico de un puerto, incrementando su intermediación y mejorando su integración con mercados internacionales.

Finalmente, la evaluación de escenarios demostró que la incorporación de Buenaventura en rutas estratégicas, como la conexión directa con México, podría incrementar su centralidad y competitividad, reduciendo distancias logísticas y diversificando flujos comerciales. No obstante, alcanzar una conectividad óptima requiere complementar las mejoras en enlaces marítimos con estrategias logísticas internas, de modo que los beneficios de una mayor integración se traduzcan en un mejor desempeño operativo y económico.

Bibliografía

[1] Tovar, B., Hernández, R., and Rodríguez-Déniz, H., Container port competitiveness and connectivity: the Canary Islands main ports case. Transport Policy, 38, pp 40–51, 2015. DOI: https://doi.org/10.1016/j.tranpol.2014.11.001

[2] Oportus, O.S., and Echeverría, P.C., External connectivity analysis of the ports of Chile as a factor of competitiveness. Ingeniare, 20(1), pp 25–39, 2012. DOI: https://doi.org/10.4067/s0718-33052012000100004

[3] Rodríguez, D., García, C., and Jaramillo, C., La accesibilidad terrestre a los puertos marítimos de Colombia. Una aproximación desde la equidad territorial. En Entorno Geográfico, 15, pp. 8–46, 2018.

[4] García, N., Adenso-Díaz, B., and Calzada-Infante, L., Identifying port maritime communities: application to the Spanish case. European Transport Research Review, 13(1), 36, 2021.

[5] Cantillo, J., Cantillo-García, V., Cantillo, V., and Arellana, J., Port choice using aggregate open data: an application to Colombian port zones. Maritime Economics and Logistics, 25(3), pp 520–548, 2023. DOI: https://doi.org/10.1057/s41278-022-00235-9

[6] Castro-Castell, O., Soler-Niño, E., and Umaña-Castellanos, R., Asimetrías entre el puerto de Buenaventura y el puerto de Cartagena para el año 2015. Infraestructura Portuaria en Colombia, 19(32), pp 87–106, 2017.

[7] Jenss, A., Global flows and everyday violence in urban space: the port-city of Buenaventura, Colombia. Political Geography, 77, Art. 102113, 2020. DOI: https://doi.org/10.1016/j.polgeo.2019.102113

[8] Ministerio de Transporte de Colombia. Boletín estadístico, tráfico portuario en Colombia, pp 1–45, [en línea]. 2022. Disponible en: https://www.supertransporte.gov.co/documentos/2022/Febrero/Puertos_07/BOLETIN-TRAFICO-PORTUARIO-2022.pdf

[9] Martínez, J.H., Costes de transporte y conectividad en el comercio internacional entre la Unión Europea y Latinoamérica. pp 1–59, 2007.

[10] Rizaldi, A., Muzwardi, A., Santoso, E., Iffan, M., and Fera, M., The strategic development of maritime connectivity in the border area in Indonesia. Journal of Eastern European and Central Asian Research (JEECAR), 10(4), pp. 701-711, 2023.

[11] Arrieta-Tejada, A.C., Cure-Gaviria, J.S., and Pérez-Buelvas, P.C., Análisis teórico de la conectividad portuaria, 2017.

[12] Liu, C., Wang, J., and Zhang, H., Spatial heterogeneity of ports in the global maritime network detected by weighted ego network analysis. Maritime Policy and Management, 45(1), pp 89–104, 2018.

[13] Rodrigue, J., The geography of maritime ranges: interfacing global maritime shipping networks with hinterlands. GeoJournal, 87(2), pp 1231–1244, 2022.

[14] Del-Rosal, I., Trade effects of liner shipping across world regions. Maritime Business Review, 9(1), pp. 2–16, 2024.
[15] Mareï, N., and Ducruet, C., The regionalization of maritime networks: evidence from a comparative analysis of maritime basins. En Maritime Networks, pp. 330–350, 2015.
[16] Tovar, B., and Wall, A., The relationship between port-level maritime connectivity and efficiency. Journal of Transport Geography, 98, art. 103213, 2022.
[17] Asariotis, R., Benamara, H., Hoffmann, J., Misovicova, M., Núñez, E., Premti, A., Sitorus, B., Valentine, V., and Violh, B., El transporte marítimo en 2010, [en línea]. 2011. Disponible en: https://www.un-ilibrary.org/content/books/9789213634493/read
[18] UNCTAD, Review of Maritime Transport, pp. 1–26, 2023. DOI: https://doi.org/10.18356/9789213584569c006
[19] Ji, Z., Wu, X., Chen, X., Zhou, W., and Song, M., Finding green performance targets globally closest to management goals for ports experiencing similar circumstances. Resources Policy, 85, art. 103897, 2023. DOI: https://doi.org/10.1016/j.resourpol.2023.103897
[20] Tongzon, J.L., Determinants of port performance and efficiency. Transportation Research Part A: Policy and Practice, 29(3), pp. 245–252, 1995. DOI: https://doi.org/10.1016/0965-8564(94)00032-4
[21] Notteboom, T., and Rodrigue, J.P., Maritime container terminal infrastructure, network corporatization, and global terminal operators: Implications for international business policy. Journal of International Business Policy, 6(1), pp 67–83, 2023.
[22] Rodrigue, J.P., and Notteboom, T., Regionalización basada en el foreland: integración de los centros intermedios con el hinterland portuario. Investigación en Economía del Transporte, 27(1), pp 19–29, 2010.
[23] Nunn, P.D., Classifying Pacific islands. Geoscience Letters, 3(7), art. 8, 2016. DOI: https://doi.org/10.1186/s40562-016-0041-8
[24] COSCO, Shipping Lines inauguró el servicio WSA5 con recalada en el Puerto de Buenaventura y conexión con Shanghái y Chancay, COSCO SHIPPING Lines News Center, [en línea]. 2025. Disponible en: https://en.coscoshipping.com/col/col6923/art/2025/art_c0cc7b98fe13464aa473c271ede75adf.html
[25] Saito, T., Shibasaki, R., Murakami, S., Tsubota, K., and Matsuda, T., Global maritime container shipping networks 1969–1981: emergence of container shipping and reopening of the Suez Canal. Journal of Marine Science and Engineering, 10(5), art. 602, 2022. DOI: https://doi.org/10.3390/jmse10050602
[26] Sarkar, B.D., and Shankar, R., Understanding the barriers of port logistics for effective operation in the industry 4.0 era: Data-driven decision making. International Journal of Information Management Data Insights, 1(2), art. 100031, 2021. DOI: https://doi.org/10.1016/j.jjimei.2021.100031

M.N. Collazos-Acosta, Investigadora del Grupo de Investigación en Transporte, Tránsito y Vías (GITTV) de la Facultad de Ingeniería de la Universidad del Valle. Su trabajo se centra en el análisis espacial aplicado al estudio de sistemas de transporte marítimo y redes logísticas, con especial énfasis en la evaluación de la conectividad y accesibilidad portuaria desde una perspectiva territorial. Ha participado en investigaciones orientadas a caracterizar patrones espaciales de flujos de carga y a modelar la estructura de redes mediante indicadores topológicos y técnicas de teoría de grafos, con el propósito de fortalecer la planificación y la competitividad portuaria.
ORCID: 0009-0001-4763-0785

J.F. Muñoz-Rebolledo, Investigador del Grupo de Investigación en Transporte, Tránsito y Vías (GITTV) de la Facultad de Ingeniería de la Universidad del Valle. Su actividad investigativa se enfoca en el análisis espacial de sistemas de transporte marítimo y logística portuaria, abordando la conectividad y la accesibilidad territorial como factores determinantes de la competitividad. Ha desarrollado estudios sobre redes portuarias utilizando métricas de teoría de grafos y análisis de componentes principales para identificar configuraciones espaciales y funcionales que optimicen la integración de los puertos en el sistema logístico global.
ORCID: 0009-0002-4048-150X

J. Gallego-Méndez, Ing. Topográfico, Sp. en Geomática de la Universidad del Valle. Docente e investigador de la Escuela de Ingeniería Civil y Geomática y miembro del Grupo de Investigación en Transporte, Tránsito y Vías (GITTV). Su labor académica e investigativa se centra en el análisis espacial aplicado a sistemas de transporte, con énfasis accesibilidad y conectividad territorial mediante sistemas de información geográfica, análisis de redes y modelación geoespacial. Ha liderado proyectos de movilidad urbana, redes portuarias y plataformas geográficas para la gestión de datos territoriales, integrando metodologías cuantitativas y herramientas de análisis geográfico.
ORCID: 0009-0006-6046-0713

C. Jaramillo-Molina, Ing. Civil de la Universidad del Valle, Dr. en Ingeniería de Transportes de la Universidad Politécnica de Valencia (España) y PhD. en Planificación Urbana y Uso del Suelo en la Universidad de Granada (España). Es profesor titular de la Escuela de Ingeniería Civil y Geomática de la Universidad del Valle e investigador y director del Grupo de Investigación en Transporte, Tránsito y Vías (GITTV). Sus líneas de investigación se centran en la accesibilidad y la equidad territorial, el análisis espacial aplicado al transporte, la conectividad y la planificación urbana, integrando metodologías cuantitativas y análisis geoespacial para el estudio de la movilidad y su relación con el uso del suelo.
ORCID: 0000-0002-8820-2314

DYNA
http://dyna.medellin.unal.edu.co/

UNIVERSIDAD NACIONAL DE COLOMBIA

Applied research with a territorial approach, a project-based pedagogical methodology

Tommy Vallejo-López, Oscar Jaime Restrepo-Baena & Jorge I. Tobón

Universidad Nacional de Colombia, Sede Medellín, Facultad de Minas, Medellín, Colombia. tvallejol@unal.edu.co, ojrestre@unal.edu.co, jitobon@unal.edu.co

Received: June 24th, 2025. Received in revised form: September 25th, 2025. Accepted: November 21st, 2025.

Abstract
In this article is presented a pedagogical methodology of applied research with a territorial approach, implemented in engineering programs at the Universidad Nacional de Colombia. Faced with the persistent gap between theoretical training and the practical competencies in demand, a Project-Based Learning (PBL) or "learning by doing" model was designed, which uses real problems from the local and national context as the axis of the educational process. The methodology was developed through an action-research cycle, involving more than 300 undergraduate and graduate students. The results demonstrate a significant impact on student motivation, social knowledge appropriation, and the development of research competencies. A bank of over 30 case studies aligned with the Sustainable Development Goals (SDG) and a pedagogical guide for the model's replicability were generated. It is concluded that the territorial anchoring of PBL not only strengthens technical training but also promotes engineering with greater social responsibility and capacity for sustainable development.

Keywords: project-based learning; territorial approach; engineering education; action-research; integral formation.

Investigación aplicada con enfoque territorial, una metodología pedagógica basada en proyectos

Resumen
Este artículo presenta una metodología pedagógica de investigación aplicada con enfoque territorial, implementada en programas de ingeniería de la Universidad Nacional de Colombia. Ante la brecha persistente entre la formación teórica y las competencias prácticas demandadas, se diseñó un modelo de Aprendizaje Basado en Proyectos (ABP) o "aprender haciendo", que utiliza problemáticas reales del contexto local y nacional como eje del proceso formativo. La metodología se desarrolló mediante un ciclo de investigación-acción, involucrando a más de 300 estudiantes. Los resultados demuestran un impacto significativo en la motivación estudiantil, la apropiación social de conocimiento y el desarrollo de competencias para la investigación. Se generó un banco con más de 30 casos de estudio alineados con los Objetivos de Desarrollo Sostenible (ODS) y una guía pedagógica para la replicabilidad del modelo. Se concluye que el anclaje territorial del ABP no solo fortalece la formación técnica, sino que promueve una ingeniería con mayor responsabilidad social y capacidad para el desarrollo sostenible.

Palabras clave: aprendizaje basado en proyectos; enfoque territorial; educación en ingeniería; investigación-acción; formación integral.

1 Introducción

La formación de ingenieros íntegros en el siglo XXI enfrenta el reto fundamental de superar la disociación entre el conocimiento teórico impartido en el aula de clase y las habilidades prácticas requeridas en un ámbito profesional dinámico y complejo [1]. Esta brecha es particularmente crítica en contextos latinoamericanos, donde los ingenieros deben ser capaces de actuar como mediadores entre el conocimiento científico-técnico y las realidades sociales, económicas y ambientales de sus territorios [2,3].

La educación tradicional a menudo centrada en la transmisión de conocimiento teórico, suele ser abstracta en su forma de presentación y oratoria, ésta, ha demostrado ser

How to cite: Vallejo-López, T., Restrepo-Baena, O.J. and Tobón, J.I., Investigación aplicada con enfoque territorial, una metodología pedagógica basada en proyectos DYNA, (93)240, pp. 132-138, January - March, 2026.

insuficiente para preparar profesionales con la capacidad de innovar y proponer soluciones contextualizadas técnico socialmente [1,4]. La rápida evolución tecnológica y las cambiantes necesidades del mercado exigen un enfoque educativo que vaya más allá de lo teórico, capacitando a los estudiantes con habilidades aplicadas para enfrentar desafíos reales [1,5], partiendo del conocimiento del territorio, de los desafíos, de las problemáticas internas y de las variables externas que afectan a la comunidad.

Como respuesta a este desafío - oportunidad, este artículo presenta el diseño, la implementación y los resultados de una metodología de "aprender haciendo", una modalidad del Aprendizaje Basado en Proyectos (ABP), enriquecida con el enfoque territorial, el cual aterriza situaciones del contexto nacional ante la perspectiva de la asignatura específica según sea el caso de aplicación.

Esta estrategia pedagógica sitúa al estudiante como protagonista de su proceso de aprendizaje, enfrentándolo a la resolución de problemas auténticos y relevantes para la comunidad [1,6]. El anclaje territorial, inspirado en los principios de la Educación Basada en el Lugar (Place-Based Education), utiliza el entorno local como un laboratorio vivo, lo que garantiza no solo la pertinencia del aprendizaje sino también su potencial impacto social [7, 8], lo que genera una trascendencia en la ingeniería, aportando desarrollo conceptual, analítico y metodológico al estudiante, futuro ingeniero o ingeniero profesional, quien es a su vez ciudadano, y quien a su vez es un ser humano racional, consciente de los múltiples desafíos que enfrenta el desarrollo territorial, no ajeno al individuo. Al conectar el currículo con la cultura, la geografía y las problemáticas locales, se fomenta una comprensión más profunda y un mayor compromiso por parte del estudiante [9,10].

La pertinencia de esta propuesta se ve reforzada por su alineación estratégica con directrices institucionales, como el Plan Global de Desarrollo de la Universidad Nacional de Colombia; nacionales, como el Plan Nacional de Desarrollo; e internacionales, como los Objetivos de Desarrollo Sostenible (ODS) [1]. Esta alineación no es una mera justificación administrativa; funciona como un eje pedagógico central que enmarca los problemas de ingeniería no como ejercicios abstractos, sino como actos de responsabilidad cívica y profesional. Al exigir que los casos de estudio aborden directamente estos marcos, la metodología obliga a los estudiantes a trascender la solución puramente técnica y a considerar las complejas implicaciones socioeconómicas y ambientales de su trabajo.

De este modo, el enfoque territorial se convierte en el mecanismo que traduce políticas macro en proyectos de ingeniería tangibles a nivel micro, enseñando a los futuros profesionales y profesionales activos, a operar como agentes activos del desarrollo desde el individuo hacia la sociedad. La literatura académica respalda sólidamente el ABP como un medio eficaz para desarrollar competencias críticas, analíticas y de colaboración [11,12], mientras que la investigación-acción se establece como el marco metodológico idóneo para la innovación pedagógica en contextos universitarios [13,14].

En virtud de esta premisa, el objetivo de este trabajo es describir y analizar el diseño, la implementación y los resultados de esta metodología pedagógica, tomando como caso de estudio la Facultad de Minas de la Universidad Nacional de Colombia, Sede Medellín.

A través de la evidencia recopilada, se busca demostrar su impacto en la formación integral de los estudiantes y proponer un modelo robusto y replicable que pueda contribuir a la necesaria transformación de la educación en ingeniería, preparándola para los desafíos del presente y del futuro.

2 Diseño de la metodología pedagógica

2.1 Fundamento teórico: el Aprendizaje Basado en Proyectos (ABP) con anclaje territorial

La metodología se fundamenta en el principio del "aprender haciendo" (learning by doing), una filosofía educativa que postula que el aprendizaje más significativo y duradero ocurre cuando los individuos se involucran activamente en la experiencia [1,15]. Este principio, articulado por pensadores como John Dewey, sostiene que la educación debe ser un proceso de experimentación y prueba, no de mera absorción de información [1,8], es decir, que resulta valioso que el estudiante se vea inmerso en prácticas extramurales que acrediten la validación de su conocimiento, estando en el territorio, percibiendo según el contexto de su profesión, sus posibilidades de aporte, desde la ingeniería, hacia los territorios.

Dentro de este marco, el Aprendizaje Basado en Proyectos (ABP) emerge como la estrategia central, donde los estudiantes trabajan de manera colaborativa durante un período extendido para investigar y responder a un problema o desafío complejo y auténtico [6,16] de origen locativo y con contexto fundamentado en la ingeniería. El proyecto se convierte en el vehículo para el aprendizaje, permitiendo la integración de teoría y práctica y el desarrollo de habilidades de resolución de problemas, pensamiento crítico y colaboración conjunta intersectorial [11,17].

La innovación clave de esta propuesta radica en la incorporación de un enfoque territorial explícito. Este enfoque va más allá de utilizar simples ejemplos locales; implica un compromiso pedagógico profundo que integra las dimensiones geográficas, culturales, socioeconómicas y políticas del lugar como componentes esenciales del proceso de aprendizaje [1,18]. Se alinea con los principios de la Educación Basada en el Lugar (Place-Based Education - PBE), que conecta el programa con las comunidades y los entornos locales para fomentar la audacia estudiantil temprana (desde semestres iniciales), el compromiso cívico y una comprensión contextualizada del conocimiento [7,10].

La sinergia entre ABP y el enfoque territorial crea un ciclo virtuoso, en primer lugar, los problemas reales del territorio motivan un aprendizaje profundo y auténtico (ABP), y adquirido este insumo, este aprendizaje se orienta a generar soluciones que tengan un impacto positivo y perdurable en ese mismo territorio. Este modelo busca, en esencia, formar ingenieros "para la vida y el entorno", formando una relación tripartita, entre la Universidad, la Empresa y la Sociedad [1].

2.2 Metodología de implementación

2.2.1 La Investigación-Acción Pedagógica

La implementación del proyecto no fue un evento estático, sino un proceso dinámico y reflexivo estructurado bajo el enfoque de la Investigación-Acción. Este lineamiento es intrínsecamente participativo y rotativo o cíclico, combinando la acción (implementar la metodología pedagógica) con la reflexión sistemática (evaluar y mejorar continuamente la práctica) [14,19]. Es particularmente adecuado para la innovación educativa en la enseñanza superior, ya que permite a los docentes convertirse en investigadores de su propia práctica, generando conocimiento contextualizado [20,21] y creando nuevos aportes e ideas que pueden contribuir al cambio auténtico de las condiciones actuales de los territorios según su contexto.

La intervención se llevó a cabo en un amplio espectro de asignaturas de pregrado y posgrado de la Facultad de Minas de la Universidad Nacional de Colombia, Sede Medellín. La población objetivo incluyó a más de 300 estudiantes de cursos tan diversos como "Rocas y Minerales en la Industria", "Fundamentos de Proyectos en Ingeniería", "Seminario de Investigación", "Tópicos Especiales en Minería", "Metalurgia extractiva", entre otros. Esta diversidad de contextos académicos y niveles de formación de las distintas ingenierías, demuestra la flexibilidad y la robustez de la metodología, que pudo ser adaptada a diferentes áreas del conocimiento en ingeniería.

El proceso siguió los ciclos iterativos característicos de la investigación-acción, como se detalla en la Tabla 1. Cada ciclo permitió ajustar y perfeccionar el modelo pedagógico basándose en la evidencia recopilada directamente de la experiencia de estudiantes y docentes.

Tabla 1.
Fases y Actividades de la Metodología de Investigación-Acción.

Fase	Objetivo de la Fase	Actividades Clave
Planificación	Definir el marco de trabajo y los instrumentos pedagógicos.	Diseño de la guía pedagógica, desarrollo de talleres de ideación y delimitación de problemas, conformación de equipos de trabajo, revisión bibliográfica.
Acción (Implementación)	Aplicar la metodología de ABP con enfoque territorial en el aula.	Desarrollo de proyectos de investigación aplicada por parte de los estudiantes, seguimiento quincenal y tutorías por parte del equipo docente.
Observación (Evaluación)	Recolectar evidencia cuantitativa y cualitativa del impacto.	Aplicación de encuestas de percepción, observación directa en el aula, análisis de los entregables de los proyectos (informes, prototipos).
Reflexión (Perfeccionamiento)	Analizar los resultados para ajustar y mejorar el modelo.	Análisis estadístico de encuestas, discusión cualitativa de resultados con docentes y estudiantes, refinamiento de la guía pedagógica para ciclos futuros.

Fuente: Elaboración propia a partir de [1].

2.3 Instrumentos para la implementación y sistematización

Dos instrumentos fueron fundamentales para la ejecución y la sistematización de la experiencia: el banco de casos de estudio y la guía pedagógica.

El banco de casos de estudio se consolidó como un resultado tangible del aprendizaje estudiantil, superando la meta inicial de 5 para llegar a más de 30 proyectos formulados. Este banco no es únicamente un repositorio, sino un instrumento pedagógico dinámico. Su creación se facilitó a través de talleres estructurados, que guiaron a los estudiantes en el proceso de identificar un problema relevante en su entorno, delimitar su alcance, formular objetivos claros y relacionarlo con su formación académica y los ODS. Los casos abarcaron líneas temáticas estratégicas como energía, aguas, infraestructura, minería, comunidad y apropiación social del conocimiento, demostrando la amplia aplicabilidad de la metodología.

La Guía Pedagógica de Investigación representa el principal producto de sistematización del conocimiento pedagógico generado. Su estructura está diseñada para funcionar como una herramienta de escalera, cada peldaño es un paso del cómo dar el siguiente, del cómo aplicar este conocimiento adquirido, proporcionando a los estudiantes un itinerario claro para "aprender a investigar" de manera autónoma. La guía abarca todo el proceso investigativo, desde la planificación (elección y delimitación del tema, formulación de problemas y objetivos) y la construcción del marco teórico, hasta la ejecución metodológica, la discusión de resultados y las recomendaciones para la comunicación científica. La existencia de esta guía es un elemento crucial para la sostenibilidad y escalabilidad de la innovación. Al sistematizar el "cómo hacer" de la metodología, se transforma una intervención exitosa pero focalizada, dependiente de sus impulsores originales, en un modelo pedagógico institucional que puede ser transferido y adoptado por otros docentes y universidades, asegurando así su perdurabilidad, su escalamiento, y ampliando su impacto más allá del contexto inicial del proyecto.

3 Resultados de la implementación

La aplicación de la metodología de ABP con enfoque territorial generó resultados significativos en múltiples dimensiones, abarcando desde la percepción y el compromiso de los estudiantes hasta la producción de conocimiento aplicado y su profundización en la comunidad académica.

3.1 Impacto en la percepción y el compromiso estudiantil

Los datos recopilados a través de una encuesta pedagógica aplicada al finalizar la intervención revelan un impacto marcadamente positivo en la comunidad estudiantil. Los resultados, sintetizados en la Tabla 2, muestran un alto grado de valoración de la investigación como componente clave de la formación profesional.

Tabla 2.
Síntesis de Resultados de la Encuesta de Percepción Estudiantil

Indicador de Percepción	Resultado Cuantitativo (% de Acuerdo/Interés)	Implicación Pedagógica
La investigación fortalece el perfil académico y profesional.	97%	La metodología conecta el aprendizaje con la empleabilidad y el desarrollo de carrera, respondiendo a una necesidad sentida por los estudiantes.
La investigación es importante para la apropiación de conocimiento.	95%	El ABP es percibido por los estudiantes como un método de aprendizaje profundo y efectivo, en contraste con enfoques más pasivos, como la oratoria tradicional de clase.
Considera importante abordar temas de investigación en el aula.	95%	Existe una demanda estudiantil por integrar la investigación en el currículo regular, validando la pertinencia del modelo propuesto.
Interés en participar en eventos de socialización de la investigación.	98%	La metodología no solo desarrolla habilidades, sino que también genera entusiasmo y deseo de participar en la comunidad investigativa.
Participación previa en grupos de investigación.	35%	La estrategia funciona como una vía de iniciación a la investigación altamente efectiva, alcanzando a una mayoría de estudiantes (65%) que no se involucraban previamente.

Fuente: Elaboración propia a partir de las conclusiones del análisis estadístico.

El análisis de estos datos revela una dinámica fundamental: si bien la mayoría de los estudiantes (65%) no había tenido una participación formal previa en semilleros o grupos de investigación, una mayoría (95%) considera crucial que estos temas se aborden directamente en las asignaturas del plan de estudios. Esto sugiere que el proyecto logró abrir una puerta de acceso a la cultura investigativa para una amplia base estudiantil que, de otro modo, podría percibir la investigación como una actividad ajena o reservada para unos pocos. La metodología, por tanto, no solo enseña a investigar, sino que despierta el interés y la oportunidad de hacerlo desde el aula tradicional.

3.2 Producción de conocimiento aplicado: el banco de proyectos

Un resultado tangible y directo del aprendizaje estudiantil fue la consolidación de un robusto banco de proyectos, que superó inclusive la meta inicial. Se obtuvieron más de 30 participaciones formales que dieron cuerpo a un documento de 183 páginas con casos de estudio. Este logro cuantitativo es un indicador del alto nivel de compromiso y productividad que la metodología es capaz de generar.

Más allá de la cantidad, la calidad y diversidad de los proyectos demuestran la eficacia del enfoque territorial. Los estudiantes abordaron problemáticas reales y pertinentes para el contexto colombiano, enmarcadas en líneas temáticas estratégicas como energía, gestión del agua, infraestructura sostenible, desarrollo comunitario y buenas prácticas de ingeniería. Estos proyectos no fueron meros ejercicios académicos, sino verdaderos intentos de aplicar el conocimiento de la ingeniería para proponer soluciones a desafíos concretos, alineados con los ODS y los planes de desarrollo nacionales.

3.3 Socialización y diseminación del conocimiento

El proyecto buscó activamente la validación y diseminación de sus resultados en la comunidad académica y profesional. Se logró una participación destacada en eventos de alto impacto para la educación en ingeniería, como el Encuentro Internacional de Educación en Ingeniería (EIEI) ACOFI 2024 y el III Coloquio Tecnología, Ingeniería y Sociedad, alcanzando a una audiencia combinada de más de 1000 personas.

La presentación de una ponencia en el EIEI ACOFI 2024, el foro más importante de educación en ingeniería en Colombia, representa una validación externa por pares académicos del más alto nivel. Esta socialización cumple un doble propósito: por un lado, contribuye al campo de la pedagogía en ingeniería compartiendo una experiencia exitosa y, por otro, somete el trabajo a un escrutinio riguroso, completando así el ciclo de la investigación-acción. Adicionalmente, se produjeron y distribuyeron materiales de divulgación como un póster científico y contenido digital, asegurando un alcance más amplio de los hallazgos del proyecto.

4 Discusión analítica

La interpretación de los resultados, a la luz de la pregunta de investigación y el marco teórico, permite extraer conclusiones robustas sobre la eficacia y las implicaciones de la metodología implementada. El alto compromiso estudiantil, la producción de casos de estudio y la validación en foros académicos indican que la implementación del "aprender haciendo" con enfoque territorial tiene un impacto positivo y medible en la calidad y eficacia de la formación integral del ingeniero, que produce iniciativas basadas en el contexto, y que las materializa acorde a su nivel de aprendizaje y de conocimiento, en continuo crecimiento.

Los hallazgos del proyecto confirman y enriquecen las teorías del Aprendizaje Basado en Proyectos. Se evidencia que el aprendizaje es más profundo y duradero cuando es activo, contextualizado y se centra en la resolución de problemas auténticos [6,16,22]. La experiencia demuestra que cuando los estudiantes se enfrentan a un desafío real y relevante, su motivación intrínseca aumenta, lo que se traduce en un mayor esfuerzo y una apropiación más significativa de los conceptos teóricos, que dejan de ser abstractos para convertirse en herramientas para la acción [1,23], la cual resulta provechosa y beneficiosa para el profesional, para la academia, la empresa y el entorno.

El "enfoque territorial" se revela como una manifestación práctica y poderosa de la Educación Basada en el Lugar

(PBE). Al anclar los proyectos en la comunidad local, se incrementa exponencialmente la relevancia del aprendizaje [7,9]. Los proyectos desarrollados por los estudiantes, al abordar problemas locales alineados con los ODS, son un ejemplo directo del principio "actuar localmente, pensar globalmente", preparando a los futuros profesionales para comprender que la ingeniería es una práctica inherentemente social. Este enfoque responde directamente a los desafíos de la educación superior en Latinoamérica, que demanda una mayor conexión con las necesidades sociales y una formación que promueva la innovación y la adaptabilidad [5,24,25].

La metodología implementada contribuye de manera decisiva a la "formación integral" del ingeniero, un concepto que trasciende la mera competencia técnica [2,3,26]. Al trabajar en proyectos territoriales, los estudiantes se ven obligados a desarrollar un conjunto de habilidades transversales: pensamiento crítico para analizar problemas complejos, creatividad para proponer soluciones innovadoras, comunicación efectiva para interactuar con diferentes actores, y trabajo en equipo para integrar conocimientos multidisciplinarios [27,28]. Fundamentalmente, desarrollan una conciencia ética y una responsabilidad social al confrontar las implicaciones humanas y ambientales de sus decisiones de diseño en ingeniería. El modelo de trabajo intersectorial que se promueve (universidad-empresa-territorio) es un reflejo de esta formación integral en acción, preparando profesionales capaces de dialogar y construir soluciones en contextos reales.

Para asegurar la rigurosidad en la evaluación de estos proyectos complejos, es crucial contar con instrumentos adecuados. La Tabla 3 presenta una rúbrica sugerida que formaliza los criterios de evaluación implícitos en la metodología, proporcionando una herramienta práctica y adaptable para otros educadores. Este tipo de instrumento es esencial para guiar a los estudiantes y para realizar una evaluación formativa propositiva que valore tanto el proceso como el producto concluido [29-31].

Tabla 3.
Rúbrica sugerida para la evaluación de proyectos con enfoque territorial

Criterio de Evaluación	Insuficiente (1)	Básico (2)	Avanzado (3)	Sobresaliente (4)
1. Pertinencia y Delimitación del Problema Territorial	El problema no es relevante para el contexto territorial o está pobremente definida.	El problema es relevante pero su delimitación es ambigua y carece de justificación con datos.	El problema está bien delimitado y su relevancia se justifica, mostrando una buena comprensión del contexto.	El problema está claramente delimitado, demuestra una profunda comprensión de las complejidades del contexto y su relevancia está sólidamente justificada con datos locales y alineación con planes de desarrollo.
2. Rigor en la Aplicación del Marco Teórico y Metodológico	No se aplica un marco teórico o metodológico adecuado. Hay errores conceptuales graves.	Se aplica un marco teórico básico, pero con imprecisiones. La metodología es simple y poco detallada.	Se aplica un marco teórico y metodológico adecuado con rigor. La selección de métodos es pertinente.	Se demuestra un dominio excepcional del marco teórico, integrando diversas fuentes. La metodología es robusta, innovadora y perfectamente alineada con los objetivos.
3. Calidad y Viabilidad de la Solución de Ingeniería Propuesta	La solución propuesta no es técnicamente funcional o es inviable.	La solución es funcional a nivel conceptual, pero presenta debilidades técnicas o de viabilidad significativas.	La solución es técnicamente sólida, viable y responde adecuadamente al problema planteado.	La solución es técnicamente sólida, viable, creativa y demuestra un alto grado de innovación, considerando restricciones realistas.
4. Análisis del Impacto Social y Ambiental (Conexión con ODS)	No se consideran los impactos sociales o ambientales de la solución.	Se mencionan los impactos de forma superficial, sin un análisis profundo ni conexión clara con los ODS.	Se realiza un análisis adecuado de los principales impactos sociales y ambientales, con una conexión explícita a los ODS.	Se realiza un análisis exhaustivo y crítico de los impactos, considerando múltiples actores y dimensiones, y se proponen medidas de mitigación o potenciación bien fundamentadas.
5. Colaboración y Comunicación del Equipo	El trabajo en equipo es deficiente. La comunicación de los resultados es confusa e ineficaz.	Hay evidencia de trabajo en equipo, pero con roles poco claros. La comunicación es comprensible pero poco profesional.	El equipo trabaja de forma colaborativa y organizada. La comunicación de los resultados es clara y profesional.	El equipo demuestra una sinergia excepcional, con roles claros y una gestión eficaz del proyecto. La comunicación es persuasiva, profesional y adaptada a diferentes audiencias.
6. Robustez técnica y desarrollo en ingeniería	El trabajo es poco explicativo, sin objetivos claros y con bajo rigor de desarrollo técnico	Hay evidencia de objetivos claros, pero con deficiencias a nivel de diseño en ingeniería, baja profundización técnica	Objetivos claros con alcance definido, con diseño de ingeniería básica, localización y tamaño.	Trabajo multidimensional aplicado, objetivos y alcance definidos, ingeniería de detalle, prototipado y solidez técnica.

Fuente: Elaboración propia a partir de los principios de evaluación en ABP y los objetivos del proyecto [1,23,31].

Finalmente, es necesario abordar de forma crítica las limitaciones del proyecto. La limitación de disponibilidad profesional para asesorías expertas en el área resalta un desafío institucional recurrente: la necesidad de estructuras

de apoyo más sólidas y ágiles para la innovación pedagógica docente. Este tipo de iniciativas, aunque exitosas, a menudo dependen del sobreesfuerzo de los profesores proponentes, lo que limita su sostenibilidad a largo plazo.

5 Conclusiones y recomendaciones

El presente estudio demuestra que la metodología de Aprendizaje Basado en Proyectos con un explícito enfoque territorial es una estrategia pedagógica de alto impacto para la educación en ingeniería. Se confirma que este modelo es eficaz para reducir la brecha entre la formación teórica y la práctica profesional, promoviendo un aprendizaje significativo que se ancla en la resolución de problemas reales y pertinentes. La implementación de esta metodología desarrolla competencias técnicas y de investigación, y también fomenta habilidades transversales indispensables como el pensamiento crítico, la colaboración conjunta, el trabajo en equipo y una profunda conciencia ética y social en los futuros ingenieros.

Se concluye que la metodología impacta positivamente la formación integral de los estudiantes al aumentar de manera demostrable su motivación y compromiso, mejorar la apropiación de conocimientos complejos a través de su aplicación directa, y alinear la educación superior con los desafíos concretos del desarrollo sostenible a nivel local, nacional y global. El proyecto ha logrado transformar el aula en un espacio de co-creación de conocimiento, donde los estudiantes no solo aprenden ingeniería, sino que aprenden a ser ingenieros responsables y agentes de cambio en sus territorios.

Con base en estos hallazgos, se formulan las siguientes recomendaciones:

Para Instituciones de Educación Superior: Es imperativo fomentar la adopción institucional de pedagogías activas y contextualizadas como el ABP con enfoque territorial. Esto requiere ir más allá del apoyo a iniciativas aisladas y crear estructuras permanentes de soporte a la innovación docente, que ofrezcan formación, recursos y reconocimiento a los profesores que lideran estos procesos de transformación.

Para Docentes e Investigadores: Se recomienda utilizar la "Guía Pedagógica de Investigación" como un recurso práctico y adaptable para implementar este modelo en diversas asignaturas y disciplinas. Es crucial promover la colaboración interdisciplinaria para abordar la complejidad de los problemas territoriales, enriqueciendo el aprendizaje de los estudiantes con múltiples perspectivas.

Como líneas de investigación futura, se sugiere realizar estudios longitudinales para evaluar el impacto a largo plazo de esta metodología en la trayectoria profesional y el desempeño laboral de los egresados. Asimismo, resulta pertinente explorar la adaptación y aplicación de este modelo en otros contextos disciplinares y geográficos, tanto en Colombia como en otras regiones de Latinoamérica. Para así entonces, continuar trabajando en el desarrollo y validación de instrumentos de evaluación robustos, como la rúbrica propuesta, que permitan medir de manera fiable el desarrollo de competencias transversales complejas, como la responsabilidad social y el pensamiento sistémico, que son el corazón de una formación ingenieril verdaderamente integral.

Referencias

[1] Aburto, P., Reflexiones sobre la Metodología de Aprender haciendo, una guía para los profesores y un acercamiento a los escenarios de aprendizajes, Managua, UNAN-Managua, 2018.

[2] Aiello-Sindoni, M., Dificultades en el aprendizaje de la metodología de la investigación, Magis, Revista Internacional de Investigación en Educación, 2(4), pp. 141-155, 2009.

[3] Alarcón, L., Estrategias metodológicas creativas para potenciar los estilos de aprendizaje, San Gregorio, 2021.

[4] Álvarez-de Zayas, C.M. y Sierra-Lombardía, V., Metodología de la investigación científica, Cochabamba, Grupo Editorial Kipus, 2019.

[5] Ardoin, N.M., Toward an interdisciplinary understanding of place: Lessons for environmental education, Canadian Journal of Environmental Education, 11(1), pp. 112-126, 2006.

[6] Barret, T., Understanding problem-based learning, in: Barret, T., Mac Labhrainn, I. and Fallon, H., Eds., Handbook of enquiry and problem-based learning, Galway, CELT, 2005, pp. 13-25.

[7] Barrows, H.S., A taxonomy of problem-based learning methods, Medical Education, 20(6), pp. 481-486, 1986.

[8] Blumenfeld, P.C., Soloway, E., Marx, R.W., Krajcik, J.S., Guzdial, M., and Palincsar, A., Motivating project-based learning: Sustaining the doing, supporting the learning, Educational Psychologist, 26(3-4), pp. 369-398, 1997.

[9] De Vincenzi, A., Diseño de rúbricas analíticas para la evaluación formativa de competencias en ciencias informáticas, EDUTEC, Revista Electrónica de Tecnología Educativa, (80), pp. 198-214, 2022. DOI: https://doi.org/10.21556/edutec.2022.80.2425

[10] Delgado, A., and Romero, I., Environmental conflict analysis using an integrated grey clustering and entropy-weight method: a case study of a mining project in Peru, Environmental Modelling and Software, 77, pp. 108-121, 2016. DOI: https://doi.org/10.1016/j.envsoft.2015.12.011

[11] Escribano, A. y Del Valle, A., El aprendizaje basado en problemas: una propuesta metodológica en educación superior, Madrid, Narcea Ediciones, 2008.

[12] Estrada, O., et al., El sistema de habilidades en la formación del tecnólogo de la carrera de Mecanización Agropecuaria, Revista Ciencias Técnicas Agropecuarias, 24(1), pp. 58-63, 2015.

[13] Fals-Borda, O., La investigación acción participativa: aporte de Fals Borda a la educación popular, Espacio Abierto, 17(4), pp. 615-627, 2008.

[14] Fawcett, S.B., Seekins, T., Whang, P.L., Muiu, C., and Suárez-Balcazar, Y., The concerns report: a strategy for needs assessment and citizen participation, Lawrence, KS, University of Kansas, USA,1982.

[15] Freire, P., Pedagogy of the oppressed, Herder and Herder, New York, USA, 1970.

[16] Glasson, G.E., Mhango, N., Phiri, A., and Lanier, M., Sustainability science education in Africa: an analysis of case studies of inquiry-based learning in Malawi, International Journal of Science Education, 32(14), pp. 1837-1856, 2010.

[17] Gruenewald, D.A., The best of both worlds: a critical pedagogy of place, Educational Researcher, 32(4), pp. 3-12, 2003.

[18] Hernández, F. y Maquilón, J.J., El proceso de investigación. Del problema al informe de investigación, en: Hernández, F., Colás, M.P. y Buendía, L., Coords., Competencias científicas para la realización de una tesis doctoral, La Coruña, Davinci Continental, 2010, pp. 31-55.

[19] Hernández-Sampieri, R., Fernández, C. y Baptista, P., Metodología de la Investigación, McGraw Hill, México D.F., México, 2018.

[20] Hoyles, C. and Noss, R., What can digital technologies take from and bring to research in mathematics education?, en: Bishop, A.J. et al., Eds., Second International Handbook of Mathematics Education, Dordrecht, Kluwer Academic, 2003, pp. 323-349. DOI: https://doi.org/10.1007/978-94-010-0273-8_11

[21] Jennings, N., Swidler, S., and Koliba, C., Place-based education in the standards-based reform era—conflict or complement?, American Journal of Education, 112(1), pp. 44-65, 2005.

[22] Leaman-Hasbún, S.D. y Cárcamo-ásquez, H.G., Investigación acción participativa: vinculación con la epistemología del sujeto conocido, desarrollo histórico y análisis de sus componentes, Espacio Abierto, 30(3), pp. 145-168, 2021.

[23] Lewin, K., Action research and minority problems, Journal of Social Issues, 2(4), pp. 34-46, 1946.

[24] Londoño, O.L., Maldonado, L.P. y Calderón, L.C., Guía para construir estados del arte, Bogotá, International Corporation of Networks of Knowledge, 2014.
[25] Marín, S.A., Apropiación social del conocimiento: una nueva dimensión de los archivos, Revista Interamericana de Bibliotecología, 35(1), pp. 55-62, 2012.
[26] Molina, A., La competencia profesional en el ingeniero del nuevo milenio, Ingeniería y Desarrollo, (9), pp. 60-71, 2001.
[27] Monereo, C., Castelló, M., Clariana, M., Palma, M. y Pérez, M.L., Estrategias de enseñanza y aprendizaje, Graó, Barcelona, España, 1999.
[28] Montoya-Suárez, L.M., Enfoque integral del ingeniero del siglo XXI: una revisión de la literatura, Revista CEA, 5(10), pp. 11-30, 2019. DOI: https://doi.org/10.22430/24223182.1309
[29] Norton, L., Action research in teaching and learning: a practical guide to conducting pedagogical research in universities, 2nd ed., Routledge, Abingdon, UK, 2018.
[30] Restrepo-Gómez, B., La investigación-acción educativa y la construcción de saber pedagógico, Educación y Educadores, (7), pp. 45-55, 2002.
[31] Rulifson, G., McClelland, C.J. and Battalora, L.A., Project-based learning as a vehicle for social responsibility and social justice in engineering education, Proceedings of ASEE Annual Conference and Exposition, 2018. DOI: https://doi.org/10.18260/1-2--30902
[32] Kellar, J.J., et al., The development of a creative and analytical (C&A) thinking program for engineering students, International Journal of Gender, Science and Technology, 7(2), pp. 178-193, 2015.
[33] Kolb, D.A., Experiential learning: experience as the source of learning and development, Englewood Cliffs, NJ, Prentice-Hall, 1984.
[34] Sánchez-Bolívar, G., El área socio-humanística y la formación integral del ingeniero, Ingeniería e Investigación, (23), pp. 20-25, 1991.
[35] Sayago, Z.B. y Chacón, M.A., Las prácticas evaluativas en la escuela básica: de la concepción a la acción, Educere, 10(34), pp. 433-442, 2006.
[36] Schank, R.C., Teaching minds: How cognitive science can save our schools, Teachers College Press, New York, USA, 2012.
[37] Smith, G.A. y Sobel, D., Place- and community-based education in schools, Routledge, New York, USA, 2010.
[38] Tamayo y Tamayo, M., Aprende a investigar, 3ra ed., Bogotá, ICFES, 1999.
[39] Vargas, A., Hernandez, L. y Aguilar, A., Exploración de competencias generales del ingeniero industrial administrador requeridas por empleadores, Revista de la Facultad de Ingeniería, 28 (52), pp. 65-80, 2019.

T. Vallejo-López, es Ing. Ingeniero de Minas y Metalurgia, estudiante de la Maestría en Ingeniería de Recursos Minerales y joven investigador en la Facultad de Minas de la Universidad Nacional de Colombia. Es miembro del grupo de investigación ÍGNEA - CEMATCO y ha participado activamente en el desarrollo e implementación del proyecto de investigación aplicada con enfoque territorial.
ORCID: 0009-0001-0312-9008

O.J. Restrepo-Baena, es PhD., Profesor Titular en la Facultad de Minas de la Universidad Nacional de Colombia, adscrito al Departamento de Materiales y Minerales e investigador senior de MinCiencias. Dirige el grupo de investigación ÍGNEA, enfocados en minería y la ciencia de materiales y su aplicación industrial, así como en la innovación pedagógica para la formación de ingenieros.
ORCID: 0000-0003-3944-9369

J.I. Tobón, es PhD., Profesor Titular en la Facultad de Minas de la Universidad Nacional de Colombia, adscrito al Departamento de Materiales y Minerales e investigador senior de MinCiencias. Dirige el grupo de investigación CEMATCO, enfocados en la química del cemento y materiales de construcción y su aplicación industrial, así como en la innovación pedagógica para la formación de ingenieros.
ORCID: 0000-0002-1451-1309

INSTRUCTIONS FOR OUR CONTRIBUTORS - DYNA JOURNAL

DYNA Journal is a general scientific publication of the technological science area founded in 1933. It is the means of expression of those who work in the area of engineering, science, and technology of the School of Mines of the Universidad Nacional de Colombia, Medellin Branch, and of researchers of the same area who are in Colombia. DYNA mainly presents scientific and technological development research articles, articles with original reflection on a particular problem or topic, and review articles which offer a general perspective of the state of a specific sphere of science and technology. Notes and communications are also included as are discussions on particular points of the theme covered by the journal: technology, science, and engineering. All of the articles published are subject to the peer or referee review by those of recognized suitability on the article's subject.

The presentation of an article should be accompanied by a Presentation Letter, requesting publication in the journal, declaring that the article is approved by all of the authors, that it has not been published or submitted for consideration in another similar publication or journal. If the article has been published in another medium with a different outreach such as seminar memoirs, newspapers, supplements, etc., these should be specified and the possible publication in DYNA should be justified. Finally, the authors should recommend possible evaluators (2 national and 2 international) for the article being presented. It will be necessary to attach copies of permissions for the reproduction of material which was already published.

The submission of articles and the Presentation Letter are handled through the Open Journal System (OJS) of the National University (UN) Virtual Library (Enter through: http://www.revistas.unal.edu.co/index.php/dyna/user).

DYNA publishes the following in each of its editions: an editorial, research articles, essays, brief communications, and diagnostic images. The journal publishes articles from the following areas:

- Organizational Engineering
- Civil Engineering
- Materials Engineering
- Geosciences and the Environment
- Computer Systems
- Chemistry and Petroleum
- Mechatronics
- Engineering and Biotechnology
- Other areas related to Engineering

 The articles which are published in DYNA are also published in an electronic version (CD-ROM), on the Internet, as well as in other electronic formats which may become important in the future; the authors of the articles accepting these and other virtual or digital forms of publication. DYNA assumes international norms for the publication of the articles such as ISI, Vancouver, and Harvard, with the specifications which shall be given shortly.

SECTION TYPES

Authors who wish to contribute to a certain section of the journal can send their contributions through the OJS system, by which the author will be notified by e-mail; understanding that this does not imply the acceptation of the paper. The Editorial Committee may reject, suggest changes, or (in certain cases), carry out modifications in the received texts. In the latter case, none of the scientific content shall be altered, but the modifications will be limited only to the literary style. The criteria which will apply to evaluate the acceptation of the articles will be the methodological scientific rigor, innovation, the relevance of the research, expositional conciseness, and the literary quality of the text. The journal will publish one or several of the following sections in each number:

1. The Editorial
These are papers written by someone recommended by the Editorial Committee, or otherwise, by one of its members. Its length should not be more than six pages, double-spaced; the bibliography (if there is one) should not contain more than 10 citations. The editorial should be placed under the consideration of the Editorial Committee for its final approval.

2. Letters to the Editor
Critical, analytical, or interpretational positions on documents published in the journal, which, by judgment of the Editorial Committee, make an important contribution to the discussion of the subject of the field, on behalf of the scientific community of reference.

3. Articles of Scientific and Technological Research
Those papers which exposit upon the outcomes of research in engineering (within previously-defined areas) will be considered as articles of scientific and technological research. These should have the following generally used structure: an introduction, the methodology, outcomes, and conclusions. They should not have more than 30 bibliographical citations.

4. Reflection Articles
These present outcomes of research from an analytical, interpretive, or critical perspective of the author, on specific topics in the area of engineering and within the previously defined areas, using original sources. They should not go beyond 10 bibliographical citations.

5. Review Articles
Documents which are a result of research in which the outcomes of published or non-published research projects are analyzed, systematized, and integrated in the field of engineering, with the objective of giving an account of the advances and the developmental trends of the previously cited topics. These articles present a careful bibliographic review of around 50 references.

6. Brief Communication and Summaries
This section allows for us to publish brief articles with greater speed. It allows authors to present their observations, initial outcomes of current research, book reviews, and even to make comments on works that have already been published in the journal. The text should not include more than 10 bibliographical citations.

7. Diagnostic Image (Case Studies)
In this section singular cases are presented which the image is decisive. For publication, one or a maximum of two images, or diagnostic cases, may be submitted. These may be from any branch of engineering and should be accompanied by a short commentary with relation to the case. The length of the commentary may not be less than 15 written lines, single spaced. This page should be sent together with another which has the information about the author or authors which shall be described further on in the presentation of papers.

8. Translations
Translations of classic or current texts, the transcriptions of historical documents, or those of particular interest in the field of the journal's publication are presented.

9. Event Notices
This shall include brief information which announces events related to engineering. It has no cost.

PRESENTATION OF PAPERS

Together with the Commitment Letter, the article shall be presented through the Open Journal System – OJS, of the UN Virtual Library (on the webpage, go to Envío de Artículos).

1. The authors shall send their articles through the Open Journal System (OJS), entering according to the instructions which are found in Envío de Artículos and, additionally will accompany it with the Presentation Letter, which they may write in accordance with the model presented in: Modelo de Carta de Presentación (in Web site: dyna.unalmed.edu.co).

2. The article should be unpublished and may not be submitted simultaneously to the scrutiny of other journals or periodical publications.

3. The maximum length of the articles will be 10 pages, single-spaced, in Spanish or English, letter-sized presentation. Include in the pages the abstract in Spanish (RESUMEN) and in English (ABSTRACT), both of a maximum of 150 words, and the "Keywords" also in Spanish (PALABRAS CLAVES) and in English (KEYWORDS). The articles may NOT be class notes and when they are translations or use material protected by intellectual property rights they should be submitted with the due author authorizations.

4. Every article shall be submitted to the evaluation of two referees designated by the Editorial Committee. The exceptions to this requirement shall be decided upon by the same Committee.

5. Regarding graphics, tables, and figures, these should be processed as objects (in order to ease the editing). Authors may use the program that they wish. These should be sent in an image format (JPG, GIF, BMP, etc.), in black and white or grey tones, avoiding polychromes.

6. The figures that are not presented in an electronic medium should be presented as photography or as vellum and Indian ink.

7. If the text includes photography, its presentation is recommended in black and white, matte, with good contrast. Photographs should be placed on pages of the same size as the text. In the rest of the aspects, the treatment given is similar to that of figures.

8. The presentation of the article will be according to the articles of this number. Footnotes are not admitted due to the typesetting requirements of the journal.

9. Under the title of the article should be included the name of the author (or authors), their professional identification or institutional affiliation, their postal and electronic (e-mail) addresses.

10. The references should go at the end of the paper in the following format:

Journal articles:
Alien, J. S., Samuelson, R. and Newberger, A. Chaos in a model of forced quasi-geostrophic flow over topography: An application of Melinkov's method, J. Fluid Mech., No. 226, pp. 511-547, 1991.

Books:
Baker, G. L. and Golub, J., Chaotic Dynamics: An introduction, Cambridge University Press, Cambridge, 1990.

Chapter of a book:
Lewis, P., Ray, B. and Stevens, J.G. Modeling time series by using Multivariate Adaptive Regression Splines (MARS), In: Time Series Prediction: Forecasting the Future and Understanding the Past (Eds. A. S. Weigend and N. A. Gershenfeid), SFI Studies in the Science of Complexity, Proc. Vol. XV, Addison-Wesley, pp. 297-318, 1994.

Conference proceedings:
Álzate, N., Botero, T. and Correa, D. Title of the Paper. Memorias XIX Congreso Latinoamericano de Ponencias Científicas. Córdoba, Argentina, Tomo II, pp. 219-228, Octubre 2000.

Organization or government report:
U.S. EPA. Status of Pesticides in Registration and Special Review. EPA 738-R-94-008. Washington, DC: U.S. Environmental Protection Agency, 1994.

Thesis:
Jacobs J., Regulation of Life History Strategies within Individuals in Predictable and Unpredictable Environments [PhD Thesis]. Seattle, WA: University of Washington, 1996.

Internet references:
NOAA-CIRES. Climate Diagnostics Center. Advancing Understanding and Predictions of Climate Variability. Available: http://www.cdc.noaa.gov [cited August 8, 1998].

Non-published data:
Last name, N. Non-published data.

Personal communication:
Last name, N. Personal communication.

OTHER CONSIDERATIONS

The author shall always keep a copy of the paper. The Editorial Committee will decide on the publication of each manuscript and will suggest possible modifications when the Committee considers it to be appropriate, after it has been submitted to the evaluation of the selected peers. This procedure will be as brief as possible.

The Journal's Editorial Committee will acknowledge receipt of the originals and will inform the author on their acceptation through communication by e-mail, through the Open Journal System.

The editorial staff of the journal will take the greatest care in avoiding errors in the final transcription of the articles to publish, however, it does not respond for the errors that may appear. If the authors detect important errors, they should recur as soon as possible to the editorial staff so that a list erratas may be prepared for the next number of the journal.

The editorial staff reserves the right to carry out small adjustments on the article titles, as well as minor rectifications in the editing, in translations, resúmenes and abstracts; although the general policy to be followed shall be to consult with the authors about these issues.

NORMAS DE PUBLICACIÓN - REVISTA DYNA
Instrucciones a los Autores

La Revista DYNA es una publicación científica general del área de las ciencias tecnológicas, fundada en 1933, es el medio de expresión de los trabajos en el área de ingeniería, ciencias y tecnología de la Facultad de Minas de la Universidad Nacional de Colombia, sede Medellín y de los investigadores del área en Colombia. DYNA presenta principalmente artículos de investigación científica y de desarrollo tecnológico, artículos de reflexión originales sobre un problema o tópico particular y artículos de revisión que brindan una perspectiva general del estado de un dominio específico de la ciencia y la tecnología. También tienen cabida notas y comunicaciones, así como discusiones sobre puntos particulares de la temática cubierta por la revista: tecnología, ciencias e ingeniería. Todos los artículos publicados se someten a revisión de pares o árbitros, de reconocida idoneidad en el tema.

La presentación de un artículo debe ir acompañada de una Carta de Presentación, solicitando su publicación en la revista, declarando que el artículo es aprobado por todos los autores, que no ha sido publicado o sometido a consideración en otra publicación o revista similar. Deben especificar si el artículo ha sido publicado en otro medio de diferente alcance divulgativo como memorias de seminarios, periódicos, separatas, etc., y justificar su posible publicación en DYNA. Finalmente recomendar posibles evaluadores (2 nacionales y 2 internacionales) para el artículo presentado; de ser necesario adjuntar copias de los permisos para reproducir material ya publicado.

El envío de los artículos y de la Carta de Presentación se hace a través del Sistema Open Jornal System (OJS) de la Biblioteca Virtual UN (Ingresar a través de: http://www.revistas.unal.edu.co/index.php/dyna/login).

DYNA publica en sus ediciones: Editorial, Artículos de Investigación, Ensayos, Comunicaciones Breves e Imágenes Diagnósticas. La revista publica artículos sobre las siguientes áreas:

- Ingeniería de la Organización
- Ingeniería Civil
- Ingeniería de Materiales
- Geociencias y Medio Ambiente
- Sistemas
- Química y Petróleos
- Mecatrónica
- Ingeniería y Biotecnología
- Otros relacionados con Ingeniería

Todo lo publicado se considerará propiedad de DYNA y solo podrá ser reproducido total o parcialmente con el permiso expreso del director. Los artículos que sean publicados en la revista DYNA podrán ser también publicados en la versión electrónica de la revista, en Internet, así como en otros formatos electrónicos (CD-ROM y otros) que surjan en el futuro, aceptando los autores de los artículos éstas y otras formas de publicación virtual o digital. DYNA asume para la publicación de los artículos las normas internacionales como ISI, Vancouver y Harvard con las especificaciones que se detallan mas adelante.

TIPOS DE SECCIONES

Los autores que deseen colaborar en algunas de las secciones de la revista pueden enviar sus aportes (a través del sistema OJS), que será notificado vía e-mail al autor; entendiéndose que ello no implica la aceptación del trabajo. El Comité Editorial podrá rechazar, sugerir cambios o llegado el caso, realizar modificaciones en los textos recibidos; en este último caso, no se alterará el contenido científico, limitándose únicamente al estilo literario. Los criterios que se aplicarán para valorar la aceptación de los artículos serán el rigor científico metodológico, novedad, trascendencia del trabajo, concisión expositiva, así como la calidad literaria del texto. La revista publicará en cada número una o varias de las siguientes secciones:

1. Editorial

Trabajos escritos por encargo del Comité Editorial, o bien, redactados por alguno de sus miembros. Su extensión no debe ser superior a 6 páginas, escritos a doble espacio; la bibliografía si la hay, no debe contener una cifra superior a 10 citas. Esta editorial debe ser puesta a consideración del Comité Editorial para su aprobación final.

2. Cartas al Editor

Posiciones críticas, analíticas o interpretativas sobre documentos publicados en la revista, que a juicio del Comité Editorial constituyen un aporte importante a la discusión del tema ambiental, por parte de la comunidad científica de referencia.

3. Artículos de Investigación Científica y Tecnológica

Tendrán tal consideración aquellos trabajos, que versen sobre resultados de investigaciones en ingeniería, dentro de las áreas definidas con anterioridad. Deben tener la siguiente estructura generalmente utilizada: Introducción, Metodología, Resultados y Conclusiones.

4. Artículos de Reflexión

Son documentos que presentan resultados de investigación desde una perspectiva analítica, interpretativa o crítica del autor, sobre temas específicos en un área de ingeniería y dentro de las áreas definidas anteriormente, recurriendo a las fuentes originales. No debe superar las 10 citas bibliográficas.

5. Artículos de Revisión

Documentos resultados de una investigación donde se analizan, sistematizan e integran los resultados de investigaciones publicadas o no publicadas, sobre el campo de ingenierías, con el fin de dar cuenta de los avances y las tendencias de desarrollo de los temas citados anteriormente. Se caracterizan por presentar una cuidadosa revisión bibliográfica alrededor de 50 referencias.

6. Comunicación Breve y Reseñas

Esta sección permite publicar artículos breves, con mayor rapidez. Ello facilita que los autores presenten observaciones, resultados iniciales de investigaciones en curso, revisiones de libros e incluso realizar comentarios a trabajos ya publicados en la revista. El texto no debe superar las 10 citas bibliográficas.

7. Imagen diagnóstica. (Reporte de Casos)

En esta sección de la revista se presentarán casos singulares en los que la imagen sea resolutoria. Para ello, se aportarán una, o como máximo dos imágenes, o casos diagnósticos, de cualquier rama de la ingeniería y acompañada de un breve comentario en relación con el caso. La extensión del comentario no será menor a 15 líneas escritas a espacio sencillo. Esta página se remitirá junto a otra, con la información del autor o autores y que se detalla mas adelante en presentación de los trabajos.

8. Traducciones

Se presentan traducciones de textos clásicos, o de actualidad, o transcripciones de documentos históricos o de interés particular en el dominio de publicación de la revista.

9. Noticias de Eventos

Incluirá breve información que anunciará eventos relacionados con la ingeniería. No tiene ningún costo.

PRESENTACIÓN DE LOS TRABAJOS

Acompañado de la Carta de Compromiso, el artículo se presentará a través del Sistema Open Journal System – OJS de la Biblioteca Virtual de la UN (ir a Envío de Artículos),

Los autores remitirán sus artículos a través del Sistema Open Journal System (OJS), ingresando según las instrucciones que encuentran en Envío de Artículos y adicionalmente acompañado de la Carta de Presentación, que pueden redactar de acuerdo con el modelo presentado en: Modelo de Carta de Presentación (en sitio Web: dyna.unalmed.edu.co).

El artículo debe ser inédito y no puede someterse simultáneamente al examen de otras revistas o publicaciones periódicas. La extensión máxima de los artículos será de 10 páginas a espacio sencillo, en castellano o en inglés, en papel tamaño carta, incluyendo en ellas el Resumen (máximo de 150 palabras) en castellano (RESUMEN), e inglés (ABSTRACT) y las "Palabras Clave", también en castellano e inglés (Keywords). Los artículos NO pueden ser notas de clase y cuando se trate de una traducción o del

uso de material protegido por "Derechos de propiedad intelectual" deberá contar con las debidas autorizaciones de los autores.

Todo artículo se someterá a la evaluación de dos jurados, designados por el Comité Editorial. Las excepciones a este requisito serán decididas por tal Comité.

Respecto a gráficas, tablas y figuras, éstas deberán procesarse como "objetos" (para facilitar la diagramación de la revista); para ello puede utilizarse el programa que se desee. Se sugiere enviarlas en blanco y negro o tonos de gris, evitando las policromías.

Las figuras que no estén en medio electrónico, se presentan en fotografía o papel albanene y tinta china.

Si el texto incluye fotografías, se recomienda su presentación en blanco y negro, mate, con buen contraste. Las fotografías se deben montar en hojas del mismo tamaño del texto. En los demás aspectos el tratamiento es similar al de las figuras.

La presentación del artículo estará de acuerdo con los artículos de este número. No se admiten "pie de página" por razones de diagramación de la revista.

Al pie del título del artículo debe incluirse el nombre del autor (o autores), su identificación profesional o filiación institucional, su dirección postal y electrónica (e-mail).

Las referencias deberán ir al final con el siguiente formato:

Artículos de revistas:
Alien, J. S., Samuelson, R. and Newberger , A. Chaos in a model offorced quasi-geostrophic flow over topography: an application of Melinkov's method, J. Fluid Mech., 226, 511-547, 1991.

Libros:
Baker, G. L. and Golub , J., Chaotíc Dynamics: An introduction, Cambridge University Press, Cambridge, 1990.

Capítulo de libro:
Lewis, P., Ray, B. and Stevens, J.G. Modeling time series by using Multivariate Adaptive Regression Spiines (MARS), En: Time Seríes Prediction: Forecasting the Futuro and Understanding the Past (Eds. A.S.Weigend y N. A. Gershenfeid), SFI Studies in the Science of Complexity, Proc. Vol. XV, Addison-Wesley, 297-318, 1994.

Memorias de congresos:
Álzate, N., Botero, T. y Correa, D. Título de la Ponencia. Memorias XIX Congreso Latinoamericano de Ponencias Científicas. Córdoba, Argentina, Tomo II, 219-228, Octubre 2000.

Reporte de un organismo o Gobierno:
U.S. EPA. Status of Pesticides in Registration and Special Review. EPA 738-R-94-008. Washington, DC:Ü.S. Environmental Protection Agency, 1994

Tesis:
Jacobs J. Regulación of Life History Strategies within Individuáis in Predictable and Unpredictable Environments [PhD Thesis]. Seattie, WA: University of Washington, 1996.

Referencias de Internet:
NOAA-CIRES Climate Diagnostics Center. Advancing Understanding and Predictions of Climate Variability. Available: http://www.cdc.noaa.gov [citado 8 de Agosto de 1998].

Datos no publicados:
Apellido, N. Datos no publicados

Comunicación Personal:
Apellido, N. Comunicación personal

OTRAS CONSIDERACIONES

El autor siempre conservará una copia del trabajo. Cada manuscrito luego de sometido al proceso de evaluación por pares seleccionados por el Comité Editorial, se decidirá o no su publicación y sugerirá posibles modificaciones cuando lo crea oportuno. Todo este trámite será lo más breve posible.

El Comité Editorial de la Revista acusará recibo de los originales e informará al autor sobre su aceptación, mediante comunicaciones vía correo electrónico.

La redacción de la revista pondrá el máximo cuidado en evitar errores en la trascripción definitiva de los artículos a publicar, no obstante no se responsabiliza de los errores que puedan aparecer. Si los autores detectaran errores importantes deberán dirigirse cuanto antes a la redacción para realizar una fe de erratas en el siguiente número de la revista.

La redacción se reserva el derecho de realizar pequeñas adecuaciones en los títulos de los artículos, así como rectificaciones menores en la redacción, en las traducciones, Resúmenes y Abstracts; aunque la política general que se seguirá será la de consultar a los autores sobre estas cuestiones.

DYNA

DYNA 93 (240), January - March, 2026
is an edition consisting of 100 printed issues
which was finished printing in the month of March of 2026
in Todograficas Ltda. Medellín - Colombia

The cover was printed on Propalcote C1S 250 g,
the interior pages on Propal Beige 90 g.
The fonts used are Times New Roman, Imprint MT Shadow

- Influence of dissolved organic carbon on the limnochemical characteristics of a tropical endorheic wetland during a hydrological period: El Eneal Wetland, Colombia
- Safety risk assessment in a drinking water treatment plant using the NTP 330 method
- Smart audit in real time: automated visual analysis from mobile devices
- Landsat 8-Based estimation of total suspended solids (1.3-43 mg/L) using NDWI, MNDWI and AWEI indices at Tecocomulco Ramsar Wetland, Mexico
- Theoretical investigation of hydrogen sulfide adsorption on doped phthalocyanine nanosheets: DFT calculations
- Design and evaluation of a high-speed centrifugal precision seed-metering device for soybean based on DEM simulation
- AUTOFIRE: an intelligent multi-agent framework for automated extraction and classification of pfSense Firewall rules
- Development of a low-cost power supply with multiple self-adjustable outputs for the operation of silicon photo-multipliers
- Development of a support vector machine-based predictive model for bored pile productivity in residential construction Projects in Iraq
- Study of the variability of physicochemical parameters in different fractions of corn and espartillo intended for the production of solid biofuels
- Identification of areas for photovoltaic projects in La Guajira using GIS and multicriteria analysis
- Evaluation of nitrogen-fixing and phosphorus-solubiling microorganisms in astromelian (*Alstroemeria aurantiaca*), cultivation
- Hybrid material of recycled pastics (PET and PP) and ágggregates for the manufacture of sustainable paving blocks
- Port connectivity assessment and its impact on competitiveness: the case of Buenaventura, Colombia
- Applied research with a territorial approach, a project-based pedagogical methodology

- Influencia del carbono orgánico disuelto en las características limnoquímicas de un humedal endorreico tropical durante un período hidrológico: Humedal El Eneal, Colombia
- Evaluación de riesgos de seguridad en una planta de tratamiento de agua potable mediante el método NTP 330
- Auditoría Inteligente en Tiempo Real: Análisis Visual Automatizado desde Dispositivos Móviles
- Estimación basada en Landsat 8 de sólidos suspendidos totales (1.3-43 mg/L) usando los índices NDWI, MNDWI y AWEI en el Humedal Ramsar de Tecocomulco, México
- Investigación teórica de la adsorción de sulfuro de hidrógeno en nanohojas de ftalocianina dopadas: cálculos DFT
- Diseño y evaluación de un dispositivo de dosificación de semillas de precisión centrífuga de alta velocidad para soja basado en simulación DEM
- AUTOFIRE: un marco inteligente multiagente para la Extracción y clasificación automatizada de reglas de Firewall pfSense
- Desarrollo de una fuente de alimentación de bajo costo con múltiples salidas ajustables para la operación de fotomultiplicadores de silicio
- Desarrollo de un modelo predictivo basado en máquinas de soporte vectorial para la productividad de pilotes perforados en proyectos de construcción residencial en Irak
- Estudio de variabilidad de parámetros fisicoquímicos en diversas fracciones de maíz y espartillo destinadas a la generación de biocombustibles sólidos
- Identificación de áreas para proyectos fotovoltaicos en La Guajira mediante SIG y análisis multicriterio
- Evaluación de microorganismos fijadores de nitrógeno y solubilizadores de fósforo en el cultivo de Astromelias (*Alstroemeria aurantiaca*)
- Material híbrido de plásticos reciclados (PET y PP) y áridos para la fabricación de adoquines sostenibles
- Port connectivity assessment and its impact on competitiveness: the case of Buenaventura, Colombia
- Investigación aplicada con enfoque territorial, una metodología pedagógica basada en proyectos